AD NUMBER

AD893965

NEW LIMITATION CHANGE

TO

Approved for public release, distribution unlimited

FROM

Distribution authorized to U.S. Gov't. agencies only; Test and Evaluation; MAR 1972. Other requests shall be referred to Air Force Materials Lab., AFSC, Wright-Patterson AFB, OH 45433.

AUTHORITY

AFML ltr, 8 May 1974

ADVANCED COMPOSITES DATA

FOR

AIRCRAFT STRUCTURAL DESIGN

Volume II: Structural Element

Behavior - Test and

Analytical Determination

I. M. Lackman

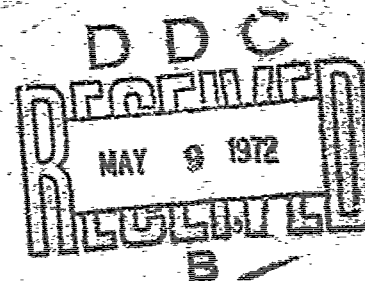D. Y. Konishi

LOS ANGELES DIVISION

NORTH AMERICAN ROCKWELL

TECHNICAL REPORT AFML-TR-70-58, VOLUME II

MARCH 1972

AIR FORCE MATERIALS LABORATORY

AIR FORCE SYSTEMS COMMAND

WRIGHT-PATTERSON AIR FORCE BASE, OHIO

NOTICE

When Government drawings, specifications, or other data are used for any purpose other than in connection with a definitely related Government procurement operation, the United States Government thereby incurs no responsibility nor any obligation whatsoever; and the fact that the government may have formulated, furnished, or in any way supplied the said drawings, specifications, or other data, is not to be regarded by implication or otherwise as in any manner licensing the holder or any other person or corporation, or conveying any rights or permission to manufacture, use, or sell any patented invention that may in any way be related thereto.

ADVANCED COMPOSITES DATA
FOR
AIRCRAFT STRUCTURAL DESIGN

Volume II: Structural Element

Behavior - Test and

Analytical Determination

L. M. Lackman

D. Y. Konishi

FOREWORD

This report was prepared by the Los Angeles Division of North American Rockwell Corporation under Contract F33615-68-C-1489, Project 6169CW, for the Advanced Composites Division, Air Force Materials Laboratory, Air Force Systems Command, Wright-Patterson Air Force Base, Ohio. Mr. R. L. Rapson (AFML/LC) was the Air Force Project Engineer, and Dr. L. M. Lackman was the North American Rockwell Program Manager.

The authors of Volume II are Dr. L. M. Lackman and Mr. D. Y. Konishi. Mr. R. B. Meadows and Mr. E. O. Dickerson supported the fabrication and testing efforts, respectively, while Mr. D. P. Murphy contributed to summarizing the testing activities and assisted in assembling the overall manuscript. Mr. G. H. Arvin, as Editor in Chief, was responsible for the organization and continuity of this volume.

This report was submitted by the authors on 24 September 1971 for publication as a technical report.

This report has been reviewed and is approved.

Robert C. Tomashot
Technical Area Manager
Advanced Composites Division

ABSTRACT

This volume is Volume II of four volumes and summarizes that portion of the program under Contract F33615-68-C-1489 concerned with the fabrication, testing, and analysis of basic element specimens composed partially or entirely of the boron/epoxy advanced composite material referred to herein as Narmco 5505.

The main body of this volume comprises independent sections devoted to the following topics:

- Fabrication of basic structural elements (section II)

- Testing of basic structural elements (section III)

- Analysis of tests (section IV) on:

  Unstiffened skin

  Honeycomb sandwich

  Stiffened skin

TABLE OF CONTENTS

LIST OF ILLUSTRATIONS

Figure	Title	Page

x

LIST OF TABLES

NOTICE

LIST OF SYMBOLS

A	-	area, general (in.^{2})
$A_{ij(i,j\,=\,1,2,6)}$	-	extensional rigidities
A_{mn}	-	subscripted coefficient where m and n generally refer to half-waves in the x and y directions, respectively
A_n	-	net area of a test panel (in.^{2})
a	-	length dimension (in.), especially of a rectangular panel
b	-	width dimension (in.), especially width of a compression panel normal to load
$D_{ij(i,j\,=\,1,2,6)}$	-	flexural rigidities
E_L	-	Young's modulus of lamina parallel to filament direction (lb/in.^{2})
E_T	-	Young's modulus of lamina transverse to filament direction (lb/in.^{2})
E_x	-	Young's modulus of laminate in X direction (lb/in.^{2})
E_y	-	Young's modulus of laminate in Y direction (lb/in.^{2})
F	-	allowable stress, general (lb/in.^{2})
F_x, F_y	-	allowable axial stresses (lb/in.^{2})
F_{xy}	-	allowable inplane shear stress (lb/in.^{2})
f	-	applied stress, general (lb/in.^{2})
f_x, f_y	-	applied axial stresses (lb/in.^{2})
f_{xy}	-	applied inplane shear stress (lb/in.^{2})
G_{LT}	-	shear modulus of lamina in the LT plane (lb/in.^{2})
G'_{cx}	-	shear modulus of honeycomb sandwich core in the XZ plane (lb/in.^{2})

ADVANCED COMPOSITES DATA

FOR

AIRCRAFT STRUCTURAL DESIGN

Volume II: Structural Element

Behavior - Test and

Analytical Determination

L. M. Lackman

D. Y. Konishi

FOREWORD

This report was prepared by the Los Angeles Division of North American Rockwell Corporation under Contract F33615-68-C-1489, Project 6169CW, for the Advanced Composites Division, Air Force Materials Laboratory, Air Force Systems Command, Wright-Patterson Air Force Base, Ohio. Mr. R. L. Rapson (AFML/LC) was the Air Force Project Engineer, and Dr. L. M. Lackman was the North American Rockwell Program Manager.

The authors of Volume II are Dr. L. M. Lackman and Mr. D. Y. Konishi. Mr. R. B. Meadows and Mr. E. O. Dickerson supported the fabrication and testing efforts, respectively, while Mr. D. P. Murphy contributed to summarizing the testing activities and assisted in assembling the overall manuscript. Mr. G. H. Arvin, as Editor in Chief, was responsible for the organization and continuity of this volume.

This report was submitted by the authors on 24 September 1971 for publication as a technical report.

This report has been reviewed and is approved.

Robert C. Tomashot
Technical Area Manager
Advanced Composites Division

G'_{cy}	-	shear modulus of honeycomb sandwich core in the YZ plane ($lb/in.^2$)
g	-	acceleration of gravity (386.4 $in./sec^2$)
h	-	thickness of a laminate (in.)
K	-	stress concentration factor (also SCF)
KiI	-	stress concentration factor (based on net area) at gage i in the I direction
M	-	moment, general (in.-lb)
m,n	-	number of half-wave lengths
N	-	number of cycles in repeated loading
N_x, N_y, N_{xy}	-	distributed force components (lb/in.)
$\left.\begin{array}{l}(n_{x,cr})_{test} \\ (n_{y,cr})_{test} \\ (n_{xy,cr})_{test}\end{array}\right\}$	-	critical values of distributed force components for general instability failure, as obtained from tests (lb/in.)
P	-	applied load (lb)
p	-	normal pressure ($lb/in.^2$)
$Q_{ij}(i,j = 1,2,6)$	-	lamina elastic constants in laminate coordinate system
q	-	normal pressure ($lb/in.^2$)
s	-	length of a side of a cell in honeycomb core
T	-	temperature ($^\circ$F)
t	-	time (units depend on application; e.g., seconds, days, etc)
$T(t_f)$	-	final temperature, when measuring a thermal gradient
$T(t_o)$	-	original temperature, when measuring a thermal gradient
t_c	-	honeycomb core thickness (in.)
t_F	-	thickness of honeycomb sandwich face sheet (in.)

ABSTRACT

This volume is Volume II of four volumes and summarizes that portion of the program under Contract F33615-68-C-1489 concerned with the fabrication, testing, and analysis of basic element specimens composed partially or entirely of the boron/epoxy advanced composite material referred to herein as Narmco 5505.

The main body of this volume comprises independent sections devoted to the following topics:

* Fabrication of basic structural elements (section II)

* Testing of basic structural elements (section III)

* Analysis of tests (section IV) on:

  Unstiffened skin

  Honeycomb sandwich

  Stiffened skin

$u_{\Delta x}, u_{\Delta y}$ –   test fixture support displacements due to thermal gradients in the X and Y directions

V –   shear force (1b)

w –   lateral deflection of a plate (in.)

$w_{,xx}, w_{,xy}, w_{,yy}$ –   shorthand notation for partial derivatives

$$\frac{\partial^2 w}{\partial x^2}, \frac{\partial^2 w}{\partial x \partial y}, \frac{\partial^2 w}{\partial y^2}$$

α –   (1) coefficient of thermal expansion (in./in./°F)
               (2) laminate invariant defined as E_x/E_y

α_L, α_T –   lamina coefficient of thermal expansion in L and T directions (in./in./°F)

Δ –   difference (used as a prefix to quantitative symbols)

θ –   angular orientation of a lamina in a laminate; i.e., the angle between the L and X axes

ν_{LT} –   Poisson's ratio relating contraction in the T direction due to extension in the L direction

ν_{TL} –   Poisson's ratio relating contraction in the L direction due to extension in the T direction

ρ –   density (1b/in.^{3})

ρ_c' –   honeycomb sandwich core density (1b/ft^3)

ρ_m –   mass density of a laminate specimen

σ –   applied normal stress

$\sigma_{ix}(i = 1,2,3...)$ –   Predicted stress in the X direction at gage i (1b/in.^{2})

ψ –   laminate invariant defined as $\dfrac{\sqrt{E_x E_y}}{(1 - \nu_{xy} \nu_{yx})}$

ω –   cyclic velocity (Hz)

$\overset{df}{=}$ –   equals by definition (in algebraic expressions)

TABLE OF CONTENTS

SUBSCRIPTS

c   -   sandwich core (used in conjunction with prime (') on basic symbol)

cr   -   critical value, in reference to instability failure

f   -   test failure value

L   -   longitudinal, in direction of L axis of lamina, parallel to filaments

pred   -   analytically predicted value

T   -   (1) transverse, in direction of T axis of lamina, inplane and perpendicular to filaments
       -   (2) value at temperature

test   -   value derived from test

ult   -   ultimate value at material failure

x,y,z   -   principal direction indicators in X,Y,Z coordinate system of laminate

xy,xz,yz   -   principal plane indicators in X,Y,Z coordinate system of laminate

SUPERSCRIPTS

ccr   -   critical compression instability value

cy   -   compression yield value

tu   -   tension ultimate value

LIST OF ILLUSTRATIONS

SECTION I

INTRODUCTION

The purpose of this program was to take the first step toward the generation and presentation of basic engineering data necessary to perform high-confidence-level structural design of primary aircraft structures utilizing advanced composite materials. The program was limited to an in-depth generation of basic material allowables for one boron/epoxy and one graphite/epoxy material system, and the determination of basic structural element response for the boron/epoxy system alone. The boron portion of this program was conducted in conjunction with a concurrent General Dynamics/ Forth Worth (GD/FW) program which was funded under Air Force Contract F33615-68-C-1474. The boron/epoxy material system highlighted by both these programs was Narmco 5505 (now available commercially as Avco 5505/4) furnished by the supplier as 3-inch prepreg tape. This is a composite material consisting of collimated 4-mil boron filaments, 208 per inch of tape width, embedded in a matrix of Narmco 2387 epoxy resin, and supported on a 1-mil layer of 104 glass scrim cloth. The graphite portion of this program is being conducted independent of any other program, and will be described in fuller detail in a later volume of this report. Additional data for all these materials, as well as for other filament/matrix material systems, were obtained from published Government, industry, and technical journal reports, and were used to augment the data generated in this program.

This program was composed of three major work task areas:

Task I   - Generation of Composite Material Design Allowables

Task II   - Structural Element Test Program and Analysis Evaluation

Task III   - Development of Advanced Composite Structural Design Manual
             for Aircraft

Task I was divided into two distinct areas of effort by the separate boron/epoxy and graphite/epoxy programs:

1. The purpose of the boron portion of task I was to complement the basic material design allowable activities conducted by GD/FW (reference 4) and to develop acceptable laminate fabrication and inspection procedures. The boron effort was divided into the following work areas:

    a. The establishment of program coordination procedures for the North American Rockwell Corporation and General Dynamics related programs

1

b. The accomplishment of a limited material development program

c. The generation of basic allowables for the constituent materials

d. Establishment of the accuracy of current analytical procedures for predicting certain basic allowables

e. The development, where reliable techniques were lacking, of prediction techniques for these basic material allowables

2. The graphite portion of task I consisted primarily of a screening, selection, and characterization of one graphite/epoxy material system. This effort will be the subject of Volume IV of this report.

The purpose of task II, which was concerned solely with boron/epoxy material, was to generate data on basic structural elements which form the building blocks from which aircraft structures are designed. A minimum evaluation of structural elements was conducted, including one basic laminate and one elevated temperature. Factors which were considered in the detail design of the structural elements included laminate orientations, panel proportions and edge restraints, effectiveness of typical forms of panel stabilization, evaluation of cutouts, and thermal gradient effects. One or more elements were selected for each primary and/or combined load applications. The test program included local and general instability of flat panels and natural frequency determinations. The results of this test program were compared to predicted response, failure mode, and strength techniques for basic structural elements.

The task III work area was originally centered on the development of an advanced composite structural design manual for aircraft structures. The first effort of this task involved revision and refinement of the Aircraft Division of the Intermediate Draft of the Structural Design Guide developed by the Southwest Research Institute, San Antonio, Texas, under Air Force Contract AF33(615)-5142. The completely revised and reorganized Aircraft Division resulting from this phase of effort was published in the Final Draft of the Design Guide in November 1968 under Contract AF33(615)-68-C-1241. Soon thereafter, a review of the Final Draft by a select industry group led to a decision by AFML to reorganize the entire Design Guide for the First Edition, which was then assigned to NR/LAD under Contract F33615-69-C-1368.

Subsequent phases of task III of this program, in light of the foregoing developments, consisted of the preparation of the Aircraft System Applications chapter of the First Edition of the Design Guide as well as the preparation of data generated by tasks I and II of this program for incorporation into the various technical function-oriented chapters. Task III also included the incorporation into the Design Guide of data generated by the concurrent GD program.

2

The bulk of the basic material allowables for the 5505 material system was generated by the General Dynamics contract. This concurrent and integrally related contract was coordinated with the Los Angeles Division program effort through scheduled periodic coordination meetings. These meetings insured the continuous flow of pertinent program data between the two contractors.

This report is divided into four separate volumes, in each of which the subject areas of interest comprise an independent segment of the overall program. Each volume is a self-contained document, complementing the other three volumes but not dependent upon them for coherence or continuity. The titles of the four volumes are:

Volume I   - Material and Basic Allowable Development - Boron/Epoxy

Volume II   - Structural Element Behavior - Test and Analytical
              Determination

Volume III - Theoretical Methods

Volume IV   - Material and Basic Allowable Development - Graphite/Epoxy

Laminate ply orientations are described and specified in this report by use of the laminate orientation code defined in the Structural Design Guide for Advanced Composite Applications.

Volume II contains the details concerned with the fabrication, testing, and analysis of basic element specimens for the boron/epoxy (Narmco 5505) system described. Three types of construction are considered: unstiffened skin, honeycomb sandwich, and stiffened skin. The stiffened-skin construction includes both zee- and hat-shaped stiffeners. The loading modes include (1) uniaxial compression, (2) biaxial compression, (3) inplane shear, (4) combined uniaxial compression and inplane shear, (5) uniform pressure, (6) uniform thermal gradient, (7) thermal gradient and pressure, (8) uniaxial compression and pressure, (9) creep buckling, and (10) uniaxial tension. Tests were conducted at room temperature and at 350°F.

Sections II and III cover the history of the problems involved in the fabrication and testing of the specimens, respectively. Processes and procedures are given for each type of specimen configuration and loading. Additionally, the reason for the various selections, as well as the problems encountered, were expounded upon so that intelligent refinements could be made in future testing. Section IV covers the analyses of the foregoing test data. Where possible, an analysis was based upon the theory developed in Volume III or presented in reference 2 . When the theory proved inadequate, an empirical modification or recommendation for future study was given.

SECTION II

FABRICATION OF BASIC STRUCTURAL ELEMENTS

FABRICATION OF BORON LAMINATES

All boron/epoxy laminates fabricated were made by the procedures described in North American Rockwell Specification ST0105LA0007. The shop area used for this fabrication is shown in figure 1.

All laminates were made by direct layup of boron/epoxy tape. To minimize scrap, 3-inch-wide Mylar templates were used to cut each piece of boron tape from the roll. The template was removed and the tape placed in the layup in its appropriate place and then the paper backing was removed as shown in figures 2 and 3. All layups were made with the 104 glass scrim down. To gain experience with Mylar full-ply templates, one laminate was laid up using this procedure, as described in ST0105LA0007 and shown in figure 4.

During layup, care was exercised to insure that gaps between boron filaments did not exceed 0.03-inch width, whether within a 3-inch-wide tape or between tapes. The boron prepreg tape was also inspected for loose or cured pieces of resin, for short or overlapped filaments, and general cleanness at the time of layup. Where a defect in the layup was noticed, it was removed by tweezers, if possible; otherwise, the entire length of filament in a strip wide enough to include the defect was removed from the tape. This area was then filled with acceptable boron/epoxy prepreg tape. After inspection, the boron layup was rubbed out parallel to the filaments with a Teflon squeegee to create intimate contact between plies and to eliminate entrapped air. The laid-up assembly was closed out with a balance ply of 104 glass fabric impregnated with the same resin system as the boron prepreg tape.

The tool used for curing was made of steel and, after cleaning with methyl ethyl ketone (MEK), the GS-3 release agent was applied and rubbed down with cheesecloth to remove the excess release agent. The prepared surface of the tool was covered with TX-1040 release cloth the same size as the boron layup to be cured. The boron/epoxy panel was placed on the TX-1040 release cloth and then covered with another layer of TX-1040 release cloth with the same dimensional restrictions as the bottom layer.

A Coroprene dam was placed around the boron/epoxy panel to a thickness of at least 0.03 inch thicker than the total layup thickness of the boron/epoxy panel. The Coroprene support material was located within 0.06 inch of the part edge to prevent filament washing during resin flow. One ply of dry 120 glass fabric was used for each five plies of boron prepreg in the layup. The 120 glass bleed fabric was cut to the same dimensions as the boron prepreg layup. A layer of Tedlar film was placed over the entire layup so that it

Figure 1. Advanced Composites Layup Area

Figure 2. Typical Laminate Layup Procedure
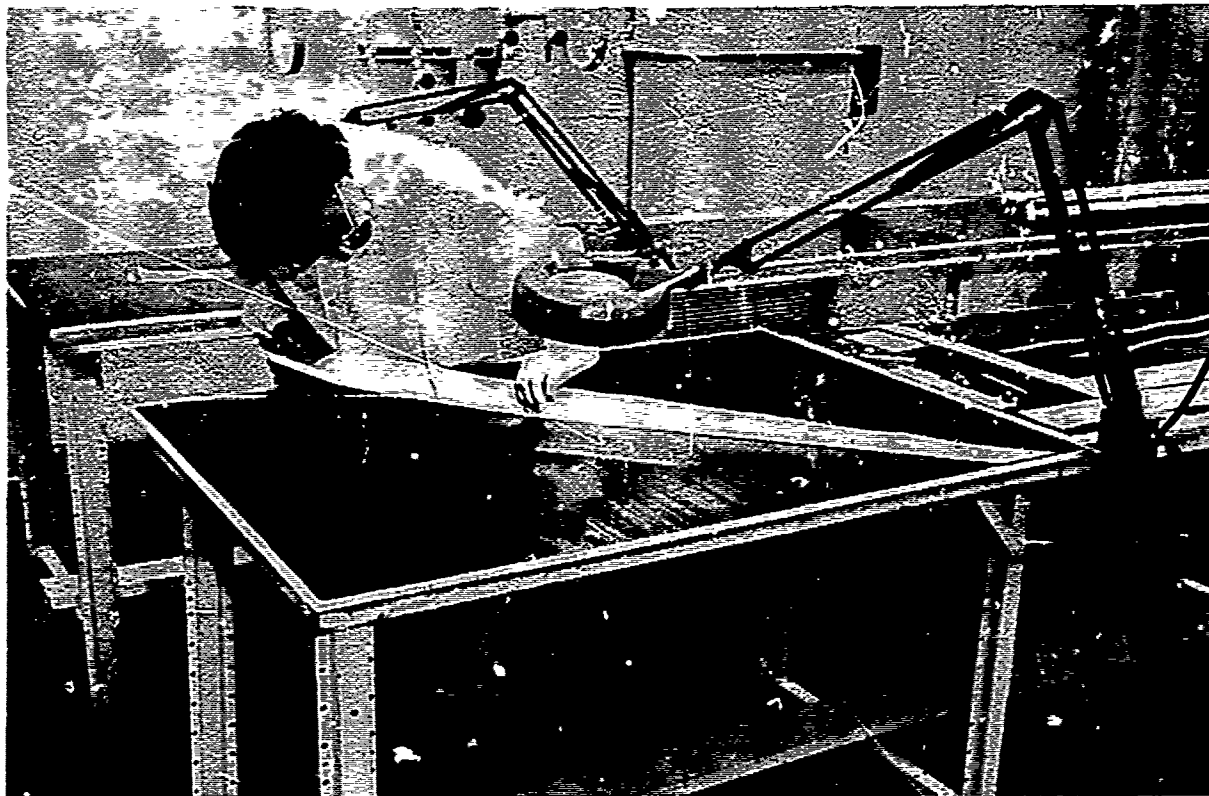
Figure 3. Typical Structural Element Being Fabricated
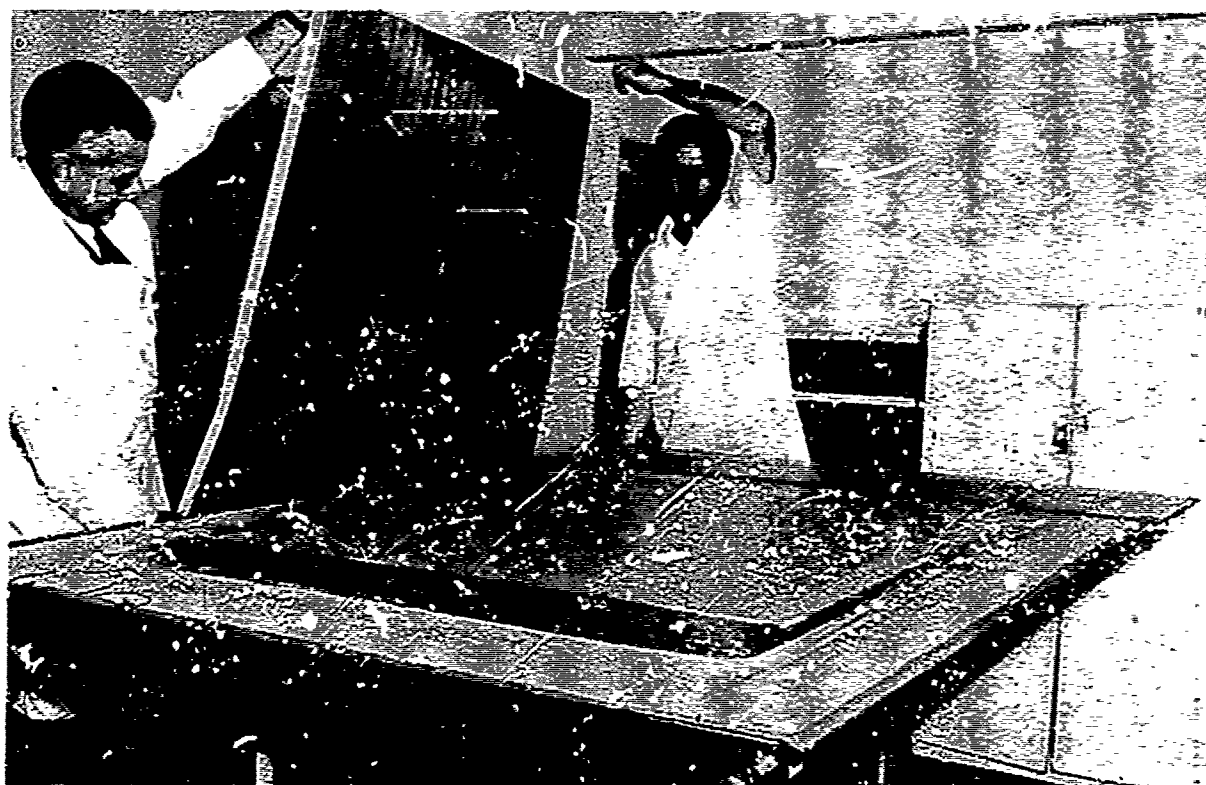
Figure 4. Mylar Ply Template Layup

extended beyond the periphery of the Coroprene dam. The escape of air from the controlled flow bleed system was obtained by perforating the Tedlar sheet on 2-inch centers starting 1/2 inch from one edge of the layup.

The layup was then covered with two plies of dry 181 glass fabric, and the completed layup was placed under vacuum pressure. When the autoclave pressure reached 30 psi, the vacuum bag was vented to the atmosphere. The autoclave pressure was raised to 85 psi and maintained at that level. The temperature was raised to 350°F ±10°F and held for 120 minutes ±10 minutes. The cured part was cooled below 150°F under pressure before removing from the autoclave. A typical cured panel is shown in figure 5.

The finished part was reinspected for crossed filaments, wrinkles, foreign objects, broken fibers, and contour discrepancies. The panel was then measured for thickness per ply to determine conformance to the specification requirement of 0.0051 inch minimum and 0.0054 inch per ply maximum.

Each panel was fabricated to include IITRI-type (figure 11 of Volume I) longitudinal and transverse tensile specimens. These specimens were used to verify that panels of an adequate strength level had been fabricated. The test coupons were provided with Scotchply end tabs (figure 6) for longitudinal and transverse tensile tests. Those specimens tested at room temperature had tabs bonded with FM-1000 adhesive, while those specimens tested at 350°F had tabs bonded with Metlbond 329 adhesive.

FABRICATION OF ZEE AND HAT STIFFENERS

Zee and hat specimens were laid up on stainless steel tooling and fabricated in accordance with NR Specification ST0105LA0007. Figures 7 and 8 show the tooling, cured rubber pressure pad, and a typical cured part. Zee stiffeners were trimmed to final size and bonded to boron/epoxy panels (figure 9), where required, with FM-1000 adhesive for room temperature testing and with Metlbond 329 adhesive for elevated temperature testing.

FABRICATION OF HONEYCOMB SANDWICH PANELS

The cured boron/epoxy laminates previously described were used as face sheets on honeycomb core. The face sheets were prepared by sanding with 240 grit abrasive paper followed by a final cleaning with MEK. An adhesive film (HT424) was placed on each face sheet, which was then placed on the honeycomb core. The entire assembly was vacuum-bagged to a flat ground steel tooling plate and cured at 350°F. After bonding, the honeycomb sandwich panels were machined for precise sizing and had doublers installed. Doubler installation for edge-loaded compression panels posed development problems because of premature failure of the adhesive bond between the doubler and the boron face sheet.

7

Figure 5. Typical Cured Structural Element

REVISED LOADING TAB FOR 16-PLY ELEMENT SPECIMEN COUPONS

FOR $[0/\pm45/0]_{2S}$ LONGITUDINAL TENSILE TESTS
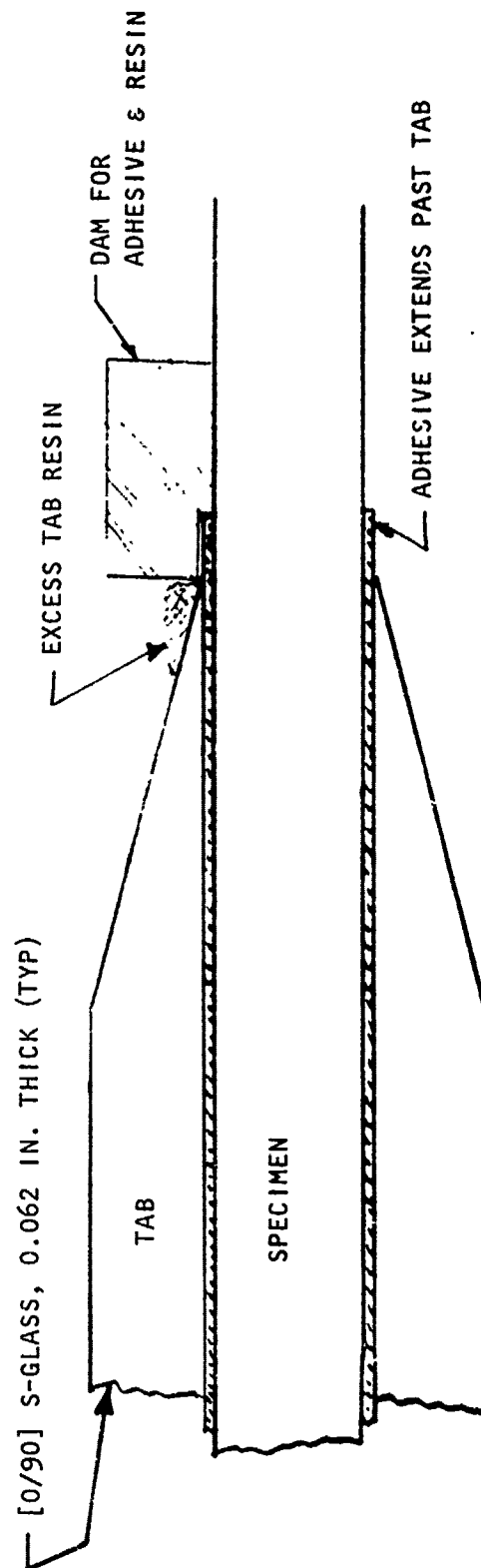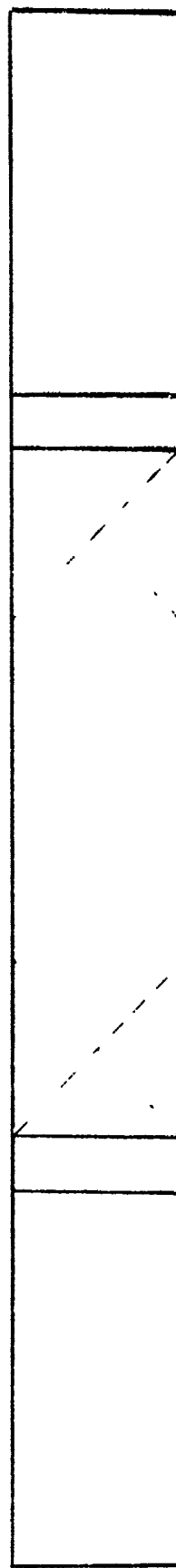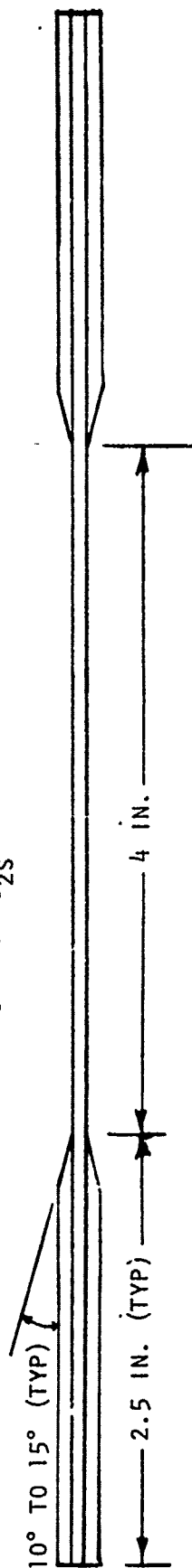
Figure 6.   Revised Loading Tab for 16-Ply Element Specimen Coupons
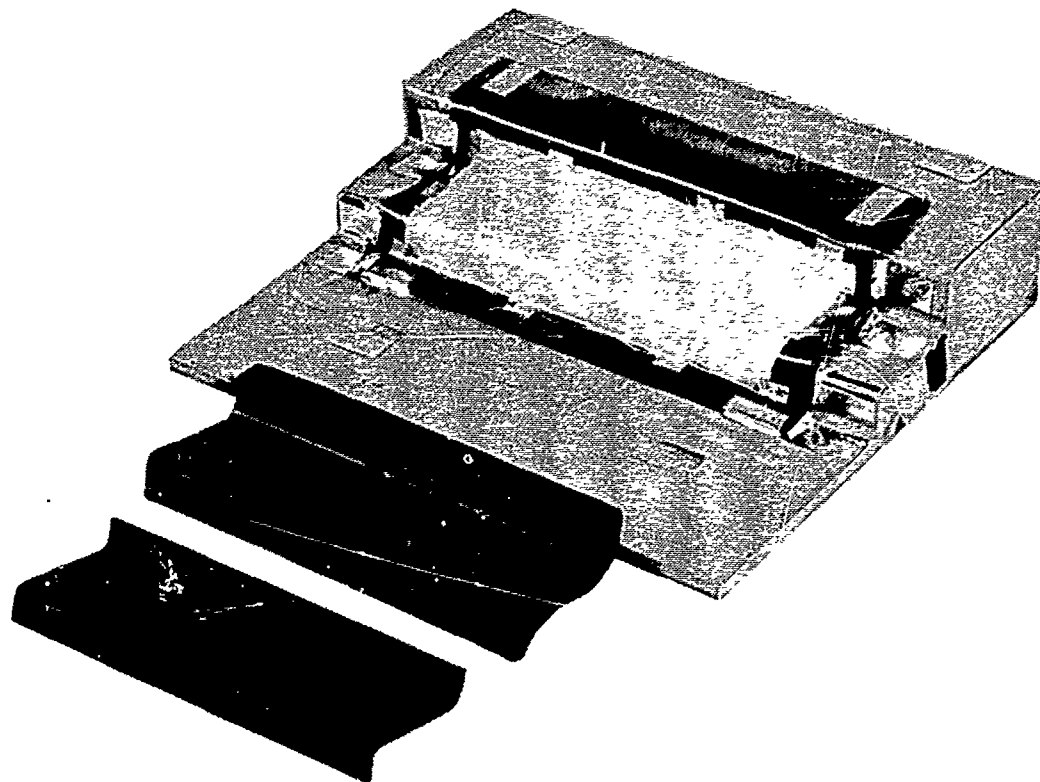
Figure 7. Zee Section and Tooling
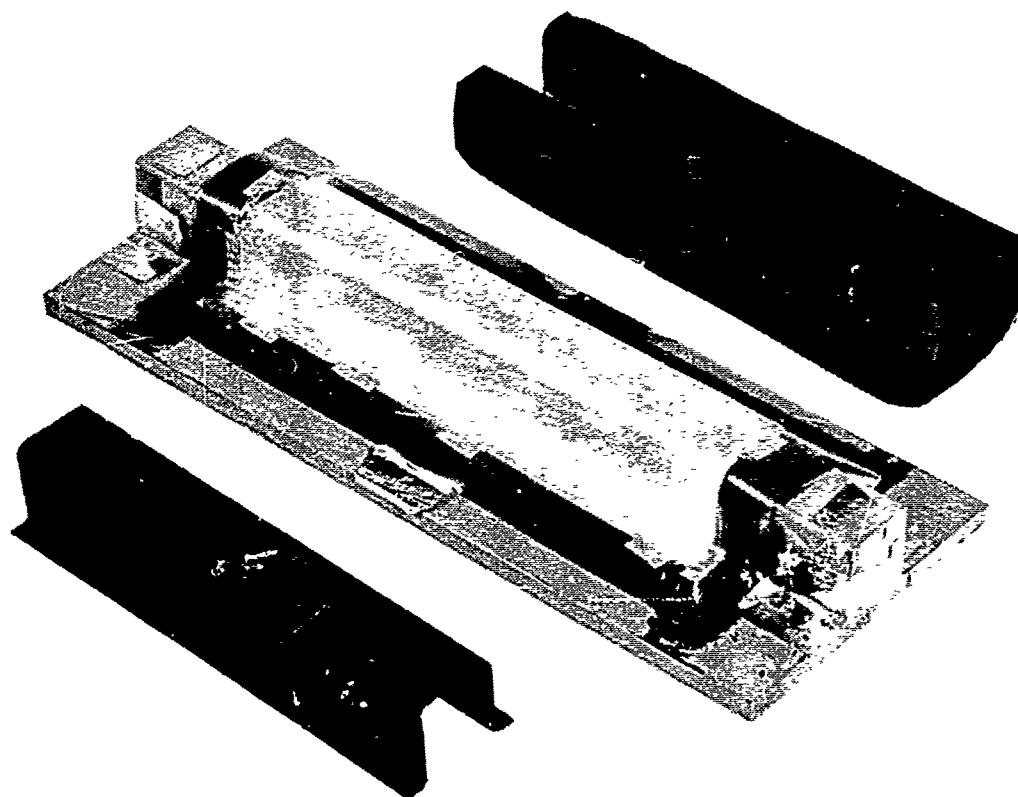
Figure 8. Hat Section and Tooling

ZEE BONDING TOOL

BORON PANEL   BOND AREA

RUBBER LOAD
DISTRIBUTION
PLATE

STAINLESS TOOL   ZEE STIFFENER

HAT BONDING TOOL

BORON PANEL   BOND AREA

RUBBER LOAD
DISTRIBUTION
PLATE

HAT STIFFENER

STEEL TOOL
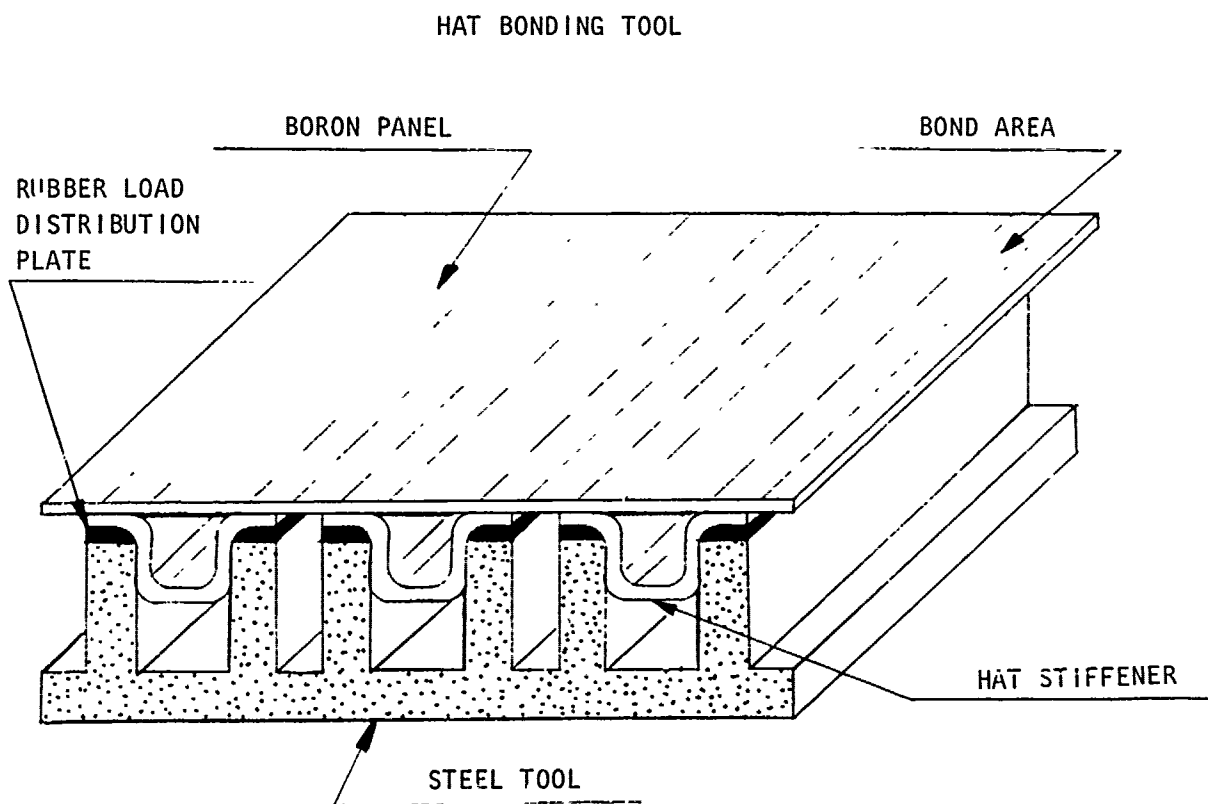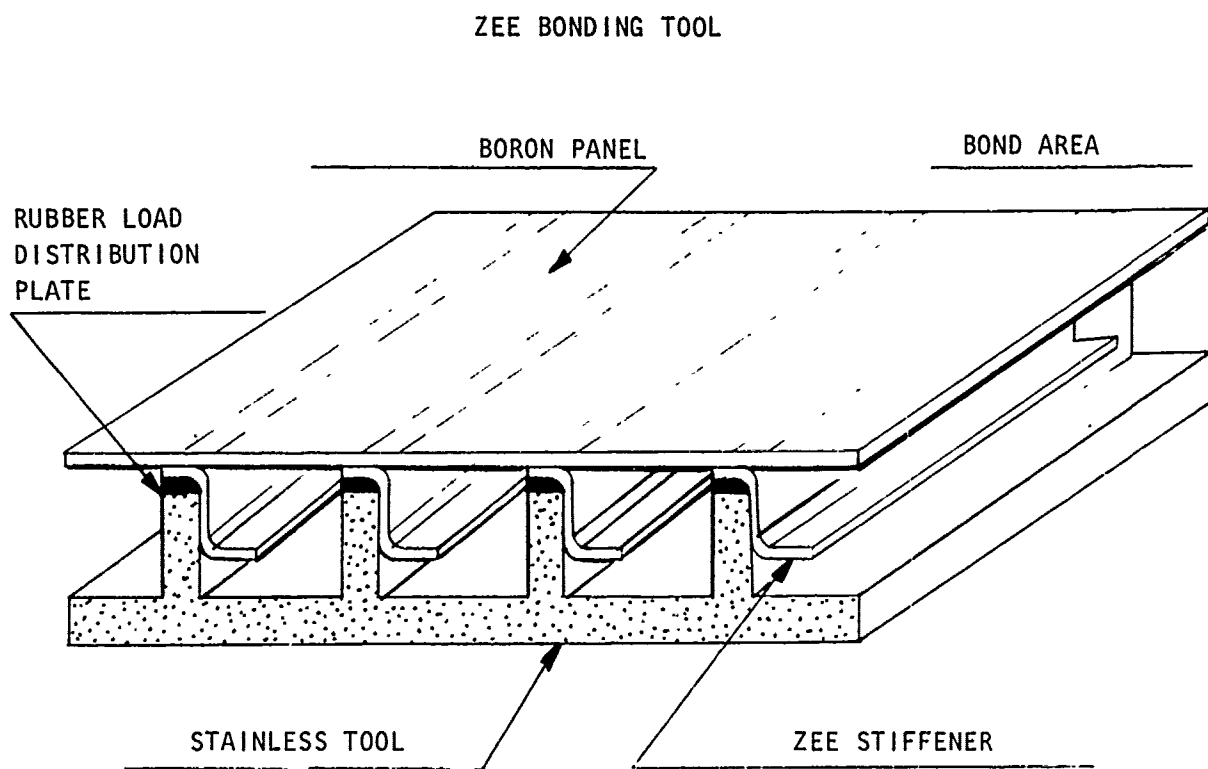
Figure 9. Tooling Schematic For Stiffened Panels

11

Initially, aluminum tapered doublers were bonded to panels using FM-1000 adhesive for room temperature tests and Metlbond 329 adhesive for 350°F tests. Induced stresses due to mismatch in coefficients of expansion between aluminum and boron/epoxy face sheets resulted in below-average failing loads.

Titanium doublers were fabricated and bonded to elevated temperature test panels. Test results revealed some improvement in load-carrying capability. To raise the anticipated failing loads further, selected panels were reinforced in the doubler system with a bonded glass laminate that served to extend the area of the doubler and to introduce the test loads into the boron face sheets with a minimum of load concentration, as shown in figure 10. The rest of the compression test panels were fabricated with steel doublers, which were used to reduce costs associated with the processing of titanium, such as raw material costs, machining costs, cleaning, and handling.

The honeycomb sandwich test panels after doubler installation were potted with an epoxy resin system on the compression-load-bearing faces of the test panels. Potting was performed to prevent brooming of face sheets and was approximately 2 cell diameters deep. To insure this depth of potting, cells were manually opened to the required depth.

The potted panels with doublers installed were final-machined to obtain the required parallelism necessary for edge-load compression tests.

Sandwich panels that were to be tested under combined loading required angle-type load introduction members. Figure 11 shows the doubler installation and figure 12 shows the tooling for bonding the doubler.
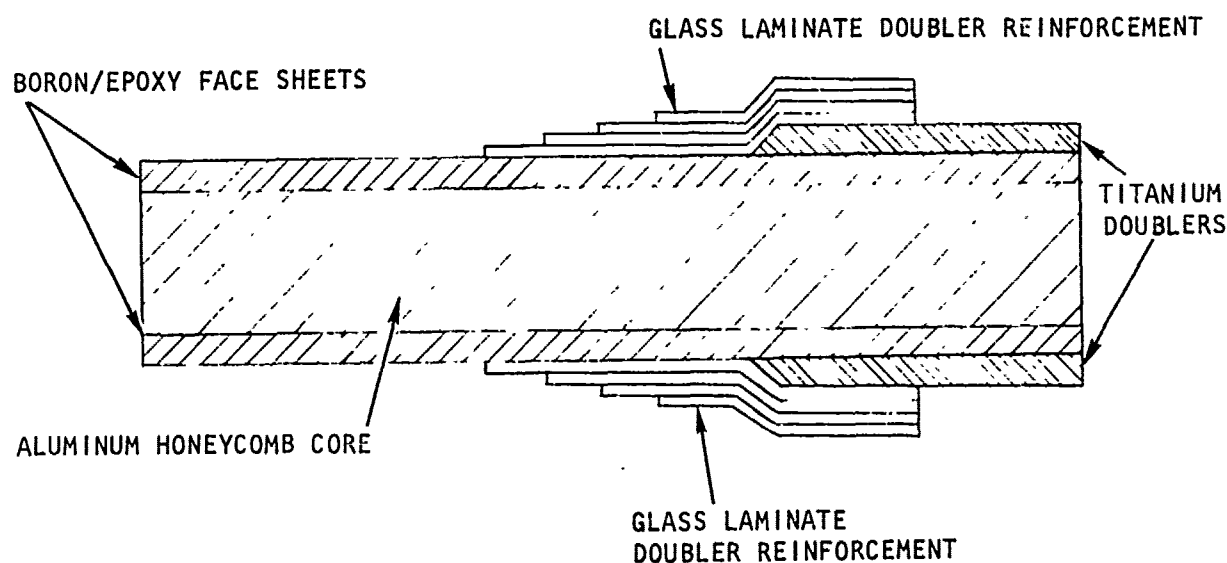
Figure 10. Glass Laminate Doubler Reinforcement
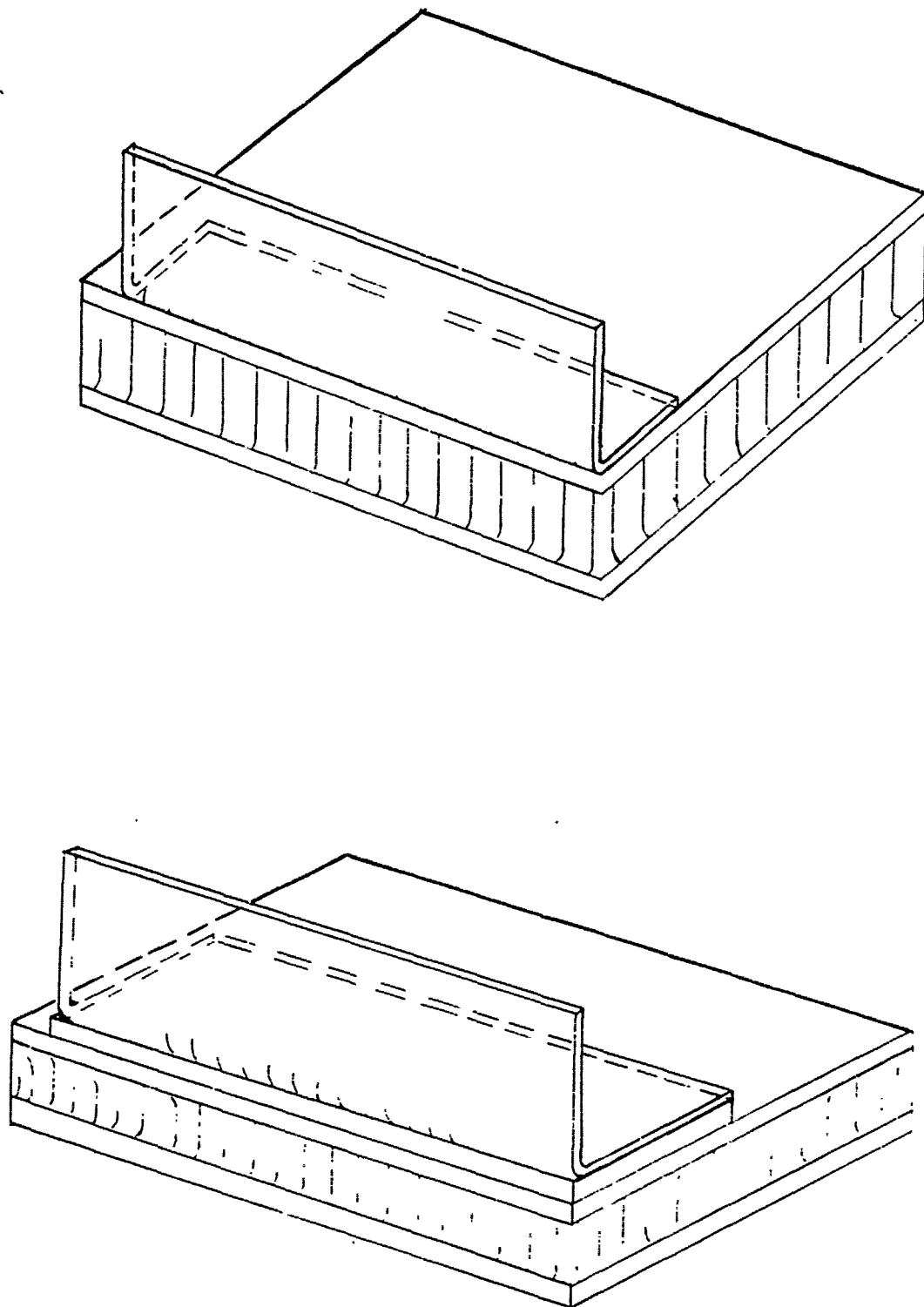
Figure 11. Design of Angle Load Introduction Doublers
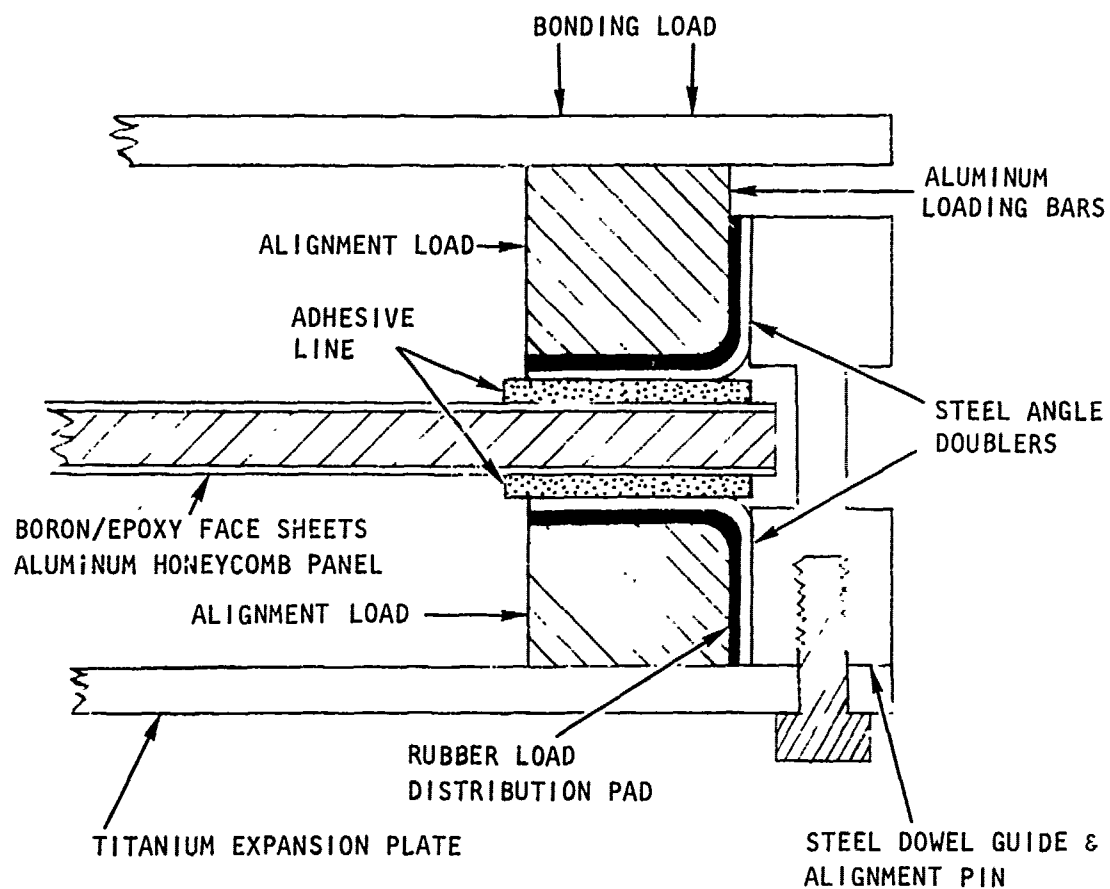
Figure 12. Angle Doubler Installation Tooling for Shear and Combined Load Boron/Epoxy Honeycomb Sandwich Specimens

14

SECTION III

TESTING OF BASIC STRUCTURAL ELEMENTS

GENERAL
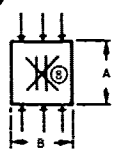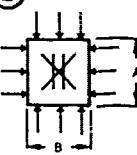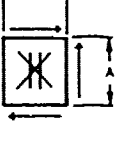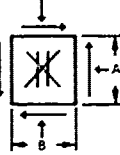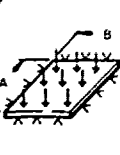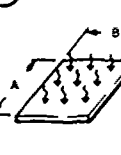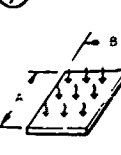
The basic objectives of this phase of the test program effort were to gather significant static, fatigue, and creep data on composite structural elements under various loading conditions, and to qualify the equipment used in these tests to reproduce accurately the loading conditions called for in subsequent analytical studies. Figure 13 outlines the test program, detailing the panel configurations and their loading conditions.

Loading equipment and jigs were designed to utilize existing test machines wherever possible, and floor-mounted jigs used for the larger, more complexly loaded panels were designed for versatility. To verify the effectiveness of the test equipment at duplicating the desired edge conditions, tests were often run on aluminum panels and the results compared with analytical predictions.

Uniaxial compression tests, loading condition No. 1, were carried out on the Riehle FS60W testing machine. A specimen edge-compression loading fixture for simple support was designed and evaluated with aluminum specimens. The fixture consists of a clevis-type fitting, which slips over the edge of the specimen, and a knife-edge loading bar. This device is shown in figure 14. The results of tests carried out with the aluminum sheet column specimens were in close agreement with theory, demonstrating the equipment effectiveness in providing an aligned true simple-support boundary condition.

The loading fixtures for the remaining specimens were designed to a large extent on the basis of this simple edge-support fixture. Schematic diagrams of the loading procedures used for unstiffened specimens are shown in figure 15. Similar setups were used for the honeycomb sandwich panels, with the clevis ends widened and stiffened to fit and support the edges of the panels.

Loading condition No. 4, which was previously shown as a biaxial compression and shear loading, was changed to uniaxial compression and shear. The longitudinal compression load was applied by a pivoting head which accommodated the shear (parallelogram type) deformation. Shear loading was applied through zee-section edge members bonded to the panel, and loaded through straps attached to hydraulic cylinders. A schematic diagram of this loading fixture is shown in figure 16. Shear fixtures for the unstiffened panels were redesigned using a simplified concept aimed at reducing costs of fabrication and testing. A sketch of this method and loading setup is shown in figure 17.

FLAT SHEET

TYPE OF STIFFENING	a/b ASPECT RATIO OF PANEL	UNIAXIAL COMPRESSION ① 4 EDGES S/S (B X A)	BIAXIAL COMPRESSION ② 4 EDGES S/S	IN PLANE SHEAR ③ 4 EDGES S/S	COMBINED LOADING ④ 4 EDGES S/S ② 3 LOAD RATIOS	PRESSURE PANEL ⑤ 4 EDGES S/S	THERMAL GRADIENT ⑥ 4 EDGES S/S	PRESSURE + THERMAL GRADIENT ⑦ 4 EDGES S/S
(A) UNSTIFFENED	1	$1/1$ $[1]^D$ (6 x 6 in., t = 0.080)	$1/1$ t = 0.080	$1/1$ t = 0.080	$1/1$ t = 0.080	$1/1$ t = 0.080	$0/1$ t = 0.080	t = 0.080
	2	—	—	—	—	—	—	—
	3	$1/1$ $[1]^D$ (6 x 12 in., t = 0.080)	$1/1$ t = 0.080	$1/1$ t = 0.080	$1/1$ t = 0.080	$1/1$ t = 0.080	$0/1$ t = 0.080	t = 0.080
(B) H/C SANDWICH	1	$2/1$ $[1]^D$ (12 x 12 IN.)	$2/1$	$2/1$	$1/1$	$2/1$	$0/1$	
	2	$2/1$ $[1]^D$ (10 x 20 IN.)	$2/1$	$2/1$	$1/1$	—	—	—
	3	$2/1$ $[1]^D$ (8 x 24 IN.)	$2/1$	$2/1$	$1/1$	2 $0,^F$ $1/1$	$0/1$	
(C) (D) SKIN STRINGER [ZEE STIFFENED] [HAT STIFFENED]	1	$(2/1) \times 2^=$ t = 0.080	—	$(2/1) \times 2^=$ t = 0.080	—	—	—	—
	2	$(2/1) \times 2^=$ t = 0.080	—	$(2/1) \times 2^=$ t = 0.080	—	—	—	—
	3	$(2/1) \times 2^=$ t = 0.080	—	$(2/1) \times 2^=$ t = 0.080	—	—	—	—
TOTALS		20/11	8/5	20/11	5/5	7/4	0/-	- -
Σ						FLAT SHEET	67/44	

BASIC ELEMENT PROGRAM (ONE LAMINATE, ELEVATED TEMPERATURE 350°F)

BASIC STRUCTURAL ELEMENT TEST PROGRAM ④, ⑤			
TYPE OF SPECIMEN	ONE CROSSPLY LAMINATE		TOTAL NO OF TESTS
	ROOM TEMP TESTS	ONE ELEVATED TEMPERATURE TEST	
FLAT PANEL	67	68	135
CRIPPLING ELEMENT	26	13	39
PANEL WITH CUTOUTS	12	6	18
TOTAL	105	87	192
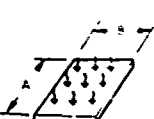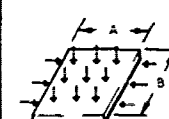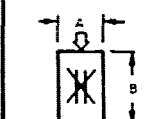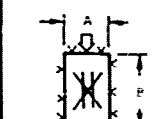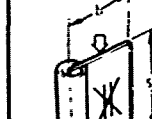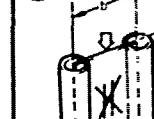
					CRIPPLING ELEMENTS			
THERMAL GRADIENT	PRESSURE + THERMAL GRADIENT	PRESSURE + COMPRESSION	CREEP BUCKLING		COMPRESSION ONE EDGE FREE	COMPRESSION NO EDGE FREE	COMPRESSION CHANNEL ELEMENT	COMPRESSION ZEE ELEMENT
	⑦	⑧	⑨	⑩	⑰	⑱	⑲	⑳

Figure 13. Basi

CRIPPLING ELEMENTS					CUT OUTS		
COMPRESSION ONE EDGE FREE	COMPRESSION NO EDGE FREE	COMPRESSION CHANNEL ELEMENT	COMPRESSION ZEE ELEMENT	COMPRESSION HAT ELEMENT	TENSION PANEL	COMPRESSION PANEL	SHEAR PANEL
⑰	⑱	⑲	⑳	㉑	㉒	㉓	㉔

Figure 13. Basic Structural Element Test Program

16

0.375

0.085-0.087

0.250

0.50

0.125

0.010-0.015R

100°

2.00

1.00

.010 R

0.25

60°

0.50

0.19

0.19

16-PLY LAMINATES

MATERIAL: PH17-4 STEEL
HEAT TREAT: 200-220 KSI

Figure 14. Simple Support Compression Edge Loading Fixture

17

Figure 15. Schematic Loading Fixtures for Unstiffened Flat Specimens
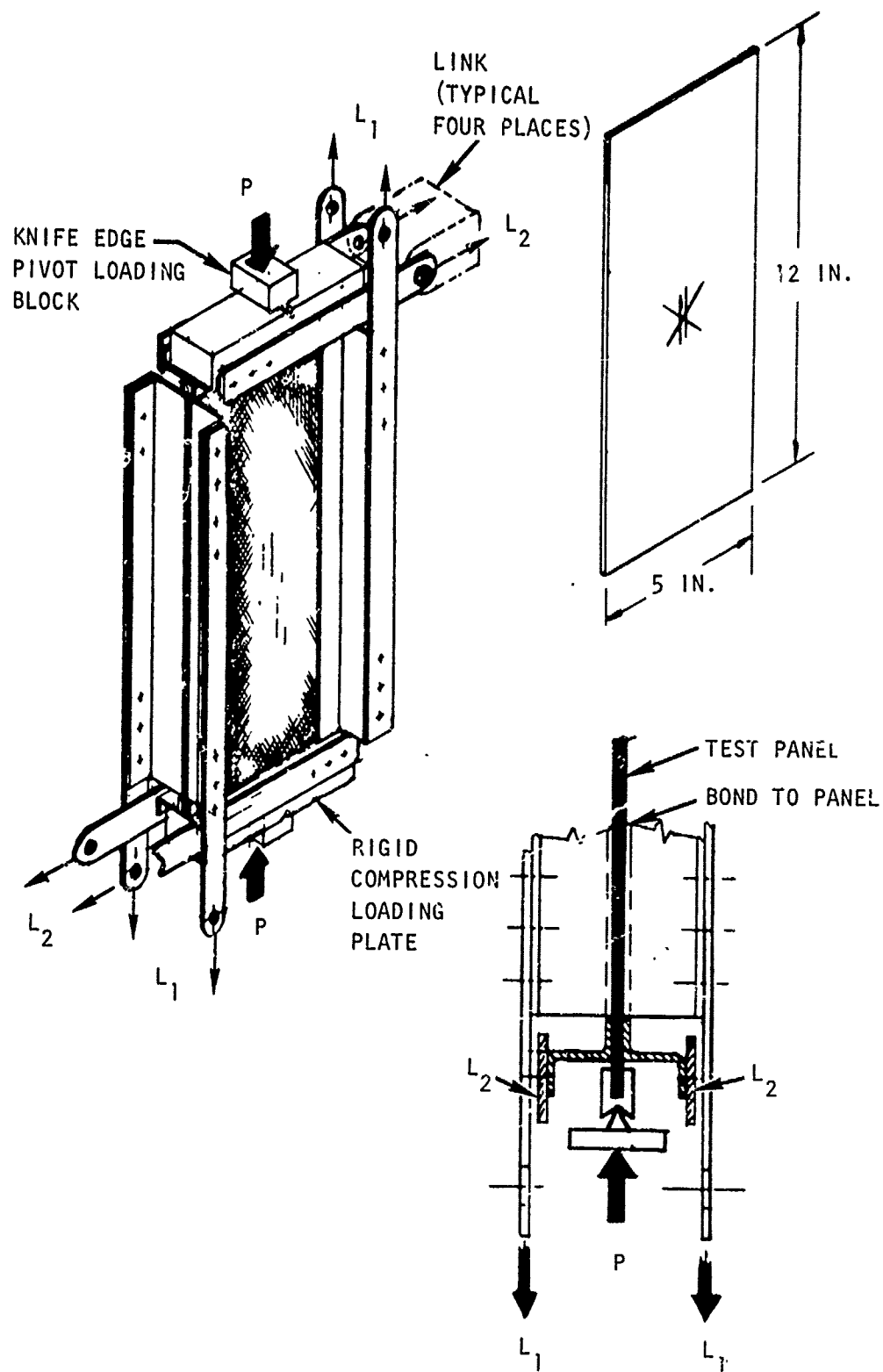
Figure 16. Combined Compression and Shear Panel Test

19

ALUMINUM ANGLES BONDED
TO PANEL

LOAD

A-A

PH17-4 STEEL
LOADING STRAPS

A

A

LONG STRAP

REINFORCEMENT

B

B

B-B

UNLOADED CORNERS
STABILIZED AGAINST
LATERAL MOVEMENT

CUTOUT IN REINFORCEMENT
CHANNEL TO PERMIT PASSAGE
OF HORIZONTAL STRAP
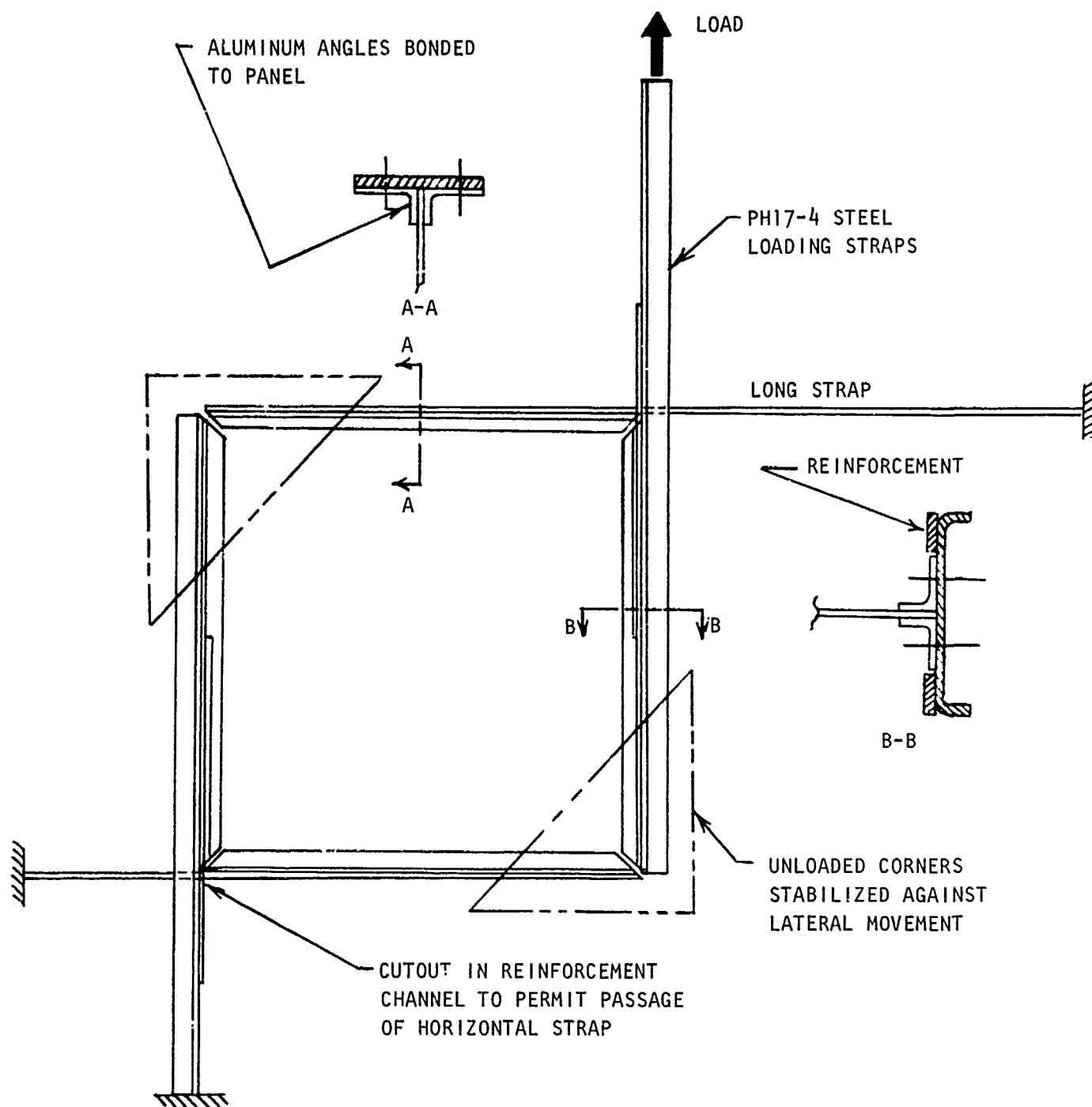
Figure 17.   Shear Fixture for Unstiffened Panel Tests

20

The initial test of unidirectional panel compressive loading used conventional split-tube edge stabilization, as shown in figures 18 and 19. At the higher loads, a severe offset occurred in the gap between the end of the edge-supporting tube and the end-loading fixture. This resulted in a premature failure because of the "punch type" offset which resulted. To correct this situation, the ends of the loading fixtures were machined to remove the sides (figure 20) and the edge-stabilizing tubes extended to overlap the loading fixture (figure 21). The revised fixture is shown in figures 22 and 23. The edges of the tube slots were also sharpened to provide a knife-edge bearing on the specimen (to reduce moment fixity) and Teflon strips inserted between the tube edges and the specimen.

In addition, to reduce the torsional stiffness of the end-loading fixture, slots were added at 1/2-inch intervals. These may be seen in figures 22 and 23. These torsional-stiffness-reducing notches were also machined into the honeycomb panel clevis bars, and this feature was subsequently incorporated into all knife-edged loading bar and channel-type panel edge bearing fixtures. A sketch of the honeycomb type clevis is shown in figure 24.

For loading conditions No. 1 and 2 on the larger, bulkier test panels, a Riehle 120K or Tinius Olsen 440K axial test machine was used. The reasons for the use of these larger machines were primarily for convenience rather than the need for greater axial loading capacity. For loading conditions No. 5, 6, 7, 8, and 10, built-up floor jigs were assembled, and edge support designs qualified in earlier phases of the program were employed. Figures 25, 26, and 27 are typical of these fixtures. Compressive loads were supplied by hydraulic cylinders and reacted through existing laboratory equipment. Normal pressure was applied by the use of a stainless steel pillow placed beneath the test panels. The required heat for thermal gradients was obtained by enclosing the test panels inside the jig and piping in dry heated air. The exterior of the test apparatus was radiantly heated with 1,000- or 2,000-watt General Electric quartz lamps. The thermal gradient setup is shown in figure 28.

Strain gages and strain gage rosettes were used to measure the panel stresses; panel midpoint deflection was measured with a dial gage; and thermocouples were used for monitoring temperatures. As the predicted failure load or deflection was approached, the dial gage was removed to prevent damage to its mechanism.

VERIFICATION OF EDGE-LOADING FIXTURE FOR HONEYCOMB PANELS

Two aluminum-alloy-faced honeycomb sandwich panels were fabricated to verify the loading fixtures, edge members, and test techniques to be used on the sandwich element tests. The aspect ratio 1 (15 x 15 inch) and aspect ratio 3 (13 x 39 inch) panels were duplicated, except for 0.040-inch
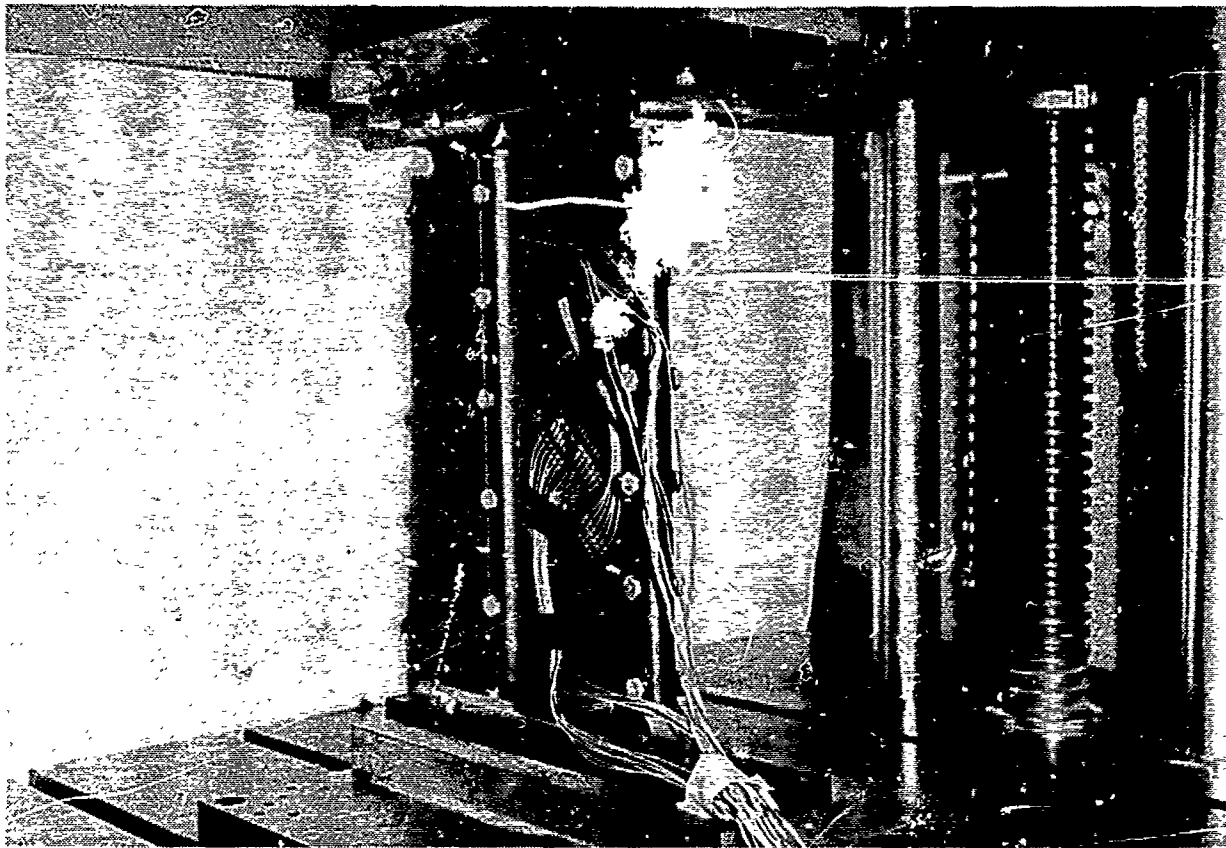
Figure 18.   Original Split-Tube Stabilization, Panel 1A3R1, Side 1
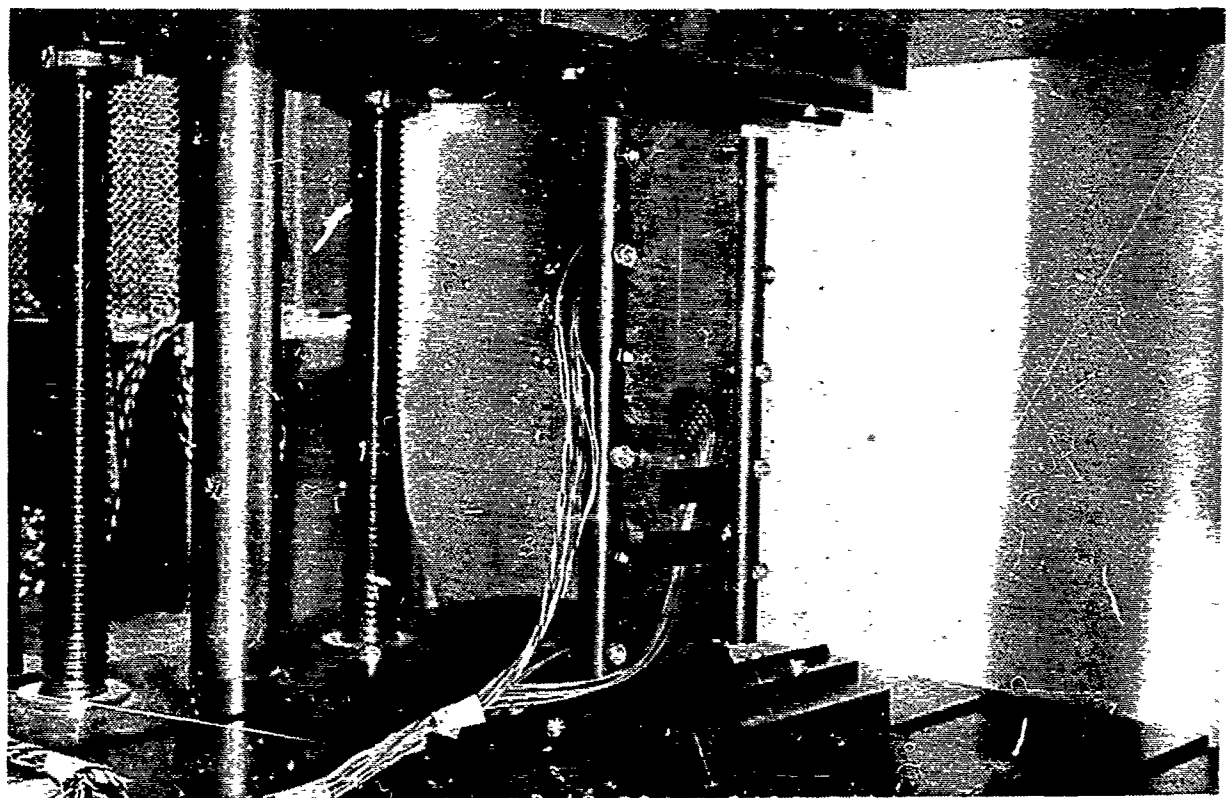
Figure 19.   Original Split-Tube Stabilization, Panel 1A3R1, Side 2

22

SIDES REMOVED
FOR 1/8 IN. AT
ENDS OF LOADING
FIXTURE
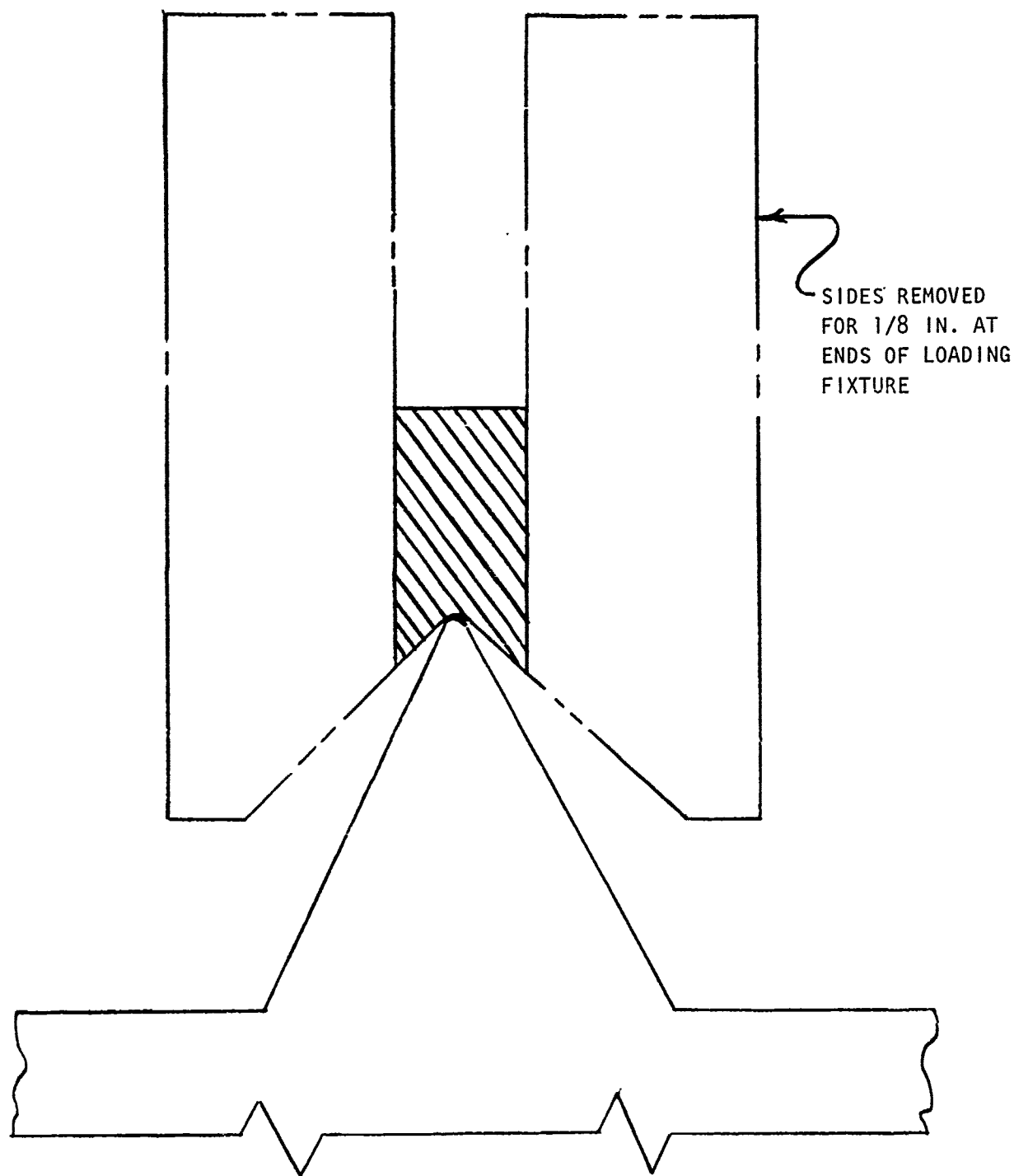
Figure 20.   Sides Removed at Ends of Loading Fixture

23
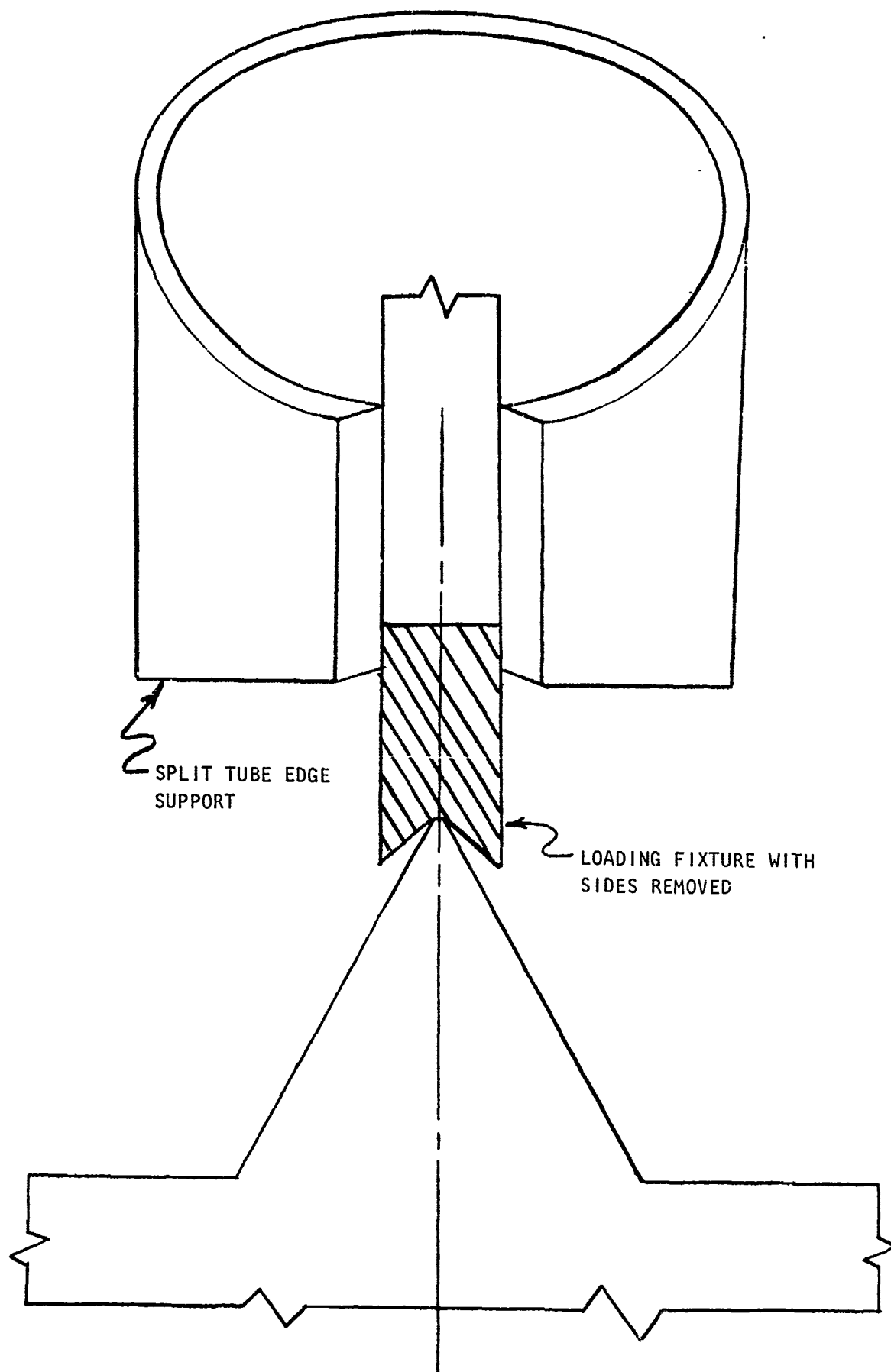
Figure 21. Modified End of Loading Fixture to Accommodate Edge Tube
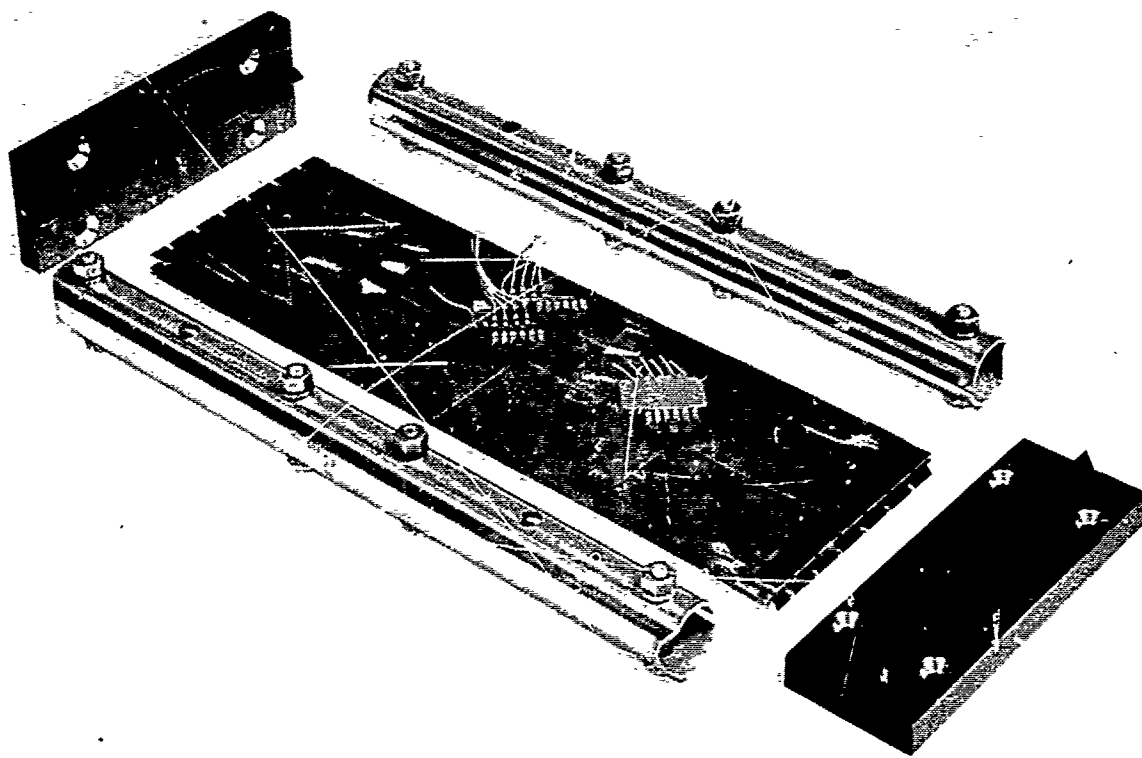
Figure 22.   Revised Split-Tube Stabilization Fixture, Panel 1A3E1
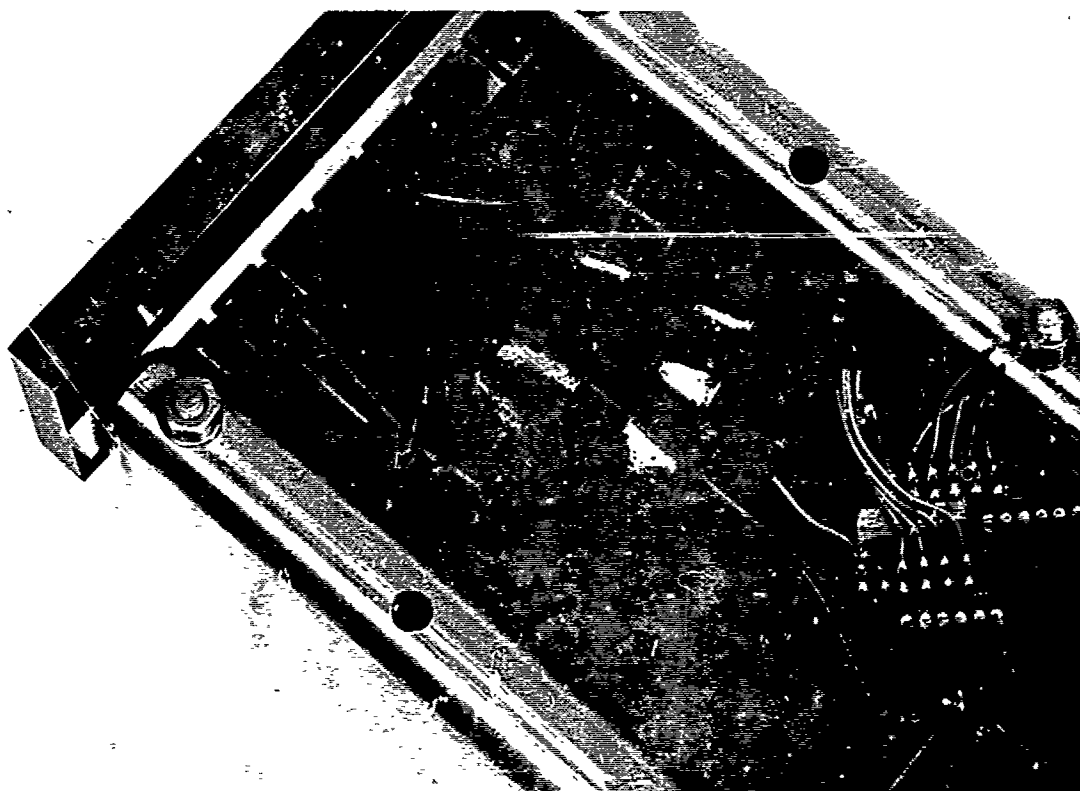
Figure 23.   Revised Split-Tube Stabilization Fixture, End Detail
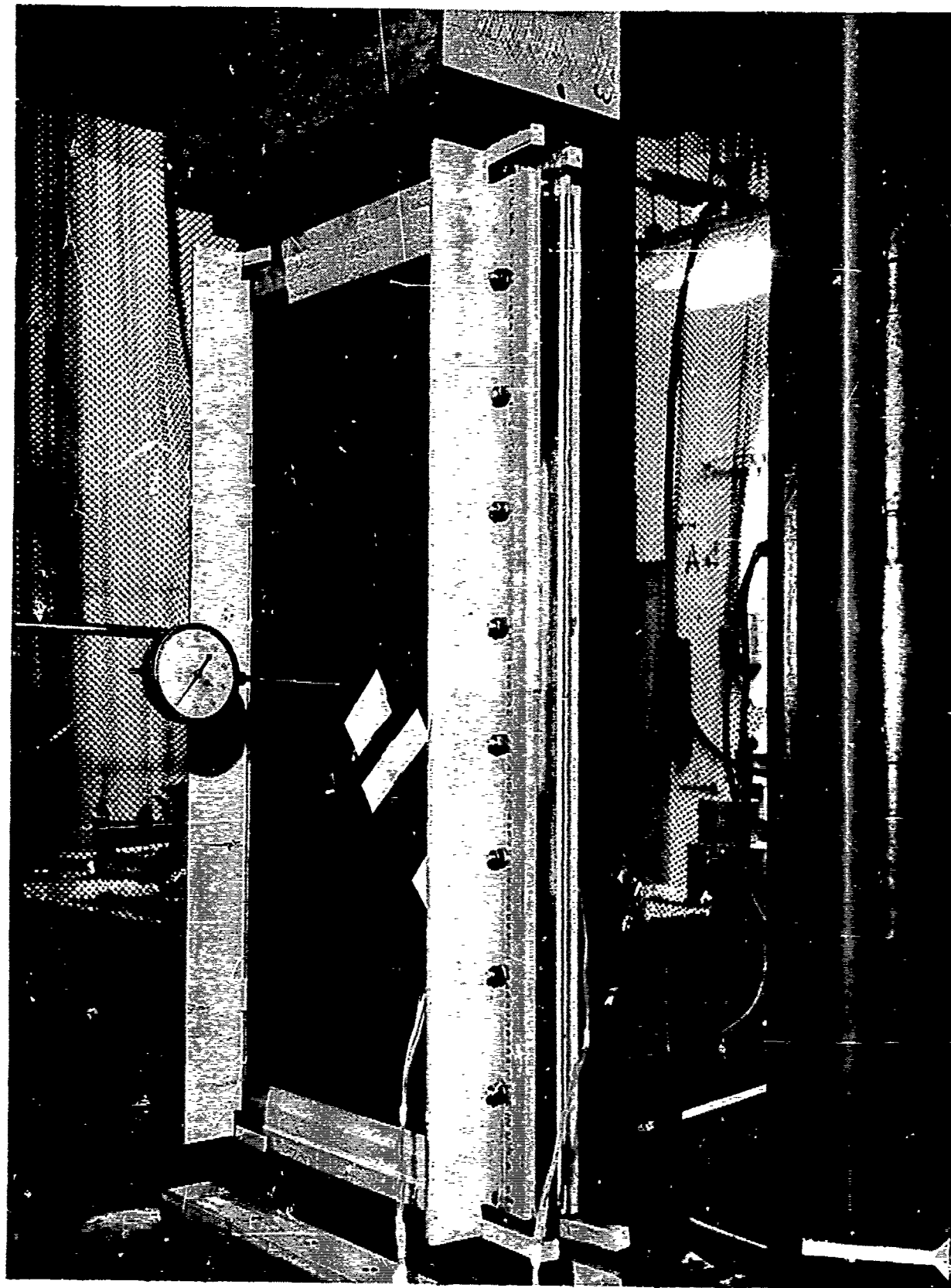
Figure 24. Honeycomb Panel Edgewise Compression Loading Fixture
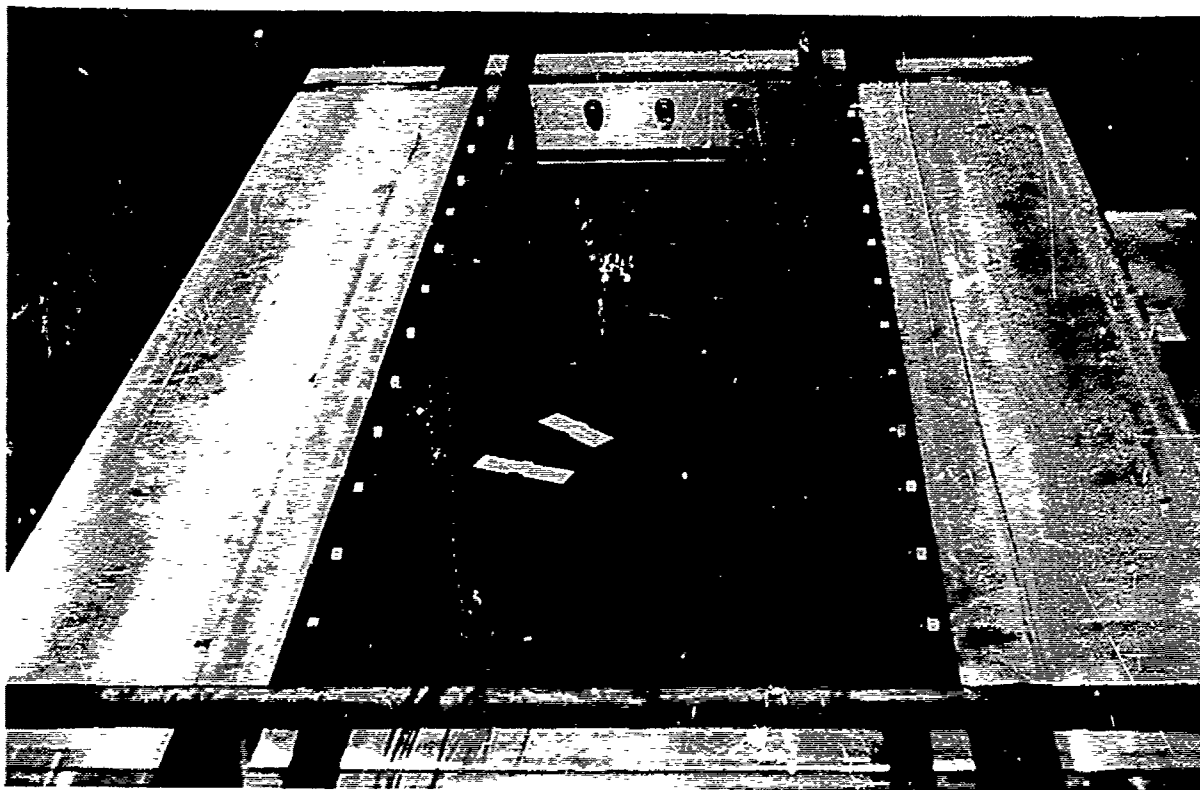
Figure 25. Normal Pressure Loading Setup, Panel 5B3R1
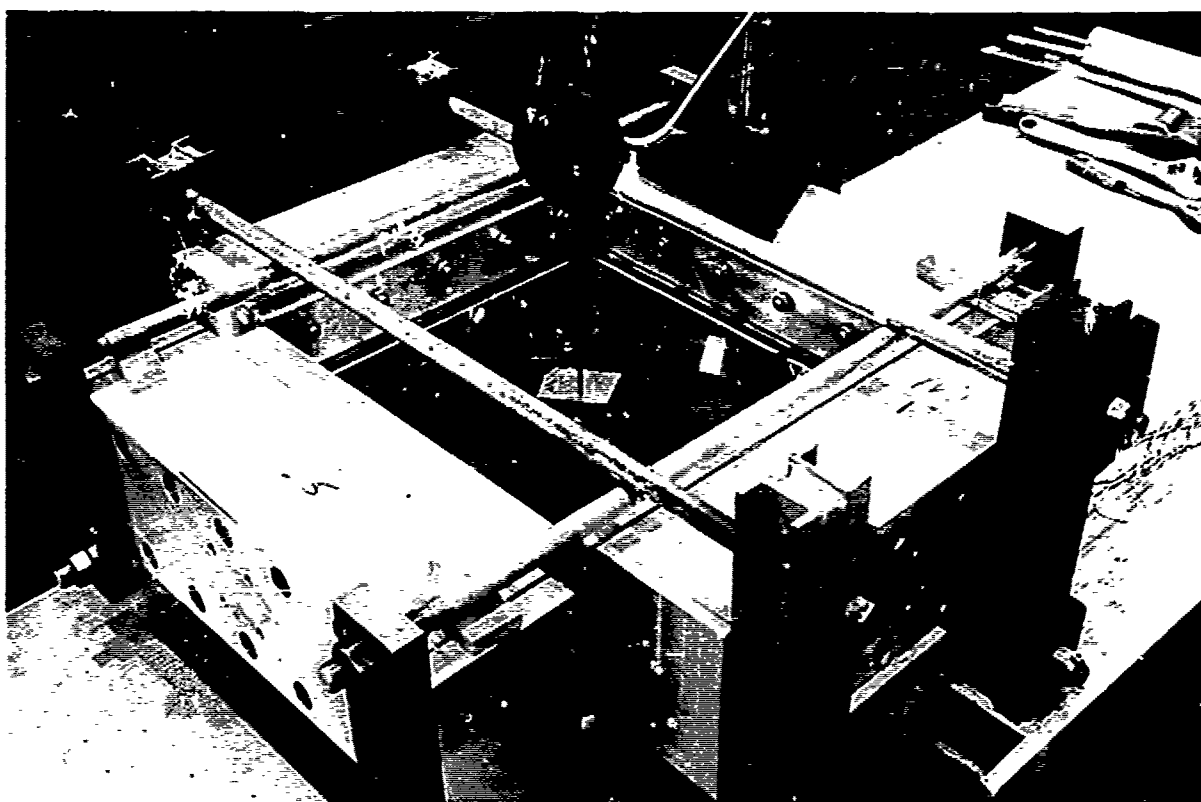
Figure 26. Normal Pressure Test Setup, Panel 5B1R1
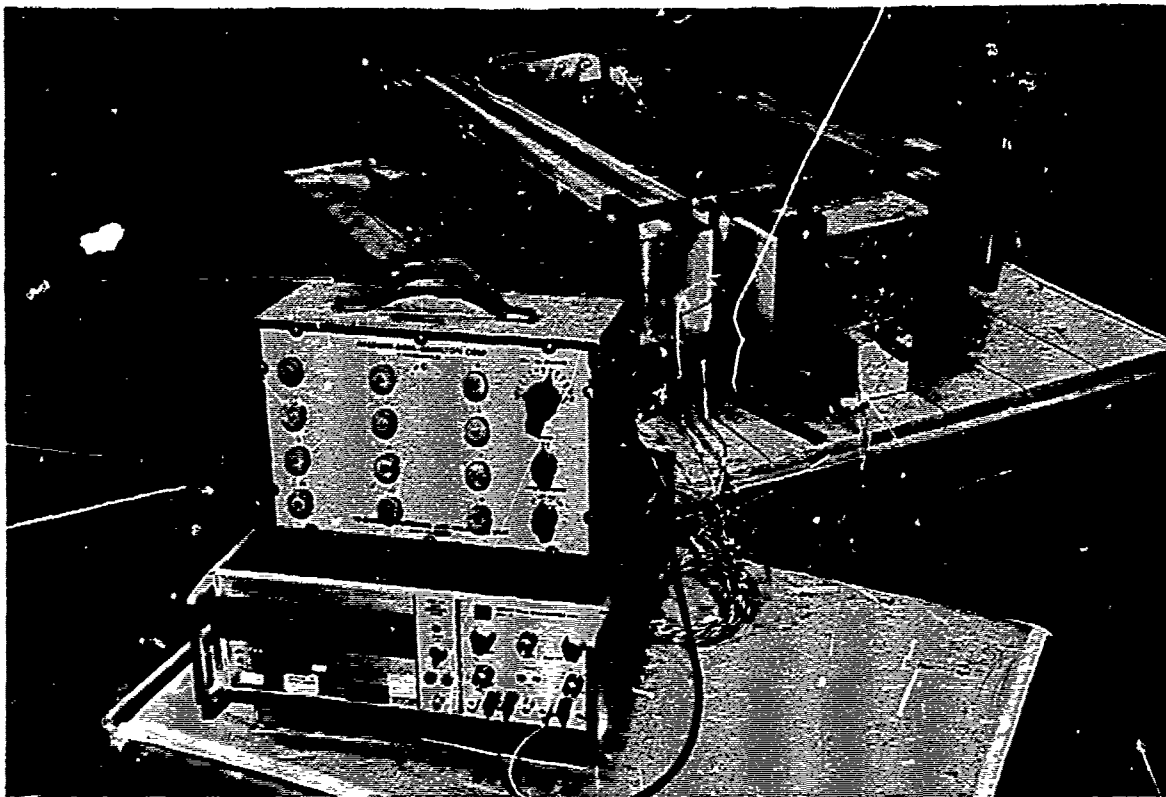
Figure 27.   Strain Gage Demonstration Setup, Panel 5B3R1
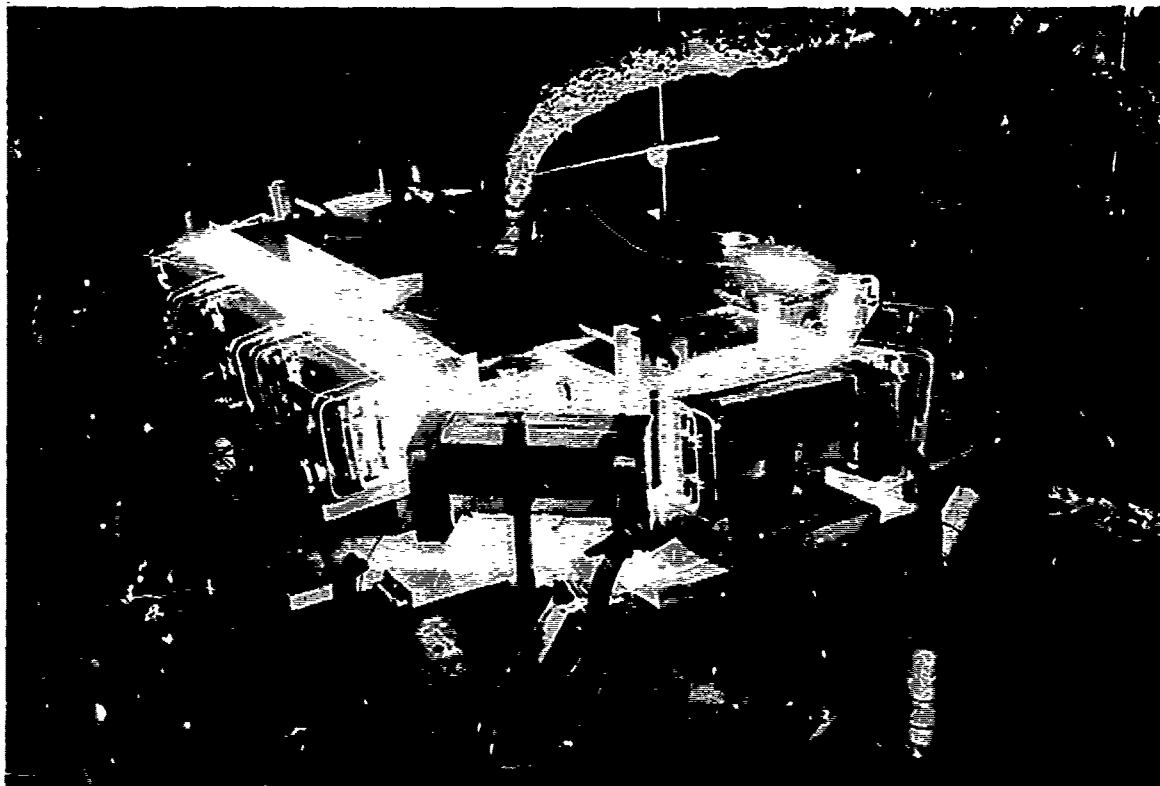
Figure 28.   Elevated Temperature Heating Setup, Panel 5B3E1

7075-T6 aluminum alloy facing instead of the $[0/\pm45/0]_S$ laminate. These panels were loaded in the pressure test fixture, with the same edge members that were used on all sandwich tests (except for the shear specimens, 3B and 4B series).

The edge-loading fixture used in these tests was a "slip-on" edge channel member designed to receive a knife-edge loading bar, as shown in figure 29. The panel edge member had been slotted to reduce its torsional stiffness, with closer slot spacing at the ends where the unstiffened panel edge member indicated the need for greater flexibility. A satisfactory pressure check on these loading fixtures is assumed to indicate that the fixtures will also be satisfactory for the compression tests (as was demonstrated for the unstiffened panels).

The test fixture used for the normal pressure (5B) series of tests with the aluminum 15 x 15 inch panel installed is shown in figure 30. The large support blocks around the edges are bigger than are required for the pressure test, but are designed to provide the stiffness needed for later thermal gradient and edgewise-compression-plus-pressure tests.

Evaluation of the validity of the test fixture was checked by comparison of the predicted and measured panel deflection under 10 psi uniform pressure load. The installation procedure prior to test was found to influence the results significantly. The best procedure found was to:

1. Torque transverse bars to remove edge looseness

2. Loosen nuts on each face to a uniform 0.015-inch gap to remove preload

3. Preload specimen to 5 psi normal pressure

4. Remove pressure, and take initial zero readings

Following this procedure, comparisons of predicted and test results for the aspect ratio 1 (15 x 15 inches) and aspect ratio 3 (13 x 39 inches) panels were as follows:

7075-T6 Honeycomb Panels		
Loading (10 psi)	Aspect Ratio 1 (15 x 15 inches)	Aspect Ratio 3 (13 x 39 inches)
Predicted deflection	0.0415	0.0685
Test run 1	0.041	0.071
Test run 2	0.041	0.069
Test run 3	0.041	0.069

+0.002
0.724 -0.000

0.375

0.250

0.047 R

90°

1.000

0.070

0.50

1.00

0.50

0.50

0.125

0.047 R

TYPICAL BOTH ENDS

1.00

1.00

1.00

2.0 (TYP)

PANEL EDGE MEMBER

0.50

1.125

0.045 R

60°
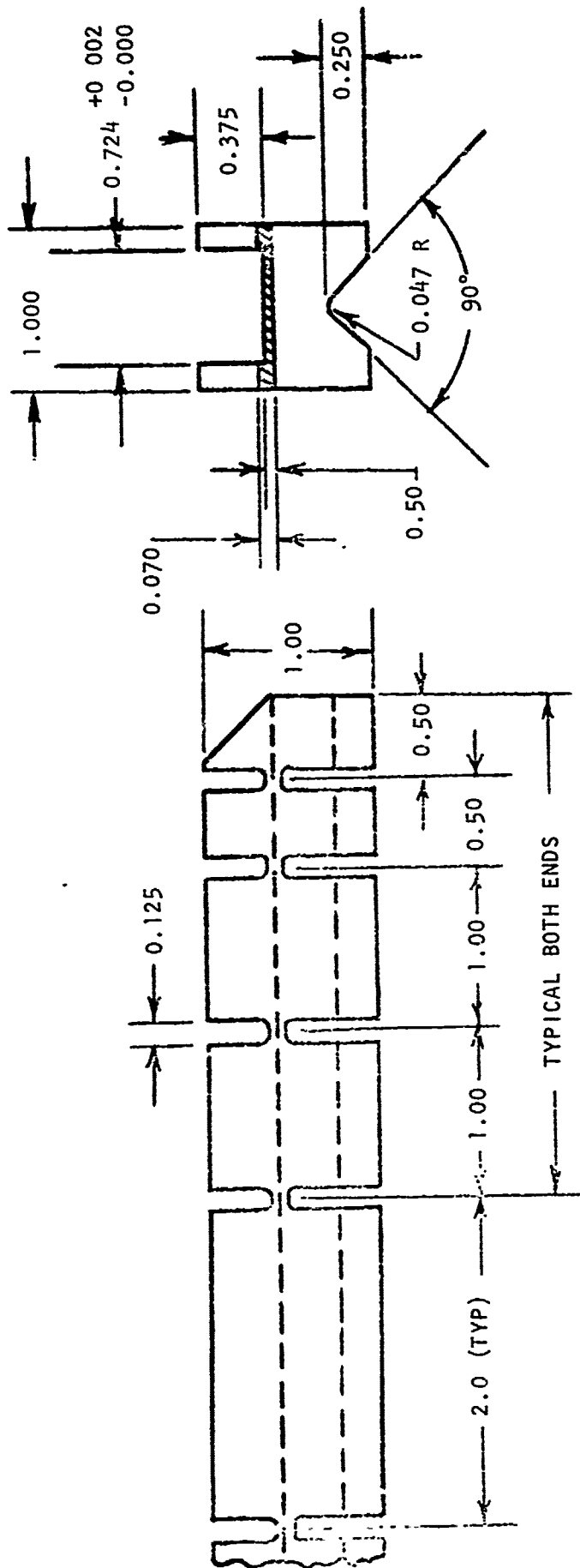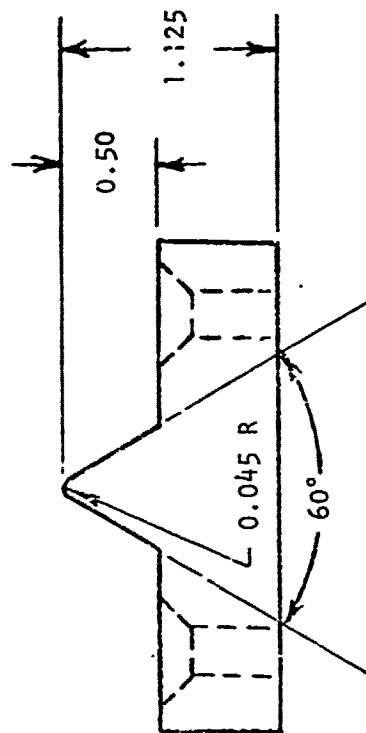
KNIFE-EDGE LOADING BAR

Figure 29. Honeycomb Panel Edgewise Compression Loading Fixture

30
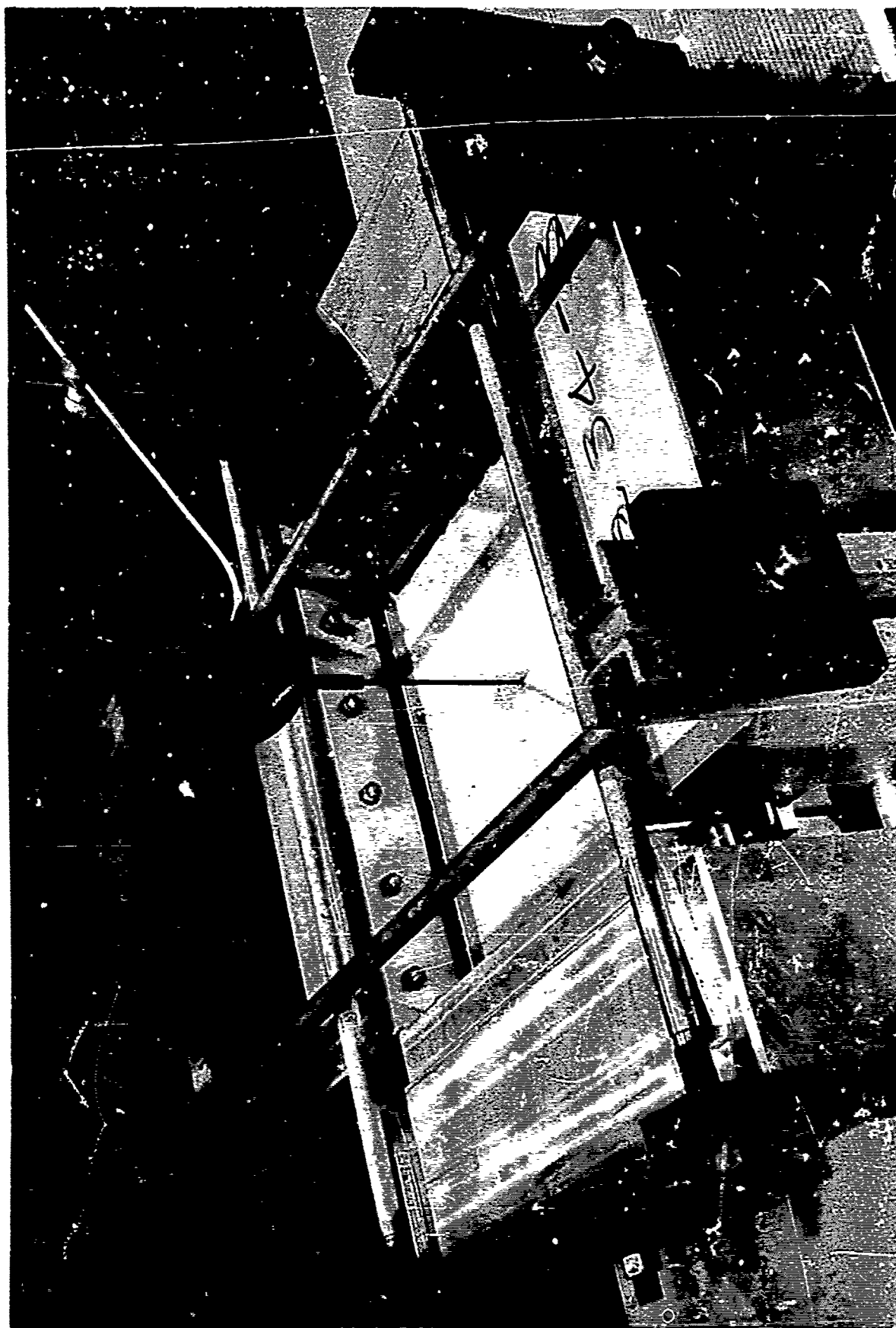
Figure 30. Aluminum Faced 15-'x 15-inch Panel Under Normal Pressure Verification Test
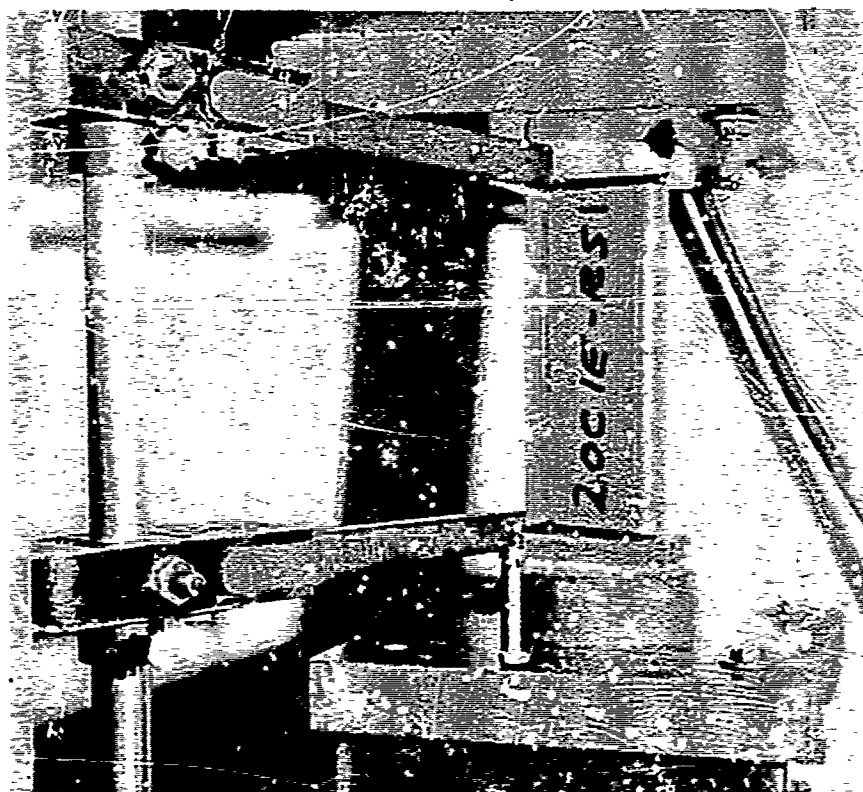
Figure 31. Test Setup for Zee Stiffener, 20D1E-RS1
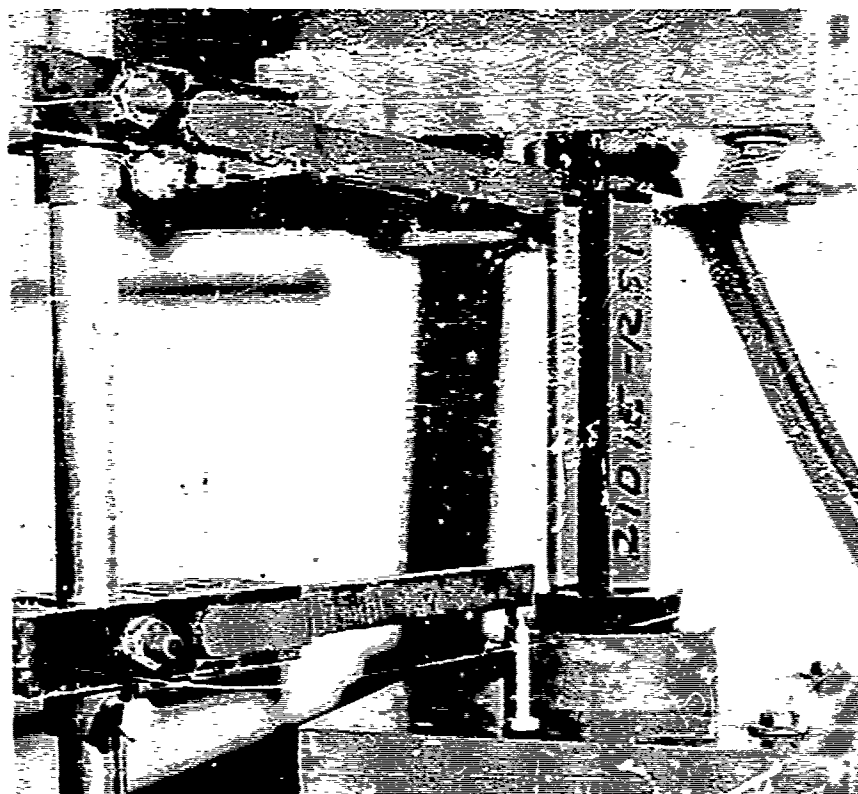
Figure 32. Test Setup for Hat Stiffener, 21D1E-RS1
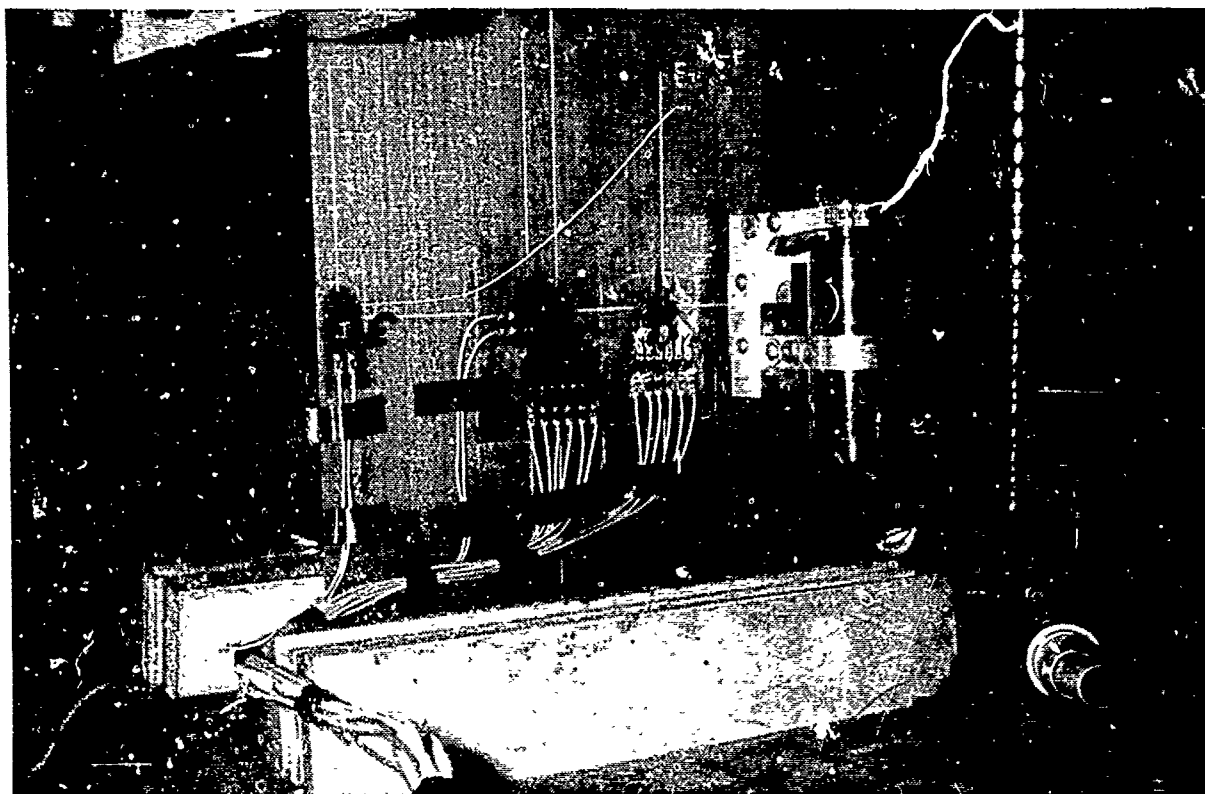
Figure 33.   Specimen 22A2R1 Tensile Test Setup
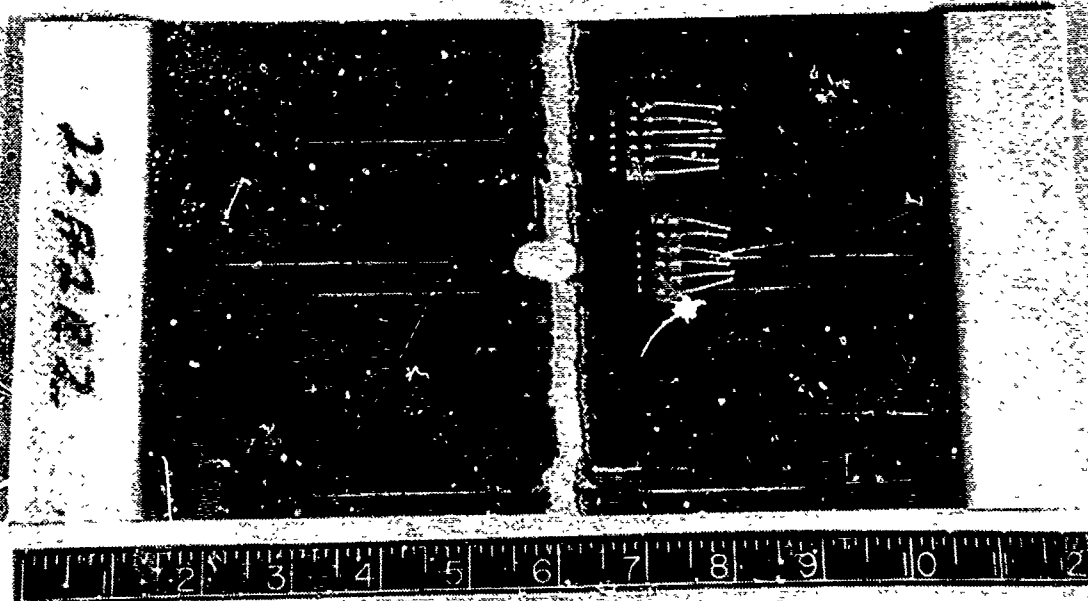
Figure 34.   Failure Under Uniaxial Tension Load, Specimen 22A2R2
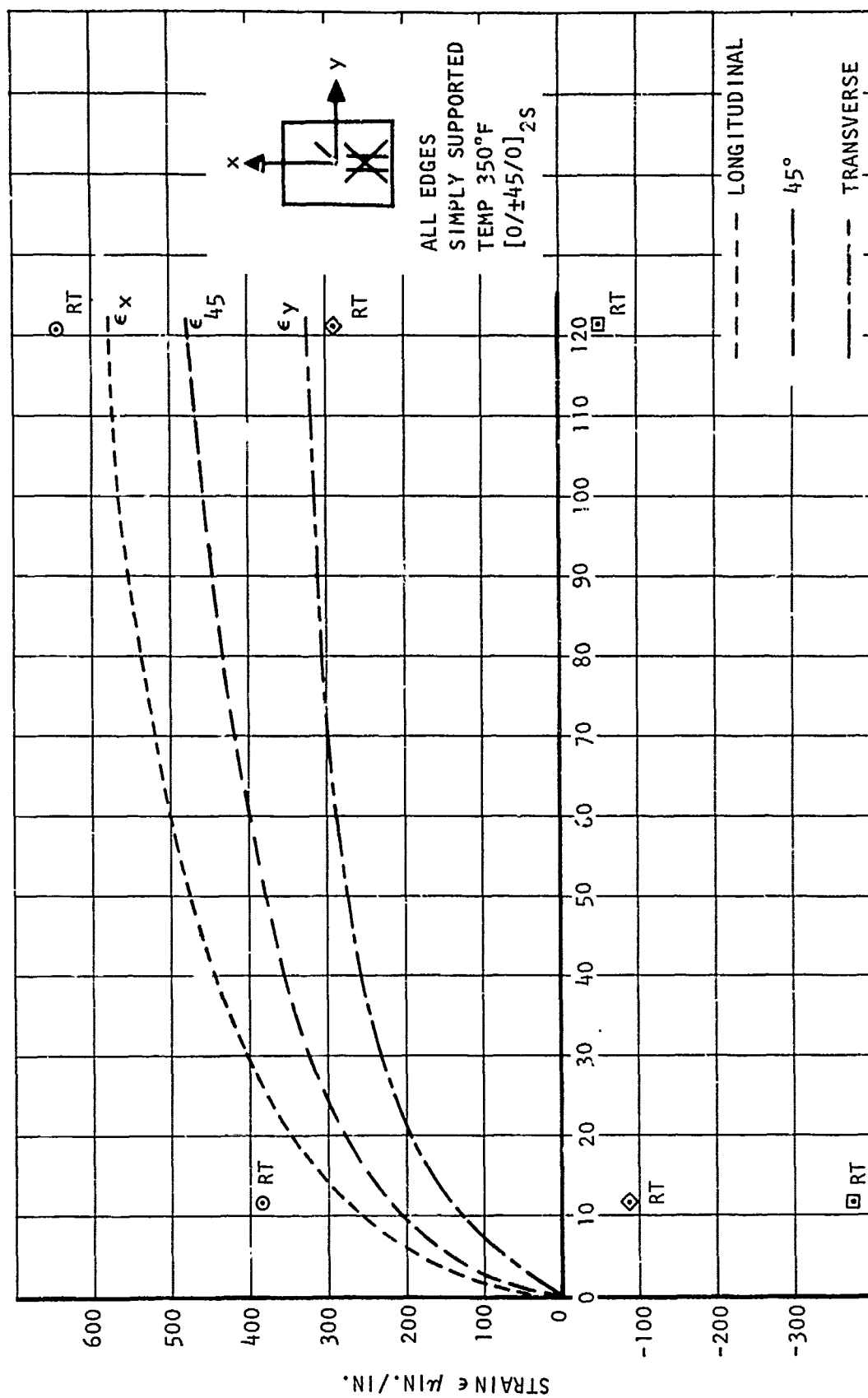
Figure 35. Strain Gage "Drift" on $[0_2/\pm45]_C$ Laminate at 350°F

Coupons from certain panels (1A through 7A) were tested for tensile failing stress and initial modulus values. Conventional (IITRI type) loading tabs were used on the initial tests. Although the resulting strength data were in good agreement with previous results, the location of the fracture for longitudinal specimens, generally at the tip of the loading tab, made results questionable. A modified loading tab, longer and with a finer taper ratio, was designed, as illustrated in figure 6. The initial test of this design resulted in a test failure away from the tab and at a slightly higher failing stress. Future loading tabs were all of the revised configuration.

The testing of the crippling elements was quite straightforward, with all loads being applied axially in compression. Loads were applied through cast resin end plugs which were ground flat and parallel. A 0.010-inch-thick aluminum sheet was placed between the test machine bearing plates and the specimen prior to loading. The machine used was the Riehle FS60W test machine. Figures 31 and 32 are typical of these tests.

Like the crippling elements, the test setup and apparatus for the cutout test panels was straightforward. Loads were applied with the edge fixture already described with the exception of the axial tension load case, which does not appear in any of the other cases. This load was applied on the Riehle FS60W test machine with the standard gripping jaws clamping a glass tape tab bonded to the specimen. Figures 33 and 34 are examples of the cutout test apparatus.

APPARENT STRAIN GAGE DRIFT AT 350°F

Strain gage readings recorded during the previously reported creep tests have indicated a tensile (elongation) panel strain. A tensile reading on one face can occur during the buckling of a panel under compression load if the local bending increment overcomes the basic axial compression. The opposite face will show an equal compressive increment to the basic axial strain. However, there were a number of cases in which both longitudinal back-to-back gages indicated a tensile type strain. To determine if this might be a characteristic of the gage or the composite material under prolonged periods of elevated temperature, a 350°F exposure test of an unloaded specimen was conducted. Panel 10A3E2 was heated to 350°F and held at this temperature (except for one return to room temperature) for a period of 120 hours. No load was applied to the panel during this time. A rather rapid initial "drift" of the gage readings was noted, followed by a reduced rate of change and almost stabilized values finally after 120 hours of exposure. The back-to-back averaged longitudinal "strains," the averaged 45-degree "strains," and the averaged transverse "strains" have been plotted versus the exposure time in figure 35. After 11 hours of exposure, the specimen was temporarily returned to room temperature and strain readings were recorded. The difference between the initial room temperature reading and the room
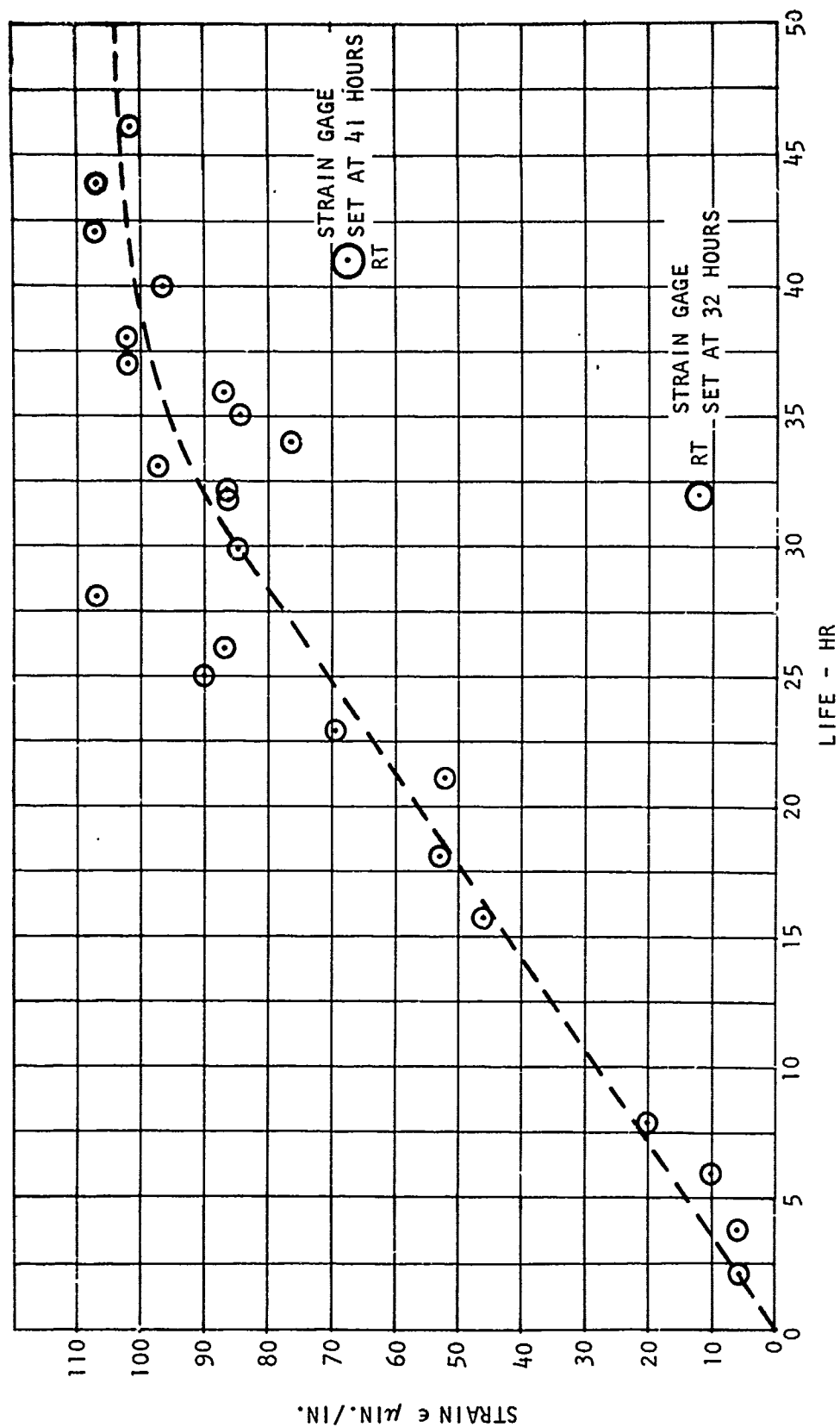
Figure 36. Strain Gage "Drift" on PH15-7Mo Steel at 350° F
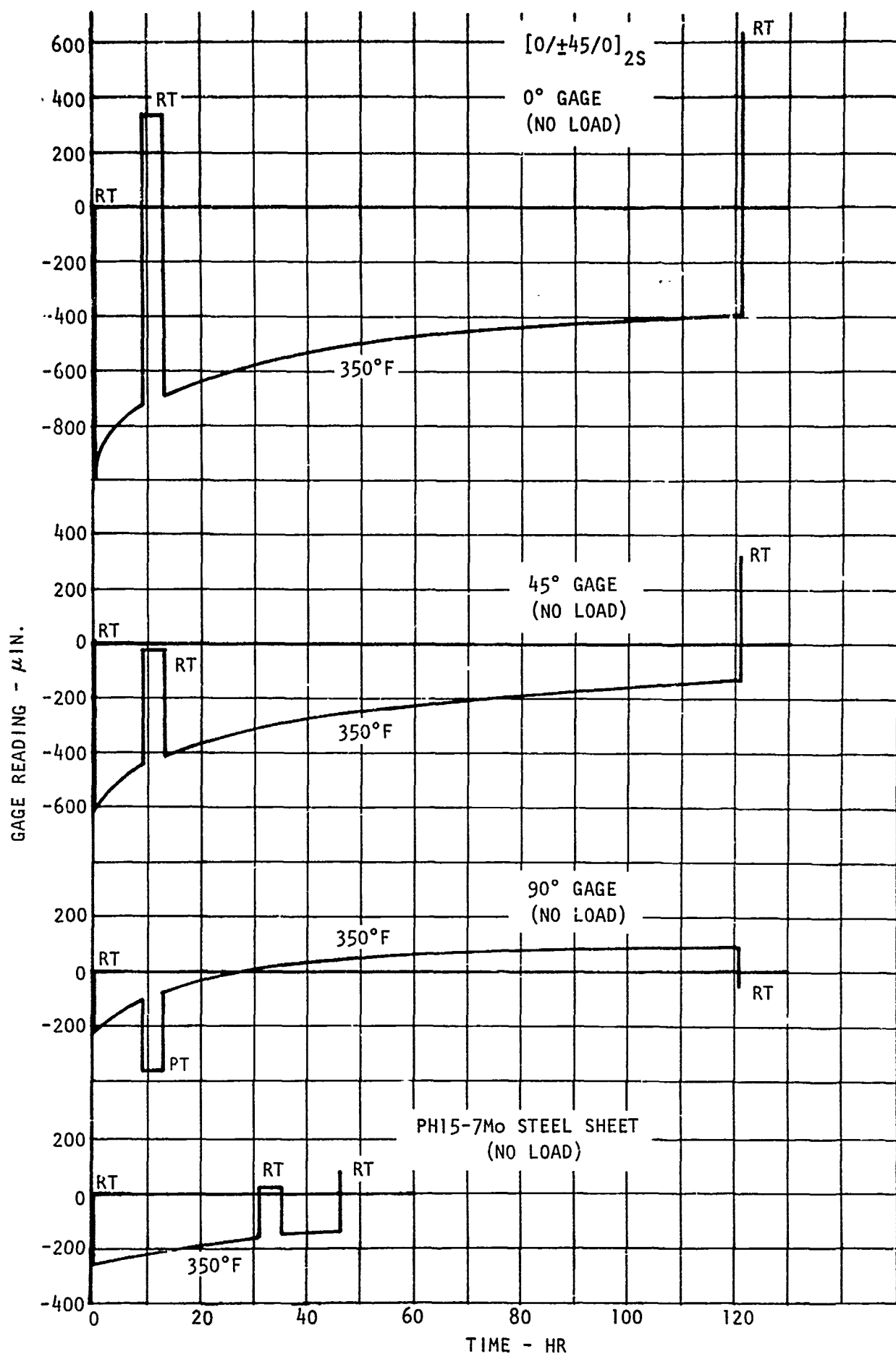
Figure 37. History of Strain Gage Drift and Apparent Thermal
Strain Readings on Composite and Steel Material

37

temperature reading after 11 hours of 350°F exposure is plotted as the larger symbols with the "RT" subscript shown in figure 35. Although all three gage orientations indicated an "apparent tensile strain drift," the room temperature "set" of only the longitudinal gage was positive, and the other two were negative, as shown. When the specimen was again heated to 350°F, the trend of original "drift" was reestablished as though there had been no room temperature interruption.

Following 120 hours of exposure, room temperature readings were again taken. The longitudinal gage "permanent set" was again in excess of the recorded "drift," whereas the 45 degree gage indicated less "set" than "drift." Again the transverse gage indicated a positive "drift" with a negative "set," but the "set" was much smaller than that recorded after 11 hours exposure.

To explore this phenomenon further, a set of similar strain gages was placed back-to-back on a piece of PH15-7Mo stainless steel sheet and exposed to 350°F for 46 hours, with a temporary return to room temperature after 32 hours. The apparent strain drift, based on the average of the gage readings during the 350°F exposure, is shown by the plot in figure 36. The result was a constant "drift" with time for the first 30 hours, and an apparent stabilized condition after 46 hours. Room temperature readings after exposures of 32 and 46 hours were compared to the initial room temperature reading, and the difference (gage "set") increments are also plotted in figure 36, indicated by the "RT" subscript after the symbol. Gage drift and set readings on the steel material are of the same type as were found on the composite, but of a lower magnitude. This indicates that some, but perhaps not all, of this effect can be attributed to the strain gage.

Values of the "apparent strain," or the incremental gage readings between room temperature and elevated temperature were also recorded. Initial readings on the boron/epoxy laminate are typical of readings found on other specimens. There is some variability of longitudinal readings with exposure, much more variation of the 45° reading with exposure, and an unexpected reversal of sign of the transverse readings after 11 hours exposure. Apparent strains of the similar unidirectional gage on PH15-7Mo steel sheet are also tabulated.

A complete plot showing both the apparent strain readings and the gage "drift" readings versus time is given in figure 37. This summarizes the "drift," "set," and apparent thermal strain readings previously discussed.

Reasons for the strain gage elevated temperature "drift," the unexpected room temperature "set" readings, and variations in the apparent strain with elevated temperature exposure are under investigation. Until more information is available on this subject, the "drift" curves of figure 37 will be used to correct strain gage readings of $[0/\pm45/0]_{2S}$ boron/epoxy laminates subject to extended periods of 350°F temperature exposure.

SECTION IV

ANALYSIS OF TESTS

INTRODUCTION

Thirty-two series of tests were conducted to verify the prediction techniques presented in Volume III. Recommendations are made for empirical modification of these techniques where necessary.

Three types of construction were considered:

1. Unstiffened skin, both with and without cutouts (18 series including stiffeners)

2. Honeycomb sandwich (10 series)

3. Stiffened skin, with zee and hat stiffeners (four series)

Ten types of loadings (elements) were considered:

1. Uniaxial compression

2. Biaxial compression

3. Inplane shear

4. Combined uniaxial compression and inplane shear

5. Uniform pressure

6. Uniform thermal gradient $[\Delta T = T(t_f) - T(t_o)]$

7. Thermal gradient and pressure

8. Uniaxial compression and pressure

9. Creep buckling

10. Uniaxial tension

Tests were conducted at both room temperature and 350°F. Both flat panels and crippling elements were tested. Figure 13 contains a summary of the specimen coding describing the geometry, loading, test temperature, etc. Tables I, II, and III contain the material properties used

39

throughout the evaluation of data. The test evaluations which follow have been grouped into categories, each of which contain a series of tests related to each other in some logical manner (i.e., having the same objectives, or where one series forms a basis for the prediction of a succeeding series). The appendix contains the specimen drawings.

MATERIAL PROPERTIES

Tables I, II, and III present the material property data used throughout this evaluation.

TABLE I. LAMINATE EXTENSIONAL PROPERTIES

Laminate Orientation	Temp (°F)	E_L (Msi)	E_T (Msi)	ν_{LT} (in./in.)	ν_{TL} (in./in.)	G_{LT} (Msi)	α_L (in./in./°F)	α_T (in./in./°F)
$[0/\pm45/0]_S$	RT	16.67	5.06	0.70	0.21	4.30	2.50	6.10
	100	16.59	4.95	0.71	0.21	---	2.55	6.28
	150	16.43	4.73	0.74	0.21	---	2.69	6.62
	200	16.27	4.51	0.76	0.21	---	2.85	6.94
	250	16.10	4.30	0.79	0.21	---	3.02	7.24
	300	15.94	4.08	0.81	0.21	---	3.18	7.48
	350	15.78	3.86	0.84	0.21	3.98	3.38	·7.68
$[0]_C$	RT	29.9	2.71	0.21	0.019	0.70	---	---
	100	29.9	2.57	0.21	0.018	---	---	---
	150	29.9	2.28	0.21	0.016	---	---	---
	200	29.9	1.99	0.21	0.014	---	---	---
	250	29.9	1.71	0.21	0.012	---	---	---
	300	29.9	1.41	0.21	0.010	---	---	---
	350	29.9	1.13	0.21	0.008	0.20	---	---
$[\pm45]_C$	RT	2.59	2.59	0.847	0.847	7.90	---	---
	350	1.16	1.16	0.927	0.927	7.05	---	---

40

TABLE II. LAMINATE FLEXURAL PROPERTIES

Laminate Orientation	Temp (°F)	D_{11} (in.-1b)	D_{12} (in.-1b)	D_{22} (in.-1b)	D_{66} (in.-1b)	D_{16}, D_{26} (in.-1b)
$[0/\pm45/0]_{2S}$	RT	963.9	192.1	278.1	198.3	31.0
	200	950.1	185.0	242.4	189.3	31.6
	350	939.7	179.6	215.7	182.5	32.0
$[0/\pm45/0]_{S}$	RT	129.3	20.9	32.0	21.7	-7.7
	350	126.6	19.3	24.0	19.7	-8.1
$[0]_{7T}$	RT	120.5	2.1	12.8	5.6	---
RSC	350	120.3	1.1	6.5	2.4	---

TABLE III. HONEYCOMB CORE PROPERTIES (Al 5056)

s (inches/16)	t_c (mils)	ρ_c' (1b/ft^3)	Temp (°F)	G_{cx}' (Ksi)	G_{cy}' (Ksi)
3	1.0	3.1	RT	45	20
			350	28	13
2	1.5	6.1	RT	90	45
			350	83	41
2	2.0	8.1	RT	143	51
			100	140	50
			150	134	48
			200	125	45
			250	116	41
			300	104	37
			350	82	32
			400	72	26
			425	57	20

Table IV summarizes tension coupon data corresponding to certain specimen sets.

TABLE IV. TENSION COUPON DATA - $[0/\pm45/0]_{2S}$

Specimen	Temp (°F)	F_x (Ksi)	E_x (Msi)	F_y (Ksi)	E_y (Msi)
1ANR	RT	99.32	16.00	15.90	4.66
1ANE	350	91.11	13.78	9.01	3.04
2ANR	RT	102.17	16.09	16.36	4.55
2ANE	350	89.91	13.44	8.82	3.06
5ANR	RT	98.42	16.12	17.13	4.89
5ANE	350	79.68	13.32	9.41	2.70
6ANE	350	83.66	13.68	9.31	3.34
9ANE	350	92.59	13.28	8.85	2.74
10ANE	350	94.59	10.78	8.91	3.38
23ANR	RT	103.98	15.92	16.75	4.18
23ANE	350	91.76	11.56	9.03	2.88

UNSTIFFENED SKIN

GENERAL INSTABILITY TESTS

Specimen series 1A, 2A, 3A, and 4A are grouped in this category. They consist of rectangular, simply supported panels loaded in uniaxial compression, biaxial compression, inplane shear, and combined uniaxial compression and inplane shear, respectively. The purposes of these tests were to (1) verify the buckling loads and (2) determine the ultimate load-carrying capacity of the panels.

The equilibrium equation for an anisotropic material, in terms of displacements, is given in Volume III as

$$D_{11} \, w,_{xxxx} + 4 \, D_{16} \, w,_{xyyy} + 2 \, (D_{12} + 2D_{66}) \, w,_{xxyy} + 4 \, D_{26} \, w,_{xyyy}$$

$$+ D_{22} \, w,_{yyyy} = q - N_x w,_{xx} - 2N_{xy} w,_{xy} - N_y w,_{yy} \tag{1}$$

where N_x, N_y, and N_{xy} are assumed to be constant.

Conventional variational techniques can be used to predict the general instability strength from this equation. The technique shown in reference 1 was used to evaluate the panels in this category. This was done by the computer program RA5.

For the case where D_{16}/D_{11} and D_{26}/D_{11} are small ($\ll 1$), the terms involving them can be neglected

$$D_{11} \, w,_{xxxx} + 2 \, (D_{12} + 2D_{66}) \, w,_{xxyy} + D_{22} \, w,_{yyyy}$$

$$= q - N_x w,_{xx} - 2N_{xy} w,_{xy} - N_y w,_{yy} \tag{2}$$

and the equilibrium equation for an orthotropic material results. The computer programs for honeycomb sandwich in the appendix of Volume III (AC5 and AC11) were used to predict the general instability strengths for this case. This was done by the artifice of prescribing the core shear modulus to approach infinity, which sets $V = 0$. Computer program AC2 was used to obtain the flexural rigidities D_{ij}.

Results for this configuration ($0.0322 < D_{16}/D_{11} = D_{26}/D_{11} < 0.0340$) indicate that there is very little difference between the two prediction

techniques. The results for the orthotropic solution may be up to 2 percent unconservative with respect to the anisotropic solution.

Table V presents the pertinent geometric data, while the material data are given in tables I through III. Table VI presents the results of the general instability analysis. Table XIX presents some failure analysis data for the uniaxial compression panels. It is presented there since it is considered as the "no hole" endpoint for the cutout failure analysis.

Two techniques are also available for determining the actual buckling load:

1. The top-of-the-knee method, which uses the results of back-to-back strain gages located at the center of the panel.

2. The Southwell method, which uses the results of the transverse deflection at the same point.

Figure 38 shows test versus predicted values for the uniaxial and biaxial compression loading tests.

Series 1A - Uniaxial Compression

The uniaxial compression tests showed reasonable correlation with the general instability analysis, although the high aspect ratio tests (a/b = 3) were about 30-percent low. The failure loads always exceeded the general instability predictions. Specimen 1A3R1 failed prematurely at the support. Specimen 1A2R1 was then made from the undamaged portion of 1A3R1 and tested. Figures 39 through 45 show the test results and setup for the uniaxial compression tests.

Series 2A - Biaxial Compression

The biaxial compression tests always exceeded predictions for general instability. This is probably due to the clamping action induced by the loading jig.

Series 3A - Inplane Shear

The inplane shear tests failed low. The failures in every case occurred at the loading angles, either as tension in the corner or as failure of the adhesive between the jig and the specimen. It is probable that an improved testing technique would produce better results. Figure 46 shows the failed specimens.

TABLE V.   GENERAL INSTABILITY PANEL GEOMETRY - $[0/\pm45/0]_{2S}$

Spec-imen	a (in.)	b (in.)	t (in.)	Test Temp (°F)	Test Type
1A1R1	6.0	6.0	0.0832	RT	Uniaxial compression
1E1	6.0	6.0	0.0832	350	
2R1*	7.6	4.0	0.0832	RT	
3R1	12.0	4.0	0.0832	RT	
3E1	12.0	4.0	0.0832	350	
2A1R1	6.0	6.0	0.0832	RT	Biaxial compression
1E1	6.0	6.0	0.0832	350	
3R1	12.0	4.0	0.0832	RT	
3E1	12.0	4.0	0.0832	350	
3A1R1	6.0	6.0	0.0832	RT	Inplane shear
1E1	6.0	6.0	0.0832	350	
3R1	12.0	4.0	0.0832	RT	
3E1	12.0	4.0	0.0832	350	
4A1R1	6.0	6.0	0.0832	RT	Compression and shear
1E1	6.0	6.0	0.0832	350	
3R1	12.0	4.0	0.0832	RT	

*Made from panel 1A3R1

TABLE VI. GENERAL INSTABILITY PANEL TEST EVALUATION

Spec- imen	Aspect Ratio a/b	Test Temp (°F)	Loading			General Instability (N_x) (lb/in.)				Ultimate Failure (lb/in.)
						Test		Predicted		
			Basic	N_y/N_x	N_{xy}/N_x	Top-of- Knee	Southwell	Anisotropic	Orthotropic	
1A1R1	1.0	RT	N_x	0	0	585	769	656	663	1,303
1E1	1.0	350	N_x	0	0	550	609	610	615	995
2R1*	1.9	RT	N_x	0	0	750	--	--	1,430	1,620
3R1*	3.0	RT	N_x	0	0	900	--	1,360	1,376	--
3E1	3.0	350	N_x	0	0	890	--	1,220	1,229	1,478
2A1R1	1.0	RT	N_x	0.5	0	450	610	436	442	1,060
1E1	1.0	350	N_x	0.5	0	430	588	--	410	900
3R1	3.0	RT	N_x	0.5	0	800	909	426	425	1,440
3E1	3.0	350	N_x	0.5	0	450	877	--	352	1,175
3A1R1	1.0	RT	N_{xy}	0	0	--	--	--	1,543	1,167
1E1	1.0	350	N_{xy}	0	0	--	--	--	1,425	667
3R1	3.0	RT	N_{xy}	0	0	--	--	--	1,625	1,000
3E1	3.0	350	N_{xy}	0	0	--	--	--	1,376	585
4A1R1	1.0	RT	N_x	0	0.36	--	--	390	--	833
1E1	1.0	350	N_x	0	1.0	--	--	553	--	500
3R1	3.0	RT	N_x	0	1.0	--	--	971	--	1,218

*Specimen 1A3R1 failed prematurely because of failure of support. Specimen 1A2R1 was then fabricated from it.
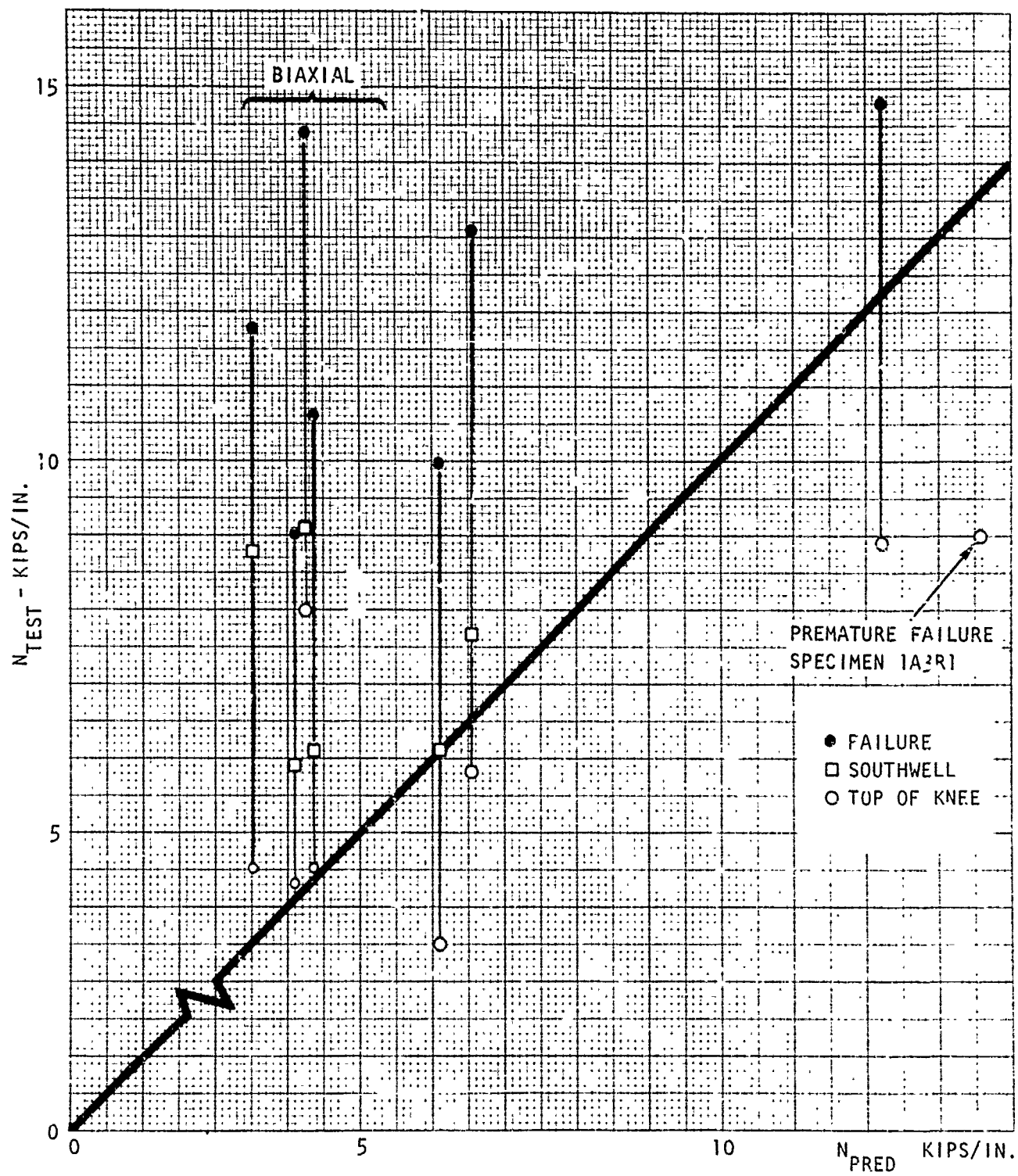
Figure 38.   Test Versus Predictions, 1A and 2A Panels
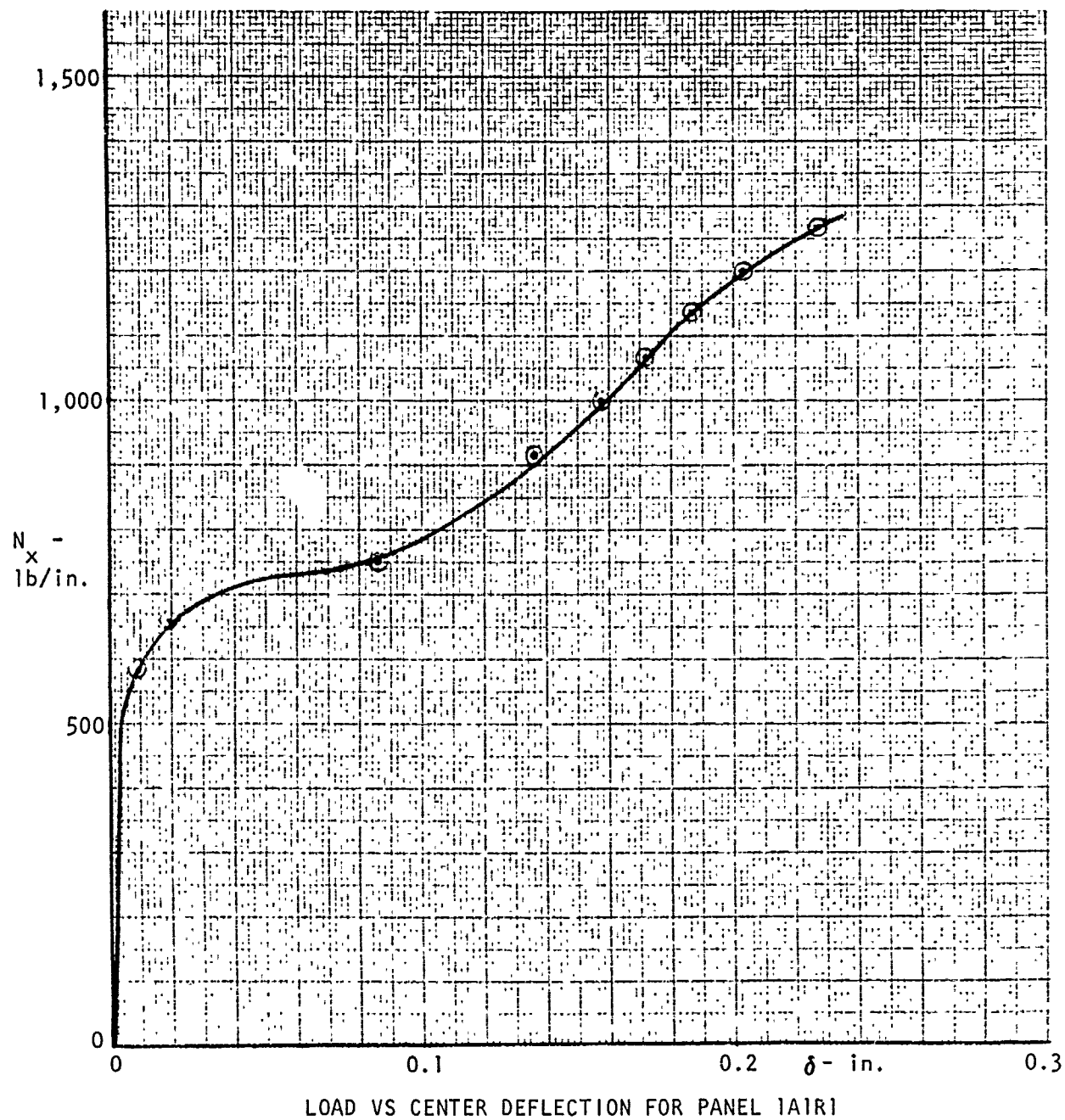
Figure 39. Load Deflection Curve for Panel 1A1R1

$$\frac{\Delta\delta}{\Delta(\delta/N_x)} = 769.23 \ \text{lb/in.} = N_{x_{cr}}$$

$\delta - $ in.

$\delta/N_x - $
$10^{-6} \ \text{in.}^2/\text{lb}$
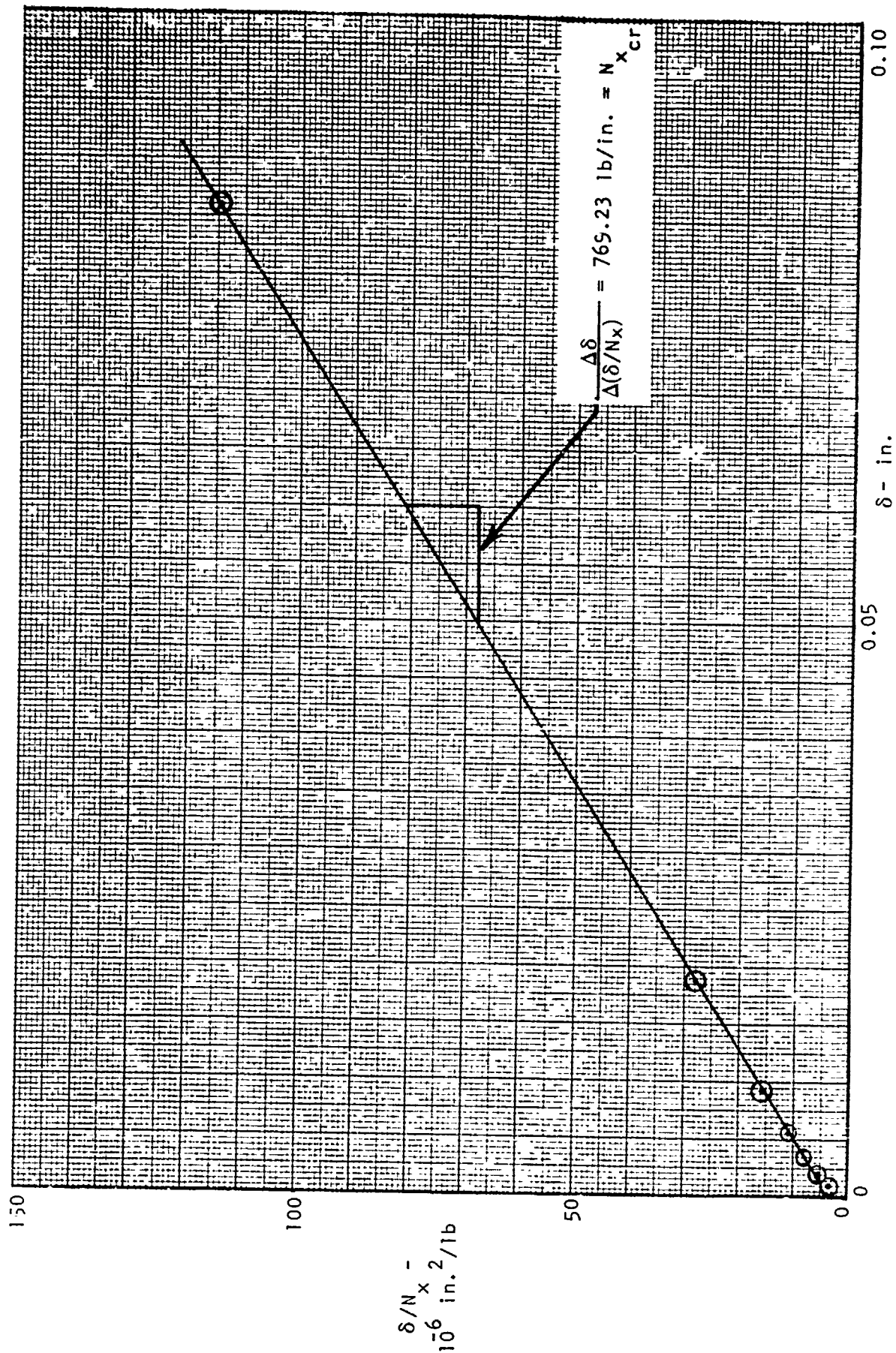
Figure 40. Southwell Plot for Panel 1A1R1

49
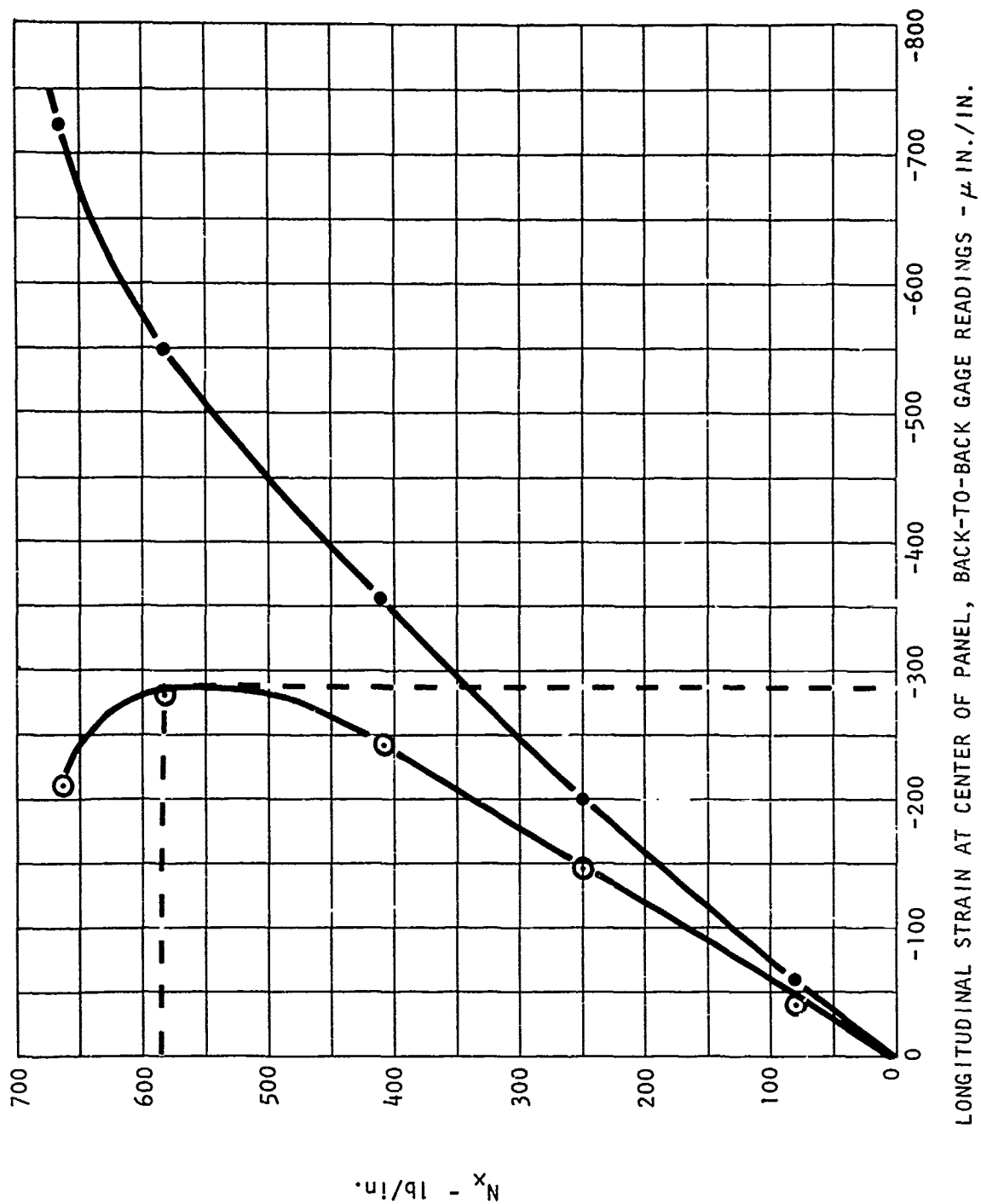
Figure 41. Top-of-Knee Plot for Panel 1A1R1

LONGITUDINAL STRAIN AT CENTER OF PANEL, BACK-TO-BACK GAGE READINGS - μ IN./IN.

N_x - lb/in.
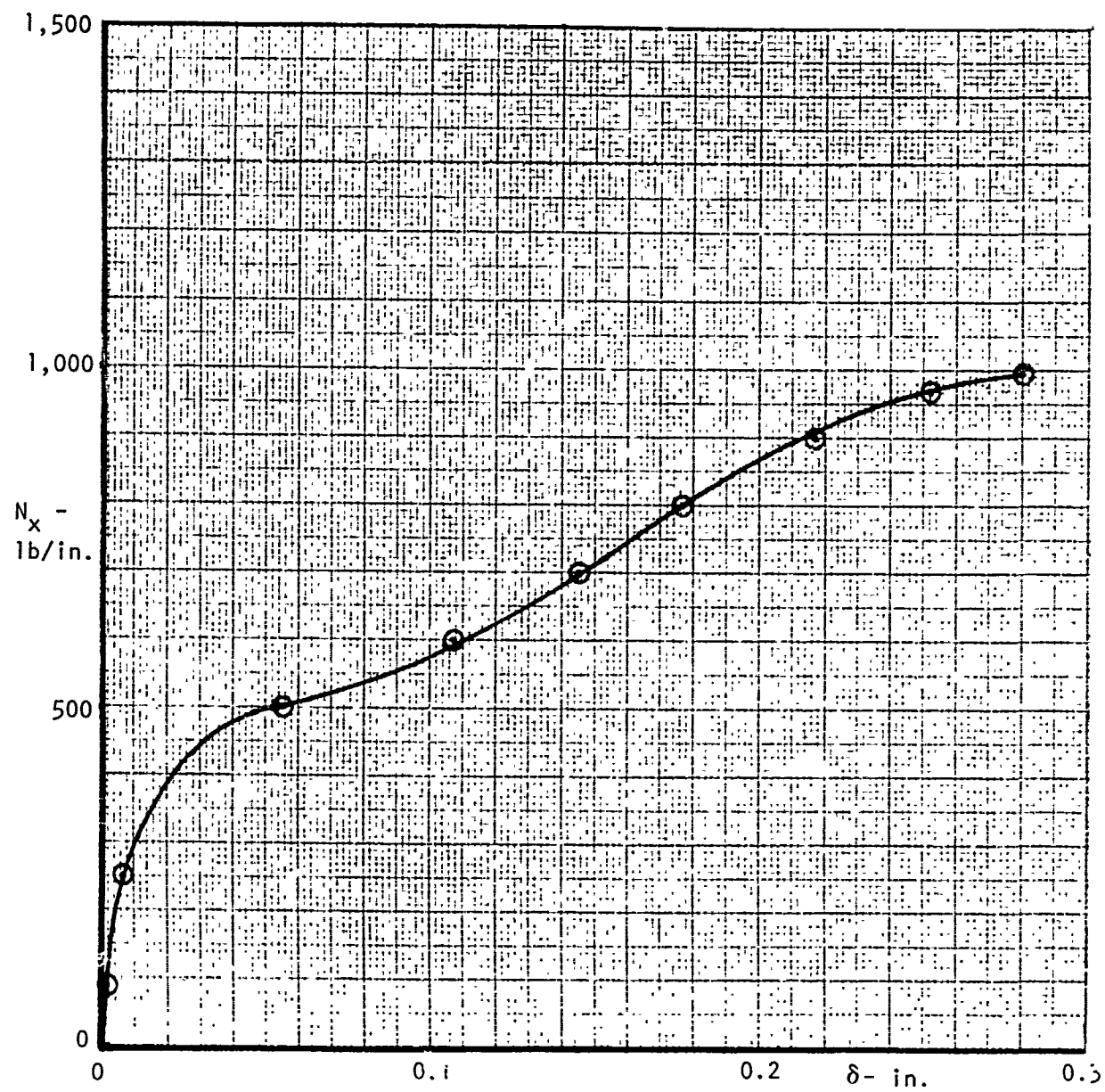
Figure 42.   Load Deflection Curve for Panel 1A1E1

$$\frac{\Delta \delta}{\Delta (\delta / N_x)} = 609.76 \text{ lb/in.}$$
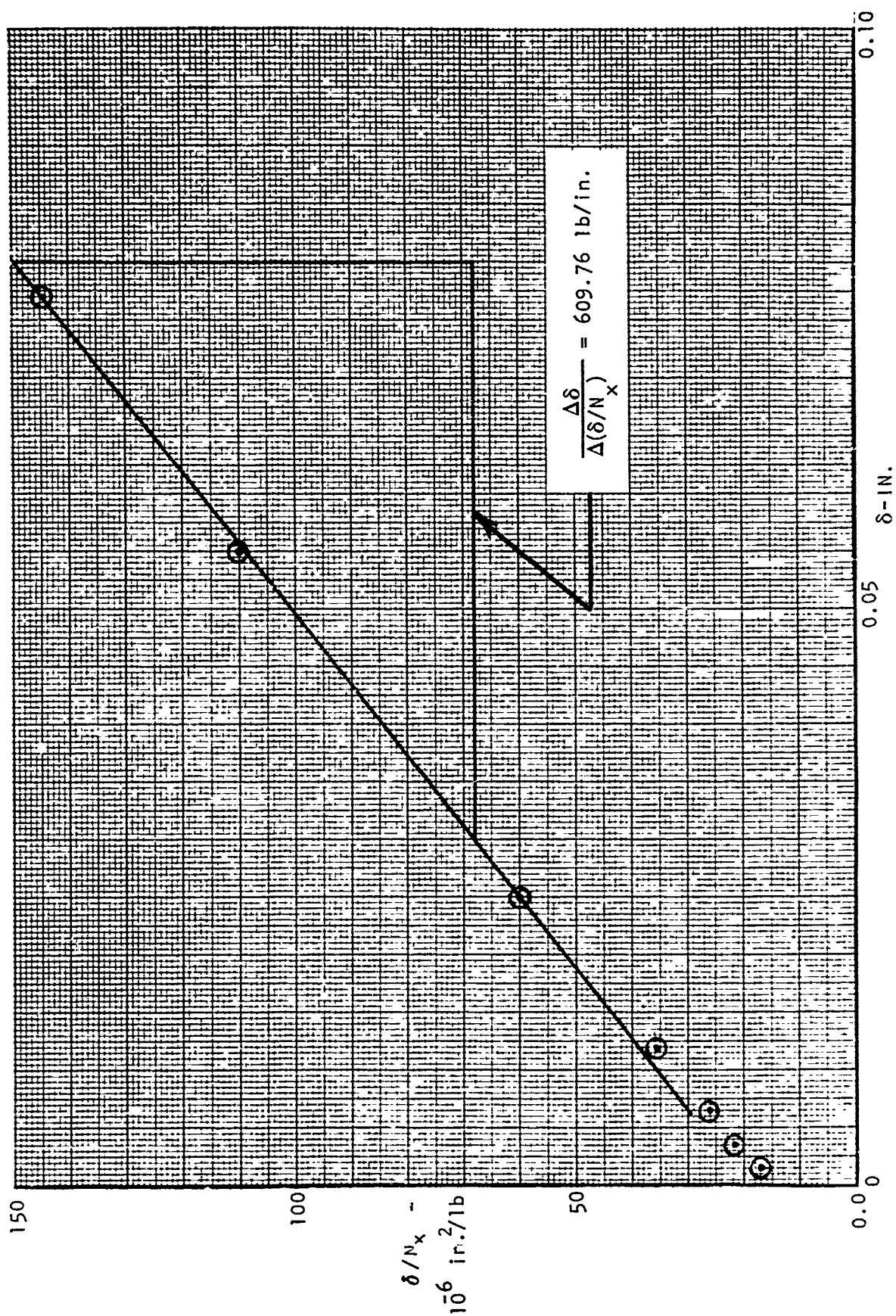
Figure 43. Southwell Plot for Panel 1A1E1

52
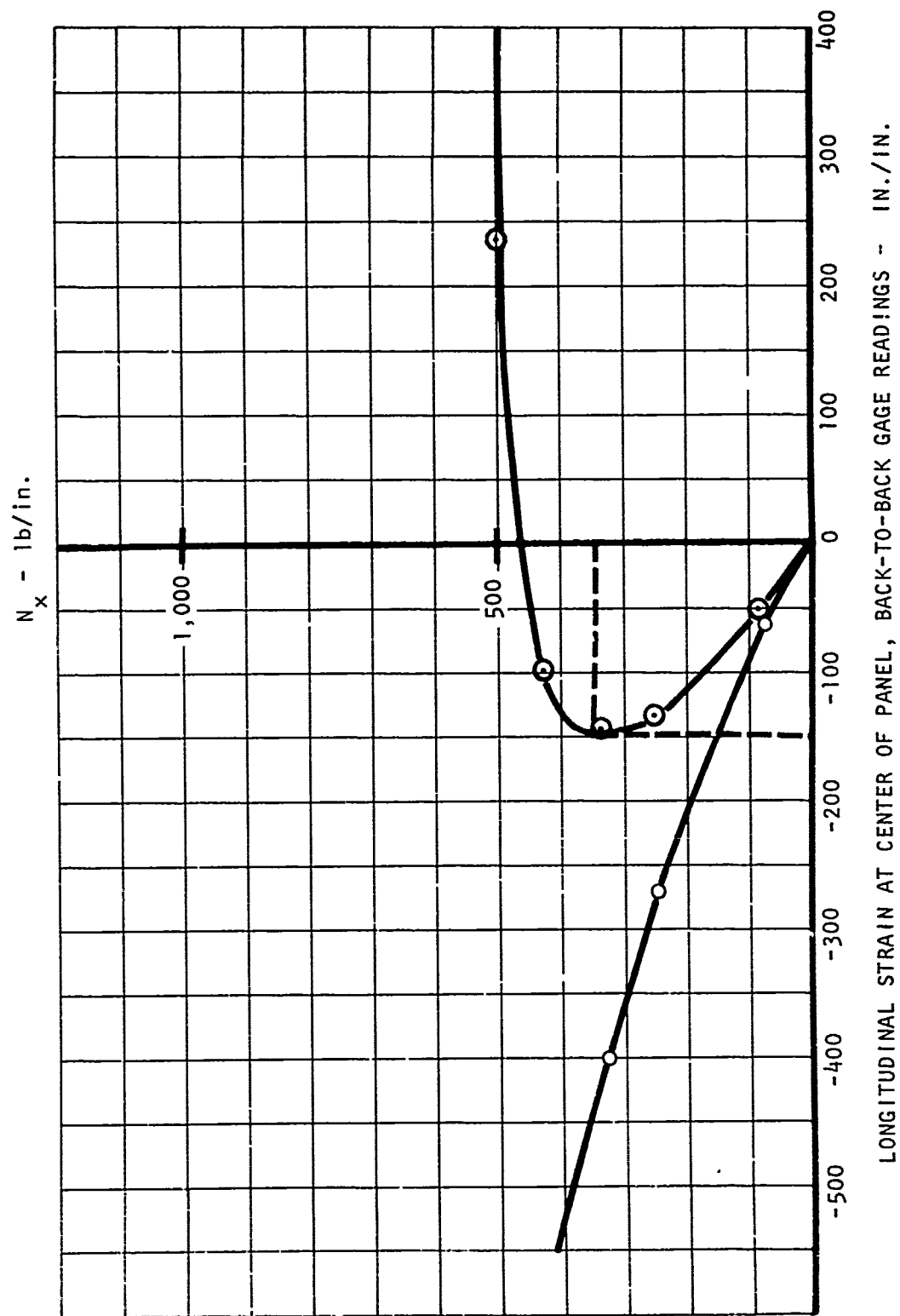
Figure 44. Top-of-Knee Plot for Panel 1A1E1

Figure 45. Specimen 1A1R1 After Testing

54

SPECIMEN 3A1R1

ULTIMATE SHEAR STRESS = 14,032 PSI
a/b = 1; a = 6 IN.
ROOM TEMPERATURE TEST

SPECIMEN 3A2E1

ULTIMATE SHEAR STRESS = 8,013 PSI
a/b = 1; a = 6 IN.

SPECIMEN 3A3R2

ULTIMATE SHEAR STRESS = 12,019 PSI
a/b = 3; a = 12 IN.
ROOM TEMPERATURE

SPECIMEN 3A3E2

ULTIMATE SHEAR STRESS = 7,011 PSI
a/b = 3; a = 12 IN.
350°F
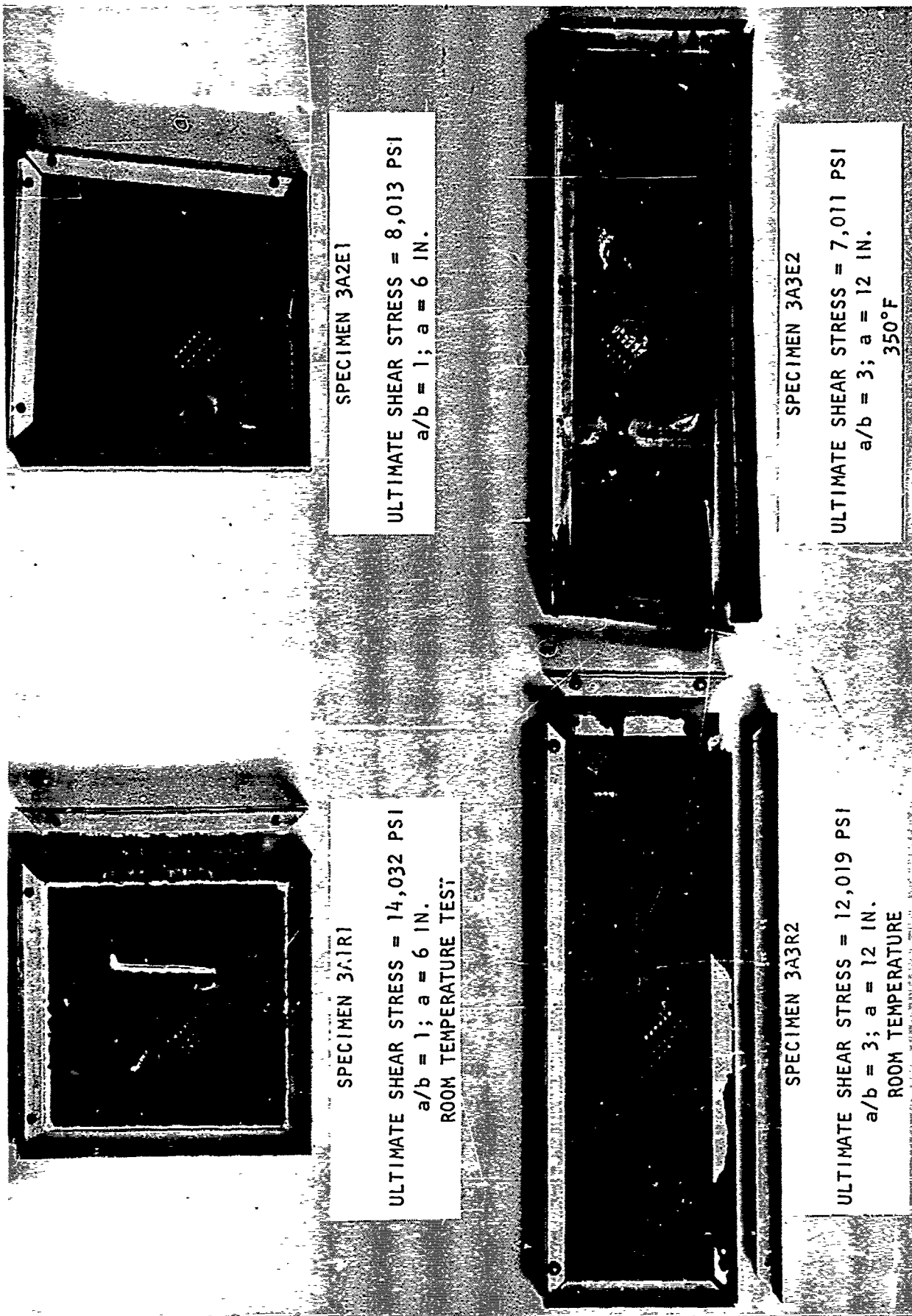
Figure 46. Specimen Failures, 3A Series

Series 4A - Combined Loading

The combined inplane shear and uniaxial compression test failure loads correlated reasonably well with the general instability predictions. Figures 47 and 48 show the failed specimens.

Verification of Plate Dynamic Behavior

The $[0/\pm45/0]_{2S}$ flat plates were tested in order to assess the validity of analytical prediction techniques with regard to the dynamic behavior of boron/epoxy plates. The plates have aspect ratios of $a/b = 1.0$ and $a/b = 3.0$ and were considered to be simply supported along all edges. The plate geometries are shown in figure 49. In both cases, the 0-degree plies were oriented along the longitudinal axis of the plates.

The plates were secured to the vibration machine by means of 2-inch-square aluminum tubing. A 0.92-inch-wide groove was machined into one side of the tubing and the tubing was cut into lengths sufficient to form a frame around the edge of each panel. Aluminum straps (1 inch by 1 inch) were used to hold this frame to the shaker table as well as to secure the panel. Then, by sharpening the edge of the grooves of the channels and by correct positioning, the plates were gripped only over a width of 1/32 inch along their four extreme edges. The test setup is shown in figure 50.

In the test phase of this verification effort, the plates were subjected to a broad frequency spectrum while searching for their first harmonic mode of vibration.

The first mode of vibration of the 6 x 6 inch plate was at 592 cycles/sec, and for the 4 x 12 inch plate was at 578 cycles/sec. These resonant frequencies were determined by monitoring through a CEC type 1-27 carrier amplifier with a CEC type 5-124 oscillograph and Ballentine vacuum tube voltmeter.

In the prediction evaluation phase of this effort, two methods were used to predict the first mode natural frequencies of the two plates. One method was to use the RA5 computer program developed by General Dynamics, Fort Worth (reference 1), and the other method was to assume the plates to be specially orthotropic (i.e., $D_{16} = D_{26} = 0$), and then to utilize a closed form of classical solution.

To find the flexural constants, computer program AC2 from Volume III of this report was used. It required as input the single-ply properties, which for the two plates are

SPECIMEN 4A1R1
FAILURE UNDER
COMBINED SHEAR
AND COMPRESSION
LOADING
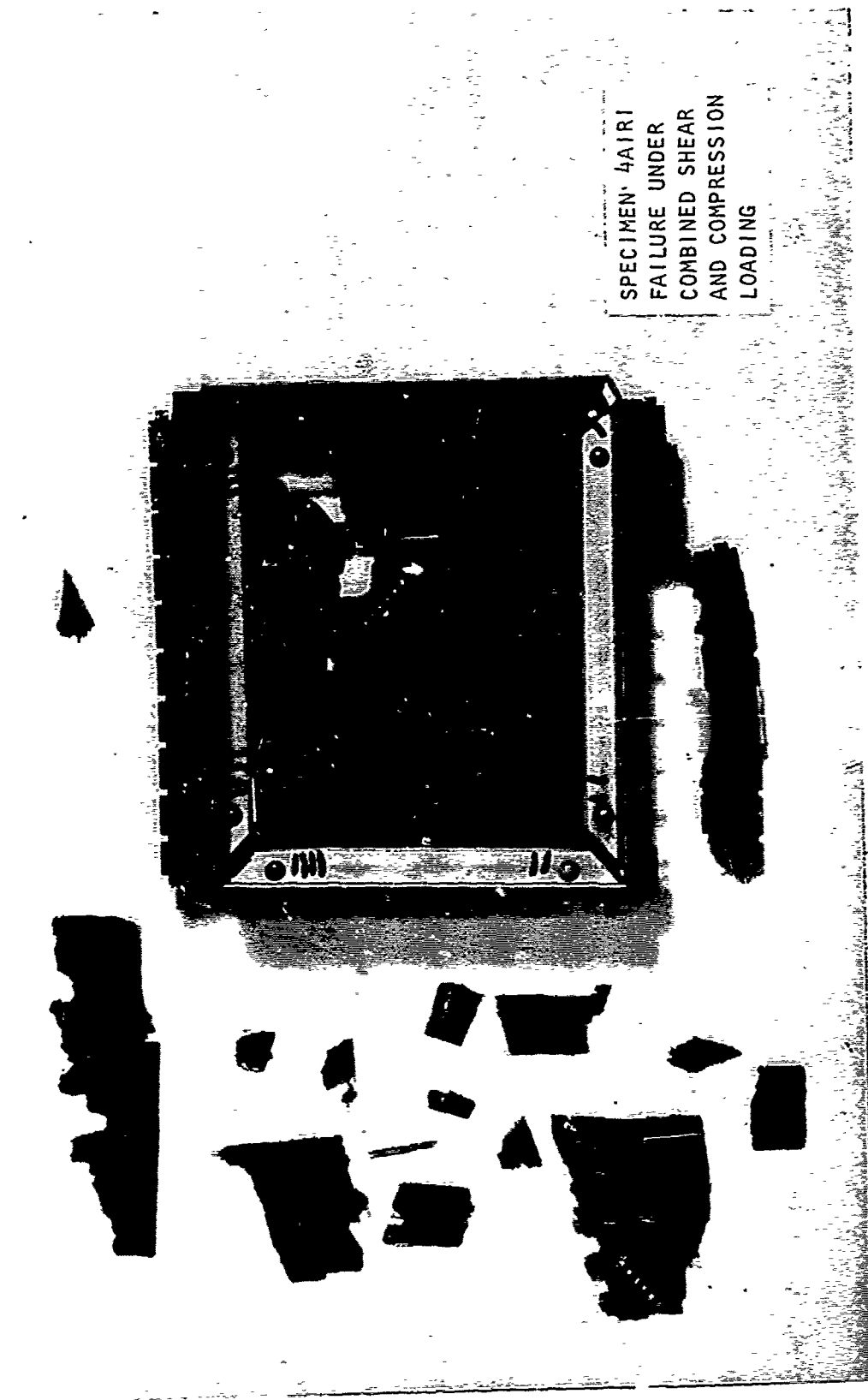
Figure 47. Specimen 4A1R1 After Failure

SPECIMEN 4A1E1
UNIAXIAL COMPRESSION AND SHEAR LOADING
$N_{xy}/N_x = 1$; $F^{su} = 6,010$ PSI
$a/b = 1$; $a = 6$ IN.
350°F

SPECIMEN 4A3R1
UNIAXIAL COMPRESSION AND SHEAR LOADING
$N_{xy}/N_x = 1$; $F^{su} = 14,624$ PSI
$a/b = 3$; $A = 12$ IN.
ROOM TEMPERATURE

Figure 48.   Specimens 4A1E1 and 4A3R1 After Testing

PANEL NO. = 4A1R1

ASPECT RATIO = a/b = 1.0

LAMINATE ORIENTATION = $[0/\pm45/0]_{2S}$

a = 6 IN.

b = 6 IN.

WEIGHT = 0.220 LB

$-45°$
$0°$
$0°$
$+45°$

L

t_{ave} = 0.0862 IN.

T

PANEL NO. = 4A3R1

ASPECT RATIO = a/b = 3.0

LAMINATE ORIENTATION = $[0/\pm45/0]_{2S}$

WEIGHT = 0.290 LB

a = 12 IN.

$-45°$
$0°$
$0°$
$+45°$

L

b = 4 IN

t_{ave} = 0.0862 IN.

T
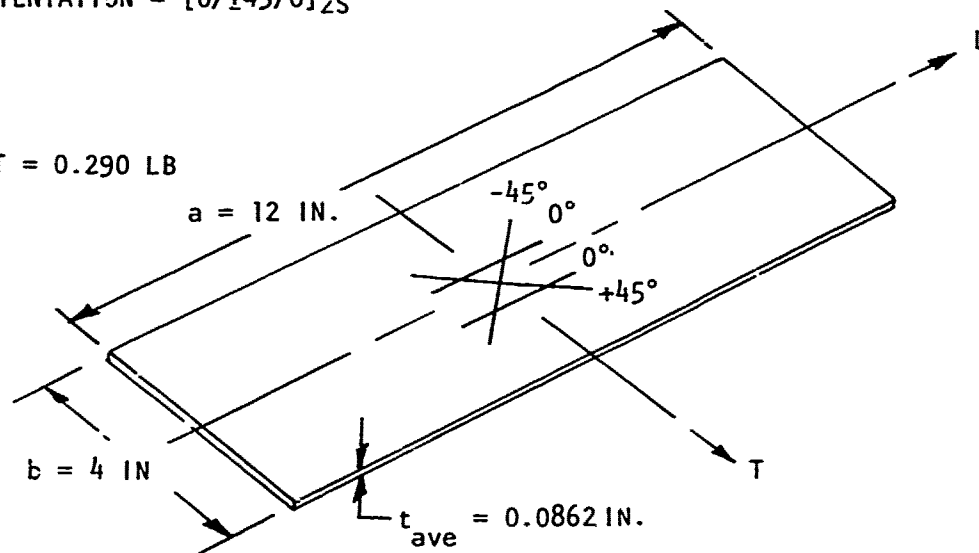
Figure 49.   Plate Geometry for Dynamic Test

ALUMINUM TIEDOWN STRAP

COMPOSITE PLATE

2 IN. GROOVED CHANNELS

SHAKER TABLE
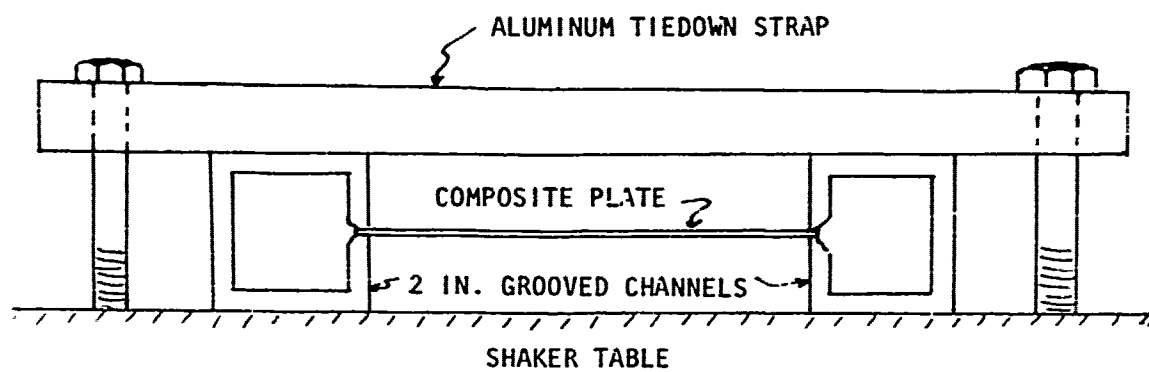
CROSS-SECTIONAL VIEW OF TEST SETUP

CHANNEL

CHANNEL

CHANNEL

COMPOSITE PLATE
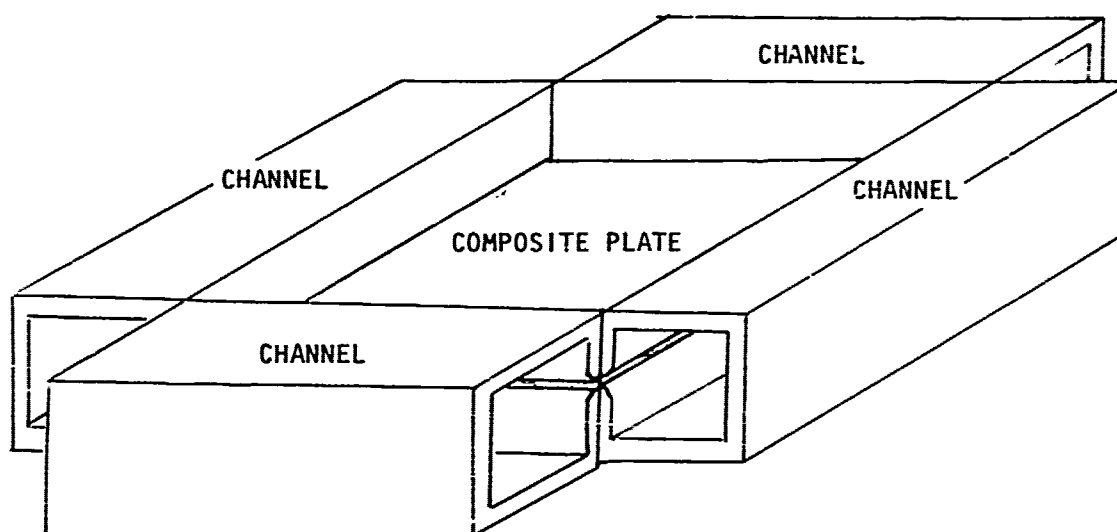
CHANNEL

PLACEMENT OF EDGE SUPPORT CHANNELS

Figure 50. Diagram of Dynamic Test Setup

$$E_L = 30.0 \times 10^6 \text{ psi}$$

$$E_T = 2.5 \times 10^6 \text{ psi}$$

$$G_{LT} = 1.0 \times 10^6 \text{ psi}$$

$$\nu_{LT} = 0.210$$

$$t/\text{ply} = 0.00533 \text{ inch*}$$

The resulting flexural stiffnesses were

$$
\begin{bmatrix}
D_{11} & D_{12} & D_{16} \\
 & D_{22} & D_{26} \\
\text{Sym} & & D_{66}
\end{bmatrix}
=
\begin{bmatrix}
1{,}046.6 & 197.0 & 33.4 \\
 & 299.9 & 33.4 \\
\text{Sym} & & 221.4
\end{bmatrix}
$$

One further constant is needed per plate for the prediction methods, and that is the plate's mass density ρ_m, which is found from

$$\rho_m = \frac{(\text{Weight of plate})}{(\text{Volume of plate})} \; \frac{1}{g}$$

where $g = 386.4 \text{ in./sec}^2$

For the 6 x 6 inch plate and the 4 x 12 inch plate, the resulting mass densities were 0.0001834 lb-sec^2/in.^{4} and 0.0001813 lb-sec^2/in.^{4}, respectively.

The first mode frequency for the 6 x 6 inch and the 4 x 12 inch plates predicted by the RA5 program are 561.4 cycles/sec and 528.7 cycles/sec, respectively.

The second prediction method, which is based on the assumption that the plates are specially orthotropic, is assumed applicable for the laminate orientation considered because

---

*The average thickness of the test plates was 0.0863 inch. Subtracting the 1-mil balance ply from this thickness and dividing by the number of plies, which is 16, one obtains t/ply = 0.00533 inch.

$$\frac{D_{16}}{D_{11}} = \frac{D_{26}}{D_{11}} = 0.03195 \cong 0$$

The equilibrium equation for a specially orthotropic plate is

$$D_{11} \frac{\partial^4 w}{\partial x^4} + 2 (D_{12} + 2D_{66}) \frac{\partial^4 w}{\partial x^2 \partial y^2} + D_{22} \frac{\partial^4 w}{\partial y^4} = \rho_m \frac{\partial^2 w}{\partial t^2}$$

where

w = lateral deflection of plate

ρ_m = mass density of plate

h = thickness of plate

If the lateral deflection w of the plate is assumed to be of the form

$$w = \sum_{i=1}^{\infty} e^{i\omega t} A_{mn} \sin \frac{m\pi x}{a} \sin \frac{n\pi y}{b}$$

where

ω = frequency of vibration

the equilibrium equation is satisfied when

$$D_{11} \left(\frac{m\pi}{a}\right)^4 + 2 (D_{12} + 2D_{66}) \left(\frac{m\pi}{a}\right)^2 \left(\frac{n\pi}{b}\right)^2 + D_{22} \left(\frac{n\pi}{b}\right)^4 = \rho_m h \omega^2$$

Solving for ω gives

$$\omega = \frac{\pi^2}{b^2}\left[\frac{D_{11}\, m^4 \left(\frac{a}{b}\right)^{-4} + 2\,(D_{12} + 2D_{66})\, m^2\, n^2 \left(\frac{a}{b}\right)^{-2} + D_{22}\, n^4}{\rho_m h}\right]^{1/2}$$

which is in radians/sec. In terms of cycles/sec (Hz), the foregoing equation must be divided by 2π. Also, the first mode occurs when $m = n = 1$, so for the first harmonic, the foregoing equation becomes

$$\omega = \frac{\pi}{2b^2}\left[\frac{D_{11}\left(\frac{a}{b}\right)^{-4} + 2\,(D_{12} + 2D_{66})\left(\frac{a}{b}\right)^{-2} + D_{22}}{\rho_m h}\right]^{1/2}$$

Using the geometry and material properties for the two plates in the foregoing equation results in

$\underline{\underline{a/b = 1.0 \qquad b = 6 \text{ inches}}}$

$$\omega = \frac{\pi}{2(6)^2}\left[\frac{1,046.6 + 2\,(197.0 + 2 \times 221.4) + 299.9}{(0.0001834)\,(0.08625)}\right]^{1/2}$$

$$= 562.2 \text{ Hz}$$

$\underline{\underline{a/b = 3.0 \qquad b = 4 \text{ inches}}}$

$$\omega = \frac{\pi}{2(4)^2}\left[\frac{1,046.6\left(\frac{1}{3}\right)^4 + 2\,(197.0 + 2 \times 221.4)\left(\frac{1}{3}\right)^2 + 299.9}{(0.0001813)\,(0.08625)}\right]^{1/2}$$

$$= 529.6 \text{ Hz}$$

63

A summary of the test and predicted results for the first mode frequencies is as follows:

a/b	a (in.)	Test	RA5 Prediction		Orthotropic Prediction	
		Hz	Hz	% of Test	Hz	% of Test
1	6	592	561.4	95	562.2	95
3	12	578	528.7	91	529.6	92

These results indicate that the prediction techniques for the first mode frequency of both panels were very good. Further, it is seen that the closed-form solution prediction, which assumed the plates to be orthotropic, was a valid procedure.

The discrepancies between the predicted versus the actual results are mainly due to the fact that the edge conditions of the panels were not true simple supports in that some edge fixity was present because of the clamping force exerted by the grooved channels on the panel edges.

LOAD DEFORMATION TESTS

Specimen series 5A, 6A, 7A, and 8A are grouped in this category. They consist of rectangular simply supported panels loaded under pressure, thermal gradient, pressure and thermal gradient, and pressure and uniaxial compression, respectively. The purpose of these tests was to verify the load-deformation properties of the material and the buckling load, if relevant. In addition, the ultimate load capacity was sought. The pertinent geometric data are given in table VII, while the material properties data are in tables I, II, and III. A summary of the predicted deflections and outer ply stresses at the center of the panels for both simply supported and clamped boundary conditions and the corresponding test data are compared in table VIII.

The classical theory for the deflections and moments of an orthotropic laminated plate, as shown in Volume III, can be obtained from equation 2 (page 43) by neglecting N_{xy} and expressing w and q as

$$w = \sum_{m=1,3}^{\infty} \sum_{n=1,3}^{\infty} A_{mn} \sin \frac{m\pi x}{a} \sin \frac{n\pi y}{b}$$

TABLE VII. LOAD-DEFORMATION PANEL GEOMETRIES - $[0/\pm 45/0]_{2S}$

Spec-imen	a (in.)	b (in.)	t (in.)	Test Temp (°F)	Test Type
5A1R1	6.0	6.0	0.0832	RT	Pressure
1E1	6.0	6.0	0.0832	350	
3R1	12.0	4.0	0.0832	RT	
3E1	12.0	4.0	0.0832	350	
6A1E1	6.0	6.0	0.0832	RT+ΔT	Thermal Gradient
3E1	12.0	4.0	0.0832	RT+ΔT	
7A1E1	6.0	6.0	0.0832	RT+125	Pressure and Thermal
3E1	12.0	4.0	0.0832	RT+125	
8A1R1	6.0	6.0	0.0832	RT	Pressure and Compression
1E1	6.0	6.0	0.0832	350	
3R1	12.0	4.0	0.0832	RT	
3E1	12.0	4.0	0.0832	350	
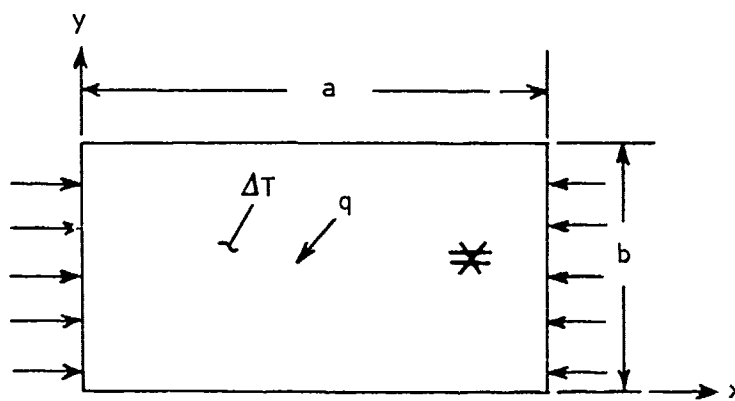
TABLE VIII. LOAD-DEFORMATION AND FAILURE ANALYSIS

(TEST VERSUS THEORY FOR P = 5 PSI (OR ΔT = 125°F) AT CENTER OF PANEL)

Speci-men	Test Temp (°F)	Loading N_x (Kips/in.)	Loading N_y (Kips/in.)	Loading ΔT (°F)	Theoretical — Simply Supported N_{xcr} (Kips/in.)	Simply Supported w (in.)	Simply Supported σ_x (Ksi)	Simply Supported σ_y (Ksi)	Clamped N_{xcr} (Kips/in.)	Clamped w (in.)	Clamped σ_x (Ksi)	Clamped σ_y (Ksi)
5A1R1	RT	---	---	---	0.66	0.043	14.26	1.41	1.73	0 0133	6.74	0.654
1E1	350	---	---	---	0.62	0.047	15.18	0.62	1.61	0.0142	7.10	0.286
3R1	RT	---	---	---	1.38	0.046	3.34	3.27	2.54	0.0118	1.67	1.27
5E1	350	---	---	---	1.23	9.058	3.75	1.65	2.28	..0149	1.85	0.664
6A1E1	RT+ΔT	---	---	ΔT	(120)	0	-6.67	-0.72	(230)	0	-6.67	-0.74
3E1	RT+ΔT	---	---	ΔT	(130)	0	-5.15	-0.55	(190)	0	-5.15	-0.55
7A1E1	RT+ΔT	0.460*	0.220*	125	(120)	---	---	---	1.15	0.0231	6.40	0.155
3E1	RT+ΔT	0.350*	0.170*	125	(130)	---	---	---	1.22	0.0189	-2.48	1.00
8A1R1	RT	0.219	---	---	0.66	0.064	16.18	2.55	1.73	0.0152	3.22	0.994
1E1	350	0.203	---	---	0.62	0.070	17.36	1.17	1.61	0.0163	3.75	0.455
3R1	RT	0.453	---	---	1.38	0.068	-6.00	5.21	2.54	0.0124	-7.92	1.76
3E1	350	0.407	---	---	1.23	0.083	-4.86	5.18	2.28	0.0158	-7.31	0.927

Specimen	Test Temp (°F)	Test w (in.)	Test σ_x (Ksi)	Test σ_y (Ksi)	Failure N_x (Kips/in.)	Failure N_y (Kips/in.)	Failure ΔT (°F)	Failure P (Ksi)
5A1R1	RT	0.022	14.26	0.94	---	---	-	55-100
1E1	350	0.061	15.18	0.93	---	---	---	36
3R1	RT	0.022	3.34	1.58	---	---	---	62
3E1	350	0.074	3.75	2.15	---	---	---	38
6A1E1	RT+ΔT	0.027	-13.62	-0.90	---	---	300	---
3E1	RT+ΔT	0.031	-6.85	-0.17	---	-	400	---
7A1E1	RT+ΔT	0.053	12.63	0.92	---	---	125	45
3E1	RT+ΔT	0.099	2.55	2.75	---	---	125	30
8A1R1	RT	0.078	19.99	2.84	0.219	---	---	55
1E1	350	0.079	25.19	1.36	0.203	---	---	60
3R1	RT	0.071	-1.69	4.44	0.453	---	---	24
3E1	350	0.091	13.56	0.03	0.407	---	---	32†

* (Δf_{cr}) Predicted loads induced by ΔT

† Delamination occurred at 20 psi

$$q = \sum_{m=1,3}^{\infty} \sum_{n=1,3}^{\infty} \frac{16q}{\pi^2 mn} \sin \frac{m\pi x}{a} \sin \frac{n\pi y}{b}$$

This procedure results in

$$w = 16 \frac{qb^4}{\pi^6} \sum_{m=1,3}^{\infty} \sum_{n=1,3}^{\infty} A'_{mn} \sin \frac{m\pi x}{a} \sin \frac{n\pi y}{b} \tag{3}$$

where

$$A'_{mn} = \frac{1}{mn\left\{D_{11}\left(\frac{mb}{a}\right)^4 + 2(D_{12} + 2D_{66})\left(\frac{mnb}{a}\right)^2 + D_{22}n^4 + \frac{b^2}{\pi^2}\left[N_x^*\left(\frac{mb}{a}\right)^2 + N_y^* n^2\right]\right\}} \tag{4}$$

and N_x^* and N_y^* are either applied inplane loads or fictitious loads imposed by a thermal gradient. For a thermal gradient

$$\begin{Bmatrix} N_x^* \\ N_y^* \end{Bmatrix} = - \int_{T_o}^{T_f} \begin{bmatrix} A_{11} & A_{12} \\ A_{21} & A_{22} \end{bmatrix} \begin{Bmatrix} \alpha_x \\ \alpha_y \end{Bmatrix} dT \tag{5}$$

The stresses can now be obtained

$$\begin{Bmatrix} \sigma_x \\ \sigma_y \end{Bmatrix} = \frac{1}{t} \begin{Bmatrix} N_x^* \\ N_y^* \end{Bmatrix} \pm z \begin{bmatrix} \overline{Q}_{11} & \overline{Q}_{12} & \overline{Q}_{16} \\ \overline{Q}_{21} & \overline{Q}_{22} & \overline{Q}_{26} \end{bmatrix} \begin{Bmatrix} -w,_{xx} \\ -w,_{yy} \\ -2w,_{xy} \end{Bmatrix} \tag{6}$$

where z is the distance from the reference surface, and A_{ij}, D_{ij}, and $\overline{Q}_{ij}$ are given in Volume III.

Series 5A - Uniform Pressure

Table VIII compares the predicted deflection and outer ply stresses at the center of the 5A series panels to the recorded test data. The comparison is for a uniform pressure of 5 psi, which constitutes the threshold where the foregoing small deflection theory begins to deviate from the actual panel response because it neglects the stretching of the plate middle surface. This stretching induces membrane forces which generally begin to influence the plate's response when the normal deflection at the center equals one-half of the plate thickness. The theoretical values are based on the truncation of

equations 3 and 4 to m and n equal to 25; i.e., $\displaystyle\sum_{m=1}^{25} \sum_{n=1}^{25}$

Figures 51 through 54 compare the test data for the 5A series panels for various values of applied normal pressures. As can be seen from these figures, the greater the plate's normal deflection, the more the stresses and deflections deviate from the linear small deflection theory because of the induced membrane forces.

Series 6A - Thermal Gradient

Table VIII compares the predicted deflections and outer ply stresses at the center of the 6A series panels to the recorded test data. The comparison is for a uniform temperature gradient of 125°F and includes the displacement of the supports, $u_{\Delta x}$ and $u_{\Delta y}$. The temperature gradient considered here is the case for which $\Delta T = T_f - T_o$, where T_f and T_o are the temperature of the panel in its final and original state, respectively, as opposed to a gradient through the thickness of the panel. The boundary conditions desired were that the boundaries were constrained from translational motion but were free to rotate. However, this was not possible and some translation u_Δ did occur. Therefore, two sets of predicted parameters were obtained:

1. Those for the desired boundary conditions (without u_Δ).

2. Those considering the measured displacement of the boundary.

These data are shown in table IX.
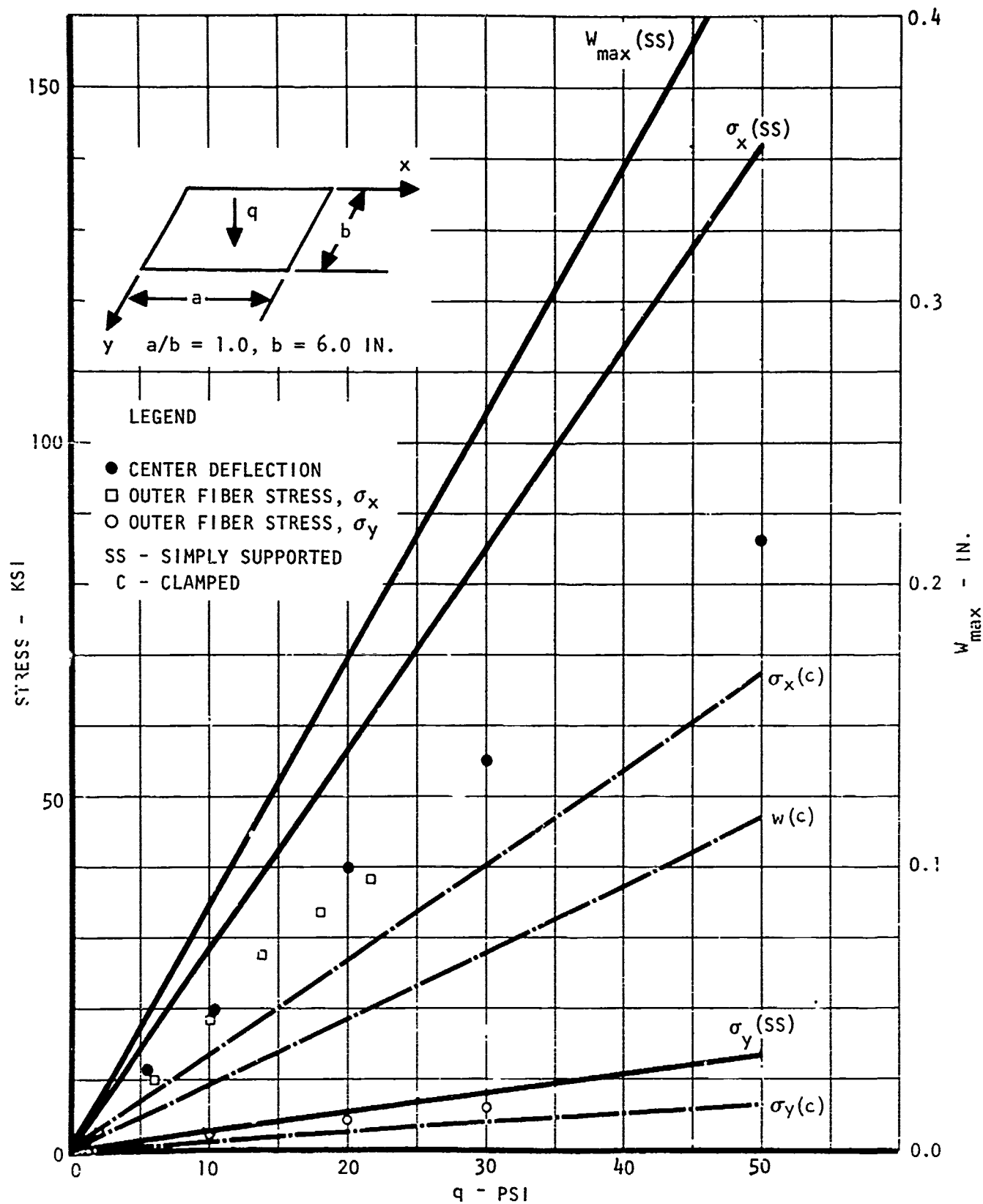
Figure 51. Test Versus Theory, Deflection and Stresses at Center of Panel 5A1R1

69
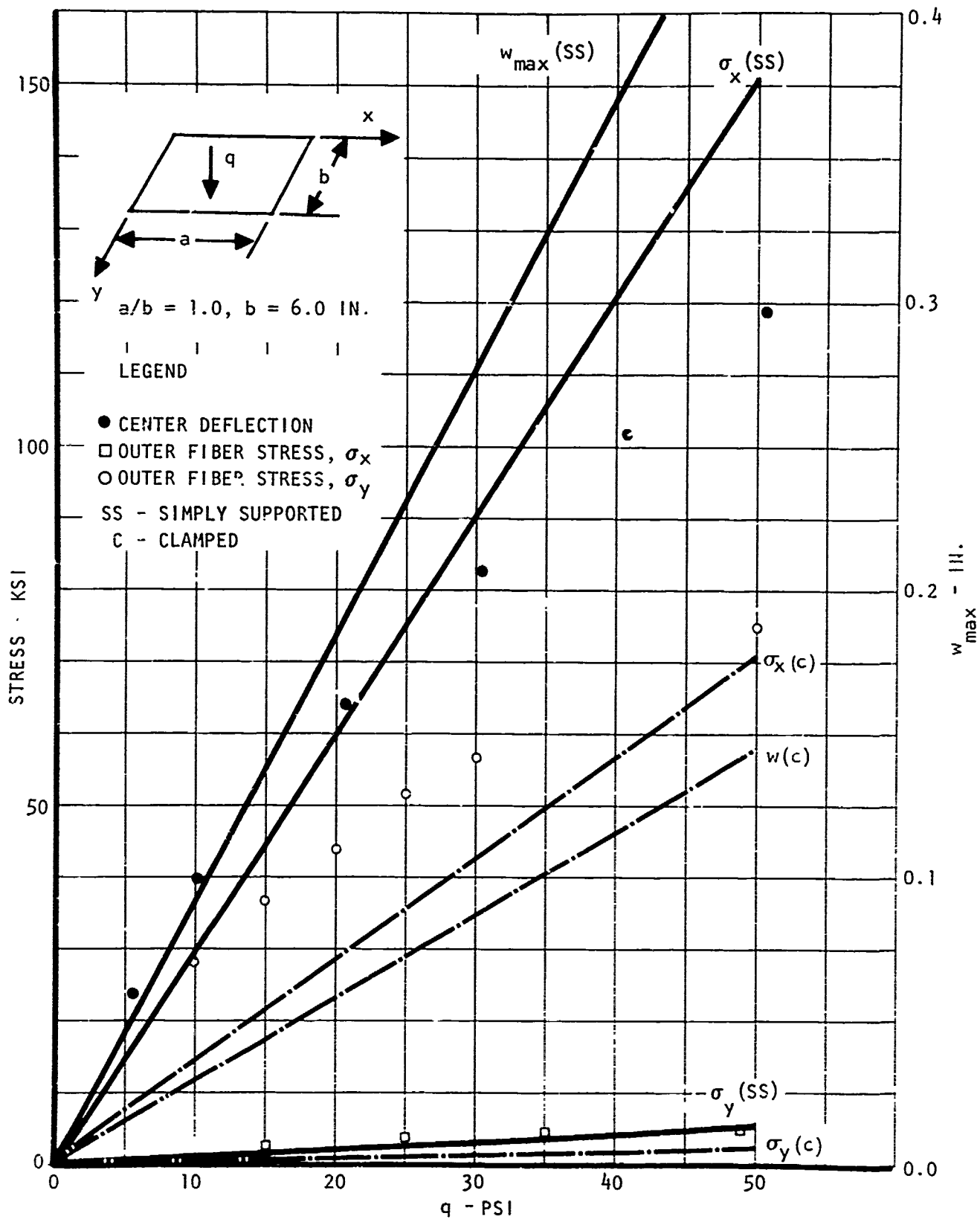
Figure 52. Test Versus Theory, Deflection and Stresses
at Center of Panel 5A1E1
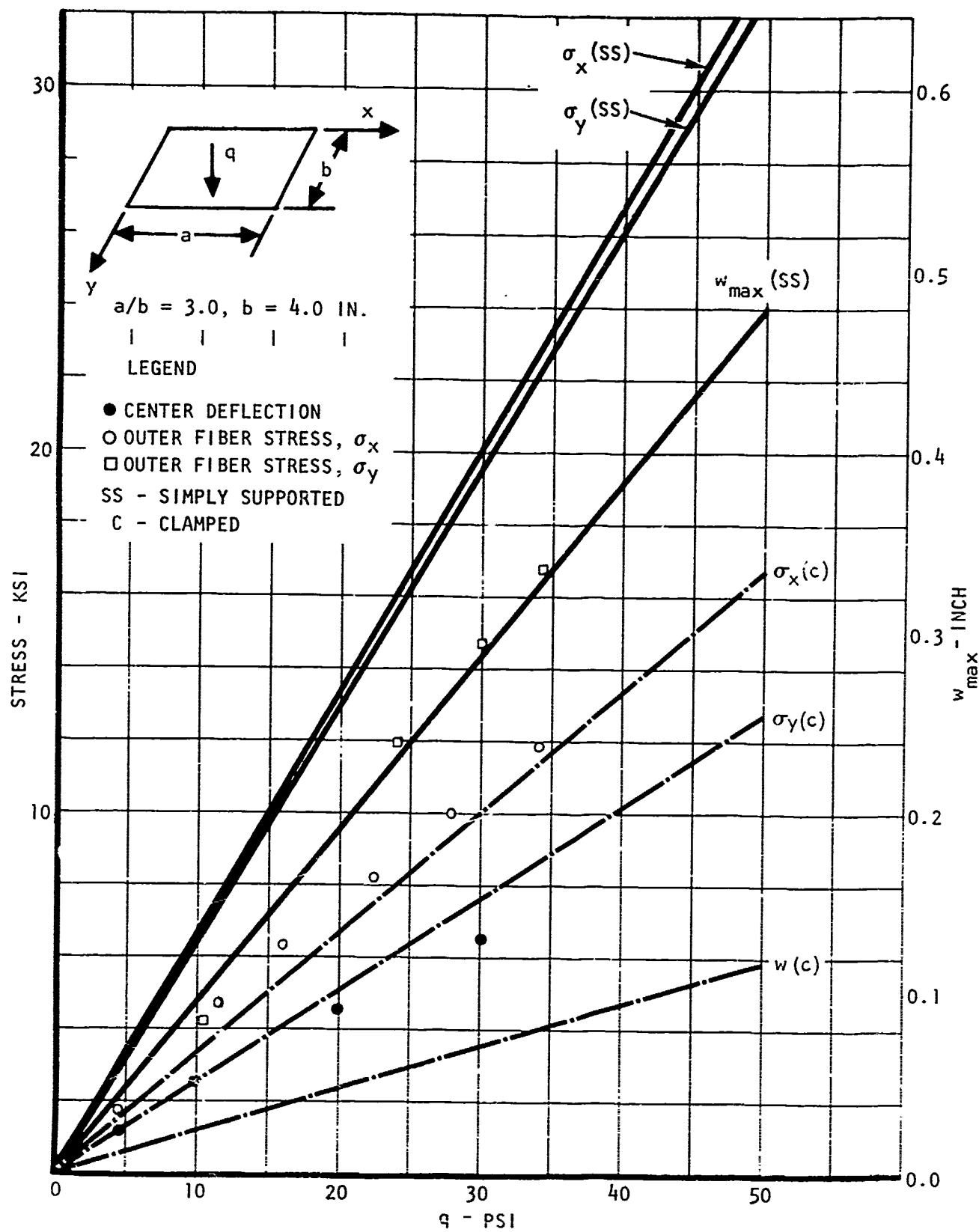
Figure 53. Test Versus Theory, Deflections and Stresses at Center of Panel 5A3R1
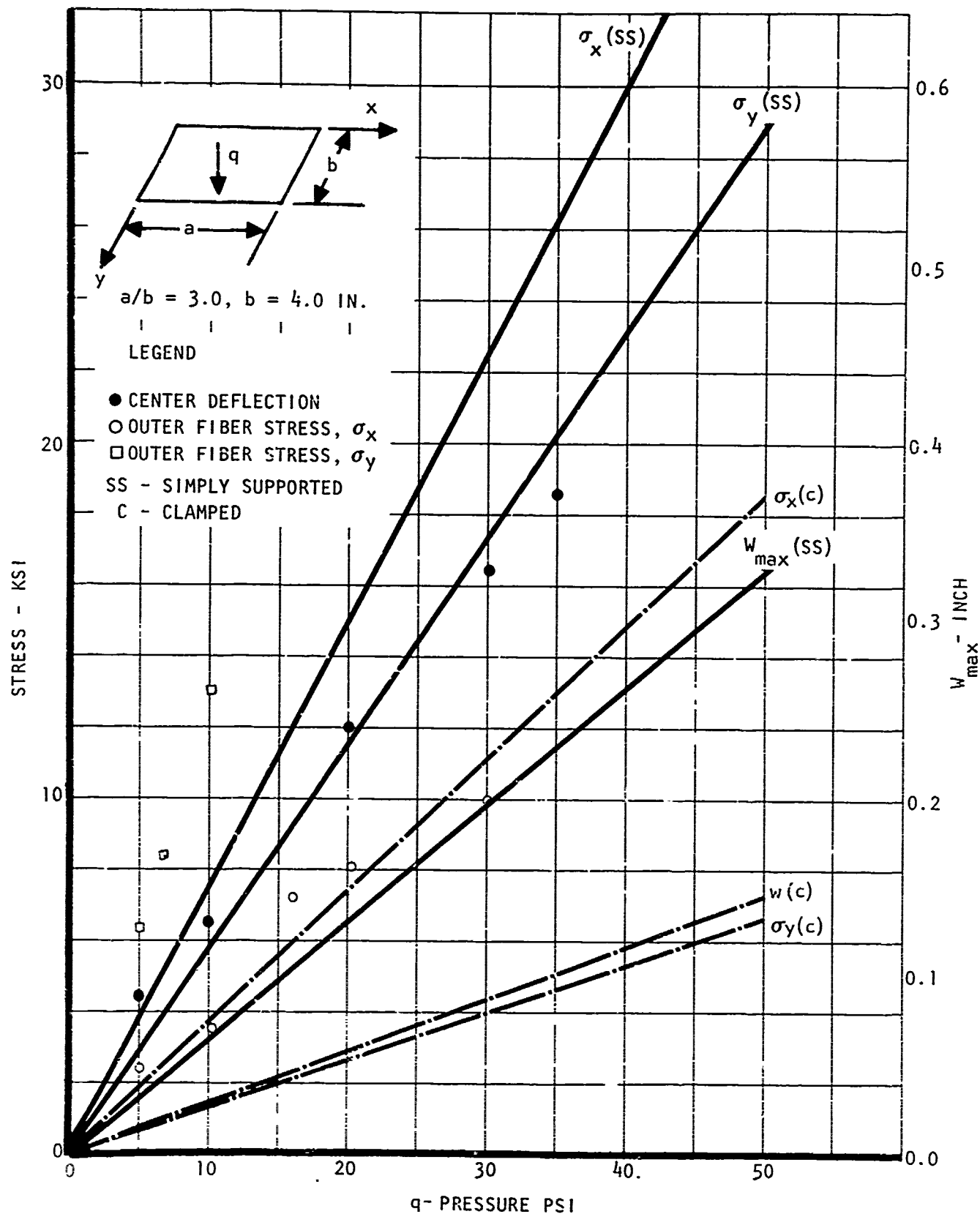
Figure 54. Test Versus Theory, Deflections and Stresses at Center of Panel 5A3E1

Panel	ΔT (°F)	Predicted								Test			
		With u_Δ		Without u_Δ		With u_Δ		Without u_Δ		Upper Face		Lower Face	
		N^*_{xT} (lb/in.)	N^*_{yT} (lb/in.)	N^*_{xT} (lb/in.)	N^*_{yT} (lb/in.)	σ_{xo} (psi)	σ_{yo} (psi)	σ_{xo} (psi)	$\sigma_{y'}$ (psi)	σ_{xo} (psi)	σ_{yo} (psi)	σ_{xo} (psi)	σ_{yo} (psi)
6A1E1*	125	460	220	820	500	6,670	720	10,390	1,770	13,620	900	---	---
3E1•	125	350	170	820	500	5,150	550	10,390	1,770	6,850	170	7,710	920

* A canning noise was heard at T = 250°F
• Strain gage data indicated delamination at T = 250° F

Local delamination occurred on both panels at temperatures much less than anticipated. This was probably due to local "hot spots" caused by uneven heat applcation. Because of this, any failure prediction comparison beyond this point is questionable.

In order to consider the measured displacement of the supports, the thermal stress resultants were modified to

$$
\left\{ \begin{array}{c} N^*_x(T_f) \\ N^*_y(T_f) \end{array} \right\} = - \int_{T_o}^{T_f} \begin{bmatrix} A_{11}(T) & A_{12}(T) \\ A_{21}(T) & A_{22}(T) \end{bmatrix} \left\{ \begin{array}{c} \alpha_x(T) \\ \alpha_y(T) \end{array} \right\} dT
$$

$$
+ \begin{bmatrix} A_{11}(T_f) & A_{12}(T_f) \\ A_{21}(T_f) & A_{22}(T_f) \end{bmatrix} \left\{ \begin{array}{c} u_{\Delta x}(T_f)/a \\ u_{\Delta y}(T_f)/b \end{array} \right\}
$$

$$
= \left\{ \begin{array}{c} N^*_{xT} \\ N^*_{yT} \end{array} \right\}
$$

where $u_{\Delta x}$ and $u_{\Delta y}$ are shown on figure 55.
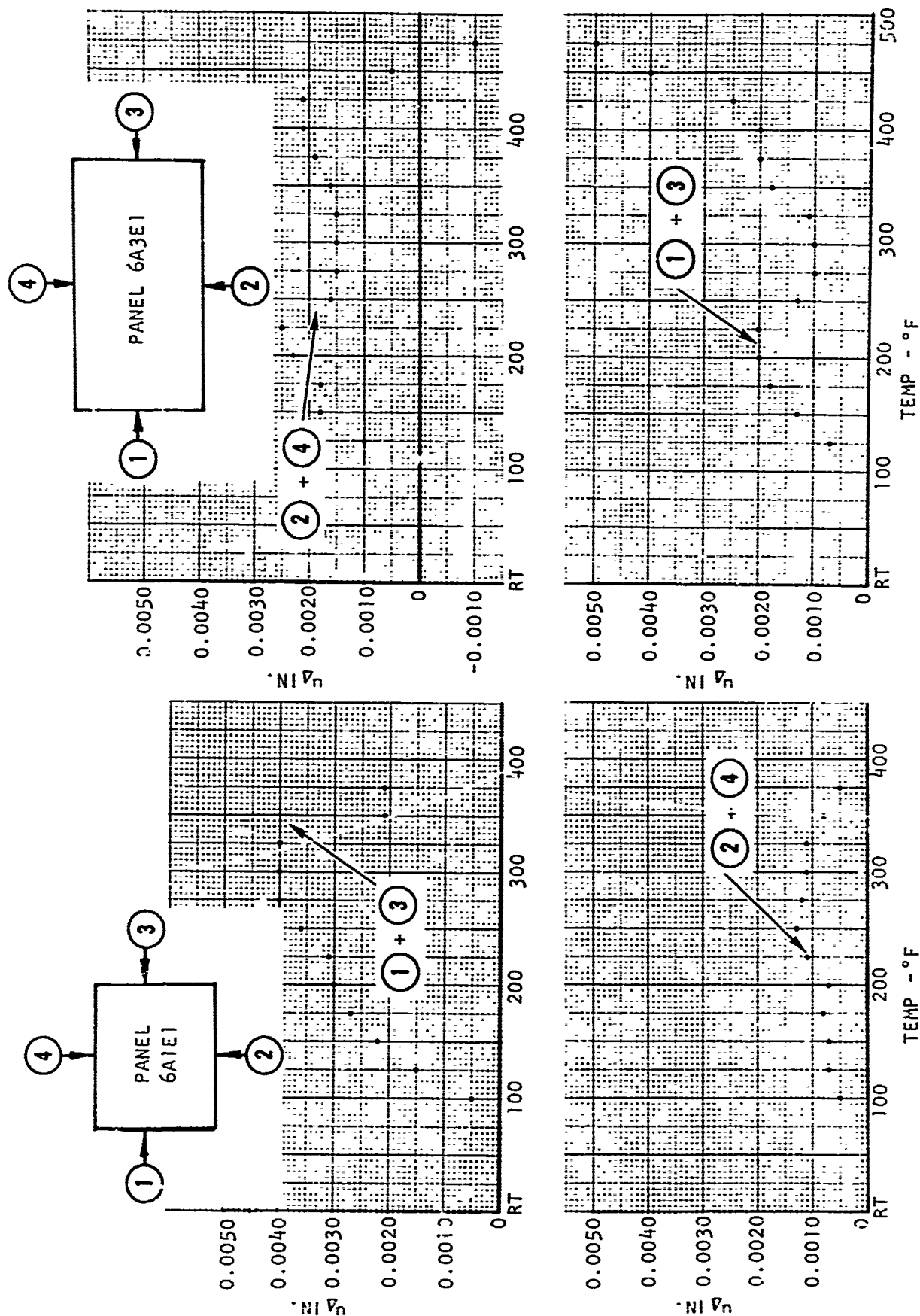
Figure 55. Edge Displacements of Panels 6A1E1 and 6A3E1 Under Thermal Gradient

Figure 56 compares the test data for various temperature gradients.

Series 7A - Pressure and Thermal Gradient

Table VIII compares the predicted deflections and outer ply stresses at the center of the 7A series panels to the recorded test data at $\Delta T = 125°F$, which was applied first, and a pressure of 5 psi. The predicted parameters are based on the assumption that the support movement due to the thermal gradient is identical to that of the corresponding 6A series panel. Difficulties were encountered in evaluating this assumption because of initial deformations in the panels which caused transverse displacements on the panel upon introduction of the thermal gradient load. The transverse displacements, in turn, introduced bending stresses in the panel. Figures 57 and 58 present the test data for the deflection and outer panel stresses versus various applied pressures. This was compared to the clamped boundary condition predictions only, since $(N_{xT}/N_{xcr_{SS}})$ was much too high to yield reasonable results. It is of interest to point out here that none of the panels delaminated prematurely.

Series 8A - Pressure and Uniaxial Compression

Table VIII compares the predicted deflections and outer ply stresses at the center of the 8A series panels to the recorded test data at the uniaxial load indicated and a uniform pressure loading of 5 psi. Panel 8A1R1 was initially pressurized to 50 psi, the pressure load was then removed and the designated axial load applied. The panel was then pressurized to failure. The remaining panels were initially loaded with the designated axial load. They were then pressurized to failure. Figures 59 through 62 compare the test data (w, σ_x, σ_y vs q) at the centers of the panels to the predictions for clamped boundary conditions. The results indicate that the actual boundary condition was somewhat less than fully clamped.

CREEP TESTS

Series 9A and 10A - Creep Buckling

Specimen series 9A and 10A are grouped in this category, and consist of creep tests for columns and panels, respectively, loaded in uniaxial compression. The columns are free on the unloaded edges while the panels are simply supported on all four sides. The purpose of these tests was to determine the load-deformation characteristics of the specimens and the time to failure.

Four tests were conducted for each series. The geometric data are presented in table X and the material data are in tables I through III. The test results are presented in table XI. Figures 65 through 78 present results of the tests, while figures 79 through 82 show the failed test specimens. Table XII is the laboratory report sheet for specimen 9A3E1, which failed prematurely.
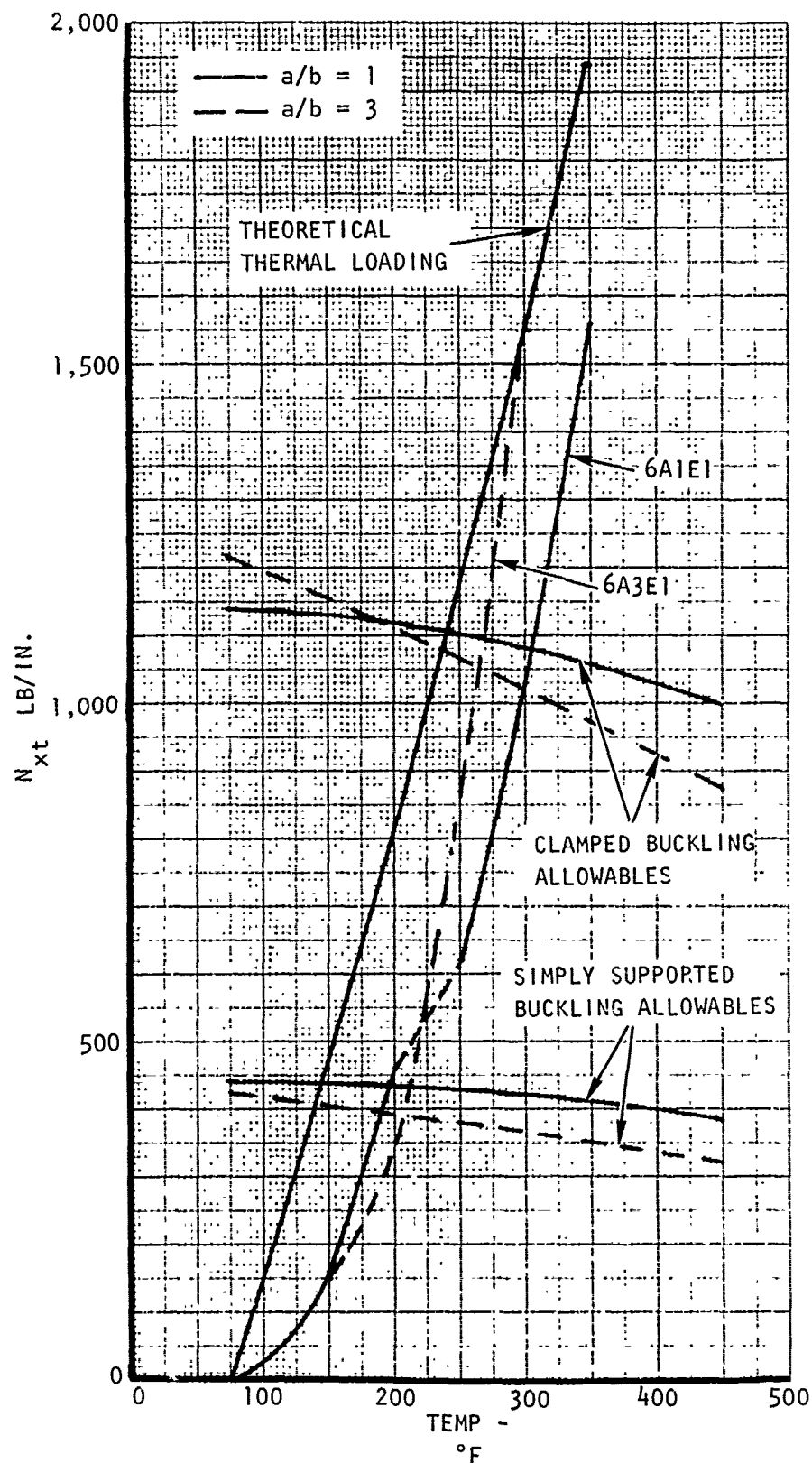
Figure 56. Thermally Induced Edge Loading in Panels 6A1E1 and 6A3E1
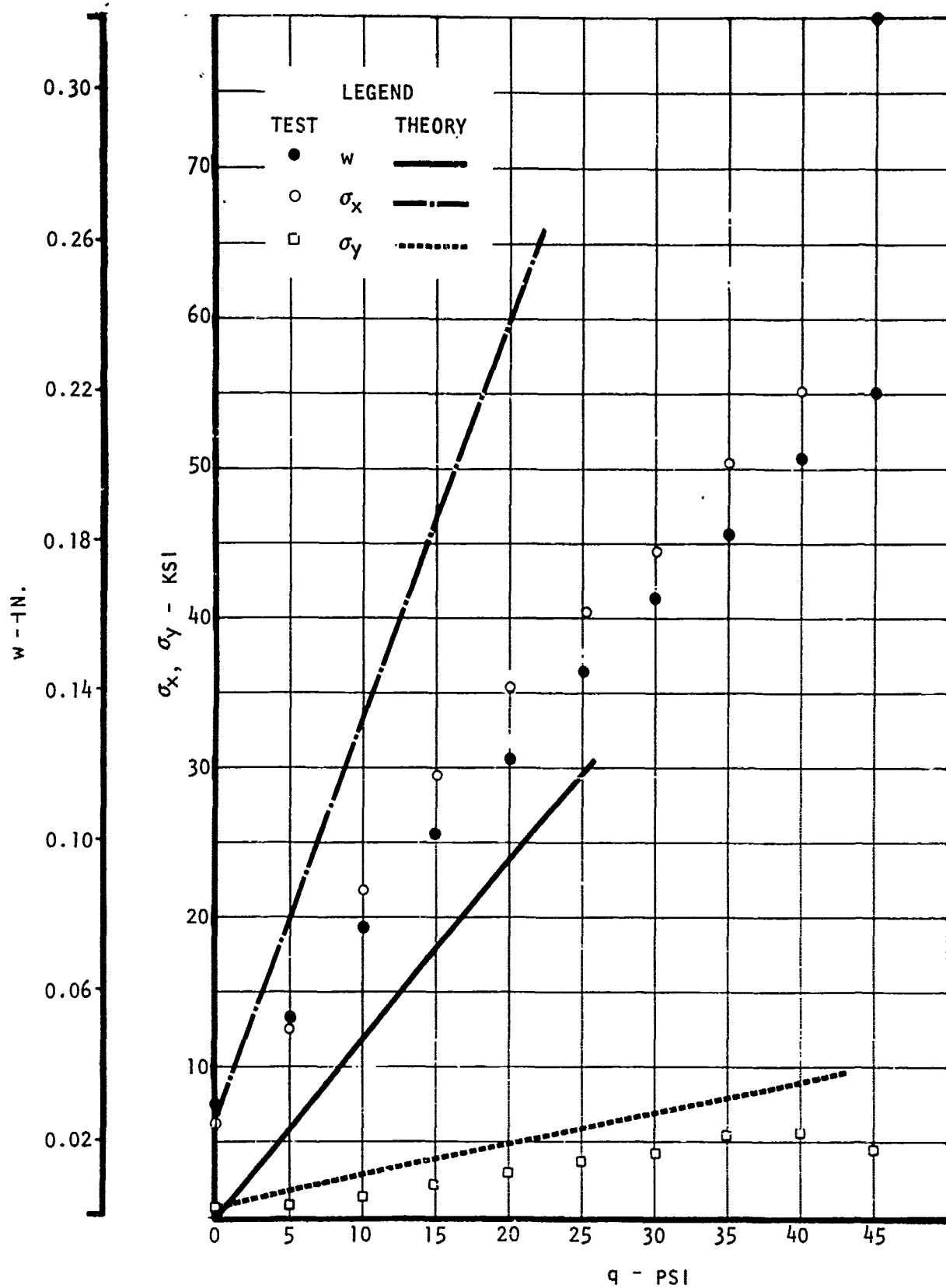
Figure 57. Test vs Theory, Deflections and Stresses at Center of Panel 7A1E1
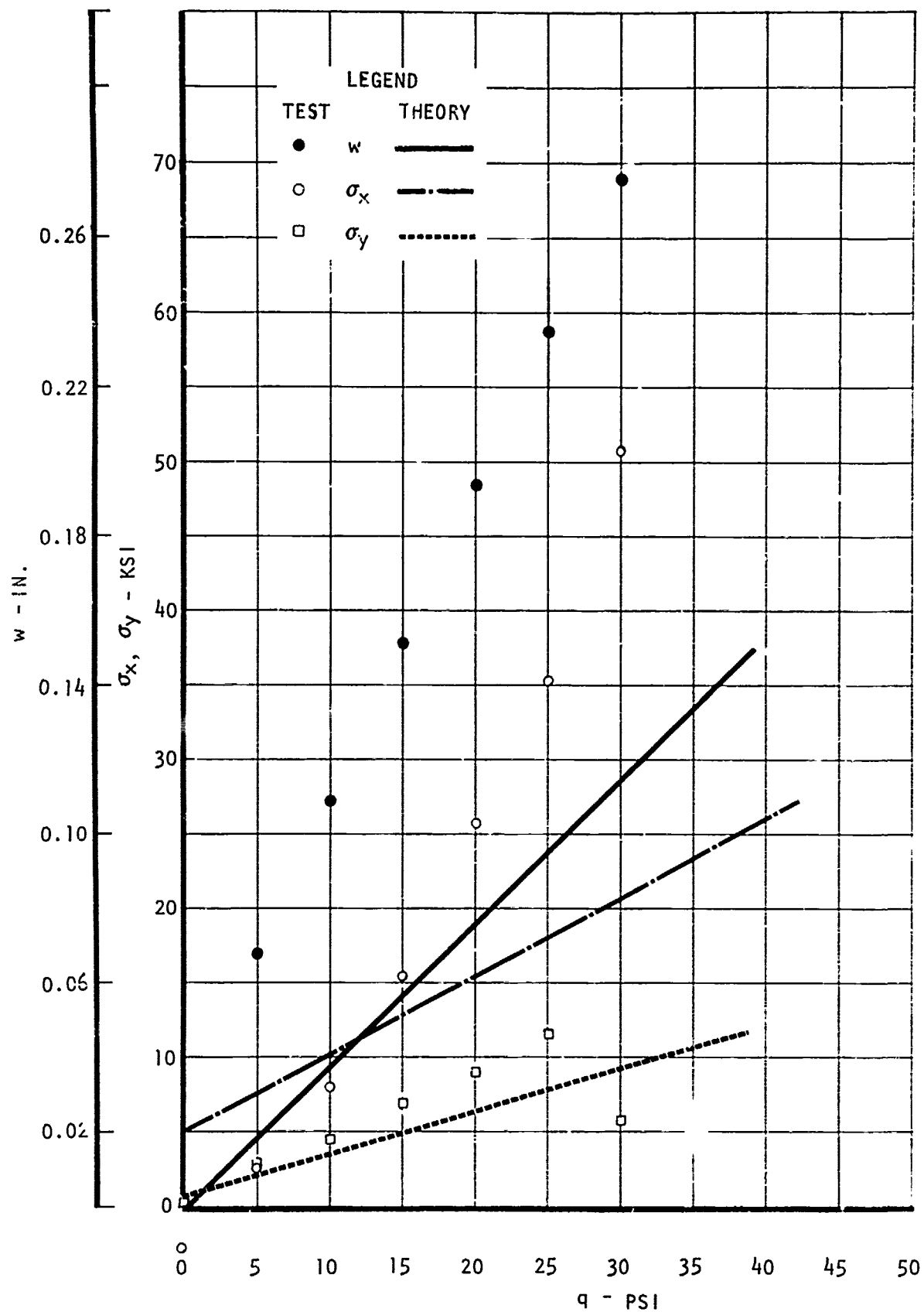
Figure 58. Test vs Theory, Deflections and Stresses at Center of Panel 7A3E1
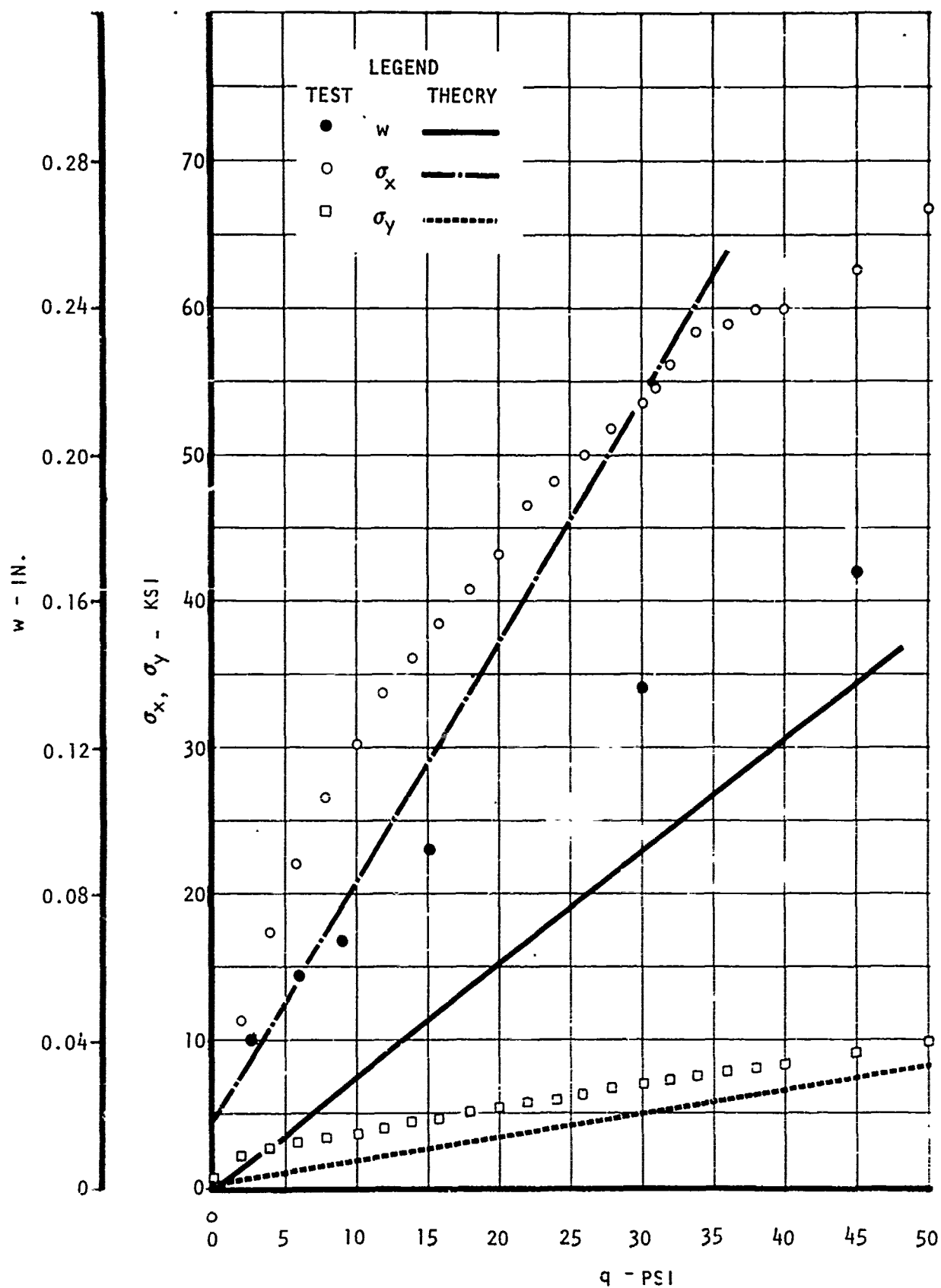
Figure 59. Test vs Theory, Deflections and Stresses at Center of Panel 8A1R1
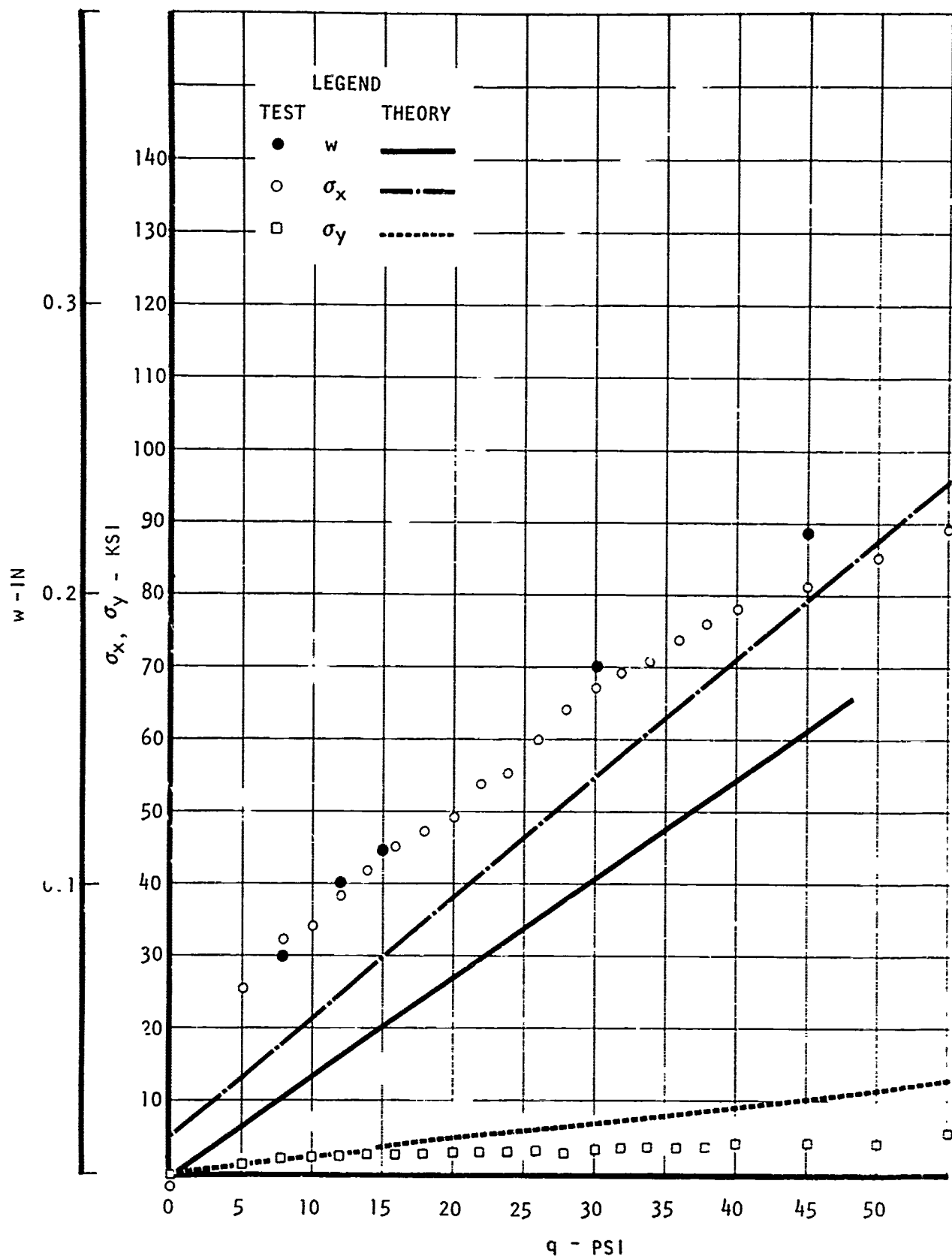
Figure 60. Test vs Theory, Deflections and Stresses at Center of Panel 8A1E1
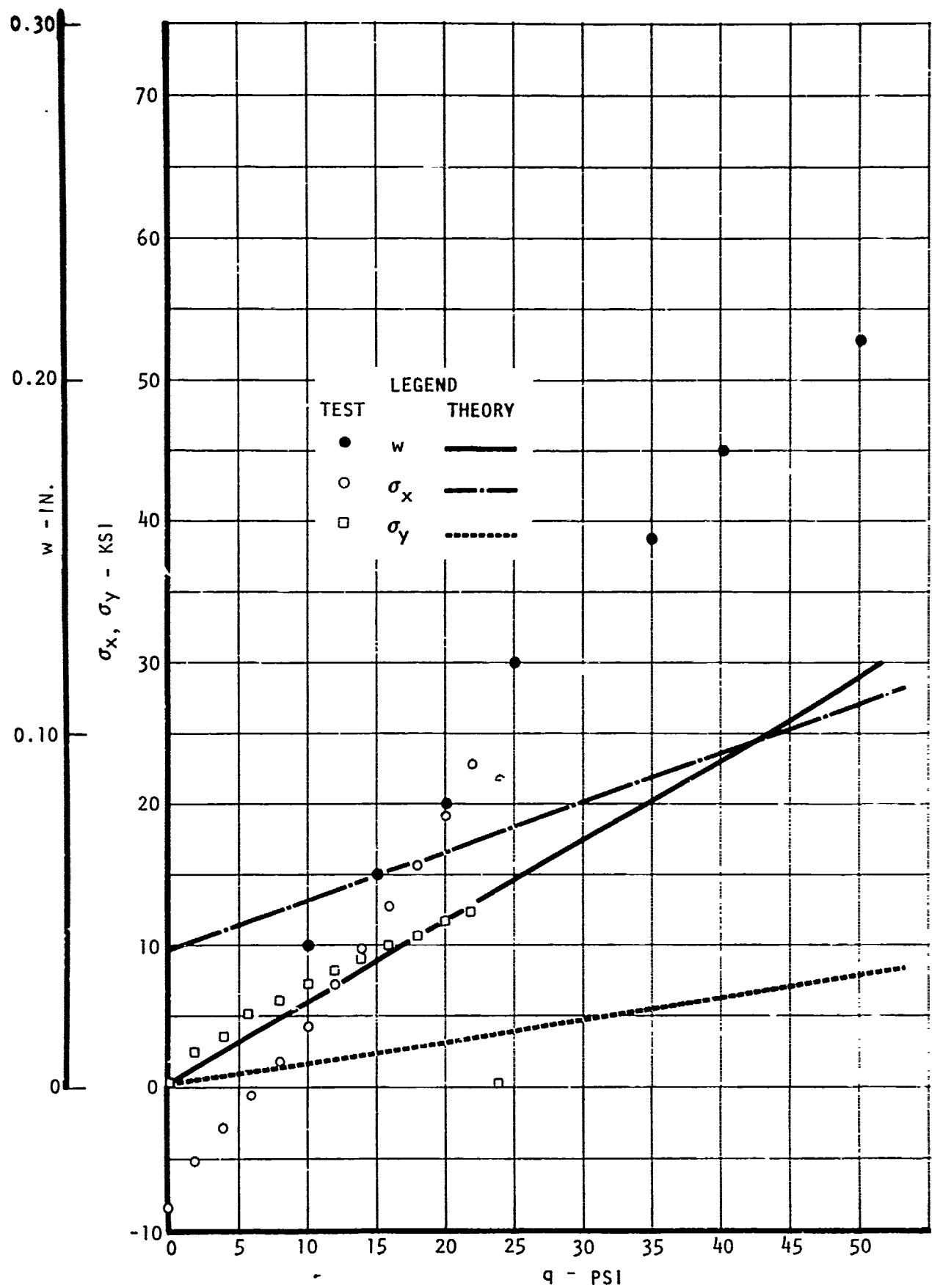
Figure 61. Test vs Theory, Deflections and Stresses at Center of Panel 8A3R1
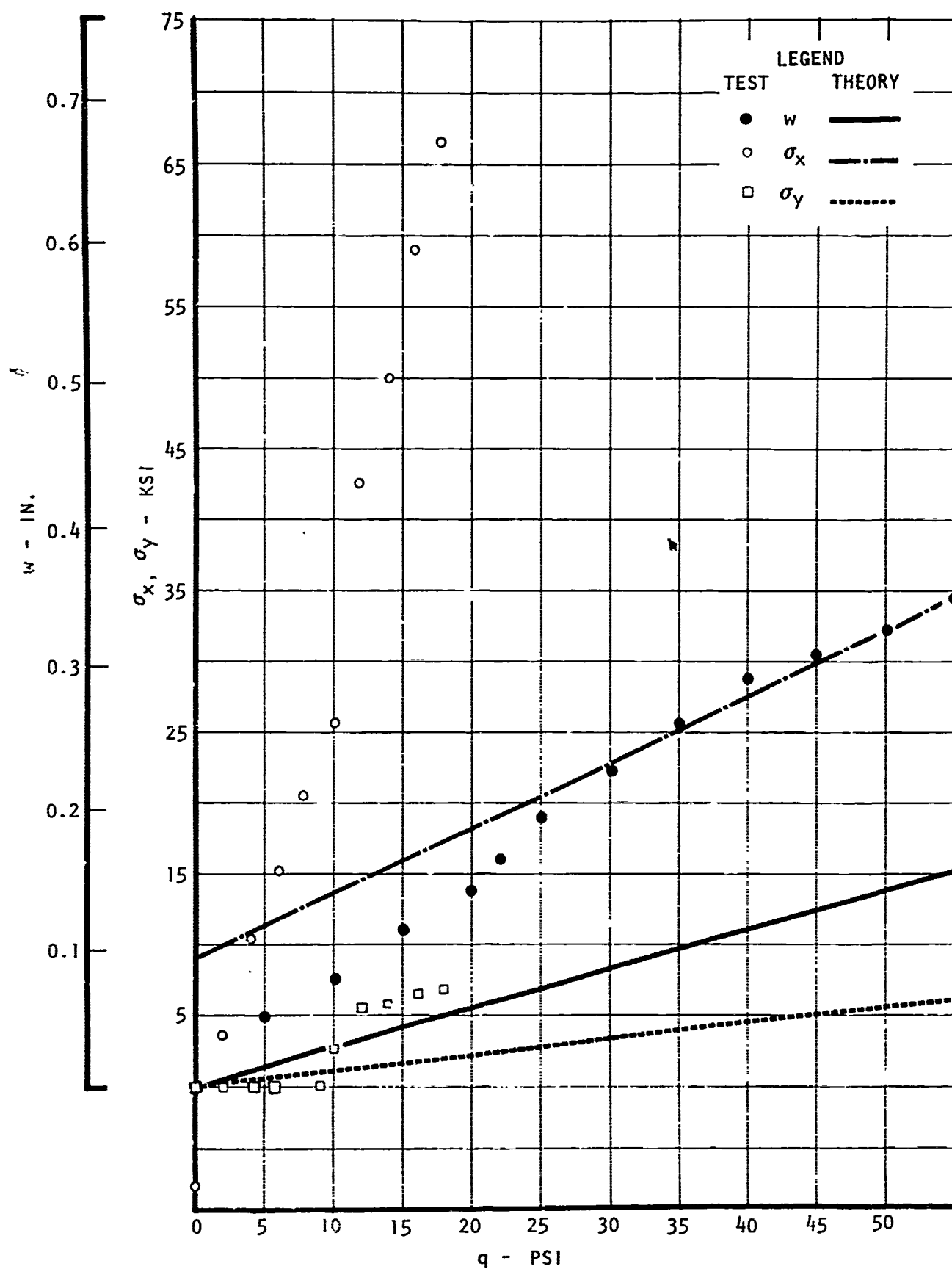
Figure 62. Test vs Theory, Deflections and Stresses at Center of Panel 8A3E1

SPECIMEN 7A1E1

SPECIMEN 7A3E1

Figure 63. Pressure Plus Thermal Loading, 7A Series Panels
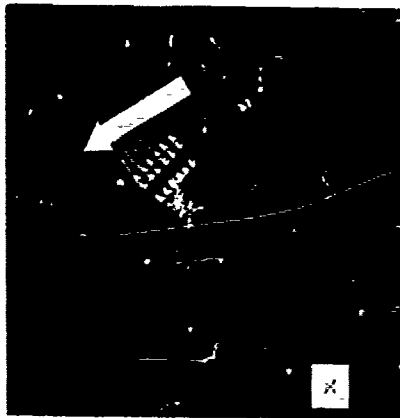
SPECIMEN 8A1R1
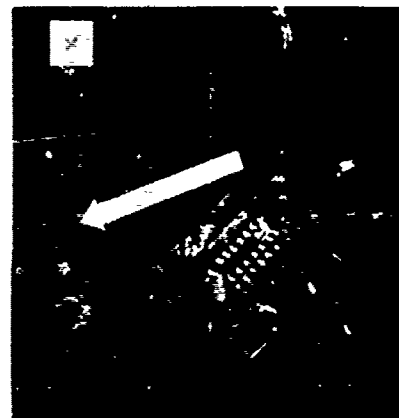
SPECIMEN 8A3R1
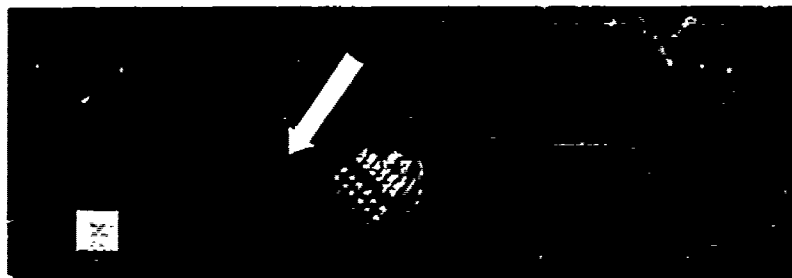
SPECIMEN 8A1E1

SPECIMEN 8A3E1

Figure 64. Pressure Plus Uniaxial Compression Loading, 8A Series Panels

TABLE X - CREEP TEST GEOMETRY $[0/\pm45/0]_{2S}$ - 350°F

Specimen	a (in.)	b (in.)	Test Type
9A1E1	6.0	6.0	Column creep
9A1E2	6.0	6.0	Column creep
9A3E1	12.0	4.0	Column creep
9A3E2	12.0	4.0	Column creep
10A1E1	6.0	6.0	Panel creep
10A1E2	6.0	6.0	Panel creep
10A3E1	12.0	4.0	Panel creep
10A3E2	12.0	4.0	Panel creep

TABLE XI - CREEP TESTS LOADING SCHEDULE

Specimen	a/b	Support	N_{x1} (lb/in.)	Time (hr)	N_{x2} (lb/in.)	Time (hr)	N_{x3} (lb/in.)	Time (hr)	N_{xcr} (lb/in.)
9A1E1	1.0	Unloaded edges free	155	60	166.7	31*	---	---	---
9A1E2	1.0	Unloaded edges free	138.3	80	155	44	171.7	23.5*	---
9A3E1	3.0	Unloaded edges free	35	0.67*	---	---	---	---	---
9A3E2	3.0	Unloaded edges free	25	281	27.5	24	30	30.3*	---
10A1E1	1.0	Unloaded edges ss	657.1	18.0*	---	---	---	---	615
10A1E2	1.0	Unloaded edges ss	592.3	74	644.3	12*	---	---	615
10A3E1	3.0	Unloaded edges ss	980	10.65 -18.15	---	---	---	---	1,229 1,229
10A3E2	3.0	Unloaded edges ss	875	H-22*	---	---	---	---	---

*Indicates failure
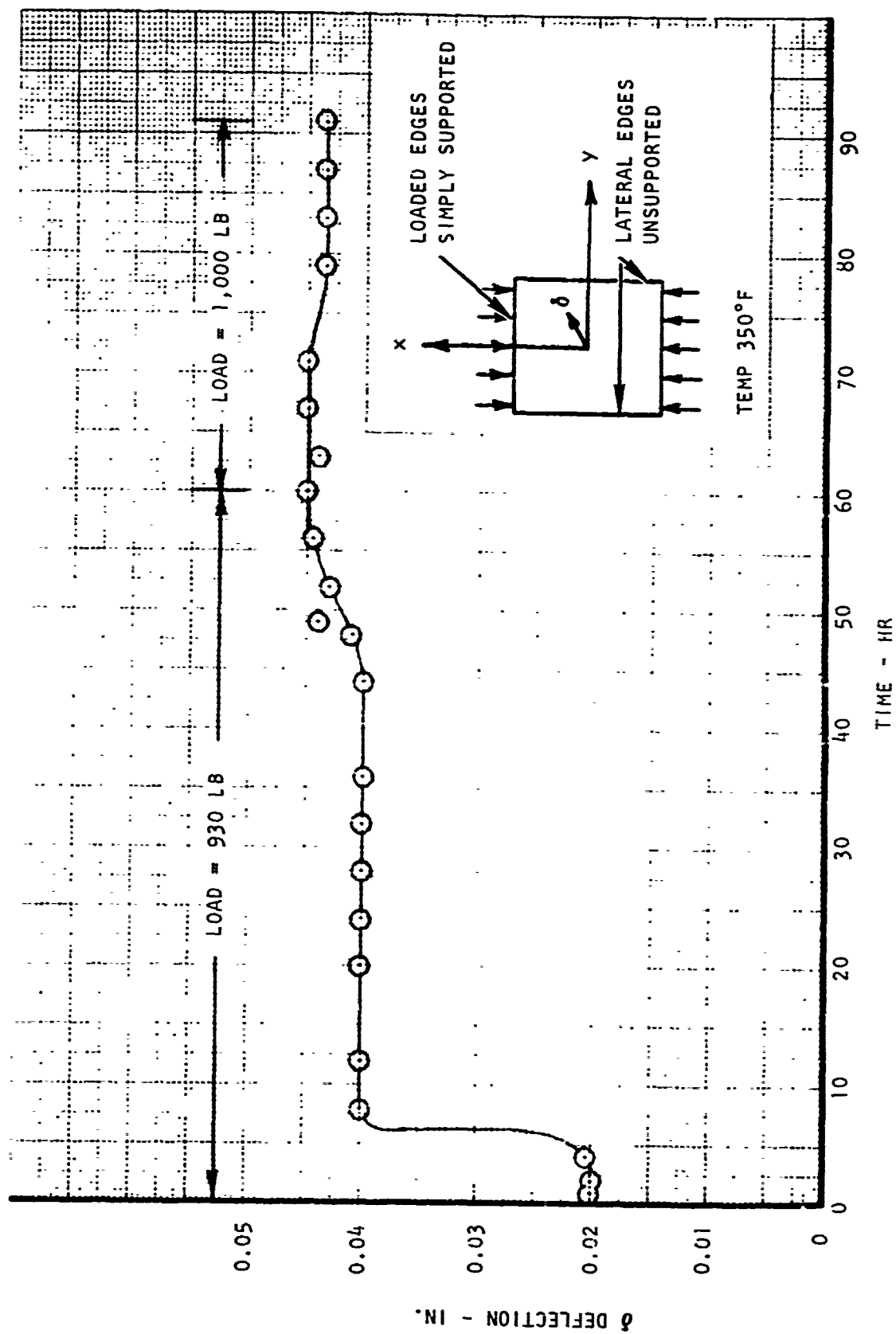
Figure 65. Midpoint Lateral Creep Deformation, Panel 9AlE1
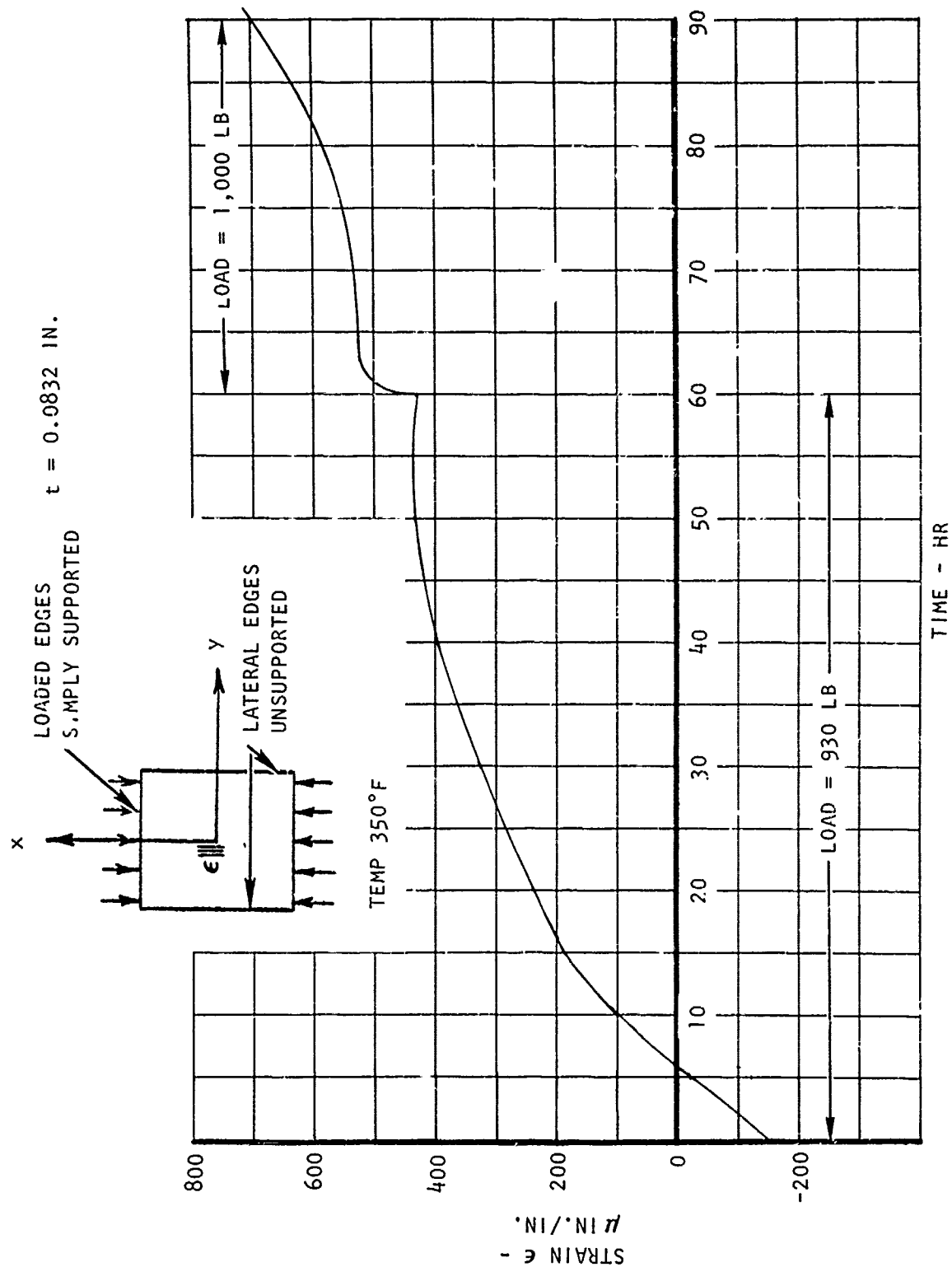
Figure 66. Midpoint Longitudinal Creep Strains from Back-to-Back
Gages, Panel 9A1E1

87
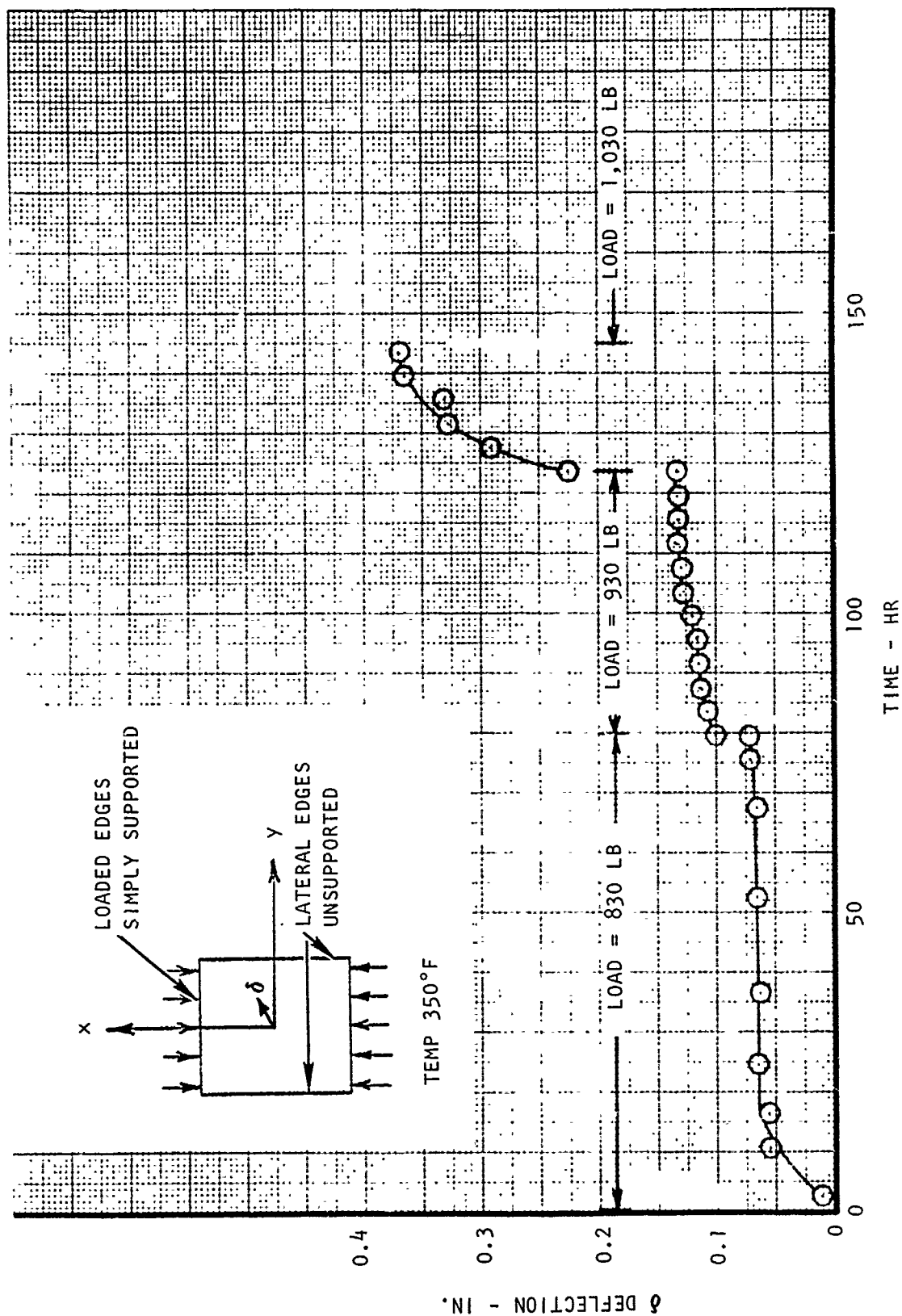
Figure 67. Midpoint Lateral Creep Deformation, Panel 9A1E2

88
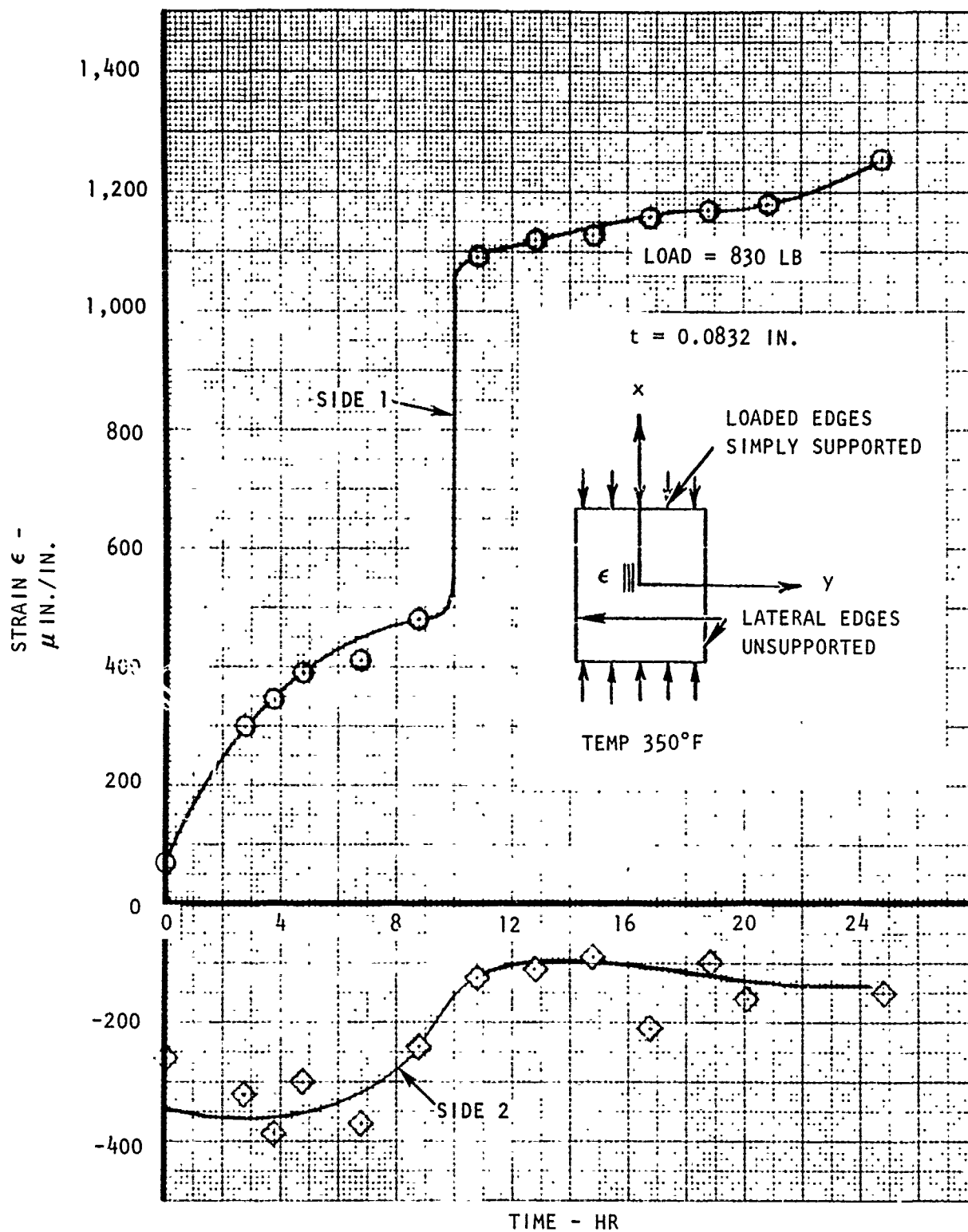
Figure 68. Midpoint Longitudinal Creep Strains from
Back-to-Back Gages, Panel 9A1E2
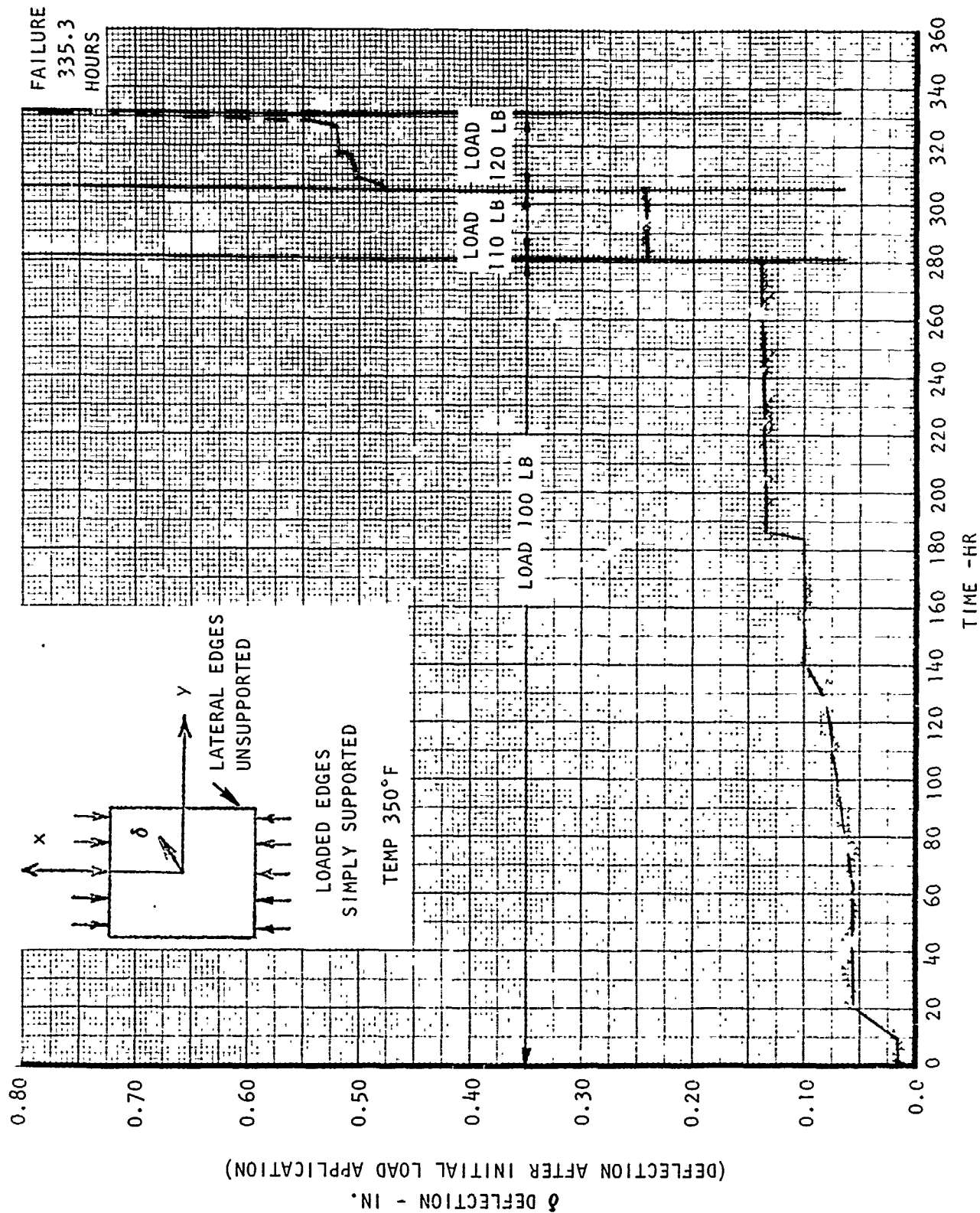
Figure 69. Midpoint Lateral Creep Deformation, Panel 9A3E2
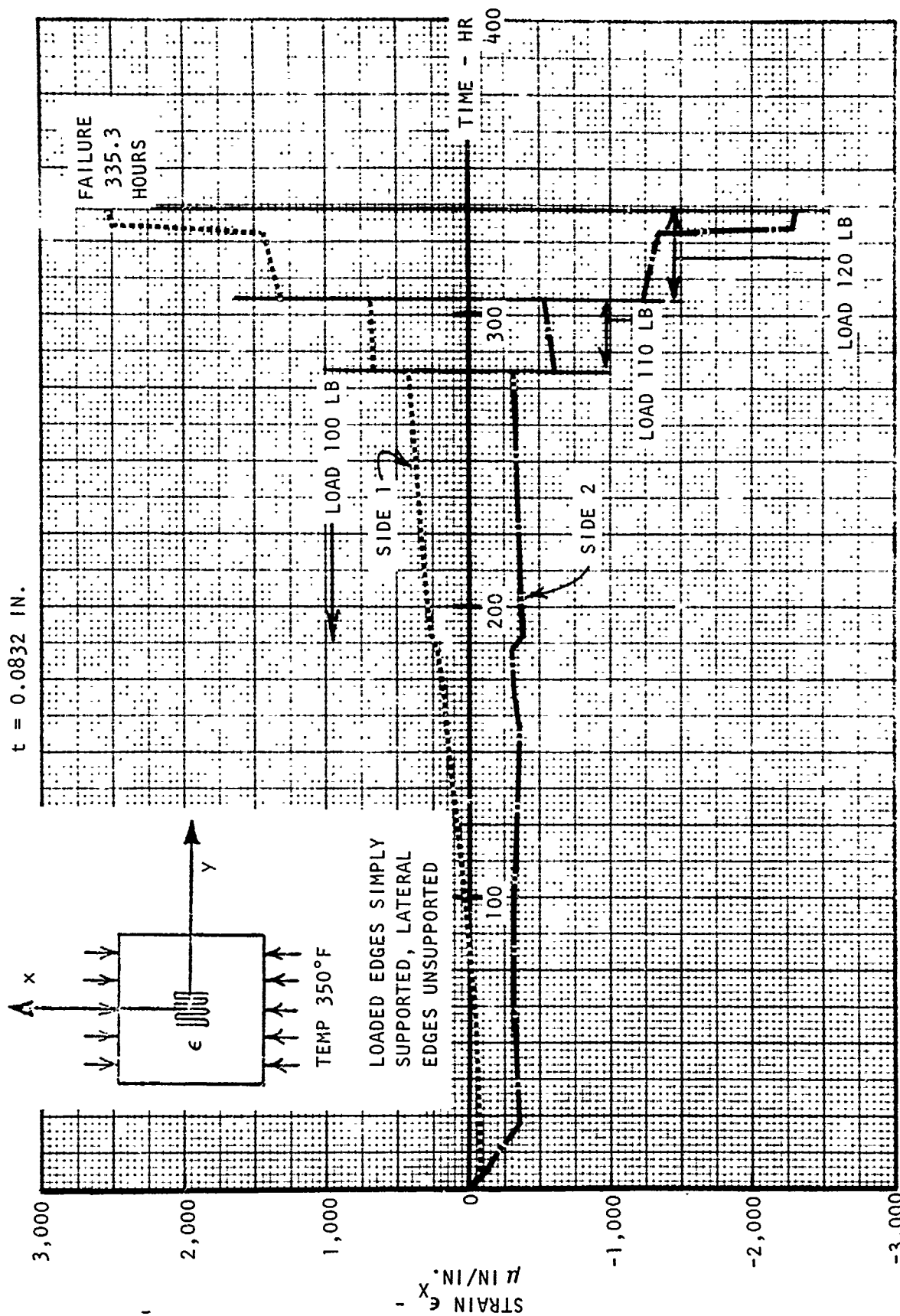
Figure 70. Midpoint Longitudinal Creep Strains From Back-to-Back Gages, Panel 9A3E2

91
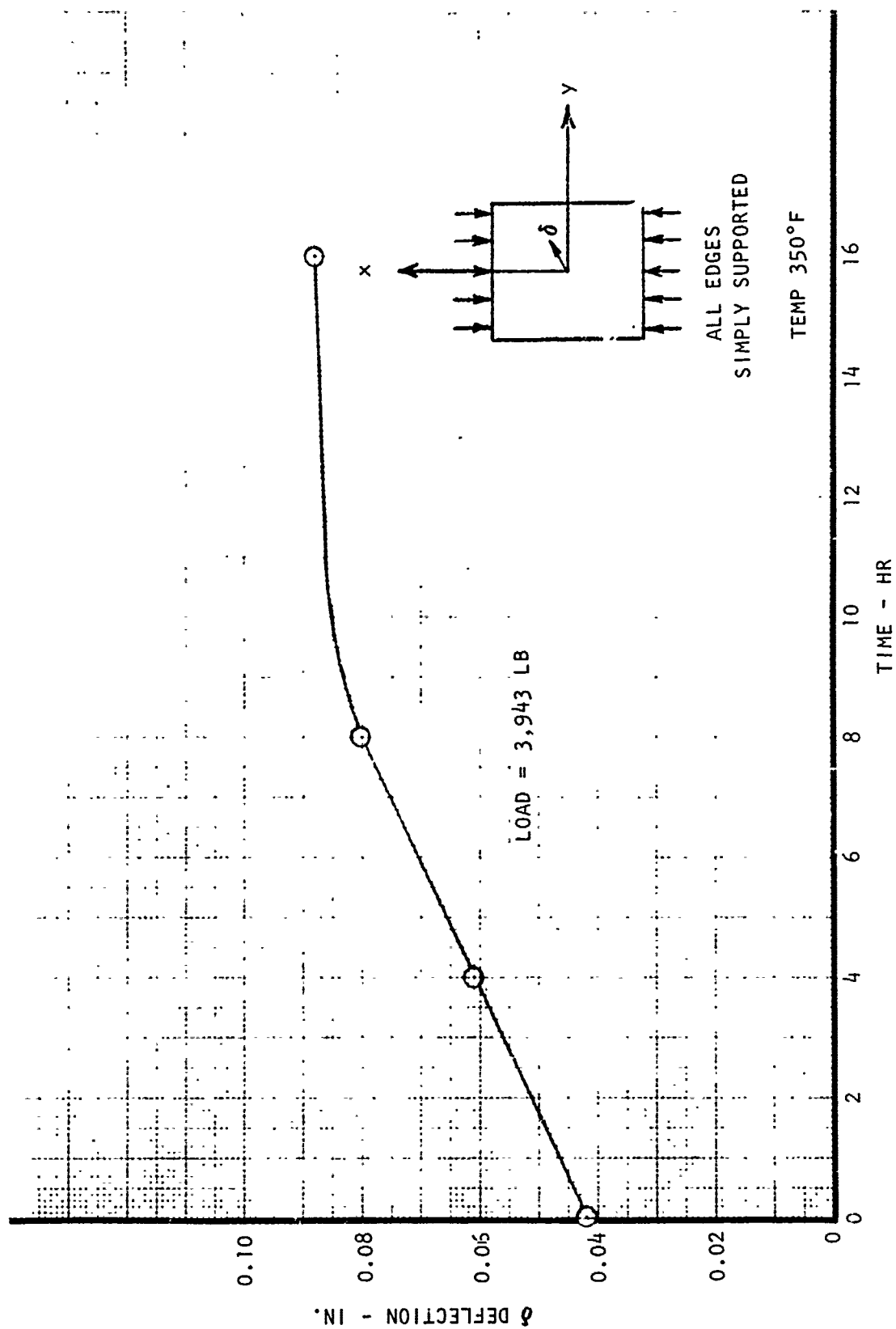
Figure 71. Midpoint Lateral Creep Deformation, Panel 10A1E1
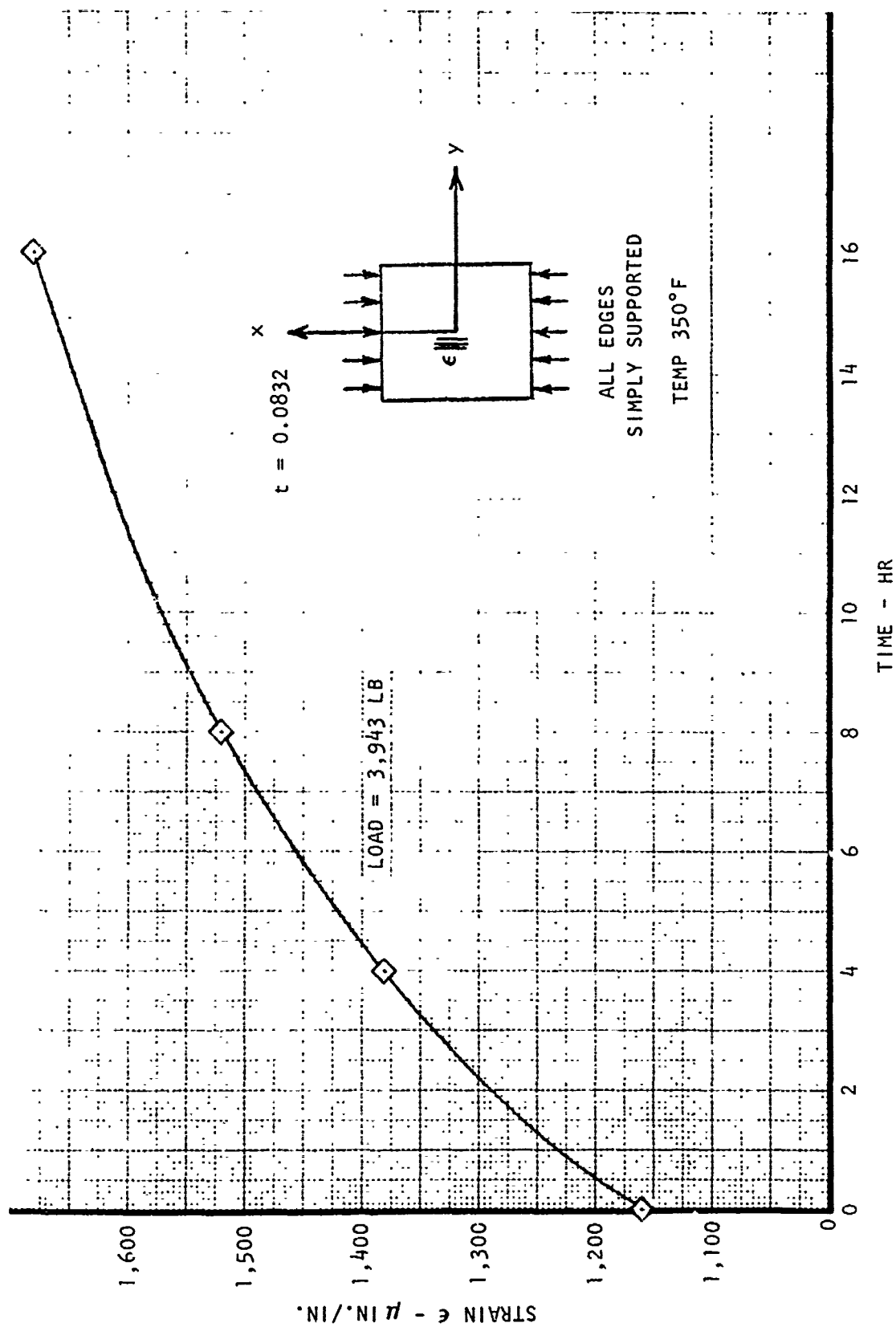
Figure 72. Midpoint Longitudinal Creep Strains from
Back-to-Back Gages, Panel 10A1E1
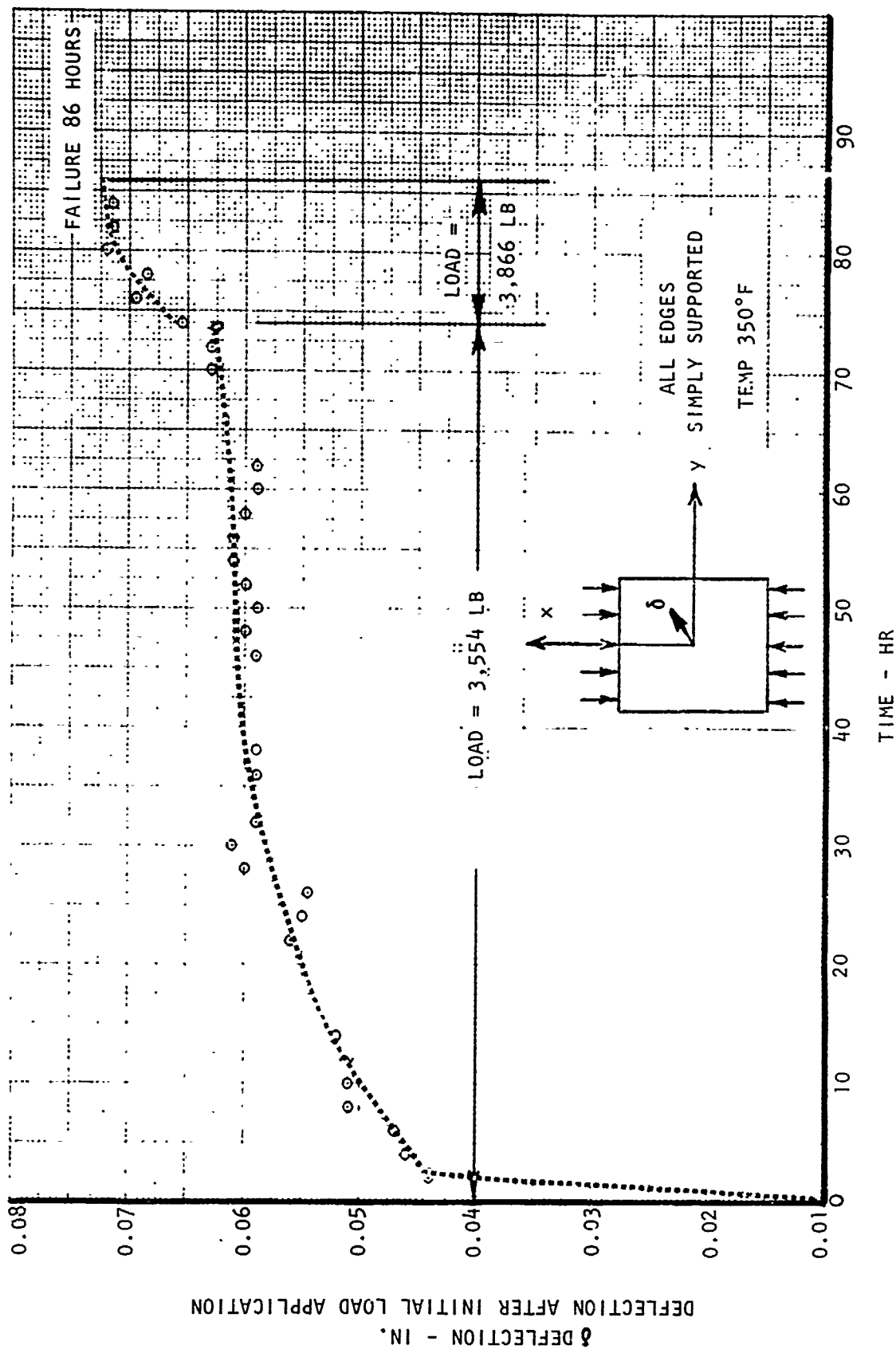
Figure 73. Midpoint Lateral Creep Deformation, Panel 10A1E2
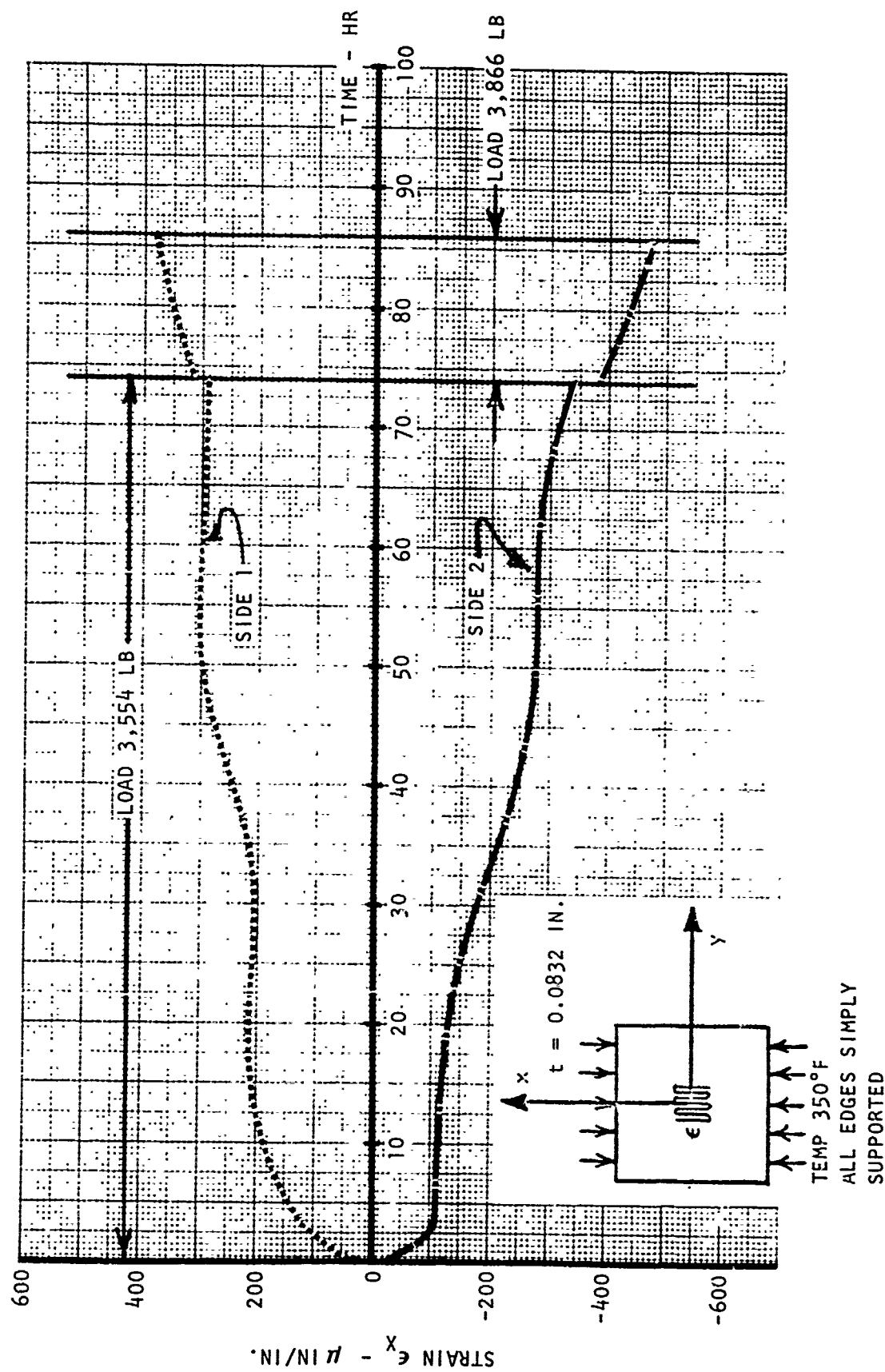
Figure 74. Midpoint Longitudinal Creep Strains from Back-to-Back Gages, Panel 10A1E2
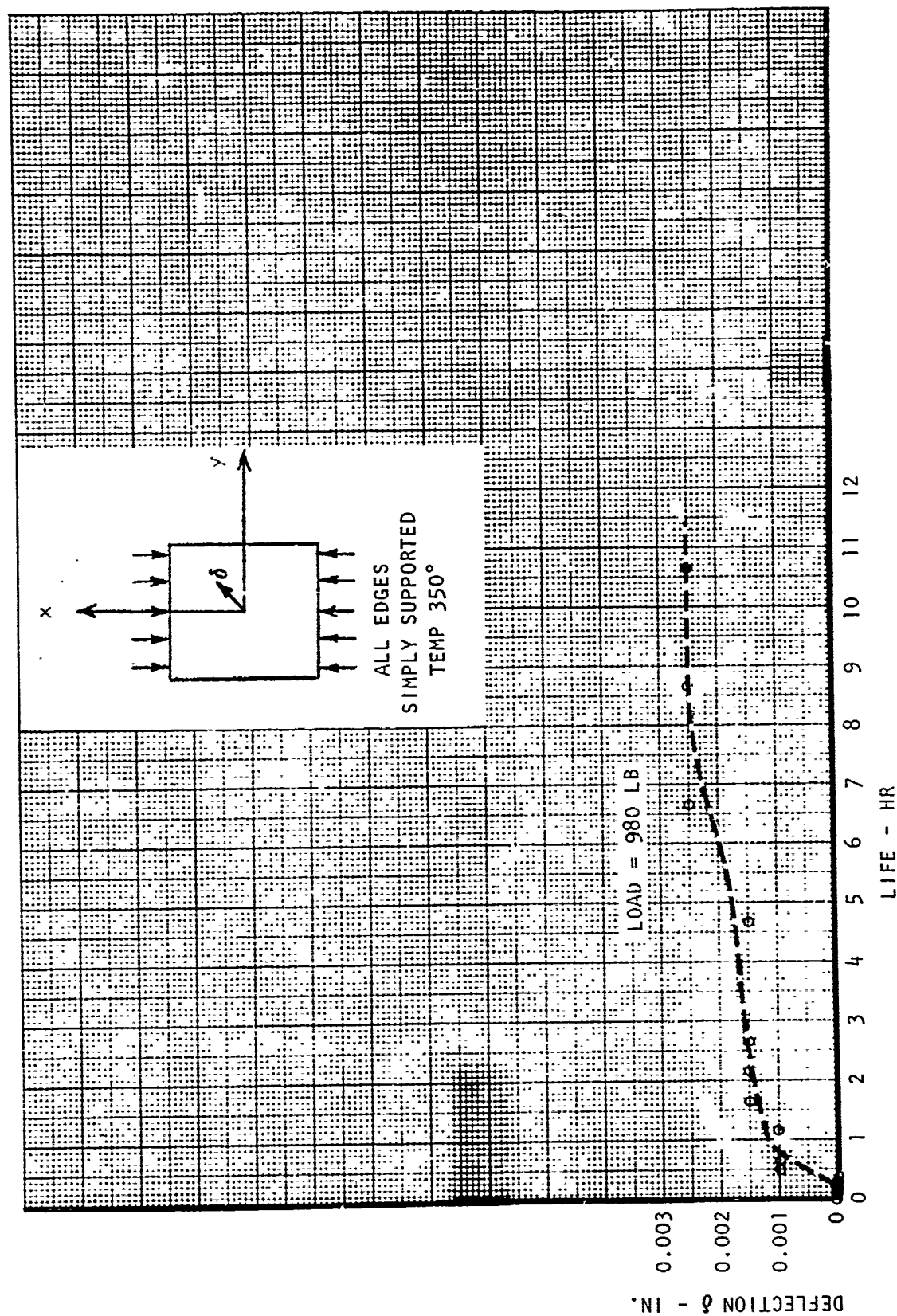
Figure 75. Midpoint Lateral Creep Deformation, Panel 10A3E1
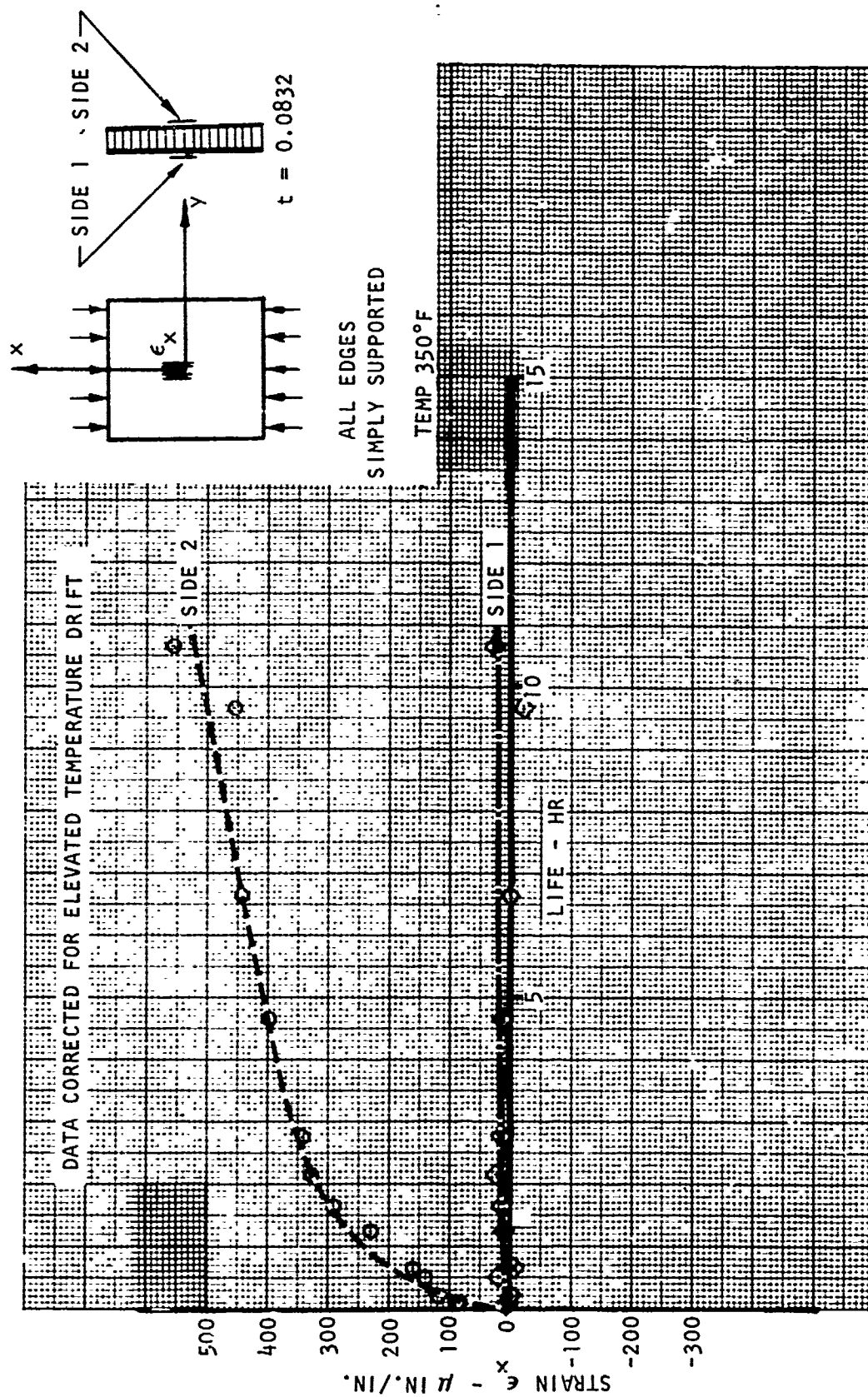
Figure 76. Midpoint Longitudinal Creep Strains from Back-to-Back
Gages, Panel 10A3E1
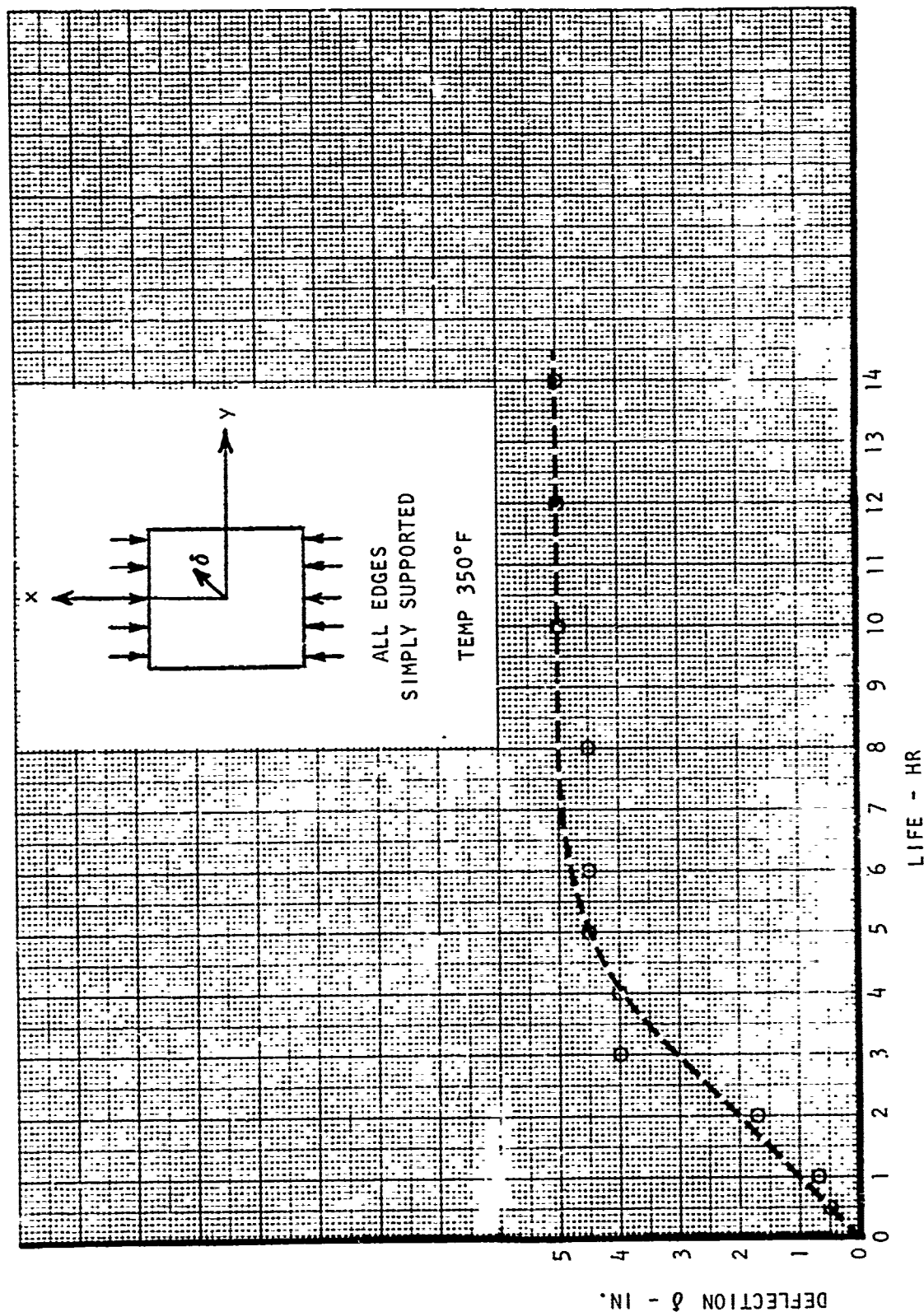
Figure 77. Midpoint Lateral Creep Deformation, Panel 10A3E2
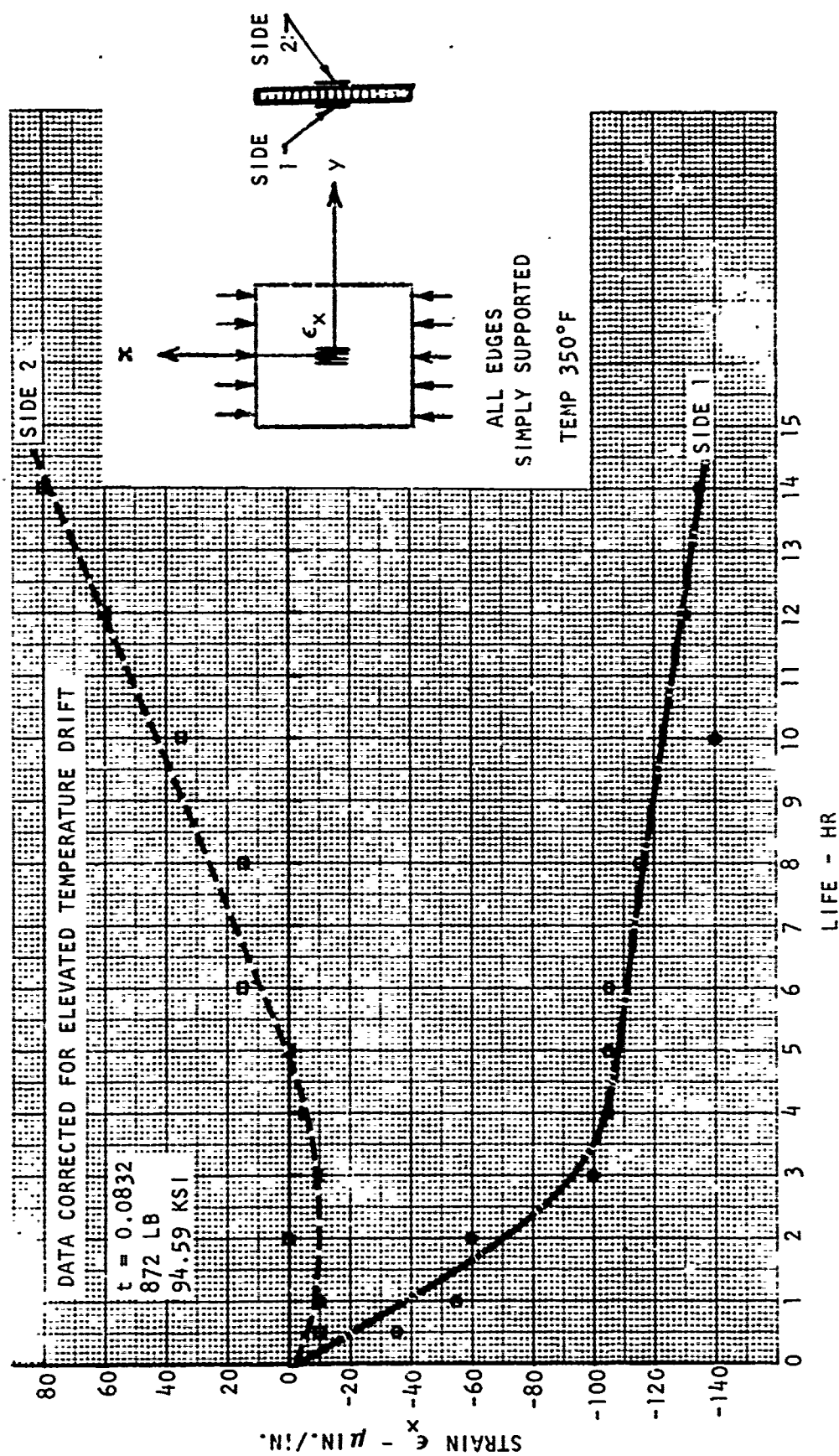
Figure 78. Midpoint Longitudinal Creep Strains From Back-to-Back Gages, Panel 10A3E2
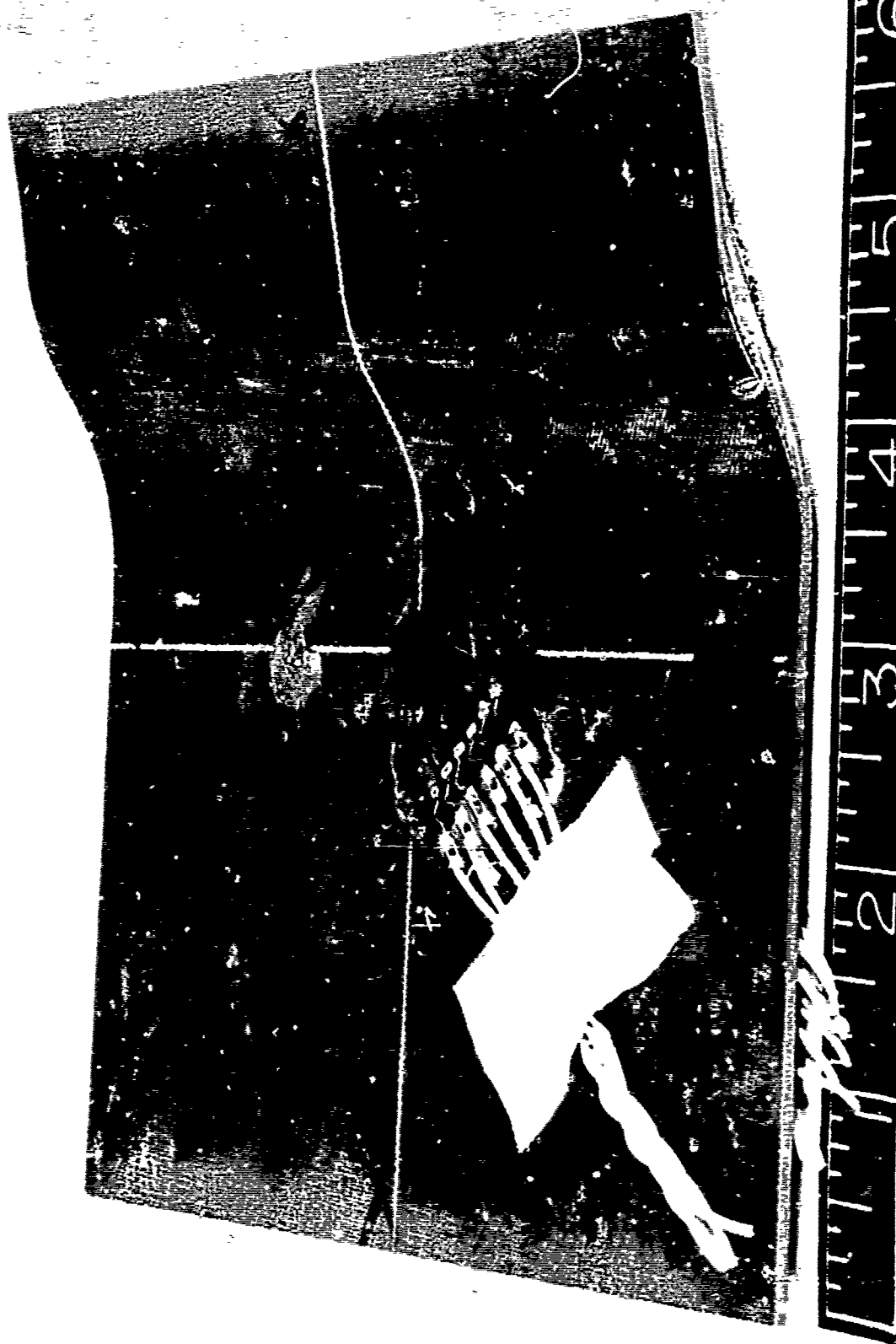
Figure 79. Panel 9A1E1 After Creep Buckling Failure
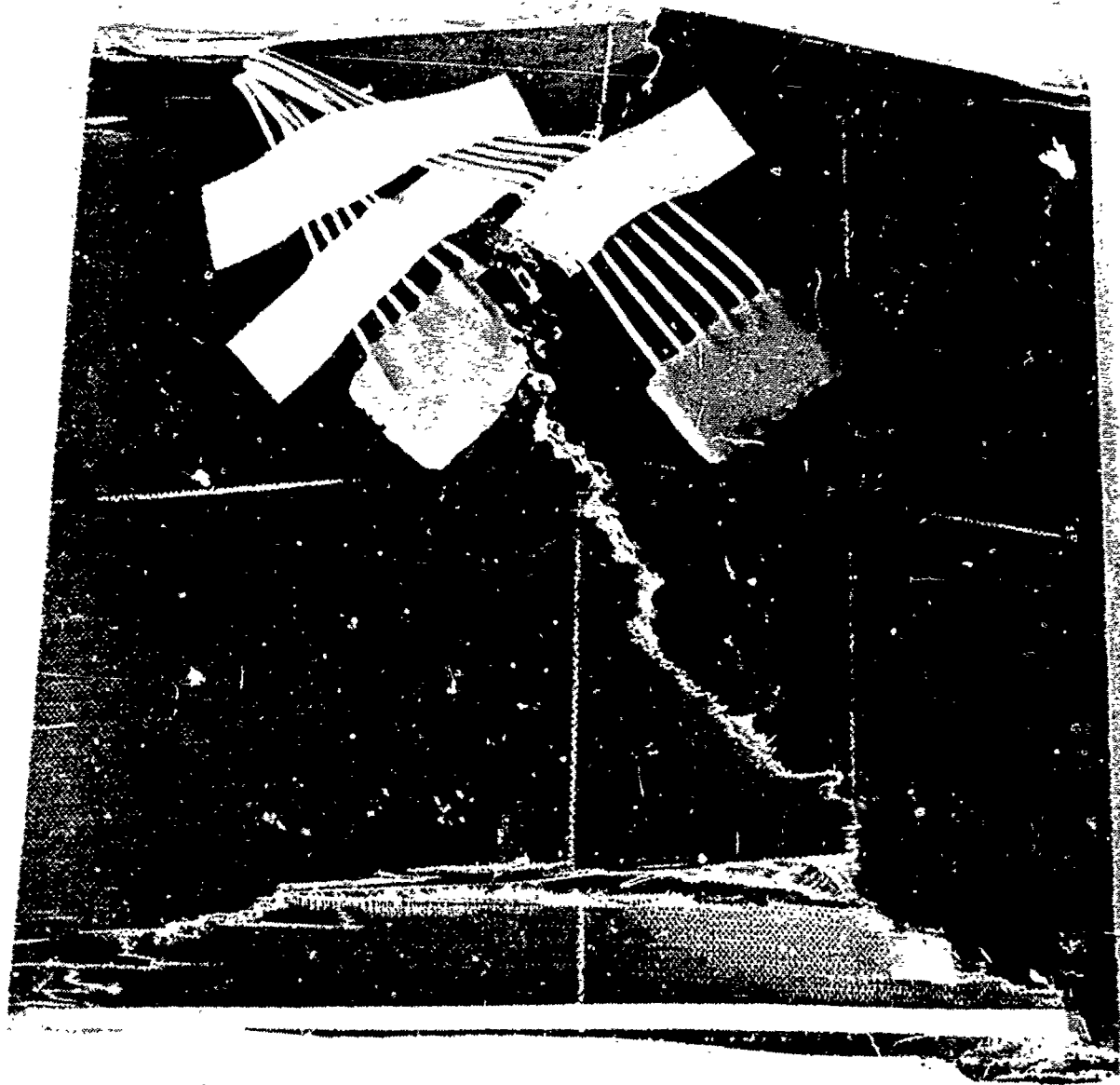
Figure 80. Panel 10A1E1 After Creep Buckling Failure

10A3E1

$[0/\pm45/0]_{2S}$

TEMP 350°F

ALL EDGES SIMPLY SUPPORTED

FAILURE: 980 LB/IN.

11,780 PSI

IN 11-18 HOURS

Figure 81. Panel 10A3E1 After Creep Buckling Failure
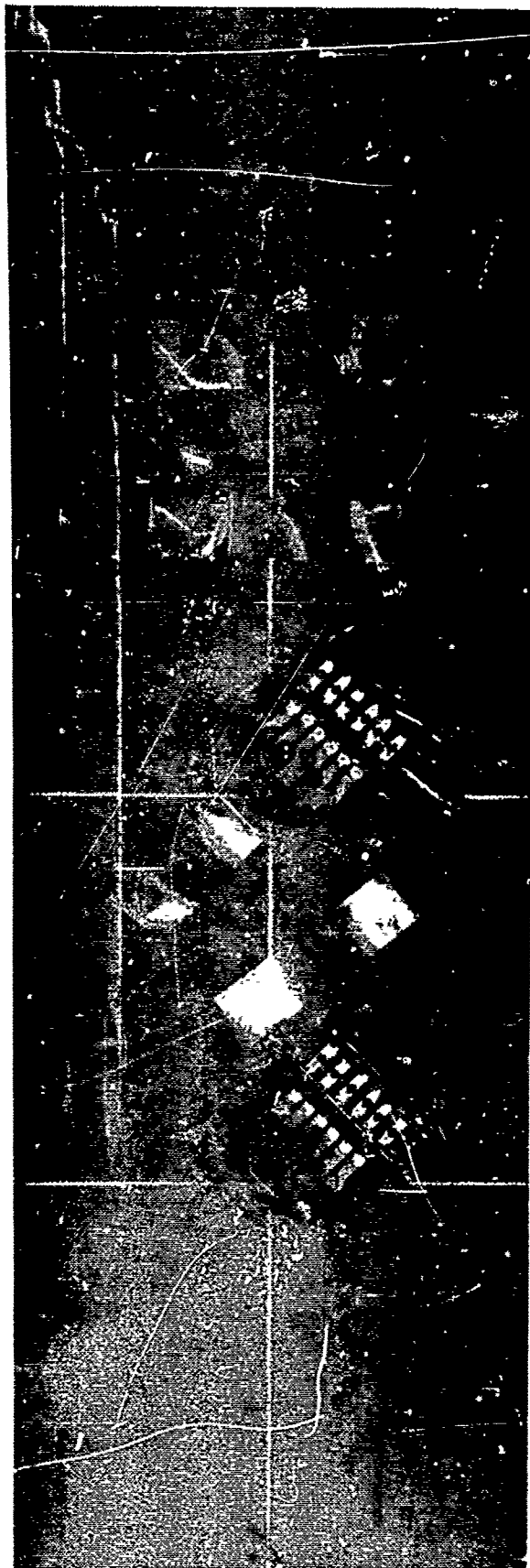
10A3E2

$[0/\pm45/0]_{2S}$

TEMP 350°F

ALL EDGES SIMPLY SUPPORTED

FAILURE: 875 LB/IN.
10,500 PSI

IN 14-22 HOURS

Figure 82. Panel 10A3E2 After Creep Buckling Failure

TABLE XII.   COMPOSITE ELEMENT STATIC TEST DATA

MATERIAL SYSTEM   Boron/Epoxy (5505)   PANEL NO.   9A3E1

LAMINATE ORIENTATION $[0/\pm45/0]_{2S}$

TYPE LOADING   Creep Buckling Column

ASPECT RATIO   3.0

EDGE SUPPORT   Loaded edges SS,
                        Lateral edges free

TEST TEMP   350°F
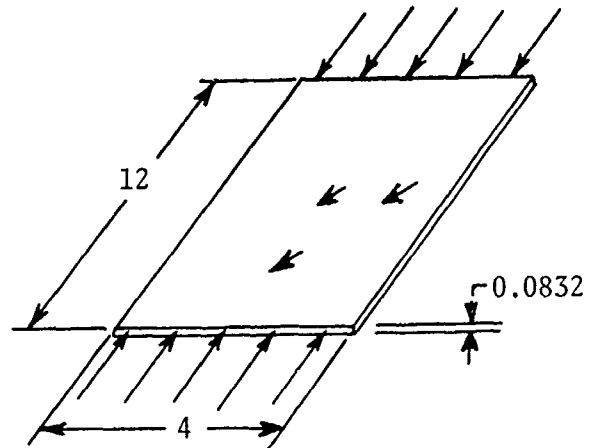
PANEL COUPON DATA   (350°F)

F_x = 92.59 Ksi E_x = 19.28 Msi F_y = 8.85 Ksi E_y = 2.74 Msi

ELEMENT TEST DATA

FAILING LOAD P_x = 140 lb

N_x = 35 lb/in.

F_x = 420.7 psi

TOTAL TIME TO FAILURE = 0.67 HOUR (40 MINUTES)

DATA FROM REPORT   L478-194   DATE   6-16-69

ORGANIZATION   NR/LAD

COMMENTS   Failure occurred after 40 minutes under load and prior to

taking initial creep readings.

104

CRIPPLING TESTS

Series 17A, 18A, 19A, 20C, 21D - Crippling Elements

Specimen series 17A, 18A, 19A, 20C, and 21D are grouped in this category. They consist of crippling elements of various cross-sections and edge conditions loaded in uniaxial compression. The purpose of these tests was to determine the ultimate strength of an element which fails in the local instability (crippling) mode.

The first two series, 17A and 18A, were conducted on the two basic shapes which can be combined to form any other desired shapes composed of straight elements; i.e., the one edge- and no-edge-free rectangular crippling elements, respectively. The series 19A, 20C, and 21D specimens are formed shapes. Series 20C and 21D are zee and hat sections, respectively, and were sized to fail in the crippling mode. Series 19A specimens were sized to determine the effect of length.

Figure 83 gives the geometry of the zee and hat specimens. The material properties data are given in tables I through III.

Table XIII show the results for the basic shapes; i.e., no- and one-edge-free rectangular elements for two temperatures, series 17A and 18A. The ultimate strength is compared to the buckling strength predictions given in Volume III. In general, sufficient data to determine the load at which the element actually buckled were not available. Therefore, the ultimate failure load is compared to the predicted buckling load. From these data it can be seen that there is a considerable amount of postbuckling load-carrying capacity. By assuming that the ultimate strength can be predicted by an equation of the form

$$F_{x,\ ult} = K\ E'\ (\tfrac{t}{b})^n$$

$$E's\ = \frac{E_x}{1 - \nu_{xy}\ \nu_{yx}}$$

where E' and t/b are known functions of the configuration and geometry, it can be seen that it suffices to determine K and n. Figure 84 shows a plot of the data, where it can be seen both that n = 1.21, and that the K's, which are a function of the boundary condition and temperature, can be conservatively used for the tests conducted.
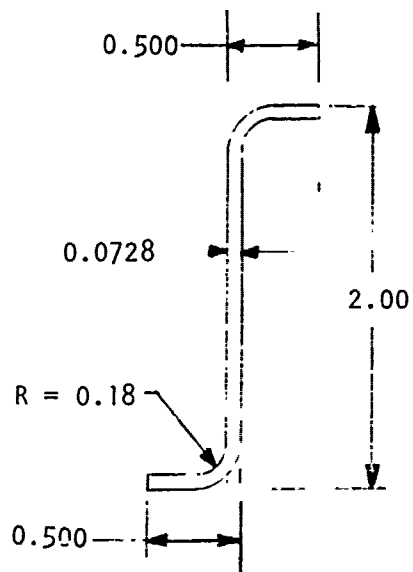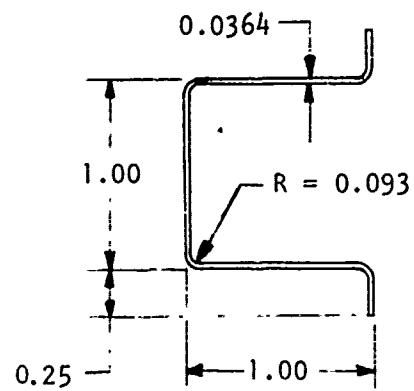
Figure 83. Cross-Sectional Geometry of Hat and Zee Crippling Elements

TABLE XIII. ANALYSIS OF BASIC SHAPES FOR CRIPPLING SPECIMENS

Specimen	Support*	Configuration	Temp (°F)	t (in.)	b (in.)	a (in.)	a/b	b/t	Test $n_{x,ult}$ (Kips/in.)	$f_{x,ult}$ (Ksi)	Theory F_{xcr} (Ksi)	$\frac{f_{x,ult}}{F_{xcr}}$
17A1RS1	SSSF	[0/±45/0]2S	RT	0.0832	1.25	6.25	5.00	15.0	2.89	34.7	22.2	1.563
2RS1	SSSF	[0/±45/0]2S	RT	0.0832	0.877	4.35	4.96	10.54	3.?	40.8	45.2	0.902
3RS1	CSCF	[0/±45/0]2S	RT	0.0832	0.7545	3.732	4.95	9.07	6.	78.4	61.1	1.283
1ES1	CSCF	[0/±45/0]2S	350	0.0832	1.252	6.225	4.97	15.05	1.82	21.9	20.8	1.052
2ES1	CSCF	[0/±45/0]2S	350	0.0832	0.878	4.35	4.95	10.6	2.70	32.4	42.2	0.767
3ES1	CSCF	[0/±45/0]2S	350	0.0832	0.750	3.73	4.97	9.0	4.95	59.5	57.8	1.029
18A1RS1	CSCS	[0/±45/0]2S	RT	0.0832	3.50	17.47	4.99	42.1	5.207	38.6	21.4	1.804
2RS1	CCCS	[0/±45/0]2S	RT	0.0832	2.508	12.46	4.97	30.1	4.29	51.6	41.0	1.259
3RS1	CSCF	[0/±45/0]2S	RT	0.0832	2.005	9.975	4.98	24.1	2.75	33.0	8.65	3.82
1ES1	CSCS	[0/±45/0]2S	350	0.0832	3.495	17.47	5.00	42.0	2.06	24.8	19.5	1.271
2ES1	CSCS	[0/±45/0]2S	350	0.0832	2.508	12.465	4.97	30.1	2.30	27.6	37.0	0.745
3ES1	CSCS	[0/±45/0]2S	350	0.0832	1.497	9.965	4.99	24.0	3.26	39.1	59.0	0.662
1R-RSC**	CSCS	[0]7T	RT	0.0364	3.690	18.46	5.00	101.4	0.67	18.4	2.0	9.2
2R-RSC	CSCS	[0]7T	RT	0.0364	2.405	11.98	4.98	66.1	1.0?	29.4	5.0	5.9
3R-RSC	CSCS	[0]7T	RT	0.0364	1.967	9.73	4.95	54.0	1.45	39.9	2.3	5.5
1E-RSC	CSCS	[0]7T	350	0.0364	2.640	13.16	4.99	72.5	0.494	13.6	2.2	6.2
2E-RSC	CSCS	[0]7T	350	0.0364	1.861	9.33	5.01	51.1	0.634	17.4	5.0	3.5
3E-RSC	CSCS	[0]7T	350	0.0364	1.521	2.57	4.97	41.8	0.644	17.7	7.8	2.3

*Support: C = clamped, S = simple support, F = free

**RSC = Rotated Scrim Cloth
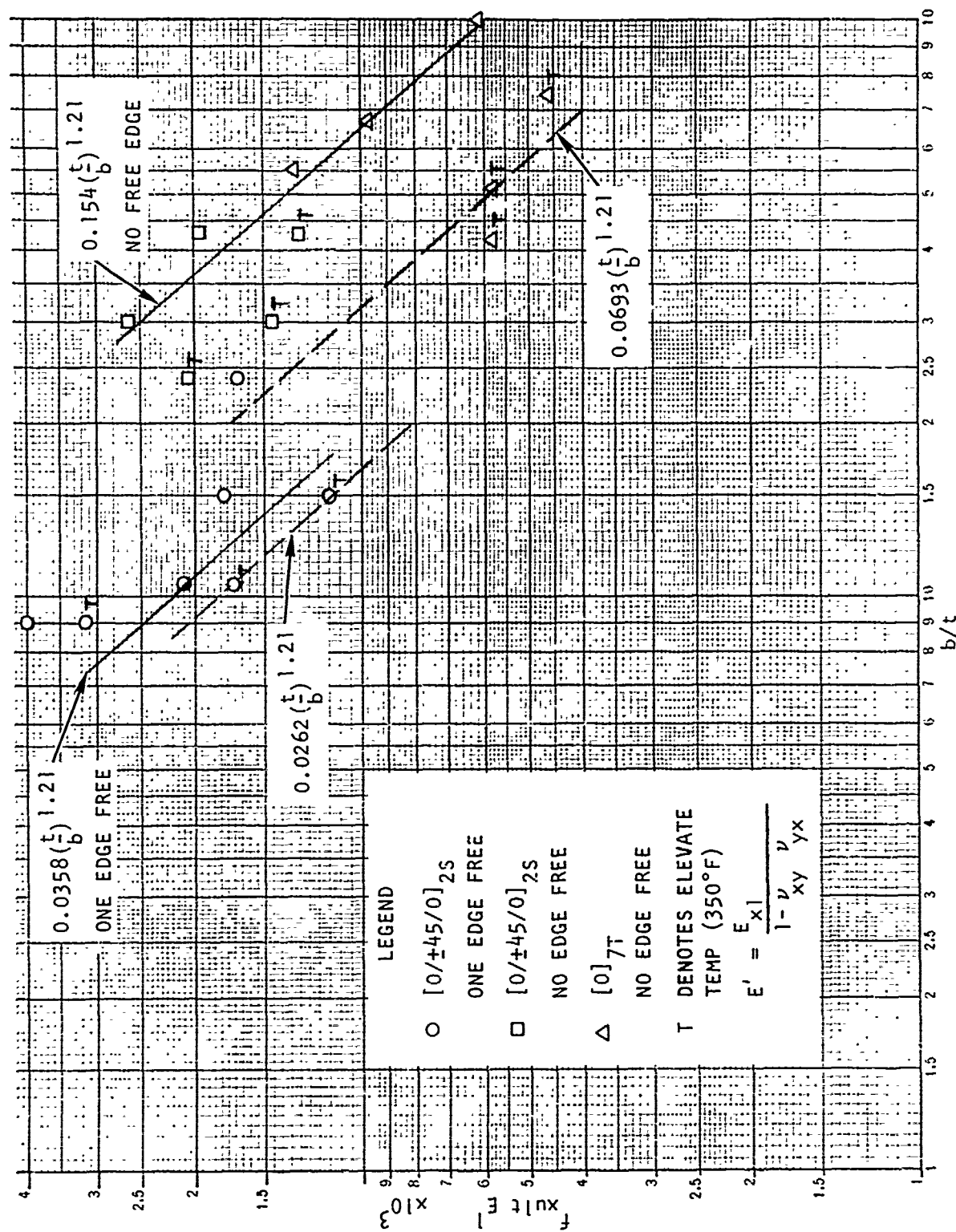
Figure 84. Ultimate Strength Prediction for Crippling Elements

108

Using these results to predict the strength of the composite shapes tested in series 19A, 20C, and 21D produces very unconservative results, as shown by table XIV and figure 85, except in the cases where the lengths are very short. The reason for this anomaly is that the curved portion of the composite shapes does not produce the necessary fixity. Thus, it is recommended that any further testing be conducted on the premise that the basic element shapes are angles and channels, rather than the less realistic rectangular plates. Figures 86 through 92 show the failed test specimens.

TABLE XIV. CRIPPLING TESTS ANALYSIS AND DATA

Specimen	Type	Configuration	t (in.)	Temp (°F)	E (Msi)	One-Edge-Free Elements					No-Edge-Free Elements					λ	L	Theory Fcc (Ksi)	Test Fcc (Ksi)	f_{cc}/F_{cc}
						No	b_1 (in.)	b_1/t	A_1 (in.²)	Fcc1 (Ksi)	No	b_2 (in.)	b_2/t	A_2 (in.²)	Fcc2 (Ksi)					
19-1	Hat	[0/±45/0]_2s	0.0416	RT	0.54x10⁶	2	0.236	5.9	0.0205	81.5	3	0.908	21.8	0.1132	71.7	0.1337	2.91	73.3	41.2x10³	0.562
-2																	2.96		65.0	0.887
-3																	2.95		60.3	0.823
-4																	1.96		63.0	0.860
-5																	1.97		62.0	0.858
-6																	1.45		109.8	1.498
-7																	1.46		116.2	1.586
-8																	1.50		102.2	1.395
20C1R-S1	Zee	[0]_14	0.0728	RT	30.02	2	0.417	5.75	0.0607	126.0	1	1.834	25.2	0.1336	93.0	0.1943	---	103.1	36.1	0.355
R-S2				RT	30.02					126.0					93.0		---	103.1	39.7	0.385
T-S1				550	29.96					94.8					41.7		---	58.4	25.6	0.438
2R-RS1*				RT	30.02					126.0					93.0		---	103.1	48.1	0.468
2R-RS2*				RT	30.02					126.0					93.0		---	103.1	46.5	0.451
2I-RS1*				550	29.96					94.8					41.7		---	58.4	35.3	0.605
21D1R-S1	Hat	[0]_7	0.0364	RT	30.02	2	0.244	6.71	0.0177	107.3	3	0.916	25.2	0.0998	93.0	0.1175	5.25	95.1	32.4	0.340
1R-S2				RT	30.02					107.3					93.0			95.1	32.3	0.339
1R-T1				550	29.96					78.6					41.7			47.2	22.6	0.479
2R-RS1*				RT	30.02					107.3					93.0			95.1	37.8	0.398
2R-RS2*				RT	30.02					107.3					93.0			95.1	40.9	0.130
2I-RS1*				550	29.96					78.6					41.7			47.2	25.8	0.547

*Rotated Section 16th

110
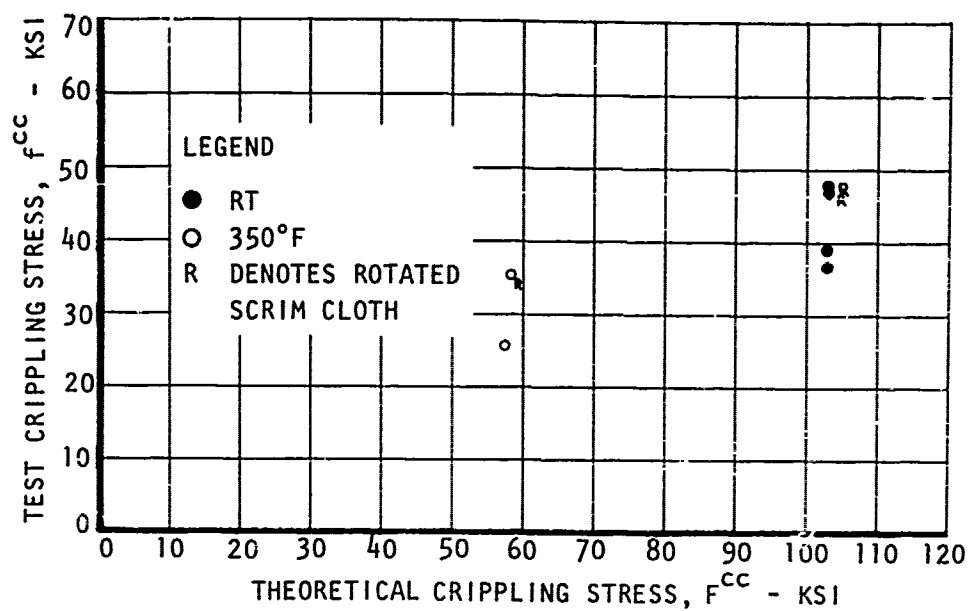
(A) Zee Section
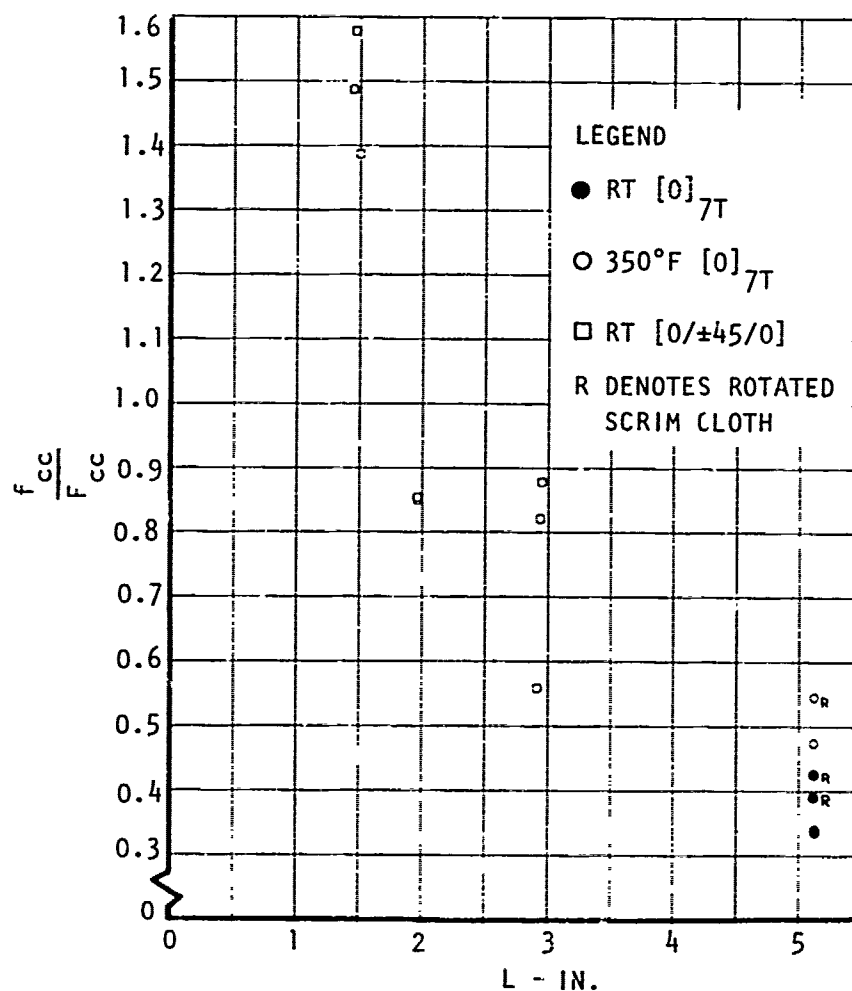
(B) Hat Section

Figure 85. Test Data Versus Theory for Zee and Hat Stiffener Elements

Figure 86. Specimens 17ARS1 After Failure
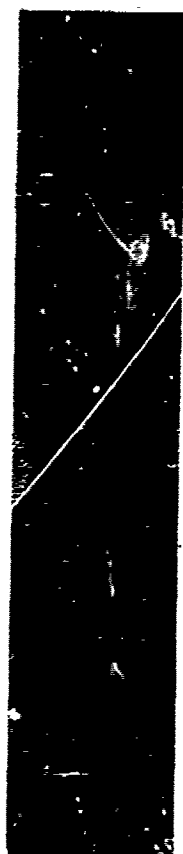
Figure 87. Specimens 18ARS1 After Failure
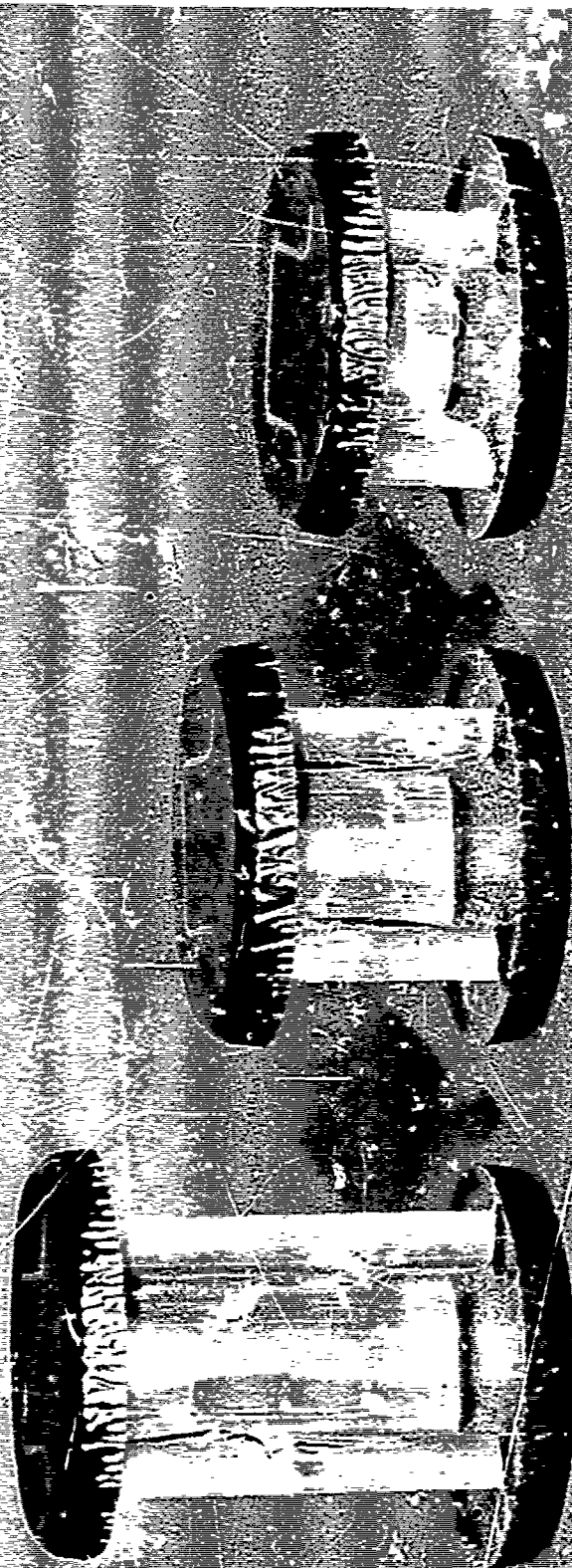
Figure 88. Typical Hat-Section Crippling Specimens After Failure

20C1E-S1
$[0]_{14T}$
350°F
5,010 LB
35,600 PSI

20C1R-S2
$[0]_{14T}$
RT
7,780 LB
39,700 PSI

20C1F-S1
$[0]_{14T}$
RT
7,140 LB
36,400 PSI

Figure 89. Standard-Scrim Zee Stiffeners, 20C1 Series, After Crippling Failure
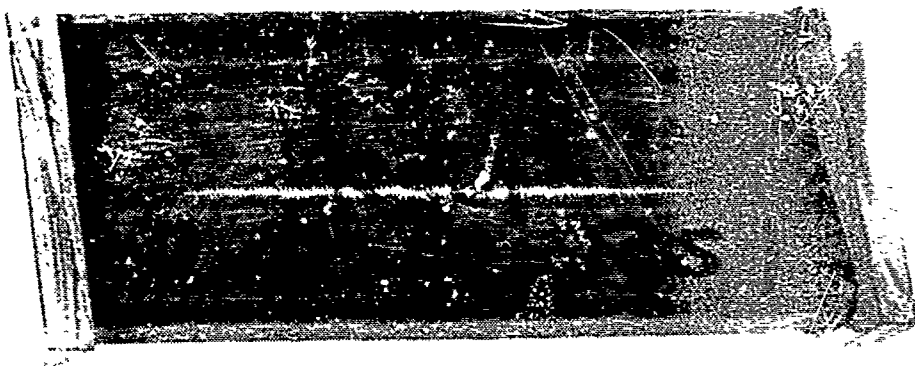
20C2R-RS1
[0]$_{14T}$ - ROTATED SCRIM

RT
9,420 LB
48,100 PSI

20C2R-RS2
[0]$_{14T}$ - ROTATED SCRIM

RT
9,130 LB
46,500 PSI
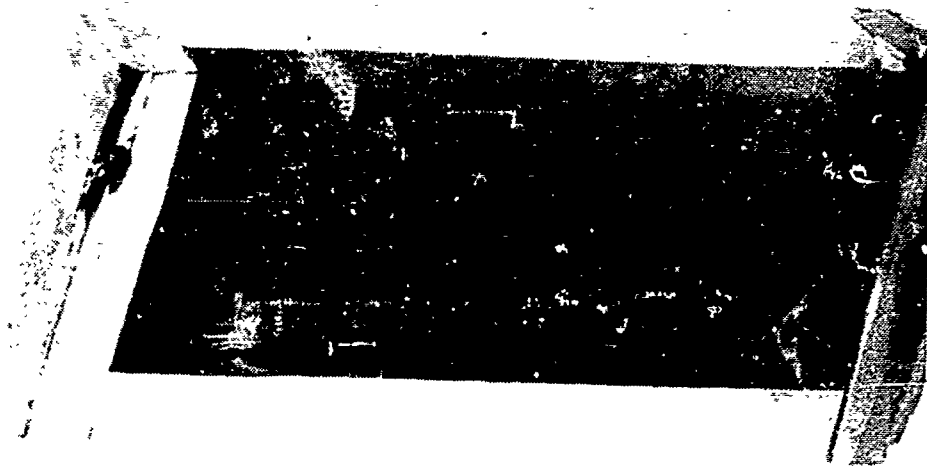
20C2E-RS1
[0]$_{14}$ - ROTATED SCRIM

350°F
6,930 LB
35,300 PSI

Figure 90. Rotated-Scrim Hat Stiffeners, 20C2 Series, After Crippling Failure

21D1E-S1
[0]$_{7T}$
RT
2,665 LB
22,600 PSI

21D1R-S1
[0]$_{7T}$
RT
3,810 LB
32,300 PSI

21D1R-S1
[0]$_{7T}$
RT
3,820 LB
32,400 PSI

Figure 91. Standard-Scrim Hat Stiffeners, 21D1 Series, After Crippling Failure

117

21D2R-RS2
[0]$_{7T}$ - ROTATED SCRIM
RT
4,815 LB
45,900 PSI

21D2R-RS1
[0]$_{7T}$ - ROTATED SCRIM
RT
350°F
3,050 LB
25,800 PSI

21D2R-RS1
[0]$_{7T}$ - ROTATED SCRIM
RT
4,460 LB
37,800 PSI
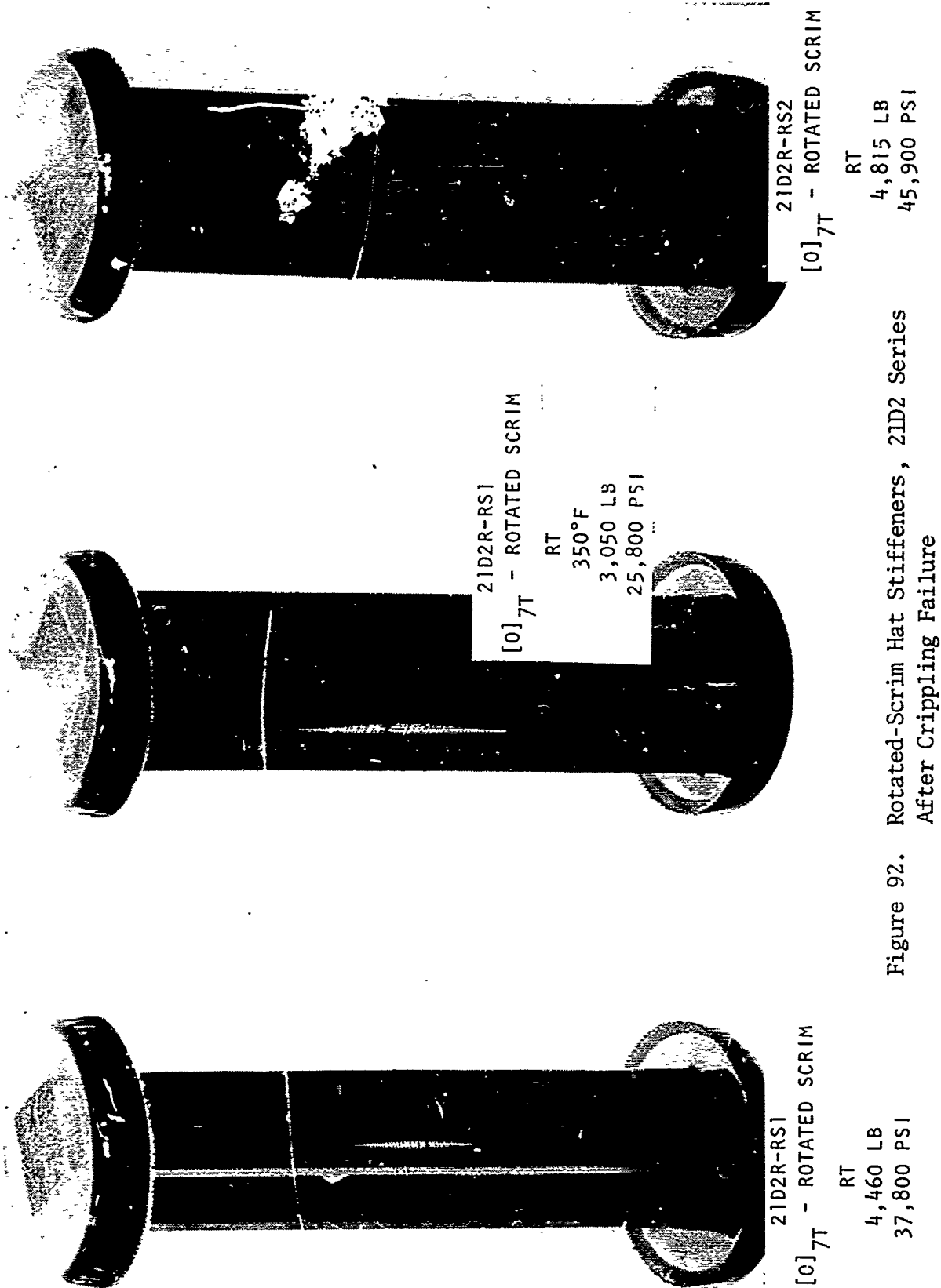
Figure 92. Rotated-Scrim Hat Stiffeners, 21D2 Series
After Crippling Failure

CUTOUT TESTS

Specimen series 22A, 23A, and 24A are grouped in this category. They consist of rectangular panels within which is a circular cutout. They were loaded in tension, compression, and shear, respectively. The tension panels were unsupported on the unloaded edges, while the compression and shear panels were simply supported on all four sides. The purpose of these tests was to determine the stress distribution within the panels, as well as the effects of this distribution on the ultimate strength. Table XV and figures 93 and 94 show the geometric and testing data for the panels.

TABLE XV.   CUTOUT SPECIMENS GEOMETRY

Specimen	a (in.)	b (in.)	D (in.)	Configuration	Test Type	t (in.)	Temp (°F)
22A1R1	12.0	6.0	2.0	$[0/\pm45/0]_S$	Tension	0.0416	RT
22A1R2			2.0				RT
22A1E1			2.0				350
22A2R1			0.5				RT
22A2R2			0.5				RT
22A2E1			0.5				350
23A1R1	6.0	6.0	2.0	$[0/\pm45/0]_{2S}$	Compression	0.0832	RT
23A1R2			2.0				RT
23A1E1			2.0				350
23A2R1			0.5				RT
23A2R2			0.5				RT
23A2E1			0.5				350
24A1R1	6.0	6.0	2.0	$[0/\pm45/0]_{2S}$	Shear	0.0832	RT
24A1R2			2.0				RT
24A1E1			2.0				350
24A2R1			0.5				RT
24A2R2			0.5				RT
24A2E1			0.5				350
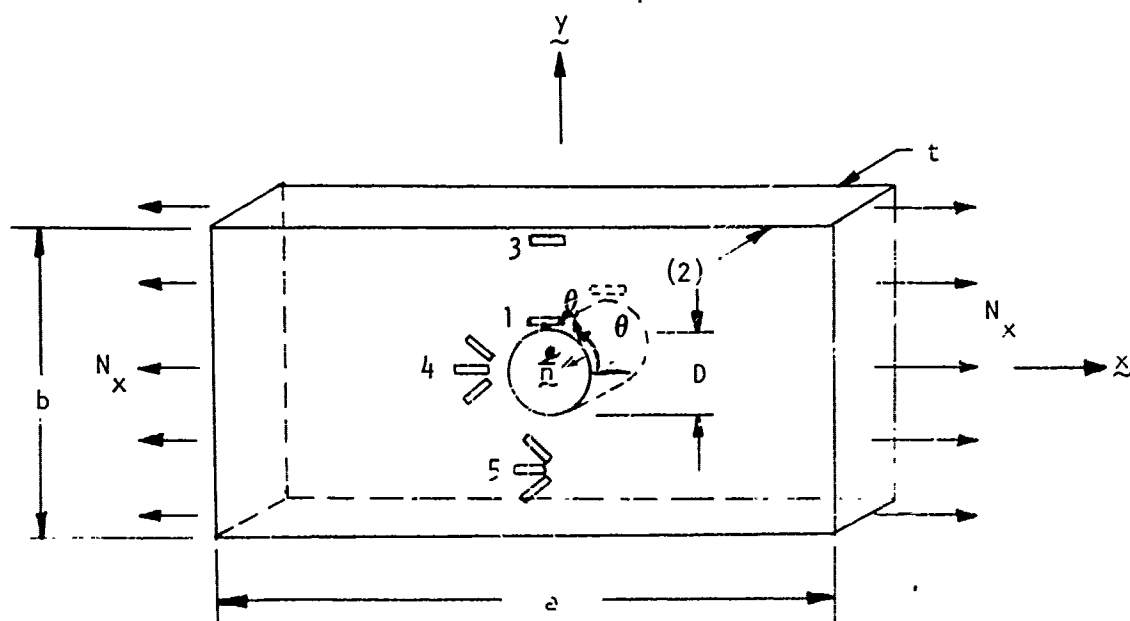
Figure 93. Flat Orthotropic Laminate With a Circular Hole, Uniaxially Loaded
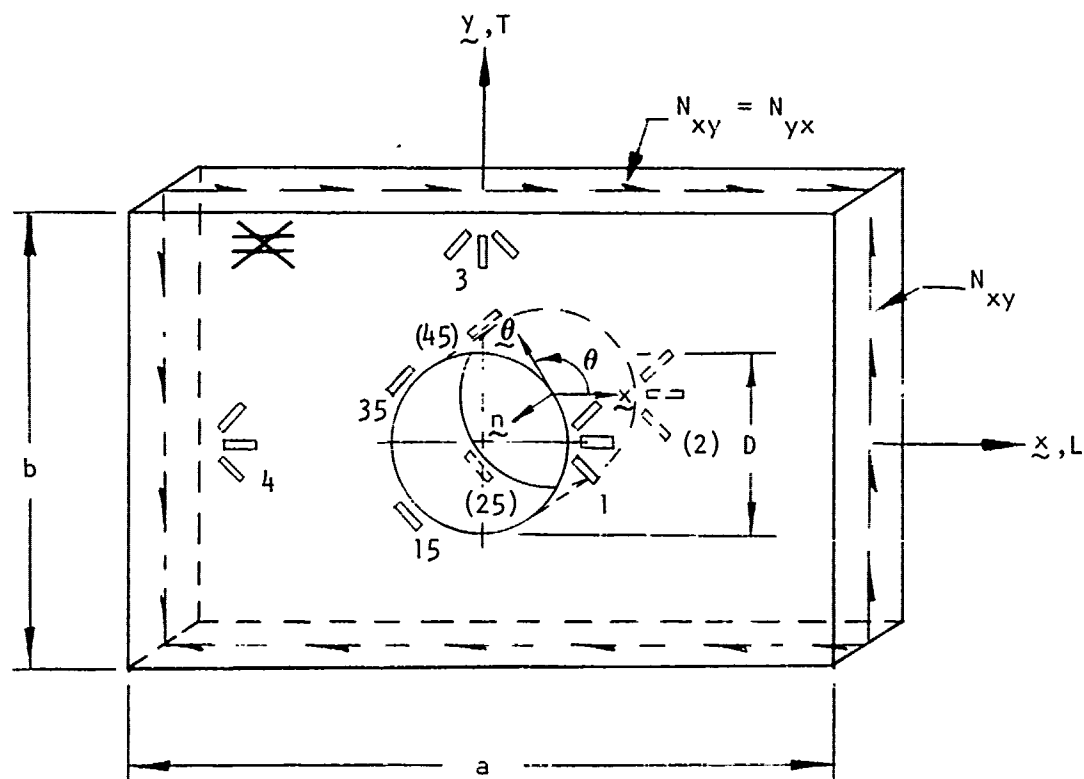
Figure 94. Flat Orthotropic Laminate With a Circular Hole,
Inplane Shear Loading

Series 22A and 23A - Tension and Compression Panels With Circular Cutouts

Stress Distribution

Reference 2 was used to predict the stress concentration factors. At the edge of the hole, the stresses are

$$\sigma_\theta = \frac{E_\theta}{E_x} \left[\psi \cos^2 \theta + (1 + n) \sin^2 \theta \right] \frac{N_x}{t}$$

$$E_\theta = E_x \Big/ \left[\sin^4 \theta + 2\rho \sin^2 \theta \cos^2 \theta + \cos^4 \theta \right]$$

$$\psi = E_x/E_y \qquad\qquad n = \sqrt{2 \ (\psi - \nu_{xy}) + E_x/G_{xy}}$$

for an infinitely wide plate with a cutout. In order to account for a finite width, the stresses were modified using Savin's results, which were derived for an isotropic material. $K_{tb}/K_{t\infty}$ (Reference 2, figure 6.3.2.3) is a reduction of the stress concentration factor based on net area stresses. Particular values are given in table XVI. Stress concentration factors are thus given in the form

$$K_{1x} = \frac{\sigma_{1x}}{\sigma_a}$$

where σ_{1x} is the predicted stress at gage 1 (see figure 93), in the x direction and σ_a is the applied stress based on net area at the cutout. Thus, the stress concentration factor becomes

$$K_{1x} = \frac{\sigma_{0°}}{\frac{N_x}{t} (\frac{b}{b-D})} \quad \frac{K_{tb}}{K_{t\infty}}$$

where $K_{tb} = K_{tb} (D/b)$. Other stress concentration factors were obtained in the same manner.

The predictions are based on the premise that strain gages 1, 2, and 4 are located at the edge of the hole, whereas they are actually 1/4 inch away. On the basis of this premise, the predicted stress concentration factors K_{iI} are:

$$K_{1x} = K_{2x} = 1 + n$$

$$K_{4y} = -1/\psi$$

In addition we see that:

$$K_{3x} \cong 1 \qquad K_{4xy} = 0 \qquad K_{4x} = 0 \qquad K_{5x} \cong 1$$

Table XVI presents the predicted stress concentration factors, while table XVII compares the test data for these panels.

The following conclusions can be drawn:

1. The data for gages 1 and 2 are in good agreement with the theory, considering that the gages are not located at the edge of the cutout. It is not possible, at the present time, to rectify this disparity other than by stating qualitatively that the stress concentration factors at the gage locations are less than those at the edge of the hole. There is no significant difference between tension or compression loading. The elevated temperatures data are somewhat higher than the room temperature data.

2. The data for strain gages 3 and 5 appear to be quite good. Gage 3 for the compression panels is somewhat low because of edge effects.

3. The data for strain gage 4 are quite good for the tension specimens. The correlation for the compression panels is not as good, although the trends indicate that the theory need not be changed.

TABLE XVI

PREDICTED STRESS CONCENTRATION FACTORS

Specimen	ψ	n	$K_{1x\,\infty}$, $K_{2x\infty}$	$K_{tw}/K_{t\infty}$	K_{1x}, K_{2x}	K_{4y}
22A1R1,2	1.817	2.472	3.47	0.77	2.67	-0.55
22A1E1	2.022	2.516	3.52	0.77	2.71	-0.49
22A2R1,2	1.817	2.472	3.47	0.93	3.23	-0.55
22A2E1	2.022	2.516	3.52	0.93	3.27	-0.49
23A1R1,2	1.817	2.472	3.47	0.77	2.67	-0.55
23A1E1	2.022	2.516	3.52	0.77	2.71	-0.49
23A2R1,2	1.817	2.472	3.47	0.93	3.23	-0.55
23A2E1	2.022	2.516	3.52	0.93	3.27	-0.49

$K_{3x} = 1$

$K_{4x} = 0$

$K_{4xy} = 0$

$K_{5x} = 1$

$K_{iIa} = \dfrac{\sigma_{iI}}{\sigma_a}$ for a plate of width a

Failure Analysis

Three prediction techniques are used to evaluate the tensile test data. The various predicted strengths, P, in terms of the applied load are:

1. P_∞ - The load when the maximum tensile stress is F^{tu} for stress concentration factors based on an infinitely wide plate.

$$P_\infty = F^{tu}A_n/K_{ix}$$

A_n is the net area

TABLE XVII.

TEST VS PREDICTED STRESS CONCENTRATION FACTORS FOR UNIAXIALLY LOADED PLATES WITH CUTOUTS

Specimen	Predicted						Datum $(\sigma_a$, Ksi)	Test				
	D/b	K_{1X}	K_{2X}	K_{3X}	K_{4y}	K_{5X}		K_{1X}	K_{2X}	K_{3X}	K_{4y}	K_{5X}
22A1R1	0.333	2.67	2.67	1.00	-0.55	1.00	12	2.08	2.05	0.65	-0.37	0.85
1R2	0.333	2.67	2.67	↓	-0.55	↓	12	2.23	1.74	0.85	-0.37	0.91
1E1 *	0.333	2.71	2.71		-0.49		12					
2R1	0.083	3.23	3.23		-0.55		17	1.52	1.38	1.20	-0.34	0.80
2R2	0.083	3.23	3.23		-0.55		17	1.56	1.60	1.25	-0.39	0.85
2E1	0.083	3.27	3.27		-0.49		17	2.94	2.30	1.90	-0.19	2.30
23A1R1	0.333	2.67	2.67		-0.55		-4.5	1.30	2.20	0.45	-0.28	0.95
1R2	0.333	2.67	2.67		-0.55		-4.5	2.35	1.86	0.18	-0.25	1.16
1E1	0.333	2.71	2.71		-0.49		-4.5	2.35	2.46	0.40	+0.02	0.74
2R1	0.083	3.23	3.23		-0.55		-4.4	1.12	1.40	0.73	-0.30	1.00
2R2	0.083	3.23	3.23		-0.55		-4.4	2.49	0.96	0.69	-0.22	2.00
2E1	0.083	3.27	3.20	1.00	-0.19	1.00	-4.4	2.40	0.32	0.48	-0.26	1.56

* Strain gage malfunction

2. P_b - The load when the maximum tensile stress is F^{tu} for stress concentration factors based on a plate of width b.

$$P_b = F^{tu} A_n / K_{1xb}$$

3. P_n - The load when the tensile stress based on uniform distribution across the net area is F^{tu}.

$$P_n = F^{tu} A_n$$

Table XVIII and figure 95 summarize the results. The following conclusions are drawn:

1. None of the foregoing prediction techniques are very good; however, P_b is much better than the other two.

2. The net area stress technique, P_n, is grossly unconservative.

3. As D/b decreases, P_b becomes more conservative.

4. As temperature increases, P_b becomes more conservative.

The method used to obtain the various stress concentration factors is given in reference 2 and the previous paragraphs on stress distribution, where the maximum tensile stress is known to occur at the edge of the hole near strain gages 1 and 2. See figure 94.

The test data show that there is some redistribution of stresses due to inelastic deformations. However, because of the brittleness of the material, the effects of stress concentration must be considered. Because of the paucity of test results, it is recommended at this time that method 2 (i.e., the maximum tensile stress, including the effects of stress concentration factors based on a plate of finite width, attains F_{tu}) be used to determine the strength of a panel with a circular cutout. As more test data become available, this criterion will be modified to include the effects of small D/b.

Three prediction techniques are used to evaluate the compression test data. The various predicted strengths, P, in terms of the applied load are:

1. $\overline{P}^{cy}$ - The "effective width" technique, as proposed by Von Kármán, reference 3, is valid; i.e., the edges of the panel attain a stress

125

TABLE XVIII. TENSILE TEST DATA

Specimen	D/b	b_n (in.)	A_n (in.^{2})	F^{tu} (Ksi)	P_∞ (lb)	P_b (lb)	P_n (lb)	P_f (lb)	P_f/P_∞	P_f/P_b	P_f/P_n
22A1R1	0.333	4.0	0.1664	103.0	4.94	6.42	17.15	7.80	1.578	1.214	0.456
1R2	0.333	4.0	0.1664	103.0	4.94	6.42	17.15	7.90	1.599	1.230	0.461
1E1	0.333	4.0	0.1664	91.5	4.33	5.62	15.23	8.90	2.055	1.583	0.584
2R1	0.083	5.5	0.2288	103.0	6.79	7.30	25.5	13.85	2.039	1.897	0.590
2R2	0.083	5.5	0.2288	103.0	6.79	7.30	23.5	14.40	2.120	1.972	0.613
2E1	0.083	5.5	0.2288	91.5	5.95	6.40	20.9	13.80	2.319	2.156	0.660

P_f is the measured load at failure.

P_∞, P_b, P_n are defined in the foregoing text.
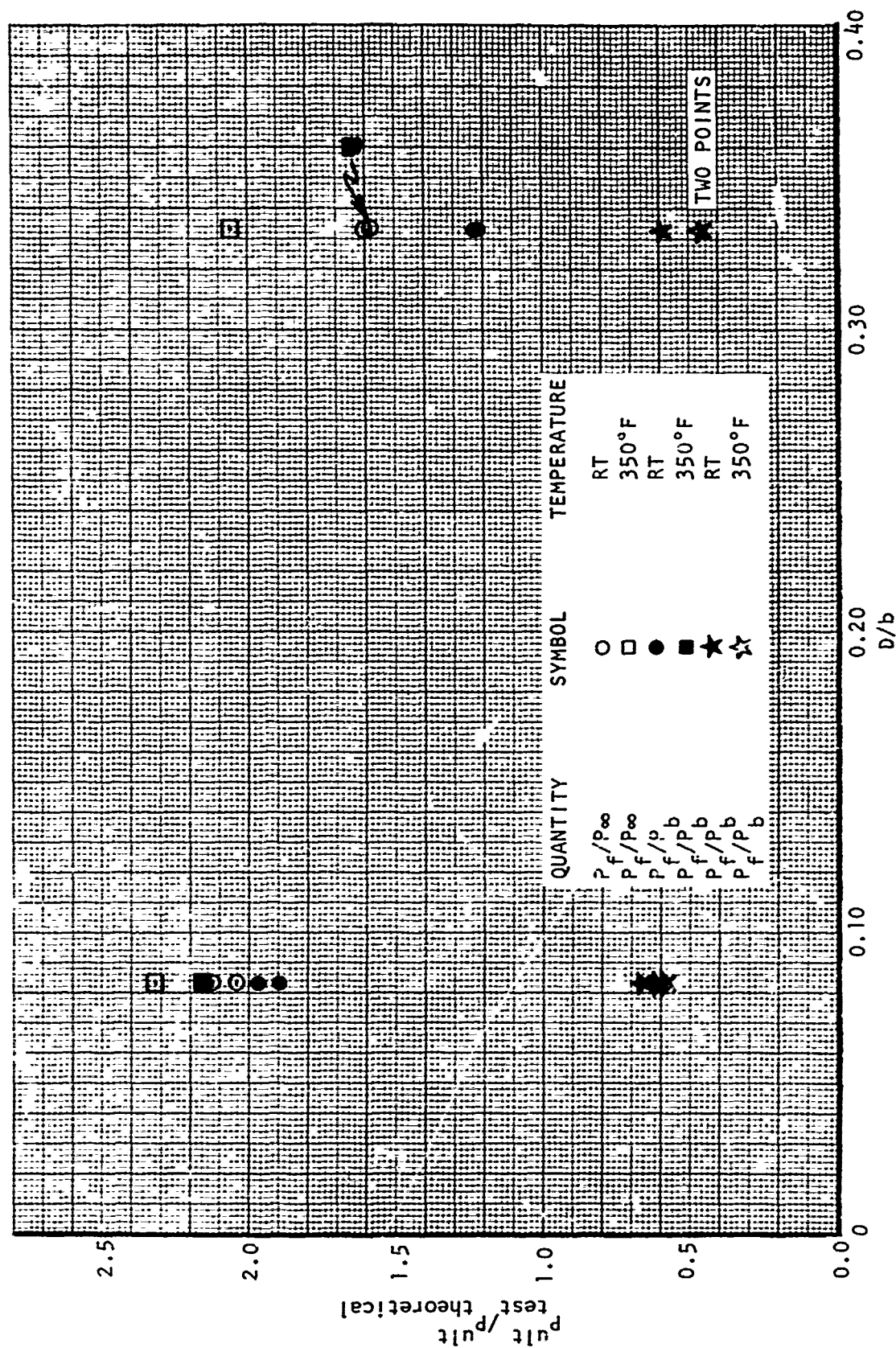
Figure 95. Test Data Versus Theory Comparison for Three Prediction Techniques

127

of F^{cy} for a width of b^{cy}, where b^{cy} is the width of a simply supported panel which can attain a stress of F^{cy}. The rest of the panel at the net cross-section attains a stress of F^{ccr}, where F^{crr} is the stress at which the panel without a hole will buckle.

$$\bar{P}^{cy} = F^{cy} b^{cy} t + F^{ccr}(b_n - b^{cy}) t$$

$$b_n = b - D$$

b^{cy} = width at which a panel without a hole and of length, L, would attain a strength of F^{cy}. See figures 100 and 101.

2. P_e - The "effective-width" technique is used but the edge stress is assumed to be that stress corresponding to the test measured b_e acting on a width of b_e. The remainder of the net cross-section attains a stress of F^{ccr}.

F^{ccr} = stress at which a panel of length, L, and width, W, would buckle.

$$P_e = F_e^{cr} b_e t + F^{ccr}(b_n - b_e) t$$

b_e = measured effective width

F_e^{cr} = stress at which a panel of width b_e and length L would buckle.

3. P^{cr} - The panel fails when the stress, based on a uniform distribution across the net section, attains F^{ccr}.

$$P^{cr} = F^{ccr} b_n t$$

Table XIX and figure 96 summarize the results. The results for the 1A specimens, which are similar to the 23A specimens, except that there is no cutout, are included so that the postbuckling strength of a panel with a cutout could be considered independently.

The following conclusions are drawn:

1. The Von Kármán effective-width approach appears to be quite promising, although the results are extremely unconservative.

TABLE XIX. COMPRESSION TEST DATA

Specimen	D/b	A_n (in²)	b^{CY} (in.)	F^{CCR} (Ksi)	b_e (in.)	F_e^{cr} (Ksi)	P^{CY} (Kips)	P_e (Kips)	P^{cr} (Kips)	P_f (Kips)	P_f/P^{CY}	P_f/P_e	P_f/P^{cr}	P_f/P^{CY}
23A1R1	0.333	0.5328	1.08	8.0	2.23	53.0	22.76	11.01	2.66	7.44	0.327	0.675	2.79	1.31
23A1R2	0.333	0.5328	1.08	8.0	2.20	55.0	22.76	11.27	2.66	6.01	0.292	0.590	2.50	1.17
23A1E1	0.333	0.5328	1.414	7.5	1.71	92.0	16.88	14.52	2.50	6.00	0.355	0.413	2.40	1.42
23A2R1	0.083	0.4576	1.08	8.0	2.22	53.0	23.76	11.97	3.66	7.50	0.315	0.626	2.05	1.26
23A2R2	0.083	0.4576	1.08	8.0	2.34	52.5	23.76	12.32	3.66	6.78	0.285	0.550	1.85	1.14
23A2E1	0.083	0.4576	1.414	7.5	1.59	106.0	17.82	16.46	3.43	6.01	0.337	0.365	1.75	1.35
1A1R1	0	0.4992	1.08	8.0	2.38	50.0	24.09	11.31	3.99	7.82	0.324	0.691	1.96	1.30
1A1E1	0	0.4992	1.414	7.5	2.00	67.0	18.15	13.65	3.74	5.96	0.328	0.456	1.59	1.31
1A2R1	0	0.3328	1.08	17.8	---	---	---	---	5.92	6.48	0.257	---	1.094	1.03
1A3R1	0	0.3328	1.08	17.8	---	---	25.14	---	5.92	---	---	---	---	---
1A3E1	0	0.5328	1.08	16.5	1.25	175.0	24.85	21.98	5.49	5.91	0.238	0.268	1.076	0.95

P_f is the measured load at failure.

129
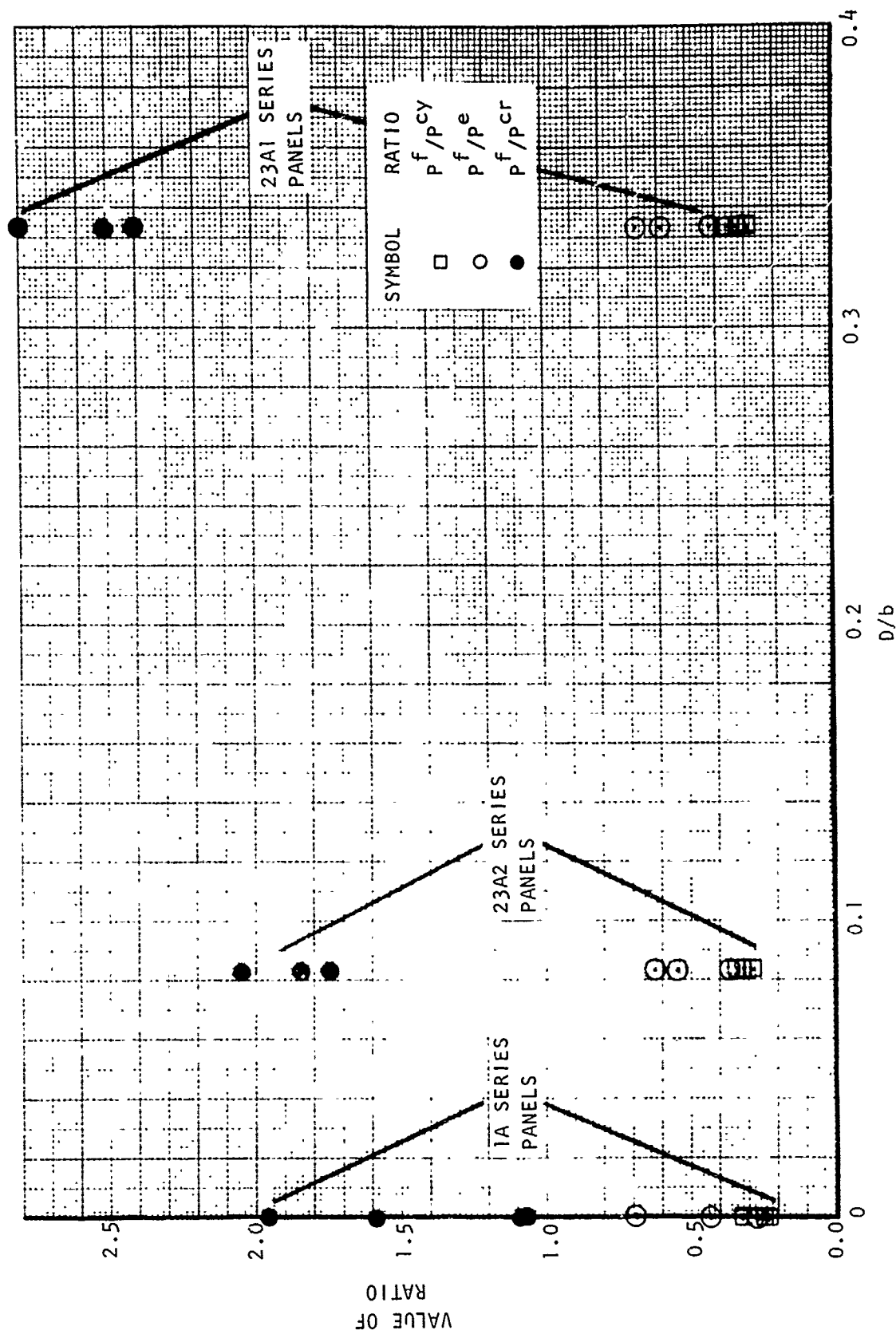
Figure 96. Panel Compression Test Data - Cutouts

Note that P_f/P^{cy} is almost a constant (figure 96). We see that for the geometry and material tested here, the following equation can be used for design:

$$P^{cy} = \gamma \overline{P}^{cy}$$

$$\gamma = .25$$

More tests are required to determine γ for other geometric and material combinations.

2. The Von Kármán effective-width approach using measured effective width looks promising. Future studies involving this approach may prove fruitful.

Figure 97 is a plot of P_f/P^{cy}. Figures 98 and 99 are plots of the test versus theoretical effective widths and test versus theoretical buckling stress based on the "top-of-the-knee" method. Figures 100 and 101 show a plot of F^{ccr} versus b/t.

Series 24A - Shear Panels With Circular Cutouts

Reference 2 was used to predict stress concentration factors. The stresses at the edge of the hole are

$$\sigma_\theta = \frac{E_\theta}{2\,E_x} \ (1 + n + \psi) \ \sin 2\theta \frac{N_{xy}}{t}$$

where n and ψ have been previously defined. The effects of finite width are considered in the same manner as for the uniaxially loaded plates. The stress concentration factors are thus:

$$K_{ix} = \frac{\sigma_{ix}}{\dfrac{N_{xy}}{t}\left(\dfrac{b}{b-D}\right)} \cdot \frac{K_{tb}}{K_{t\infty}}$$

Table XX compares the theoretical versus test stress concentration factors for N_{xy} = 166.7 lb/in.

The failure prediction criteria used are:

1. V_T is such that failure is due solely to the transverse stress, σ_T, at $\theta = 60°$. The stress concentration at this point is $K_\theta = 1.77$ at room temperature and 1.50 at 350°F.

131
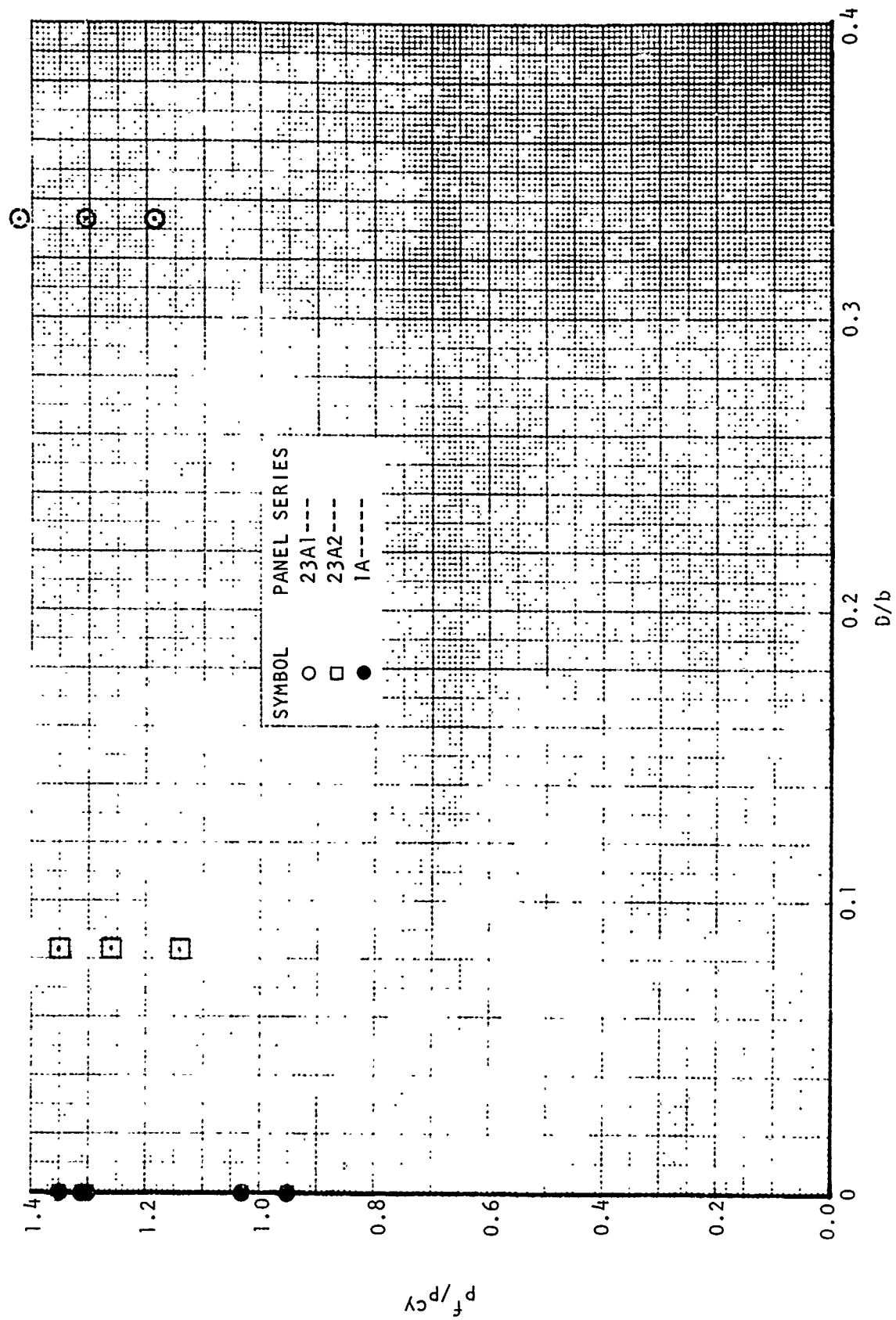
Figure 97. Panel Compression Test Data - Cutouts
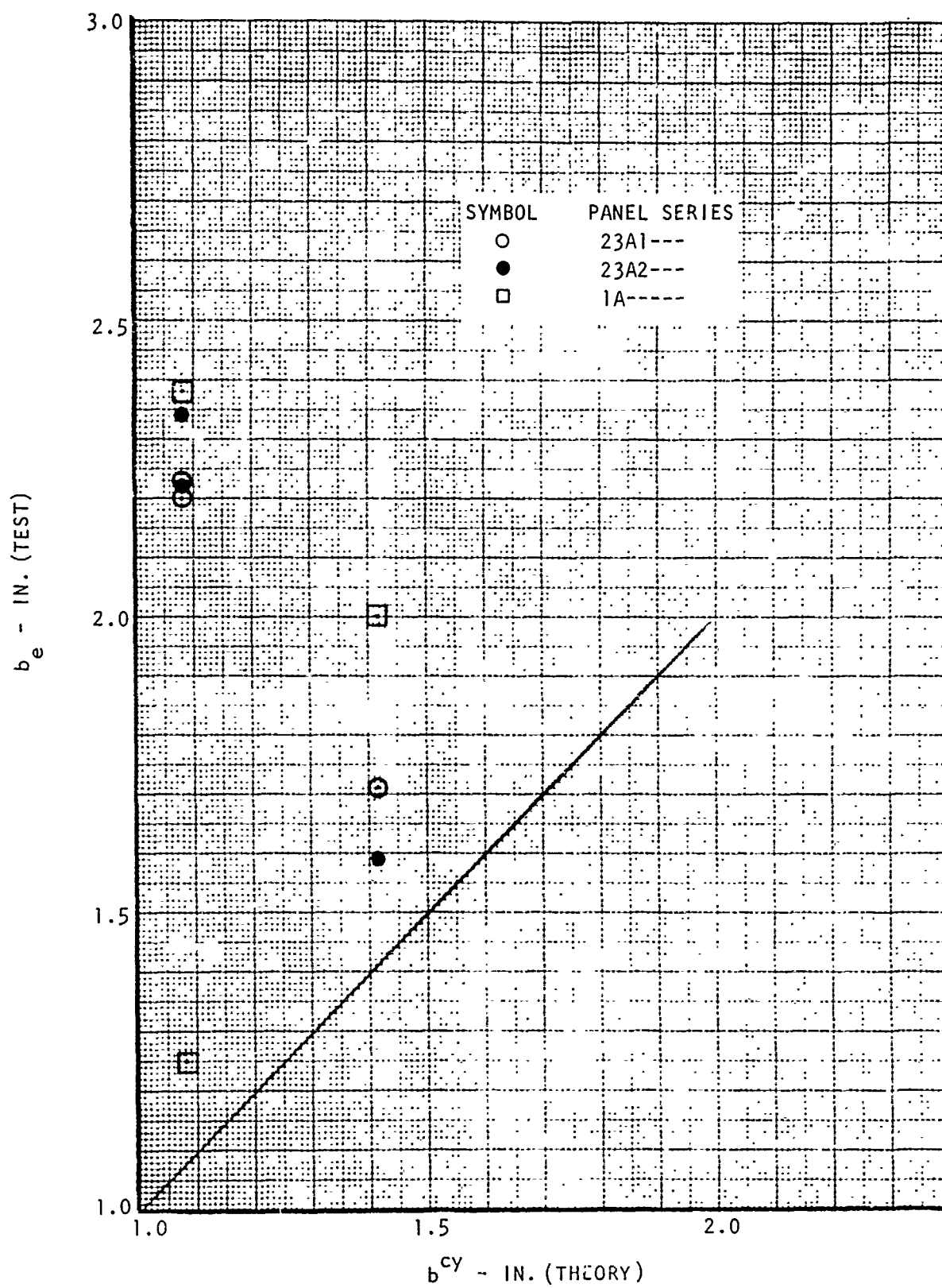
Figure 98. Test Versus Theoretical Effective Width
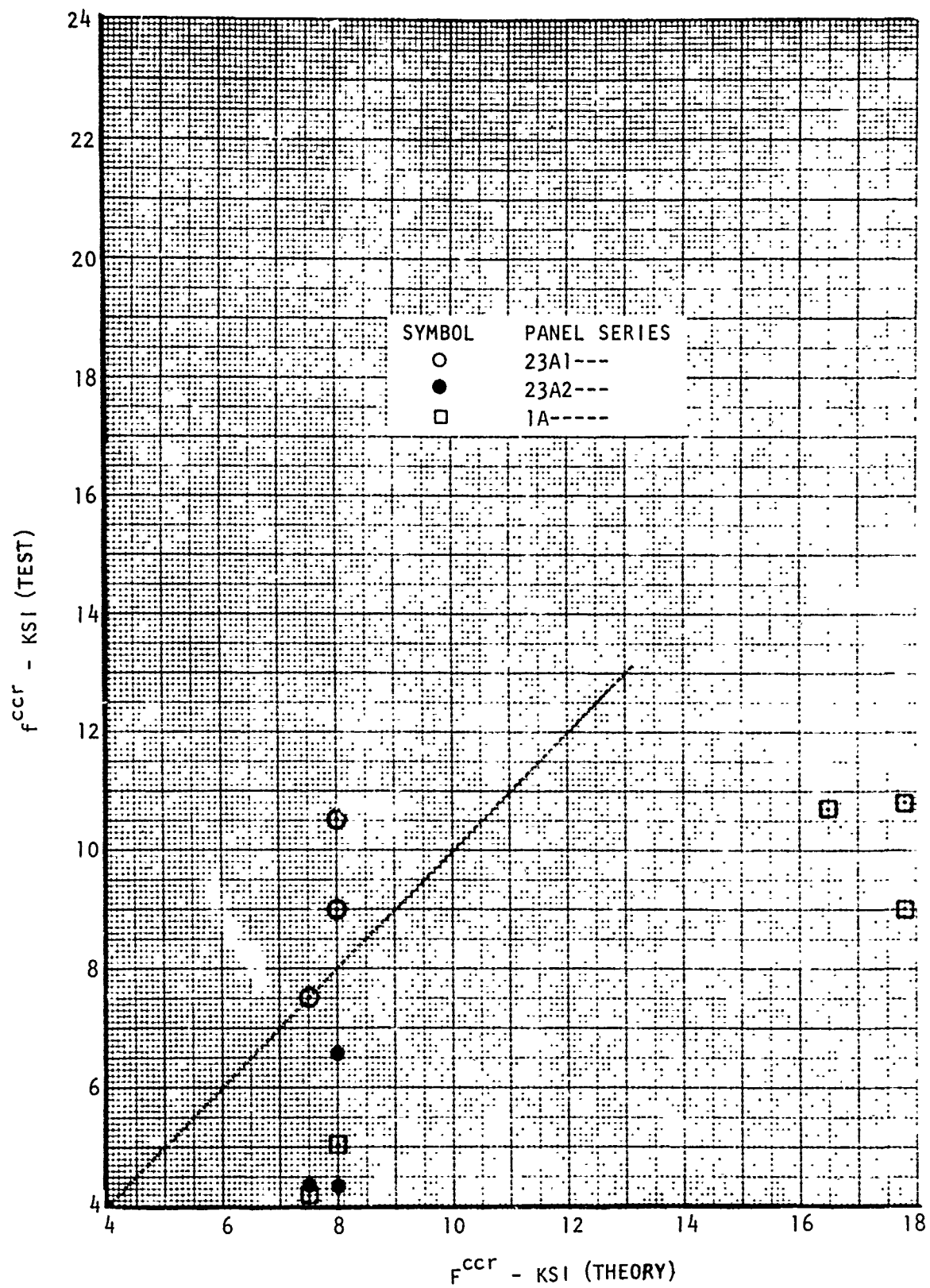
Figure 99. Test Versus Theoretical Buckling Stress
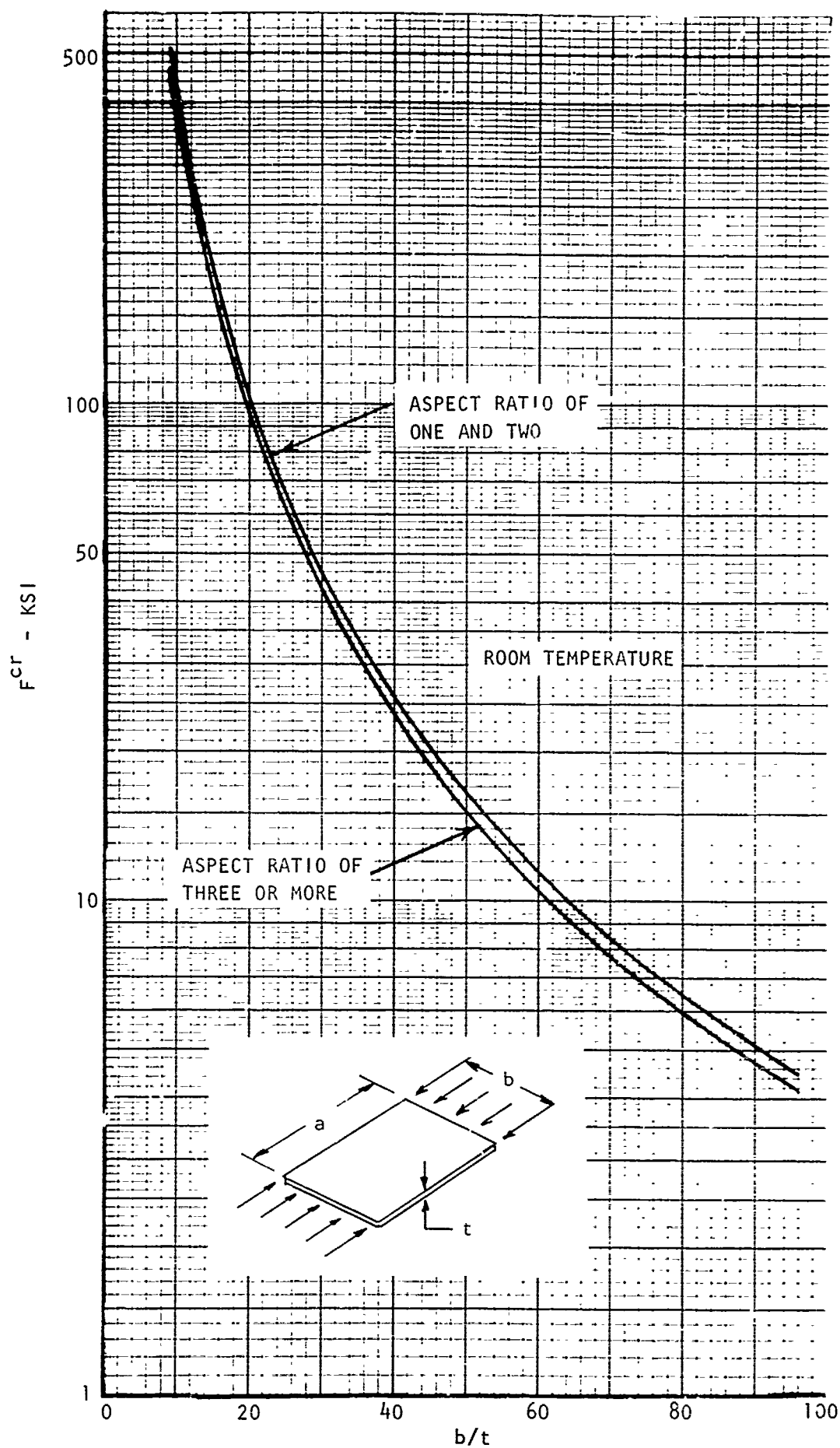
Figure 100. Predicted General Instability Strength for $\left[0_2/\pm45\right]_{4c}$ Laminates Simply Supported on Four Edges (Room Temperature)
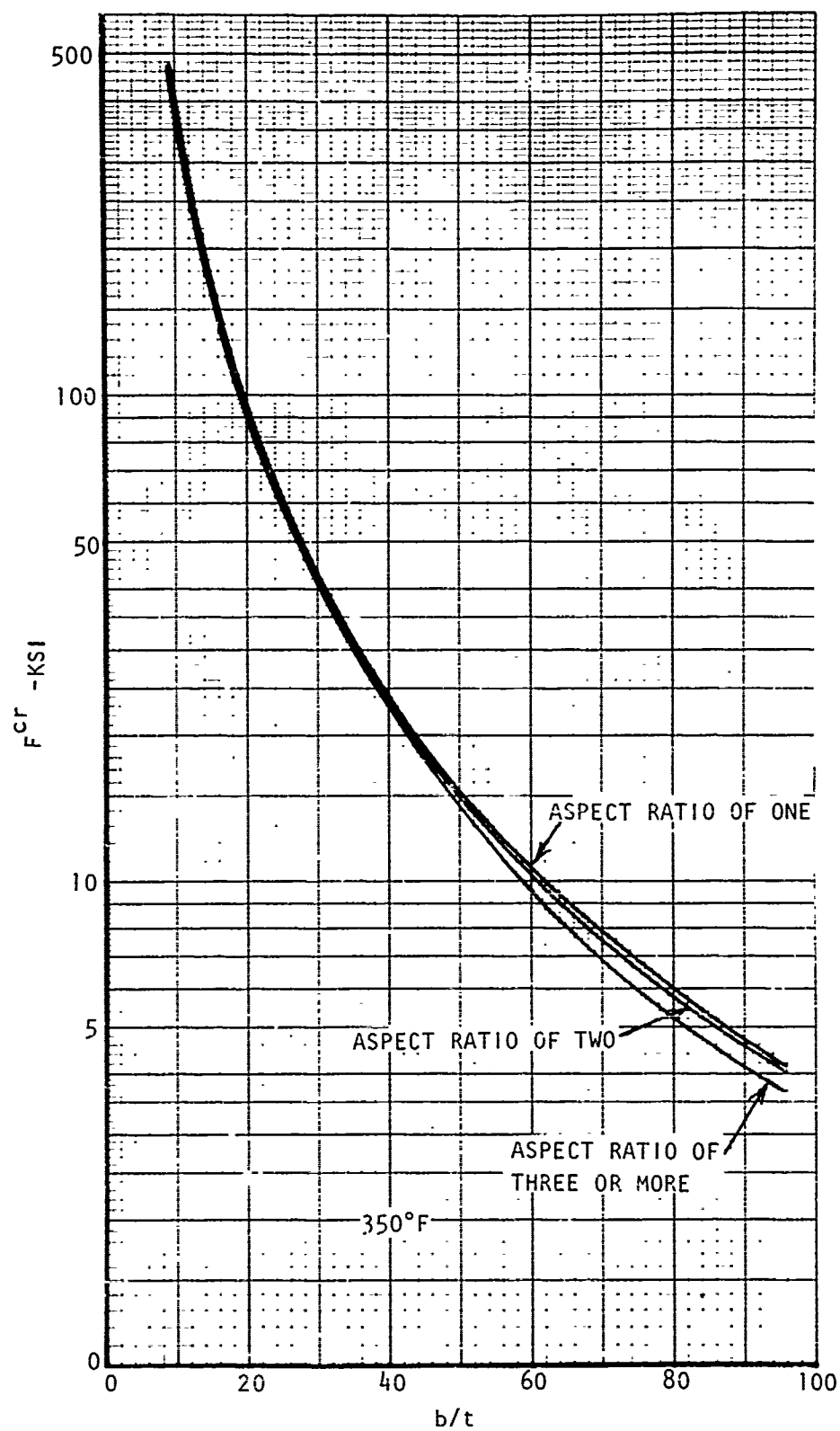
Figure 101. Predicted General Instability Strength for $[0_2/\pm45]_{4C}$ Laminates With Simple Support on Four Edges - 350° F

TABLE XX. SHEAR PANEL (CUTOUT) STRESS CONCENTRATION FACTOR SUMMARY

Specimen	D/b	K_{1x}	K_{1y}	K_{2x}	K_{2y}	K_{3x}	K_{3y}	K_{4x}	K_{4y}	$K_{15y'}$	$K_{25y'}$	$K_{35x'}$	$K_{45x'}$
24A1R1,2(Th)	0.555	0.00	0.00	0.00	0.00	1.00	-1.00	1.00	-1.00	-3.39	-3.39	1.77	1.77
24A1R1	0.555	0.25	-0.15	0.55	-0.41	0.74	-0.81	0.89	-0.72	-0.72	-1.07	7.73	7.63
24A1R2	0.555	-0.15	0.27	-0.42	0.46	---	---	---	---	---	---	-4.53	-5.60
24A1L1(Th)	0.555	0.00	0.00	0.00	0.00	---	---	---	---	---	---	1.50	1.50
24A1L1	0.555	-0.16	-0.07	-0.22	0.15	---	---	---	---	---	---	-6.85	-7.12
24A2R1,2(Th)	0.085	0.00	0.00	0.00	0.00	1.00	-1.00	1.00	-1.00	-3.39	-3.39	1.77	1.77
24A2R1	0.085	0.70	-0.59	-0.51	-0.12	0.94	-0.78	0.95	-0.85	-0.58	0.07	5.51	4.5o
24A2R2	0.085	0.59	-0.55	0.58	-0.54	---	---	0.73	-0.67	-0.68	-1.04	---	---
24A2L1(Th)	0.085	0.00	0.00	0.00	0.00	---	---	1.00	-1.00	-3.32	-3.32	---	---
24A2L1	0.085	0.28	-0.15	0.68	-0.67	---	---	0.36	-0.86	-0.47	-1.15	---	---

(Th) = Theoretical

$N_{xY} = 166.7$ LB/IN.

157

2. V_{cr} is such that the shear stress on the net section is equal to the theoretical buckling stress for a simply supported panel.

The results are shown in table XXI and figure 102, where V_f is the actual failure load. Figures 103 through 105 show test data for the compression panels, while figures 106 through 112 are the failed test specimens.
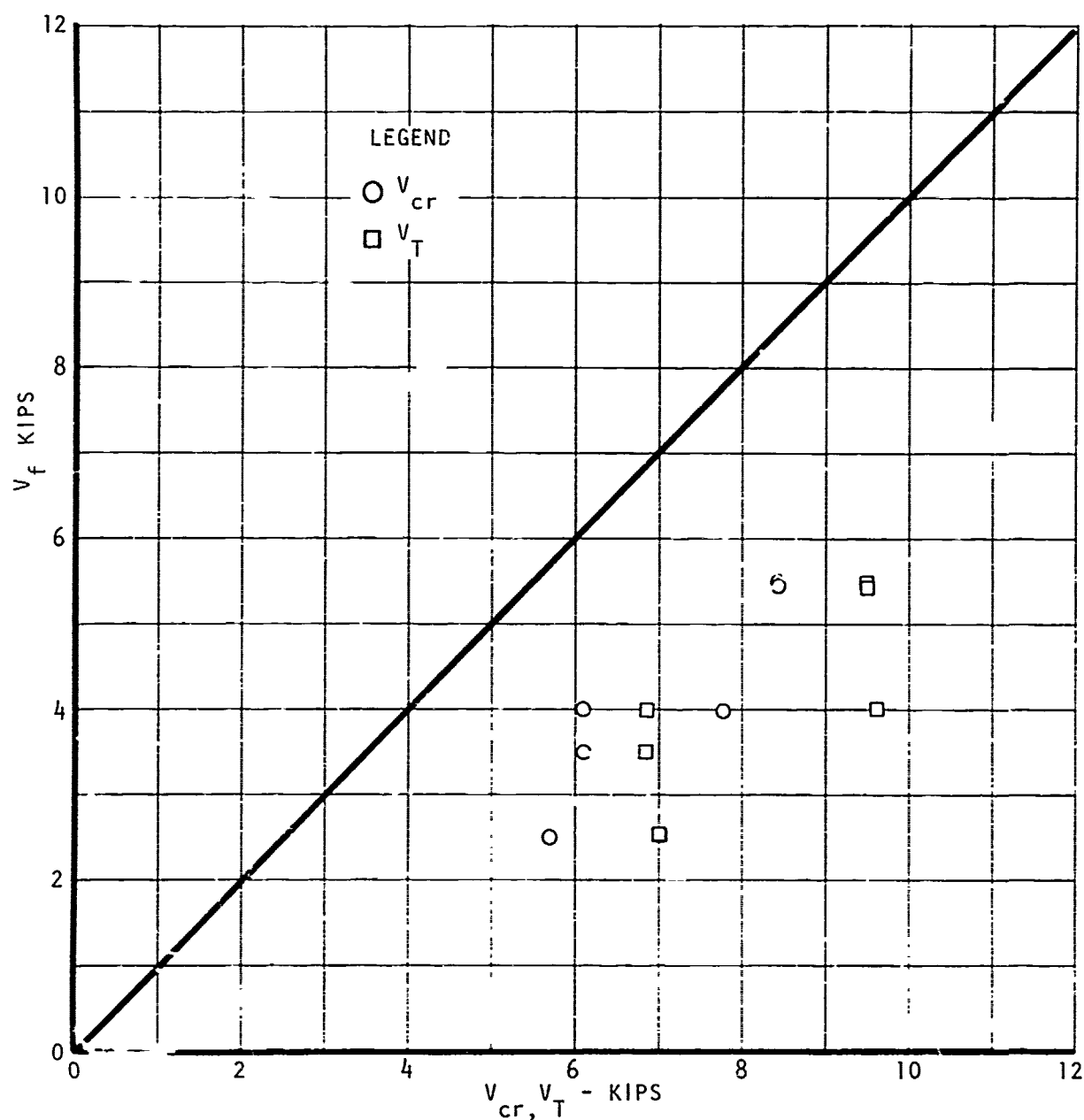
Figure 102. Test Results Versus Theory for
Inplane Shear Specimens With Cutouts

TABLE XXI. TEST VERSUS THEORY FOR THE ULTIMATE STRENGTH OF A SHEAR PANEL WITH A CIRCULAR CUTOUT

Specimen	D/b	T (°F)	F_{ct}^{tu} (Ksi)	K_θ	V_T (Kips)	V'_{cr} (Kips)	V_f (Kips)
24A1R1	0.333	RT	16.0	1.77	6.9	6.17	4.0
1R2	0.333	RT	16.0	1.77	6.9	6.17	3.5
1E1	0.333	350	13.8	1.50	7.0	5.70	2.5
2R1	0.085	RT	16.0	1.77	9.5	8.49	5.5
2R2	0.085	RT	16.0	1.77	9.5	8.49	5.5
2E1	0.085	350	13.8	1.50	9.6	7.84	4.0

V_T is such that $(\sigma_T = F_T^{tu})$ at $\theta = 60$ degrees.

V'_{cr} is such that $N_{x, net} = N_{xcr}$ (no hole).

V_f is the failure load.
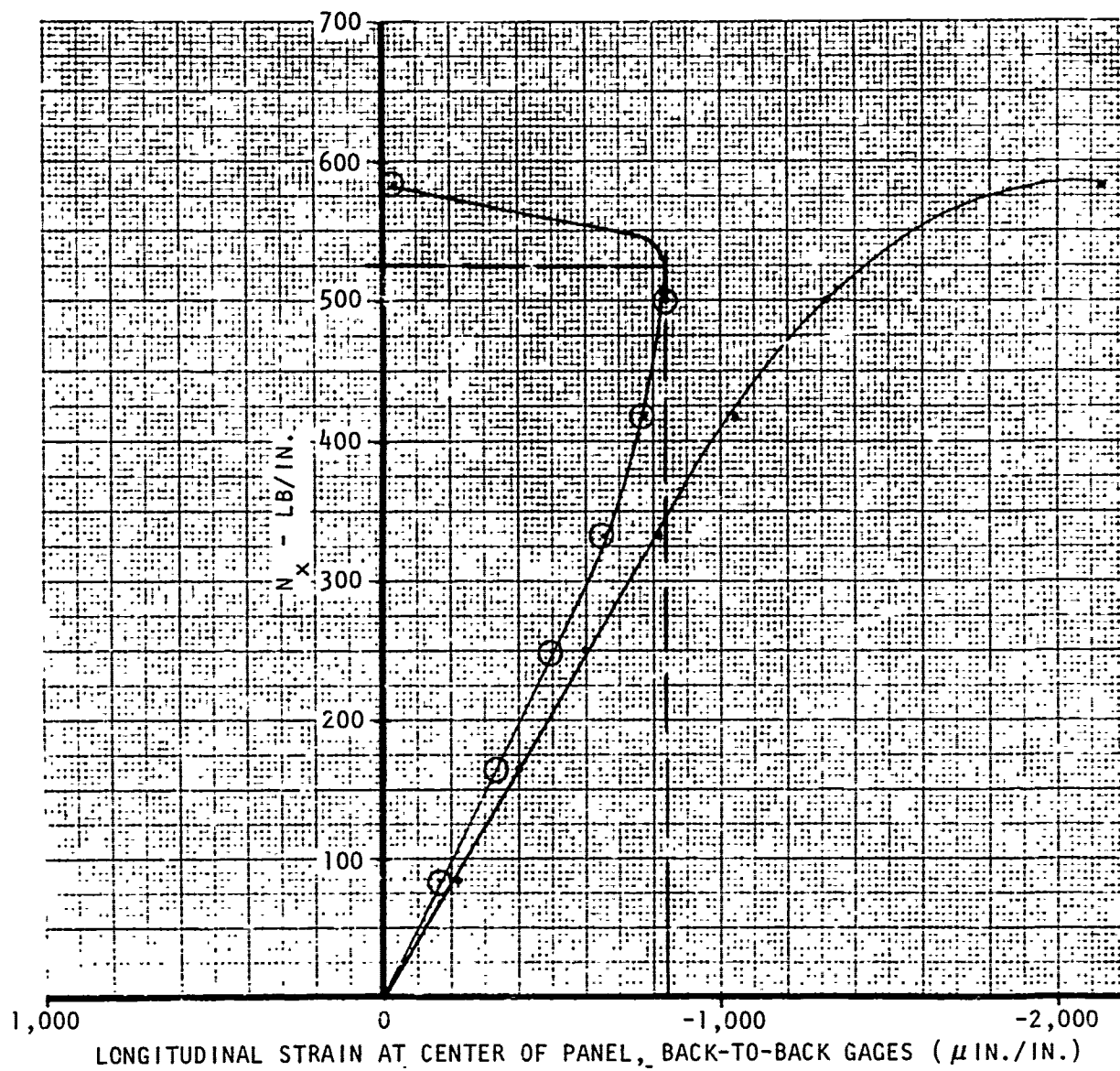
Figure 103. Longitudinal Strain Buckling Plot for Panel 23A1R1
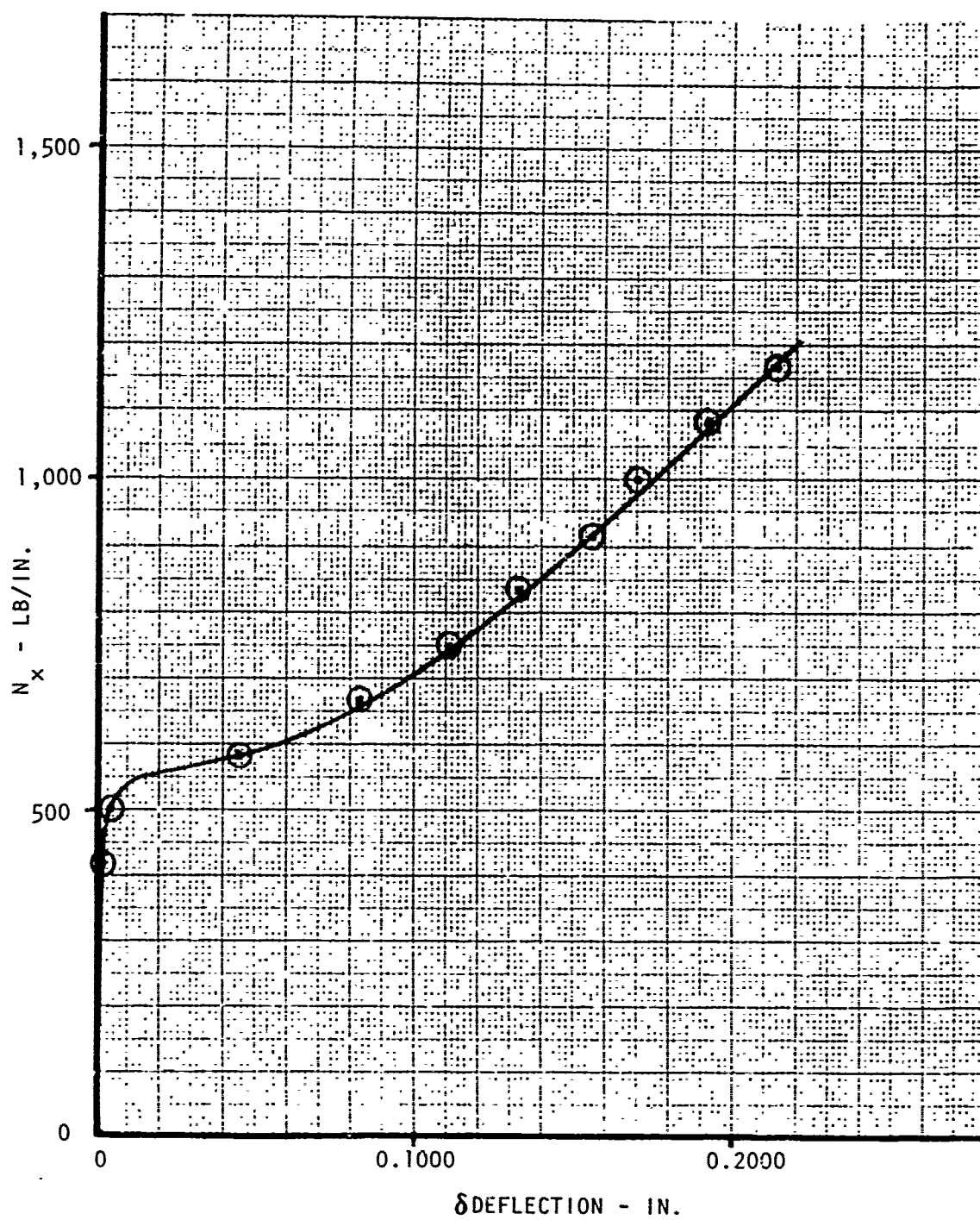
Figure 104. Midspan, Hole Edge, Lateral Deflection for Panel 23A1R1
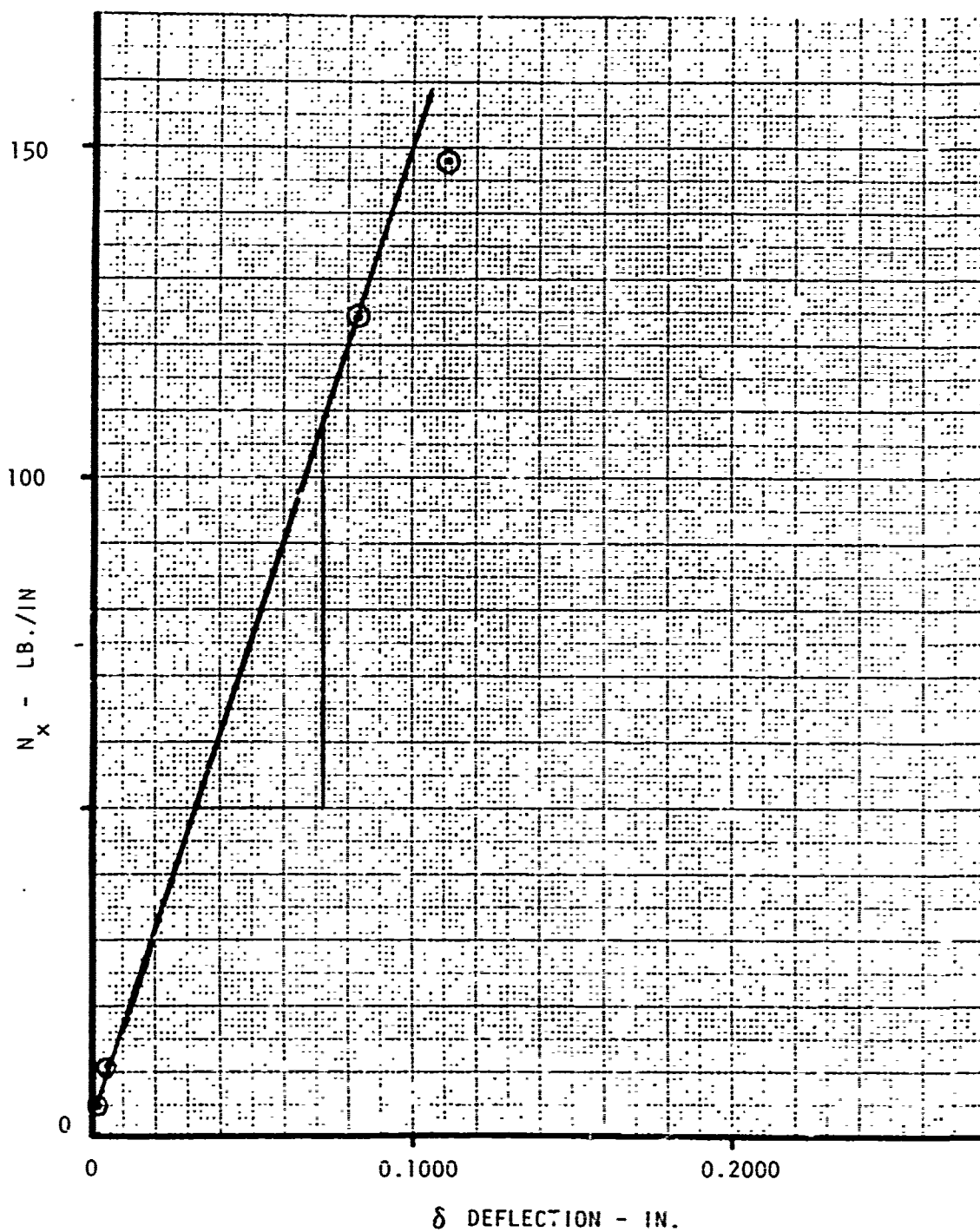
Figure 105.   Southwell Buckling Plot for Panel 25A1R1
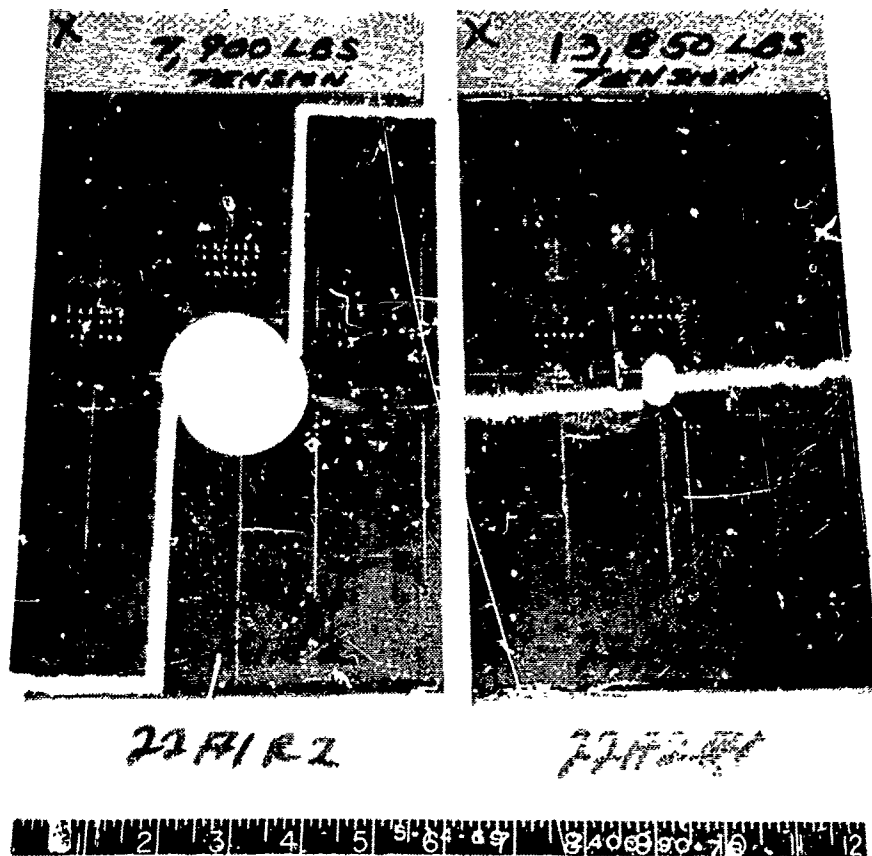
Figure 106. Failure Under Uniaxial Load, Specimens 22A2Ri and 22A1R2
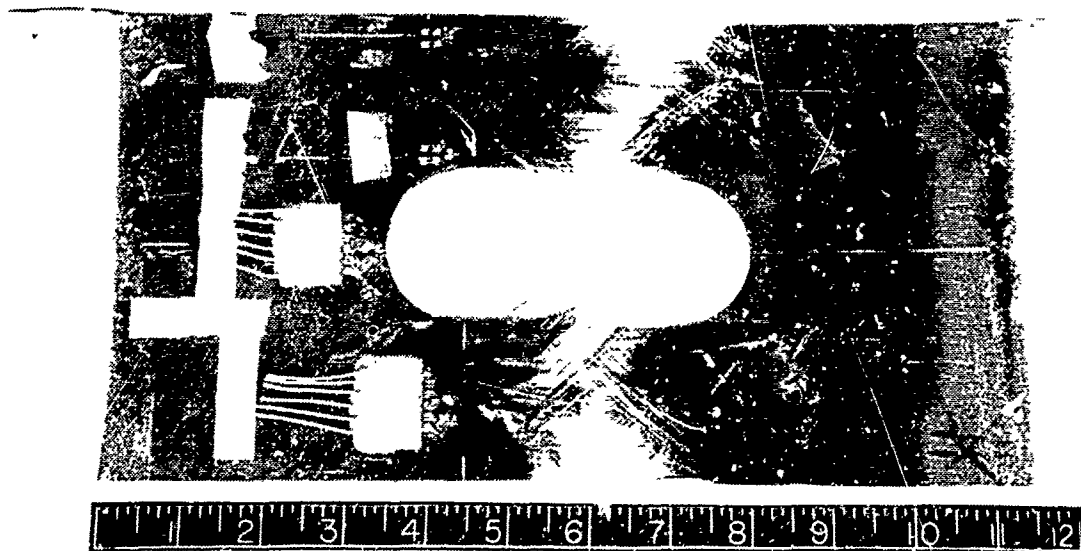
Figure 107. Failure Under Uniaxial Tension Load, Specimen 22A1E1
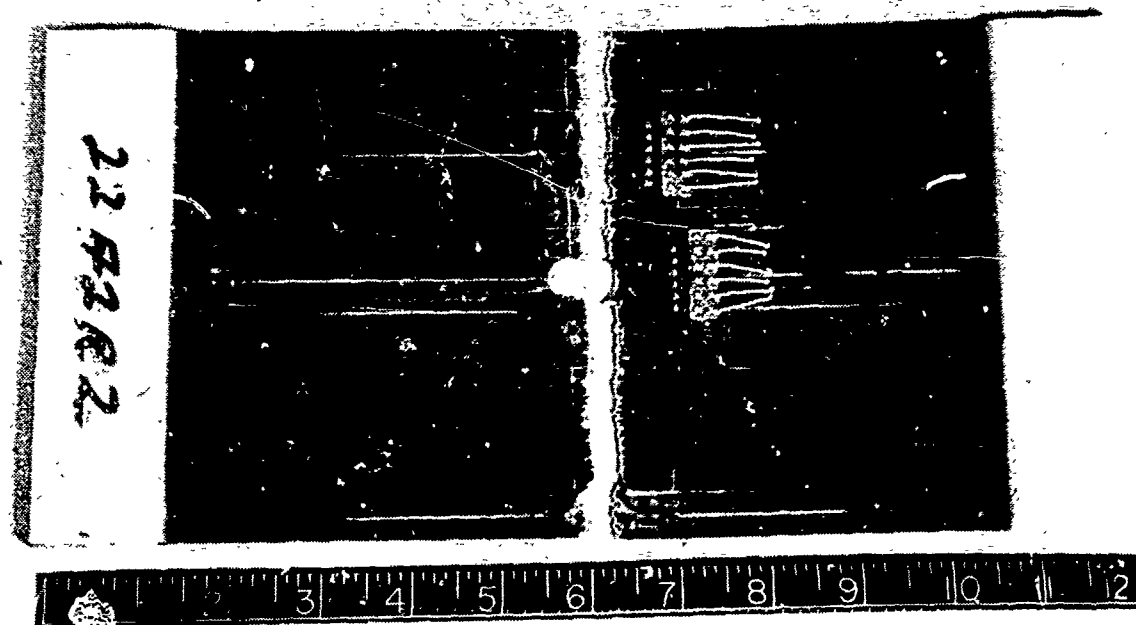
Figure 108.   Failure Under Uniaxial Tension Load, Specimen 22A2R2
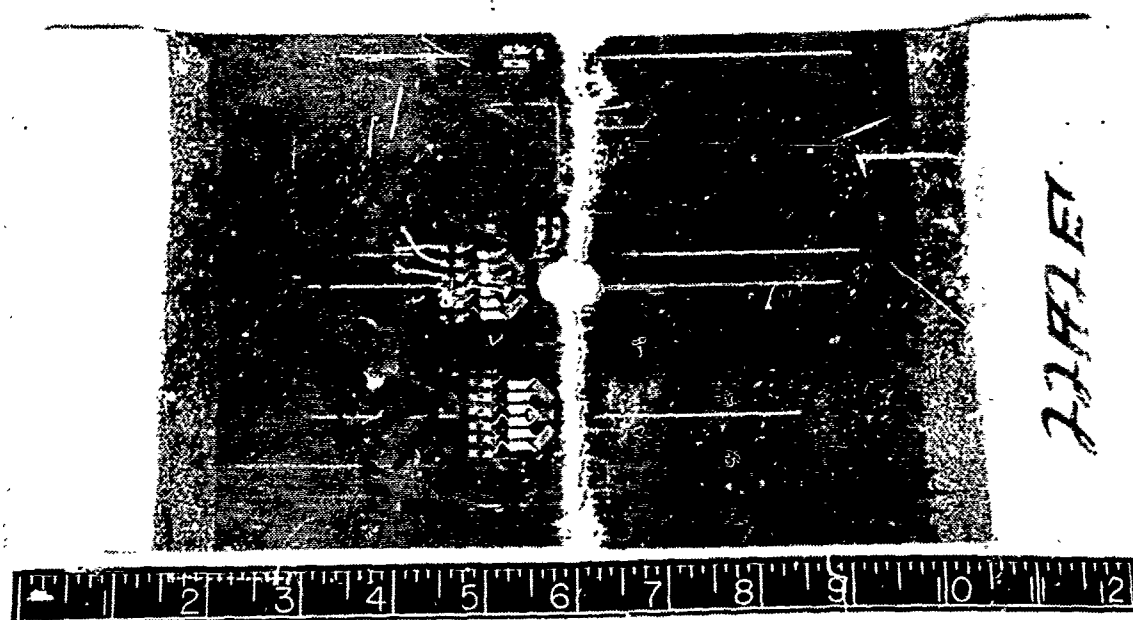
Figure 109.   Failure Under Uniaxial Tension Load, Specimen 22A2E1

144
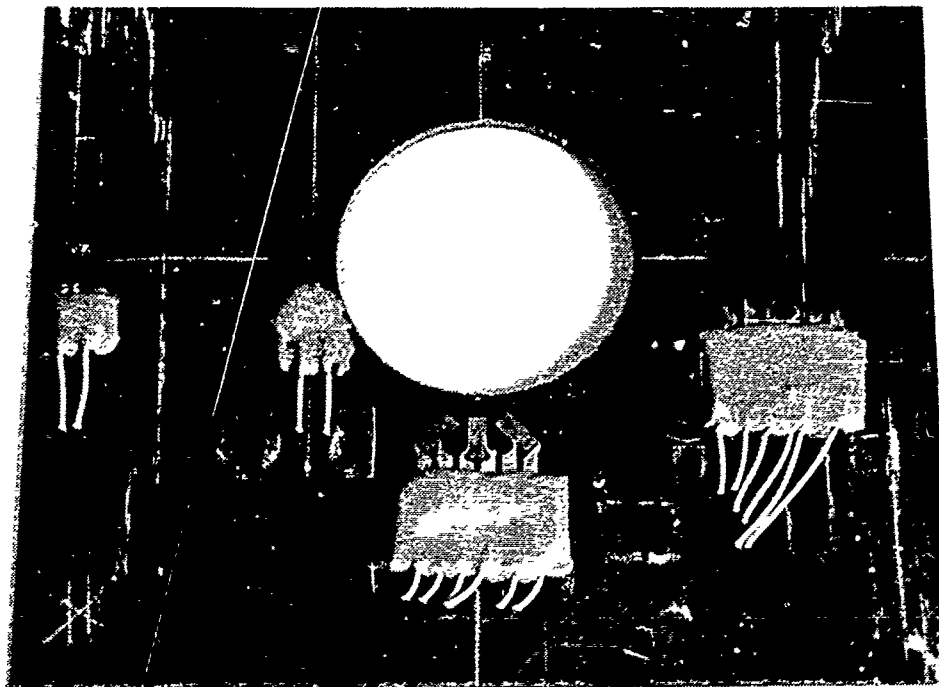
Figure 110. Buckling Failure Along Edges, Panel 23A1E1
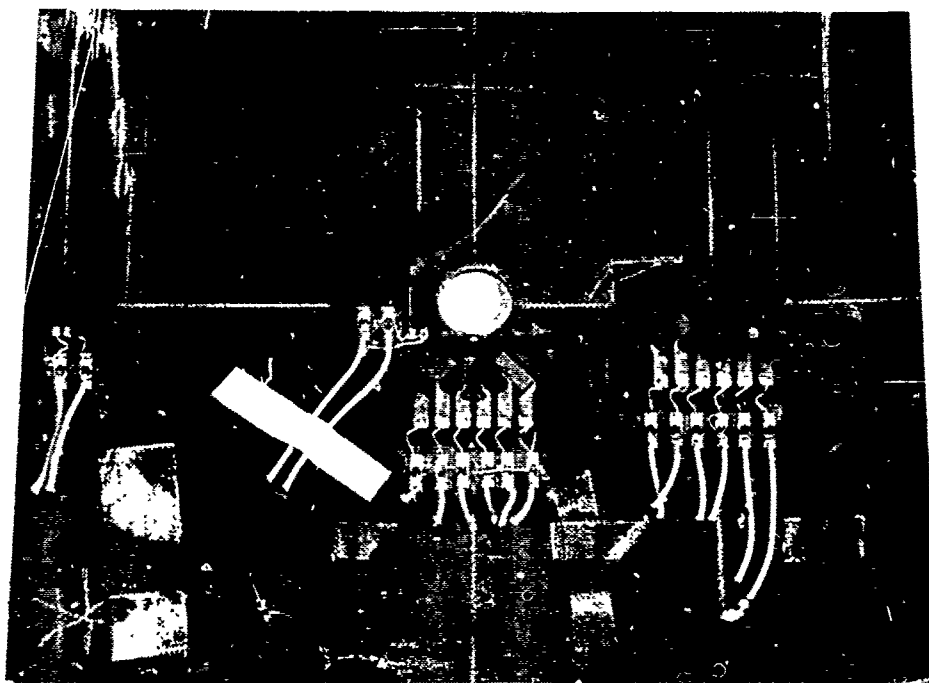
Figure 111. Buckling Failure Along Edges Panel 23A2E1

SPECIMEN 24A2E1
GROSS SHEAR STRESS = 8,013 PSI
A/B = 1; A = 6 IN.; D = 0.5 IN.
350°F.

SPECIMEN 24A1E1
GROSS SHEAR STRESS = 5,008 PSI
A/B = 1; A = 6 IN.; D = 2.0 IN.
350°F

SPECIMEN 24A2R2
GROSS SHEAR STRESS = 11,018 PSI
A/B = 1; A = 6 IN.; D = 0.5 IN.
RT.

SPECIMEN 24A1R2
GROSS SHEAR STRESS = 7,011 PSI
A/B = 1; A = 6 IN.; D = 2.0 IN.
RT

SPECIMEN 24A2R1
GROSS SHEAR STRESS = 11,018 PSI
A/B = 1; A = 6 IN.; D = 0.5 IN.
RT

SPECIMEN 24A1R1
GROSS SHEAR STRESS = 8,013 PSI
A/B = 1; A = 6 IN.; D = 2.0 IN.
RT

Figure 112.   Failed Shear Specimens With Cutouts, Series 24A1 and 24A2

HONEYCOMB SANDWICH PANELS

UNIAXIAL COMPRESSION (SERIES 1B)

The 1B series, simply supported uniaxial compression panels, were all fabricated with $[0/\pm45/0]_S$ face sheets and 5056 aluminum core, 6.1 lb/ft^3 density for the RT specimens and 8.1 lb/ft^3 for the 350°F specimens. The basic properties used to calculate predicted values for the typical simply supported test panel illustrated in figure 113 are as follows:

t_F = 8 plies x 0.0052 in./ply = 0.0416 in.
c = 0.500 in.

	6.1 lb/ft^3	8.1 lb/ft^3
$(G'_{Cx})_{RT}$	90,000 psi	126,000 psi
$(G'_{Cx})_{350°F}$	82,800 psi	116,000 psi
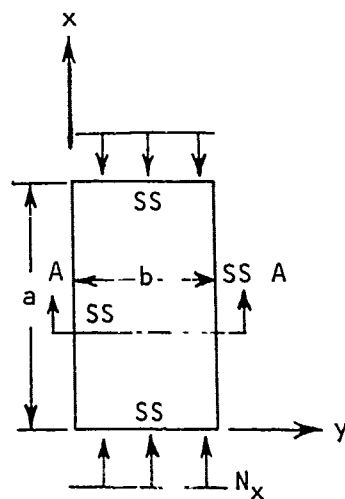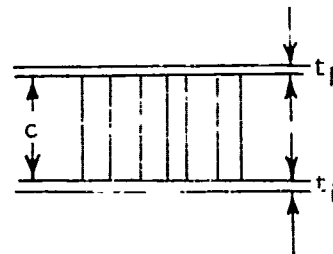
PLAN VIEW   SECT A-A

Figure 113. Typical Simply Supported Uniaxial Compression Honeycomb Panel

Tables XXII and XXIII present the data used in the analysis, while table XXIV presents the results.

TABLE XXII. MATERIAL PROPERTIES FOR SERIES 1B PANELS

| Temp (°F) | Face Sheet Properties | | | | | Core Density ρ'_c (lb/ft^3) | Sandwich Properties | | |
	E_x (Msi)	E_y (Msi)	G_{xy} (Msi)	ν_{xy}	ν_{yx}		α	ψ (Msi)	Vb^2 (in.^{2})
RT	16.67	5.06	4.30	0.701	0.213	6.1	1.82	10.79	13.31
						8.1	1.82	10.79	9.50
350	15.78	3.86	3.97	0.840	0.205	6.1	2.02	9.42	12.69
						8.1	2.02	9.42	9.05

where

$$V = \frac{\pi^2 \psi \, (t_F/c)(1+t_F/c)}{2 \, G'_{cx} \, (b/c)^2}$$

$$\psi = \left(\sqrt{E_x E_y}\right) / (1 - \nu_{xy}\nu_{yz})$$

$$\alpha = \sqrt{E_x/E_y}$$

For these sandwich properties, we obtain from figures 29 and 30 of section IV of Volume III the following buckling coefficients.

TABLE XXIII. BUCKLING COEFFICIENTS FOR SERIES 1B PANELS*

Panel Aspect Ratio a/b	Panel Width b (in.)	Temp (°F)	Core Density (lb/ft^3)	V	k_x
1.0	15.0	RT	6.1	0.059	3.87
		350	8.1	0.040	4.40
2.0	14.0	RT	6.1	0.068	3.80
		350	8.1	0.046	4.52
3.0	13.0	RT	6.1	0.079	3.65
		350	8.1	0.054	4.07

$$* \quad \frac{G'_{cx}}{G'_{cy}} = \frac{D_{qx}}{D_{qy}} = 2.0$$

$$(N_x)_{cr} = \frac{k_x \, \pi^2 \, \psi \, t_F c \, (c + t_F)}{2b^2}$$

TABLE XXIV.   TEST VERSUS THEORY - UNIAXIAL COMPRESSION HONEYCOMB
SANDWICH PANELS

Panel No.	a/b	b (in.)	Temp (°F)	ψ (Msi)	$(N_x)_a$ Test (lb/in.)	$(N_x)_a$ Theory (lb/in.)
1B1R1	1.0	15.0	RT	10.79	9,130	10,300
1E1	1.0	15.0	350	9.42	6,670*(1)	10,240
2R1	2.0	14.0	RT	10.79	12,960	11,600
2R2	2.0	14.0	RT	10.79	*(2)	11,600
1B2E1	2.0	14.0	350	9.42	6,210*(3)	11,150
3R1	3.0	13.0	RT	10.79	13,500*(4)	12,900
3R2	3.0	13.0	RT	10.79	13,000	12,900
3E1	3.0	13.0	350	9.42	10,300	12,590

*Unable to determine buckling load because of dial gage malfunction and pre-
mature panel failures at load introduction points. Numbers shown were
calculated by the pseudodeflection method.

   (1)   Failure at N_x = 5,540 lb/in.

   (2)   Failure at N_x = 7,857 lb/in.

   (3)   Failure at N_x = 5,714 lb/in.

   (4)   Failure at N_x = 6,846 lb/in.

In many cases, as noted, a dial gage malfunction occurred and conventional techniques could not be used to obtain the loads at which buckling occurred. Where possible, in these cases, an artifice involving pseudodeflections based on back-to-back strain gage readings was used. The basic hypothesis is that the strain gage readings are the result of deflections of a prescribed form:

$$w = w_o \, \phi(x,y)$$

Consider first a beam undergoing sinusoidal deflection

$$\phi = \sin \frac{\pi x}{L}$$

The radius of curvature is

$$R = - \frac{1}{w_{,xx}} = - \frac{1}{w_o \, \phi_{,xx}} = \frac{L^2}{\pi^2 w}$$

and, at the center

$$R(L/2) = \frac{L^2}{\pi^2 w_o} \overset{df}{=} R_c$$
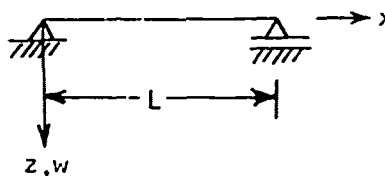
It now remains to determine R_c from the strain gage data. From figure 114

$$\frac{(1-\epsilon_x) \, \Delta_x}{\Delta_x} = \frac{R_c - h/2}{R_c} \qquad\qquad R_c = \frac{h}{2 \epsilon_x}$$
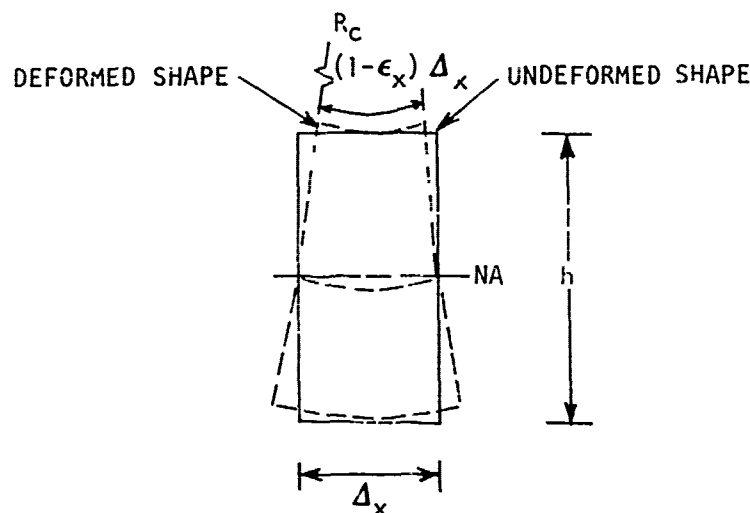
Figure 114.   Typical Beam Element

In order to plot a Southwell diagram, w_o versus N_x must be obtained. The parameter w_o is the pseudodeflection mentioned previously. Consider that $w_o(t_{i+1})$ is desired, given $w_o(t_i)$ (t is an arbitrary parameter), where $N_x(t_i)$ and $\epsilon_x(t_i)$ are known. Assume

$$w_o(t_o) = 0$$

The load $N_x(t_i)$ is then applied

$$w_o(t_1) = \frac{L^2}{\pi^2}\left[\frac{1}{R_c(t_1)}\right] = \frac{2L^2\epsilon_x(t_1)}{\pi^2 h}$$

The load $N_x(t_2) = N_x(t_1) + \Delta N_x$ is then applied

$$w_o(t_2) = \frac{L^2}{\pi^2}\left[\frac{1}{R_c(t_2)}\right] = \frac{2L^2\epsilon_x(t_2)}{\pi^2 h}$$

$$\Delta\, w_o(t_1) = w_o(t_2) - w_o(t_1) = \frac{2L^2}{\pi^2 h}\left[\epsilon_x(t_2) - \epsilon_x(t_1)\right]$$

The Southwell diagram can now be drawn and analyzed in the conventional manner. Figure 115 shows the method used for panel 1B1R1, for which a conventional Southwell diagram (figure 116) is available. For this case, this method obtains an $N_{xcr} = 9.11$ Kips/inch, whereas the conventional method obtains 9.13 Kips/inch. Agreement of this type was not expected nor will it normally be in the future. However, the reliability of the method is somewhat enhanced.

It is of interest to note that the choice of

$$\phi = \frac{-(R - w_o) + \sqrt{R^2 - (x-L)^2}}{w_o}$$

which is a circular segment, produces an identical load for critical buckling, although the constants used to calculate the pseudodeflections change somewhat. Figures 117 through 120 are photographs of the test specimens after failure.

The figure shows a Pseudo-Southwell plot with the following labeled content:

Y-axis: W/P 10^{-10} IN./LB (scale 0 to 700)

X-axis: W μ - IN. (scale 0 to 6,000)

$$P_{cr} = \frac{2800 \times 10^{-6}}{205 \times 10^{-10}} = 13.7 \times 10^{4} \; K$$

$$N_{xcr} = 9.11 \; K/IN.$$
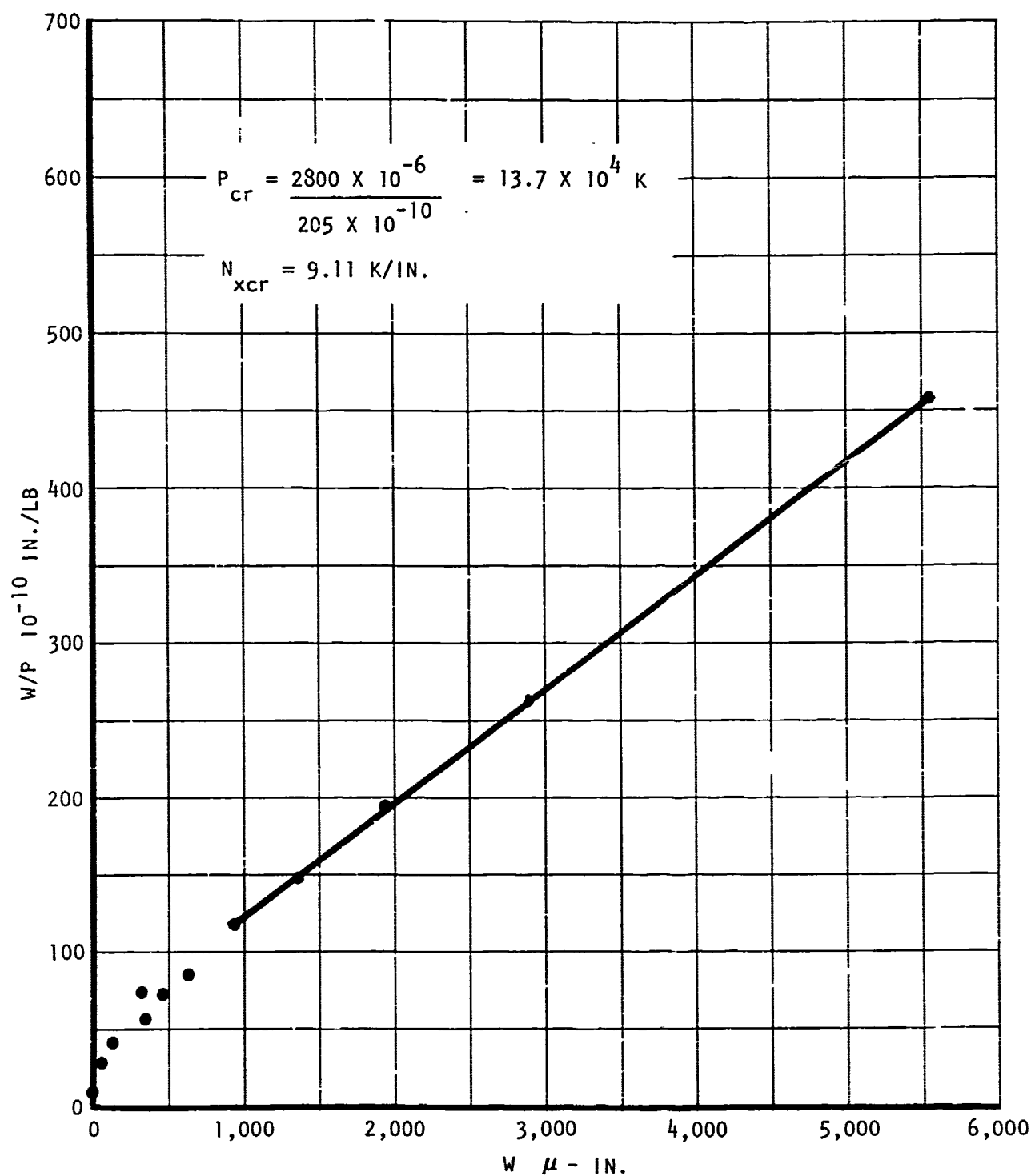
Figure 115.   Typical Pseudo-Southwell Plot, Specimen 1B1R1

153
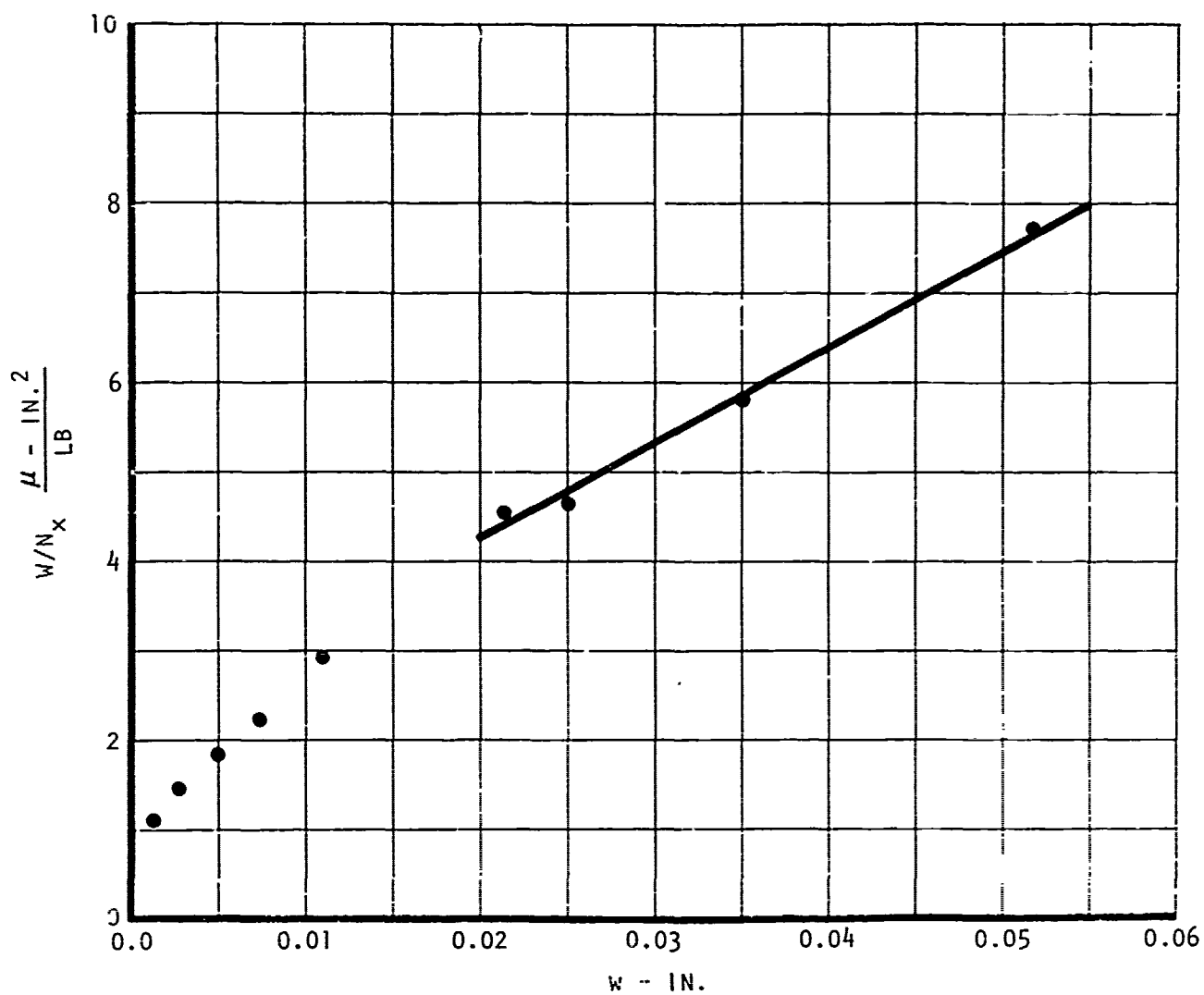
Figure 116. A Typical Southwell Plot Specimen No. IB1R1
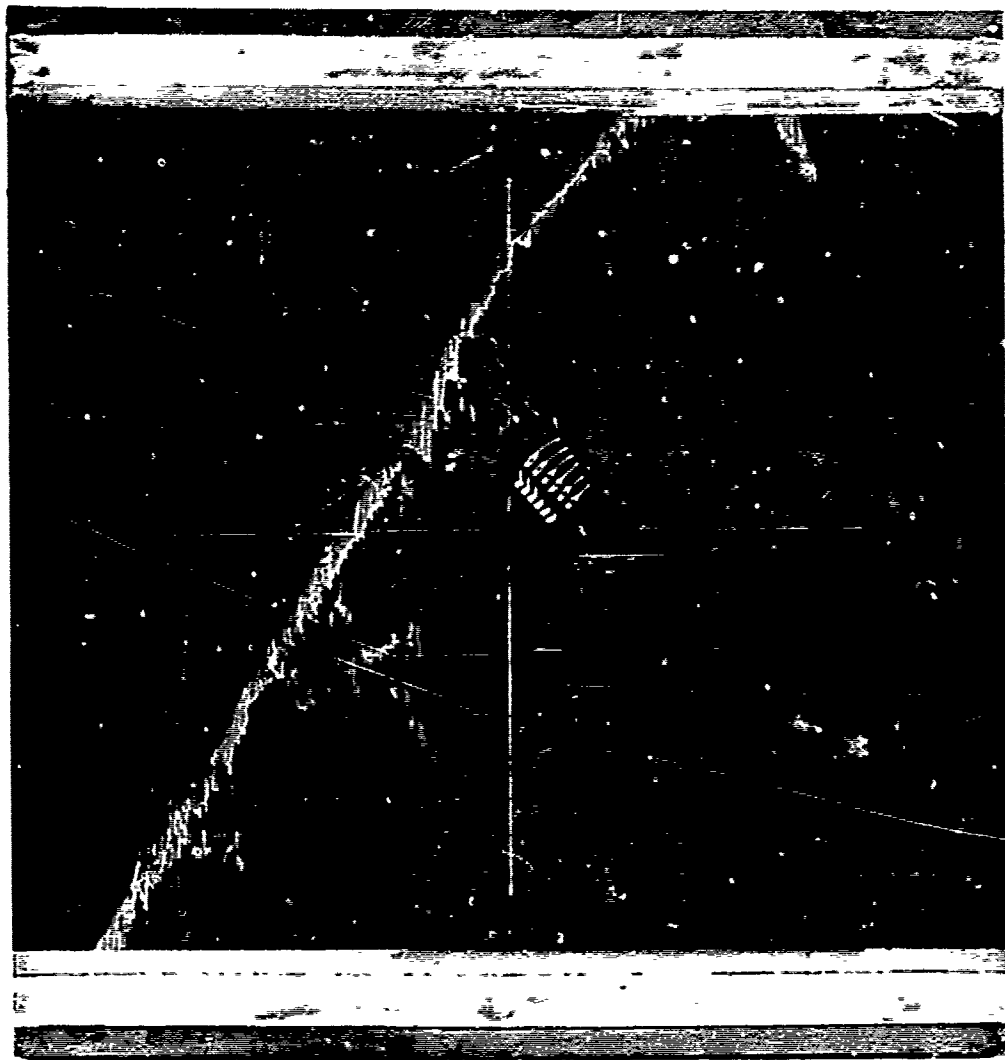
Figure 117. Failed ecimen 1B1R1, Uniaxial Compression
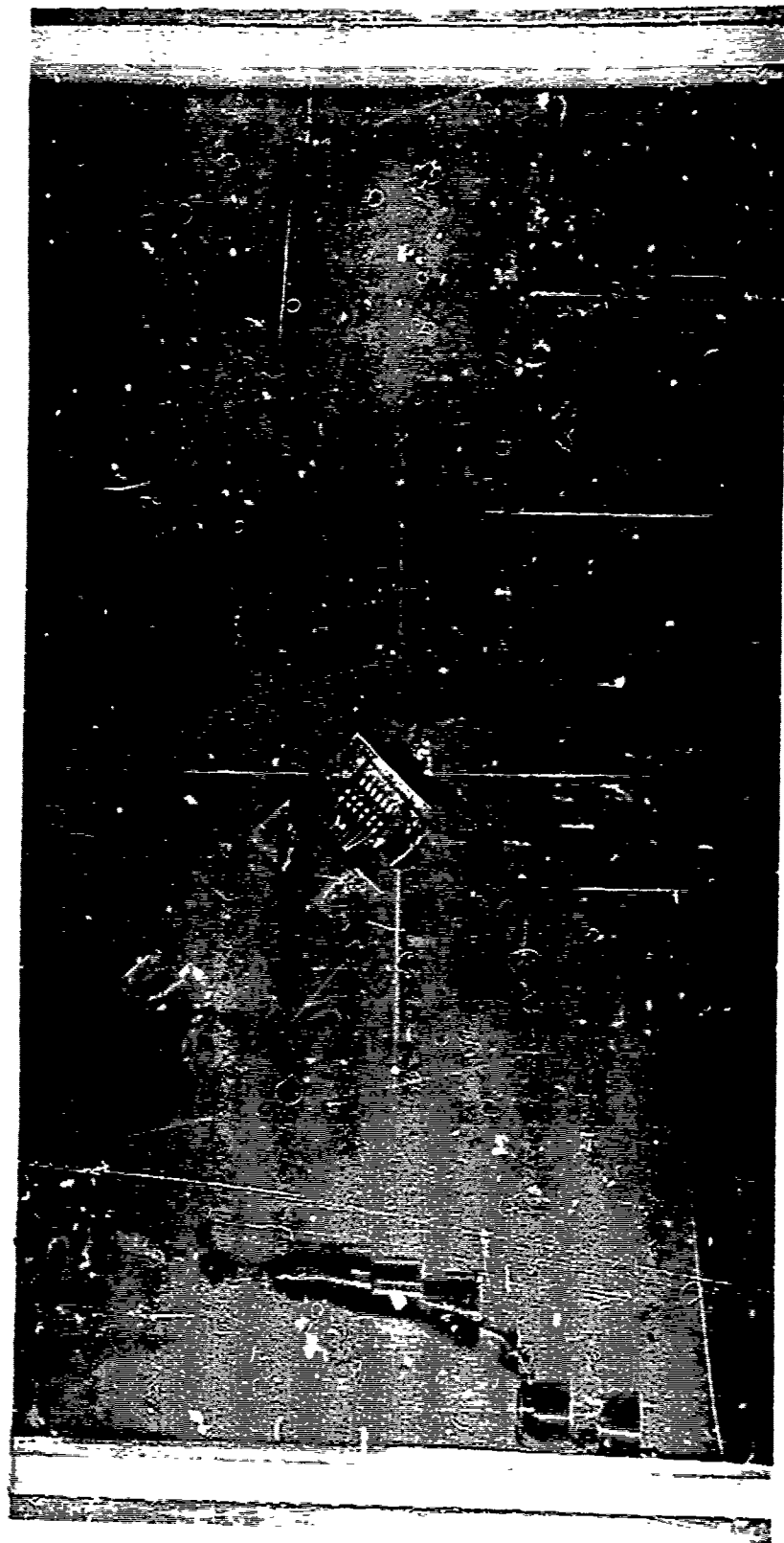
Figure 118. Failed Specimen 1B2E1, Uniaxial Compression

Figure 119. Failed Specimen 1B3R1, Uniaxial Compression

157
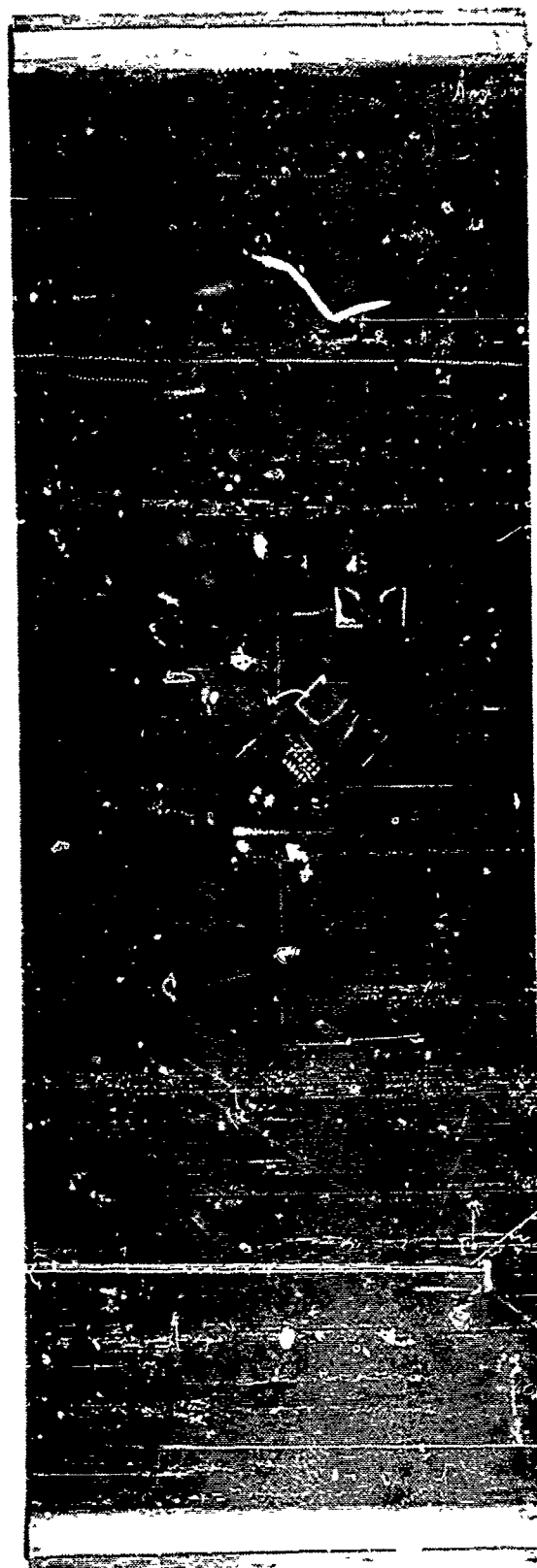
Figure 120.   Failed Specimen 1B3E1, Uniaxial Compression

BIAXIAL COMPRESSION (SERIES 2B)

The 2B series, simply supported, biaxially loaded, compression panels
were identical in geometry to the 1B series panels described in the previous
paragraphs. The predicted buckling loads were obtained from the data
presented in figures 31 through 36 of section IV of Volume III; the pertinent
data are summarized in table XXV.

TABLE XXV. BUCKLING COEFFICIENTS FOR SERIES 2B PANELS

Panel Aspect Ratio a/b	Panel Width b (in.)	Temp (°F)	Core Density (lb/ft³)	Applied Load Ratio N_y/N_x	V	k_x
1.0	15.0	RT	6.1	0.50	0.059	2.67
1.0	15.0	350	8.1	0.50	0.040	2.99
2.0	14.0	RT	6.1	1.0	0.068	0.90
2.0	14.0	350	8.1	1.0	0.046	0.93
3.0	13.0	RT	6.1	1.0	0.079	0.67
3.0	13.0	350	8.1	1.0	0.054	0.67

Where the basic material properties for the panels are presented in the
previous sections for the series 1B panels and

$$(N_x)_{cr} = \frac{k_x \pi^2 \psi t_F c (c+t_F)}{2b^2}$$

$$\frac{G'_{cx}}{G'_{cy}} = \frac{D_{qx}}{D_{qz}} = 2.0$$

with a typically loaded panel shown in figure 121.

Table XXVI shows the results for the tests. Figures 122 through 129 are
photographs of the test specimens after failure.
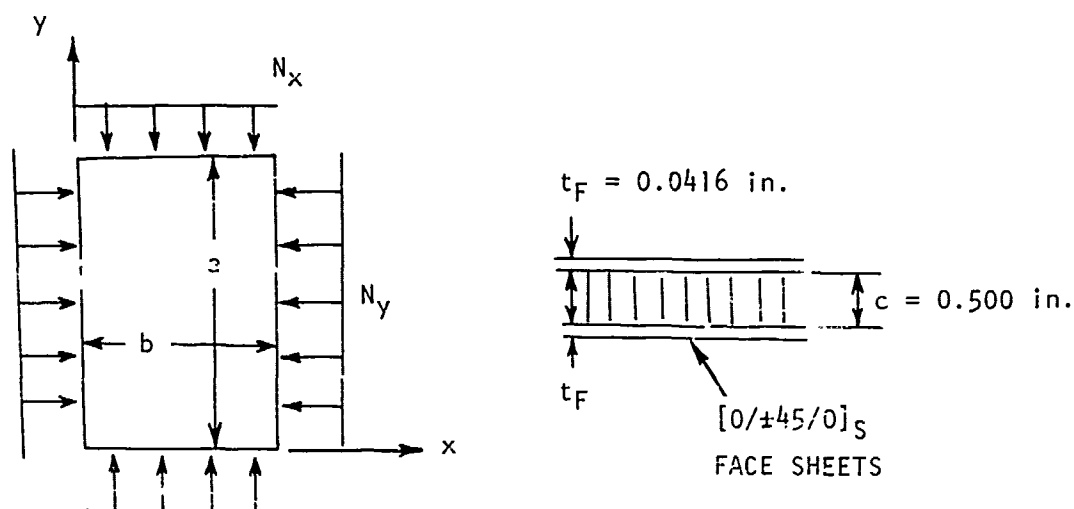
Figure 121. Typical Simply Supported, Biaxially Loaded,
Honeycomb Compression Panel

TABLE XXVI. TEST VERSUS THEORY FOR BIAXIAL COMPRESSION
HONEYCOMB SANDWICH PANELS

Panel No.	a/b	b (in.)	Temp (°F)	ψ (Msi)	Applied Load Ratio (N_y/N_x)	Theory (N_x)cr (lb/in.)	Test (N_x)cr (lb/in.)
2B1R1	1.0	15.0	RT	10.79	0.50	7,118	10,200
1R2	1.0	15.0	RT	10.79	0.50	7,118	*
1E1	1.0	15.0	350	9.42	0.50	6,959	9,700
2R1	2.0	14.0	RT	10.79	1.0	2,749	**
2R2	2.0	14.0	RT	10.79	1.0	2,749	5,600
2E1	2.0	14.0	350	9.42	1.0	2,400	5,800
3R1	3.0	13.0	RT	10.79	1.0	2,374	4,255
3R2	3.0	13.0	RT	10.79	1.0	2,374	3,400
3E1	3.0	13.0	350	9.42	1.0	2,073	4,000

*Nonoperative dial deflection gage; panel failed locally near corner at
N_x = 6,800 lb/in.
**Damaged during fabrication.
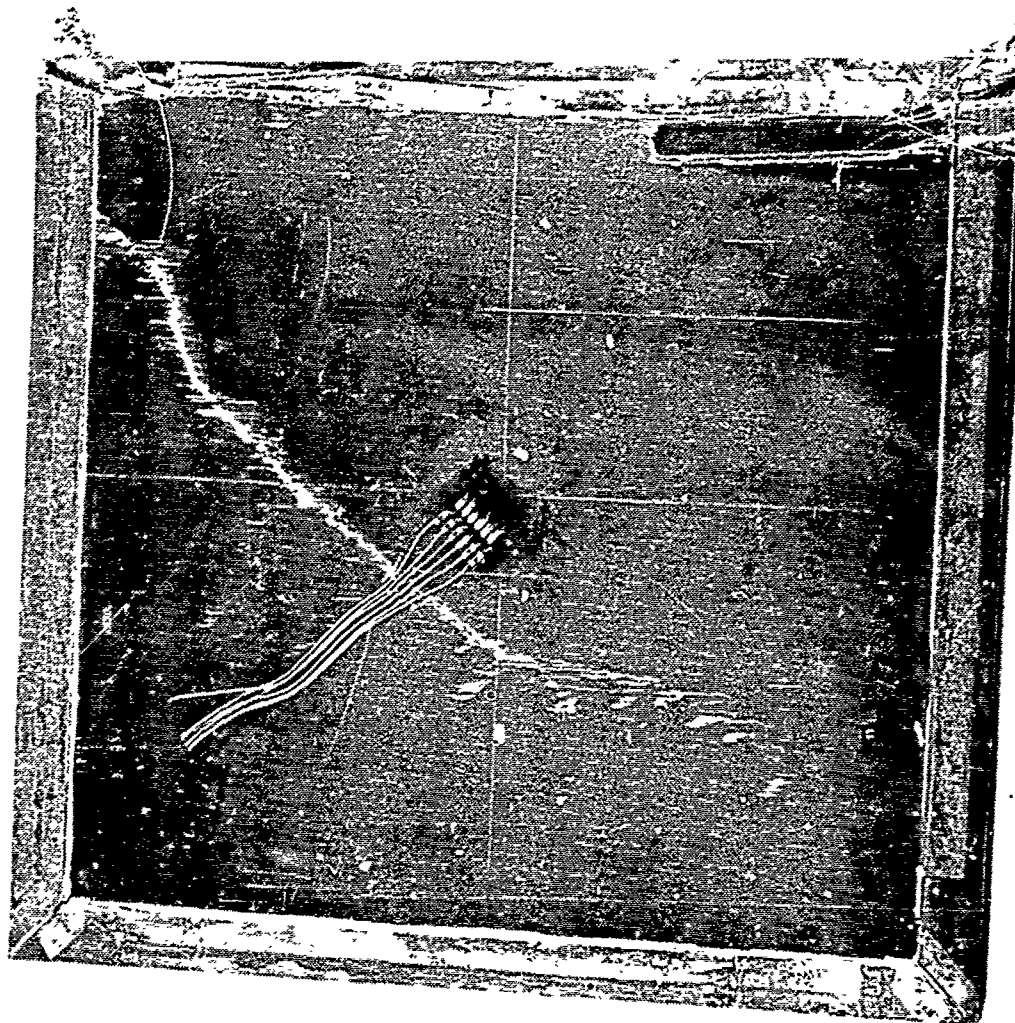
Figure 122. Test Specimen 2B1R1 After Failure, Biaxial Compression
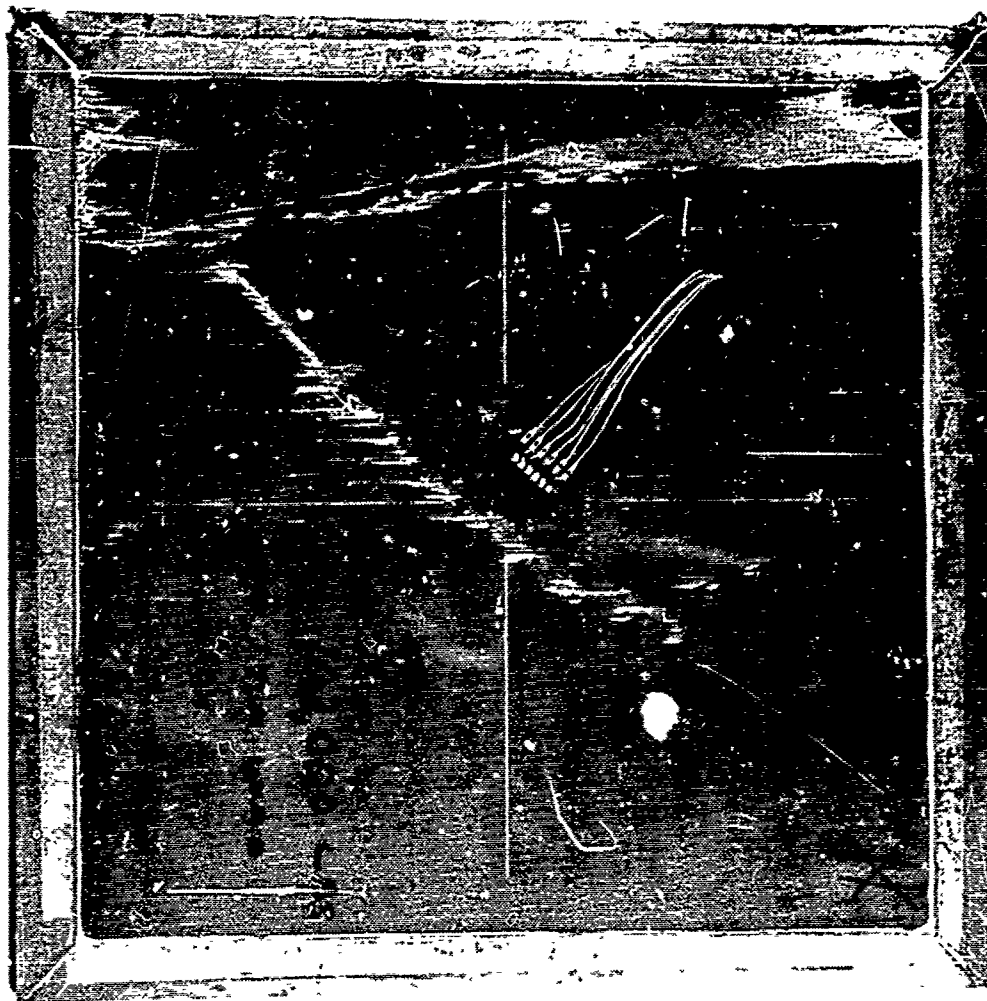
Figure 123. Test Specimen 2B1R2 After Failure, Biaxial Compression
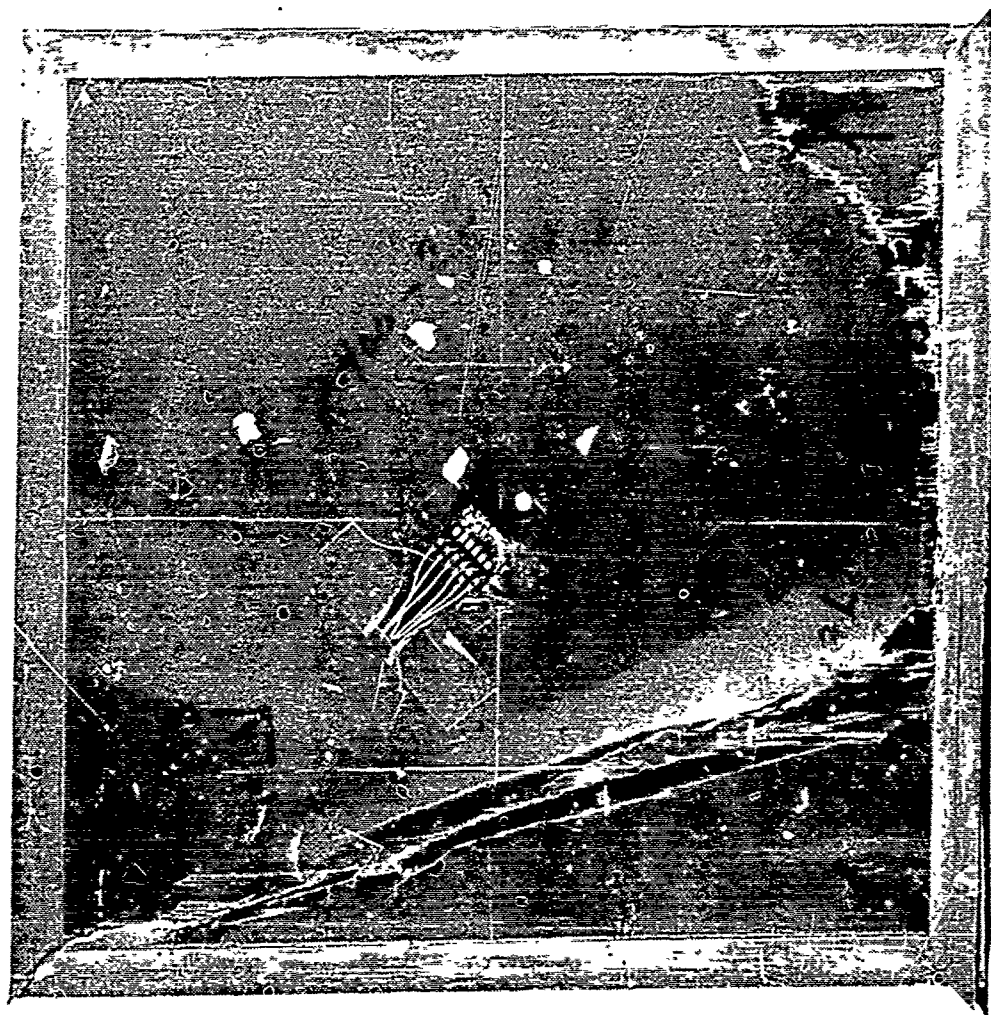
Figure 124. Test Specimen 2B1E1 After Failure, Biaxial Compression

Figure 125. Test Specimen 2B2R1 After Failure, Biaxial Compression
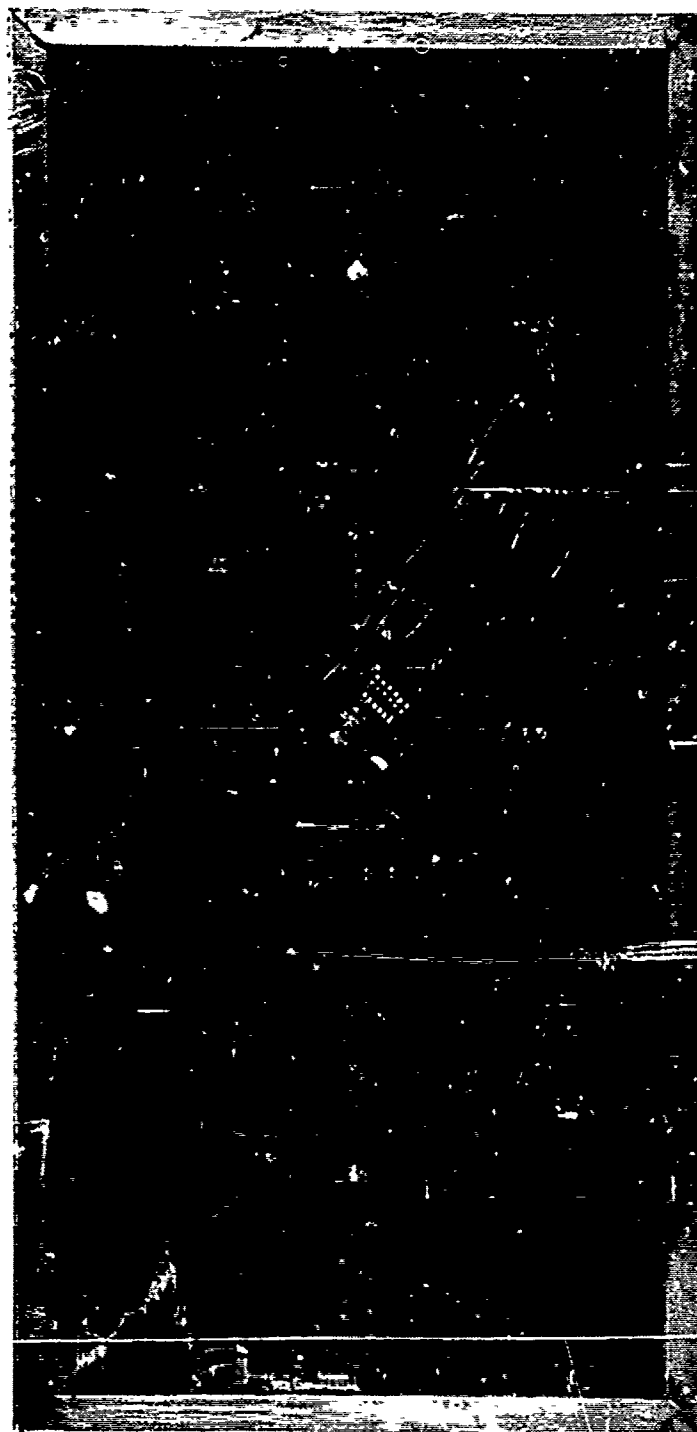
Figure 126. Test Specimen 2B2E1 After Failure, Biaxial Compression

Figure 127. Test Specimen 2B3R1 After Failure, Biaxial Compression
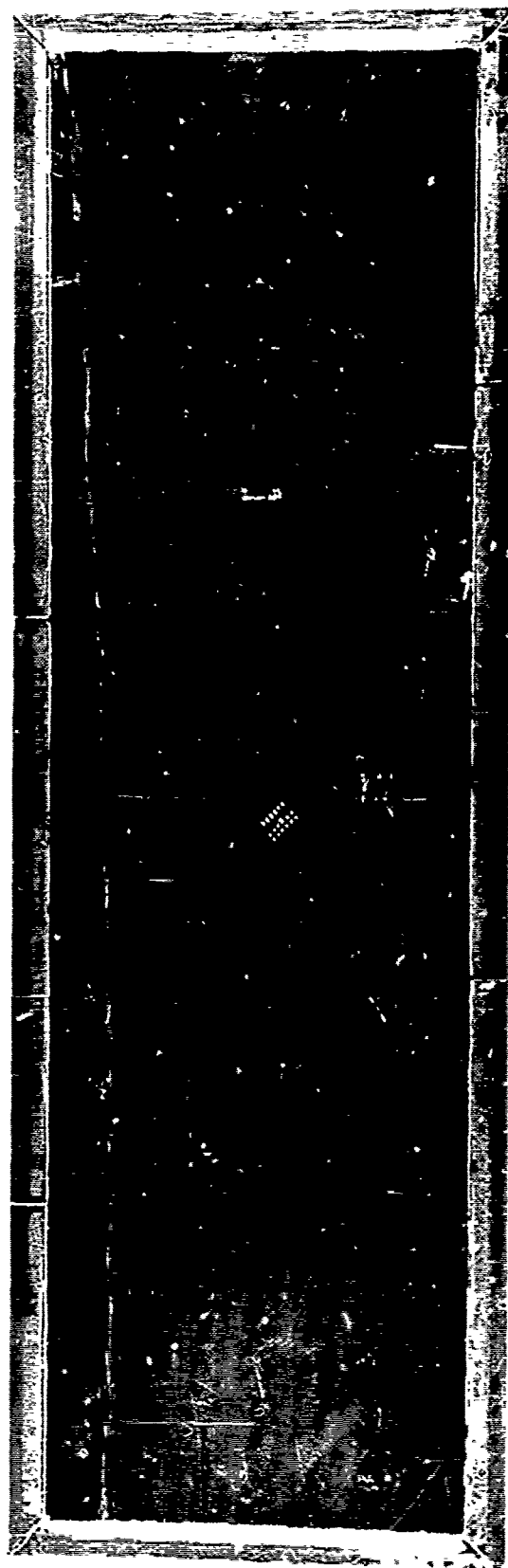
Figure 128. Test Specimen 2B3R2 After Failure, Biaxial Compression

Figure 129.   Test Specimen 2B5E1 After Failure, Biaxial Compression

INPLANE SHEAR (SERIES 3B)

The 3B series honeycomb inplane shear panels were fabricated with $[\pm 45]_T$ face sheets and 3.1 lb/ft^3 (3-10) 5056 aluminum honeycomb core. The boundary condition was somewhere between simple support and fixed. Tests were conducted at both room temperature and 350°F. The basic properties used to calculate the predicted panel buckling loads are given in tables I through III. Also,

$$t_F = 0.0104 \text{ in.} \qquad\qquad c = 0.25 \text{ in.}$$
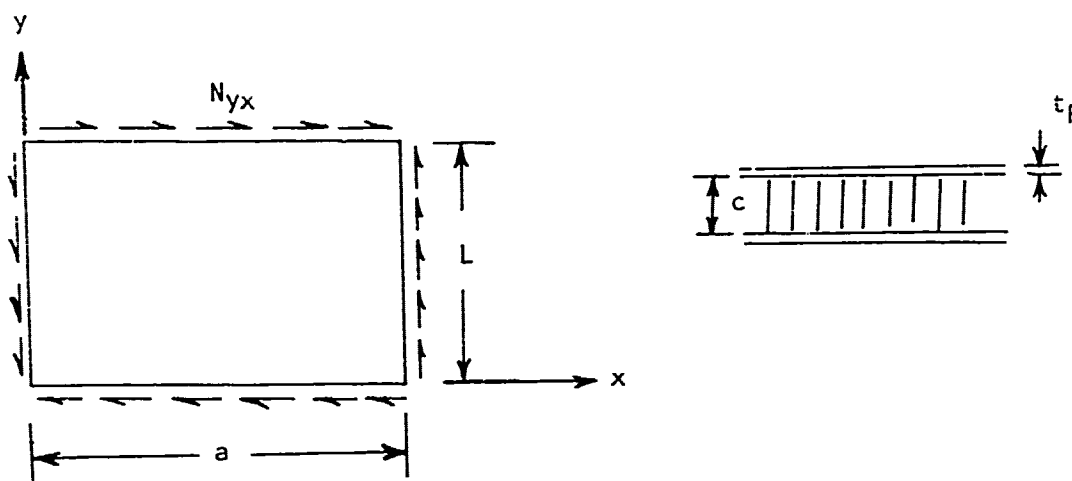
IBM program AC11 of Volume III was used to obtain the predicted buckling load. Table XXVII gives the results, as well as pertinent geometric parameters not heretofore defined. The predicted buckling loads are based on four sides simply supported.

In order to obtain the test buckling load, $(n_{xycr})_{test}$, the pseudo-deflection method shown in the chapter for uniaxially loaded compression panels was used, utilizing the back-to-back diagonal gages of the center rosettes. A typical result is given in figure 130. All the panels failed in tension, with the fracture emanating from a corner. Panel 3B2R1 subsequently had a compression failure in the opposite direction.

The room-temperature projected results for buckling were very high, though this should be mitigated by the fact that the failure loads were much less than the projected buckling loads. The elevated-temperature values were inexpliciably
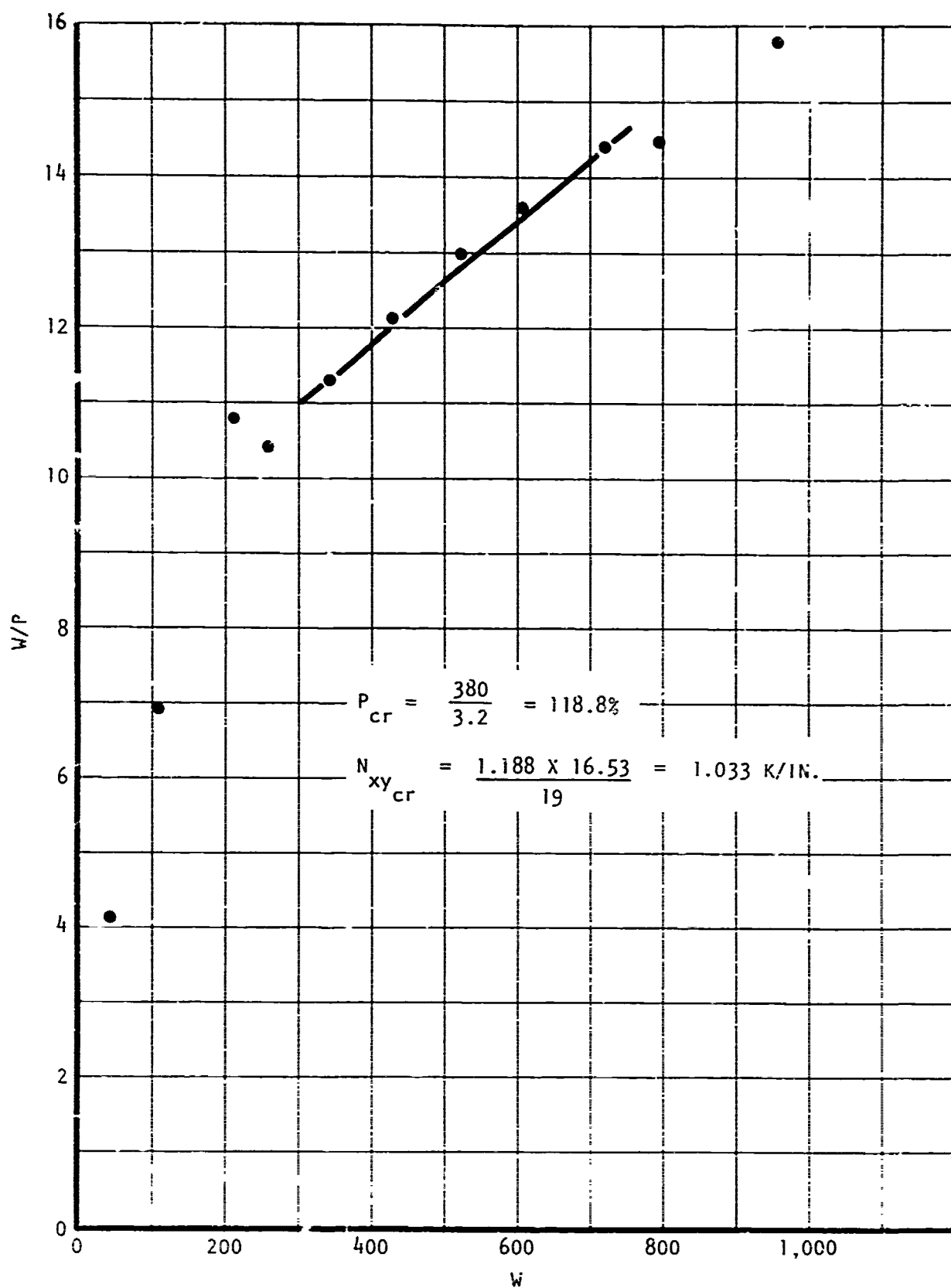
Figure 130. Typical Pseudo-Southwell Plot for Shear Specimen 3B2R1

TABLE XXVII. TEST VERSUS THEORY FOR SHEAR-LOADED HONEYCOMB SANDWICH PANELS

Panel	Temp (°F)	a (in.)	b (in.)	α	ψ (Msi)	V	Theory		Test			
							K^s	N_{xycr}	n_{xycr}	n_{fail}	R_{xy}	f^s_{fail}
3B1R1	RT	26	26	1.0	9.15	0.0040	15.4	726	1,324	364	1.82	17,500
1R2	RT	26	26	1.0	9.15	0.0040	15.4	726	1,409	364	1.94	17,500
1E1	350	26	26	1.0	8.19	0.0058	16.0	674	171	173	0.25	8,300
1E2	350	26	26	1.0	8.19	0.0058	16.0	674	250	187	0.37	9,000
2R1	RT	38	19	1.0	9.15	0.0075	9.80	865	1,299	583	1.50	28,000
2E1	350	38	19	1.0	8.19	0.0108	10.65	840	638	347	0.76	16,700

Results are highly inconclusive.

low. The effects of thermal stresses due to edge constraints should probably be considered in future studies. The ultimate failure loads were all low. This is probably due to stress concentrations at the corner of the plates. Figures 131 through 141 are photographs of the test specimens after failure.

UNIAXIAL COMPRESSION AND INPLANE SHEAR (SERIES 4B)

The 4B series honeycomb panels were loaded in combined uniaxial compression and inplane shear. The face sheets were Narmco 5505 $[\pm 45]_T$ and the core was 5056 aluminum, 3.1 pcf (3-10) honeycomb. Tests were conducted at both room temperature and 350°F. The basic properties used to determine the predicted strengths are given in tables I through III.

Computer program AC5 of Volume III of this report was used to obtain the uniaxial compression strength predictions, while the shear predictions were given in the paragraph pertaining to the series 3B tests. The results are presented in the form of an interaction curve, figure 142, where

$$R_x = \frac{(n_{xcr})_{test}}{(N_{xcr})_{theory}}$$

$$R_{xy} = \frac{(n_{xycr})_{test}}{(N_{xycr})_{theory}}$$

Figure 131. Test Specimen 3B1R1 After Failure, Front Side, Inplane Shear

Figure 132. Test Specimen 3B1R1 After Failure, Back Side, Inplane Shear

Figure 133. Test Specimen 3B1R1 After Failure, Back Side, Inplane Shear

Figure 134.   Test Specimen 3B1R2 After Failure, Front Side, Inplane Shear

Figure 135. Test Specimen 3B1R2 After Failure, Back Side, Inplane Shear
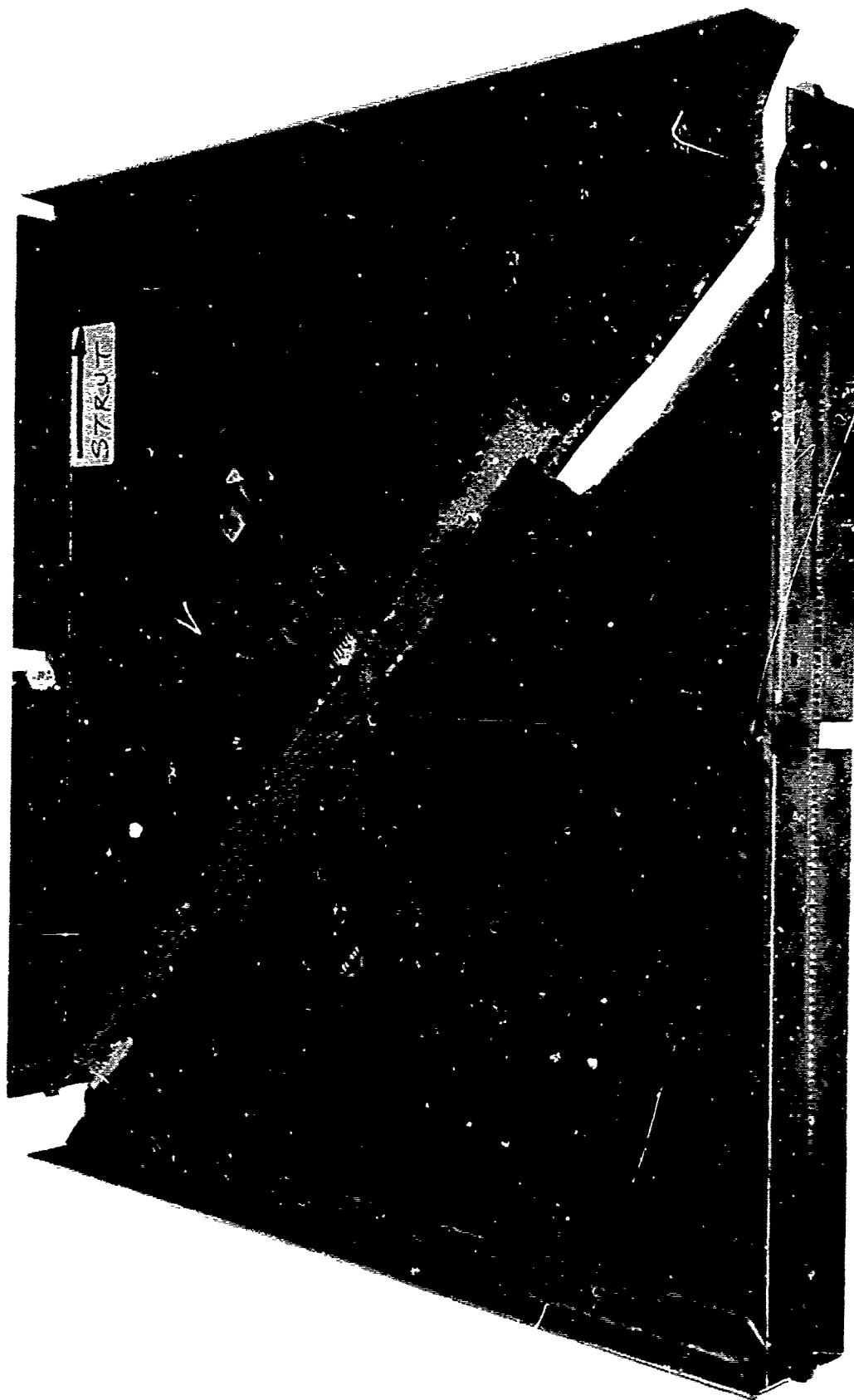
Figure 136. Test Specimen 3B1E1 After Failure, Front Side, Inplane Shear

177
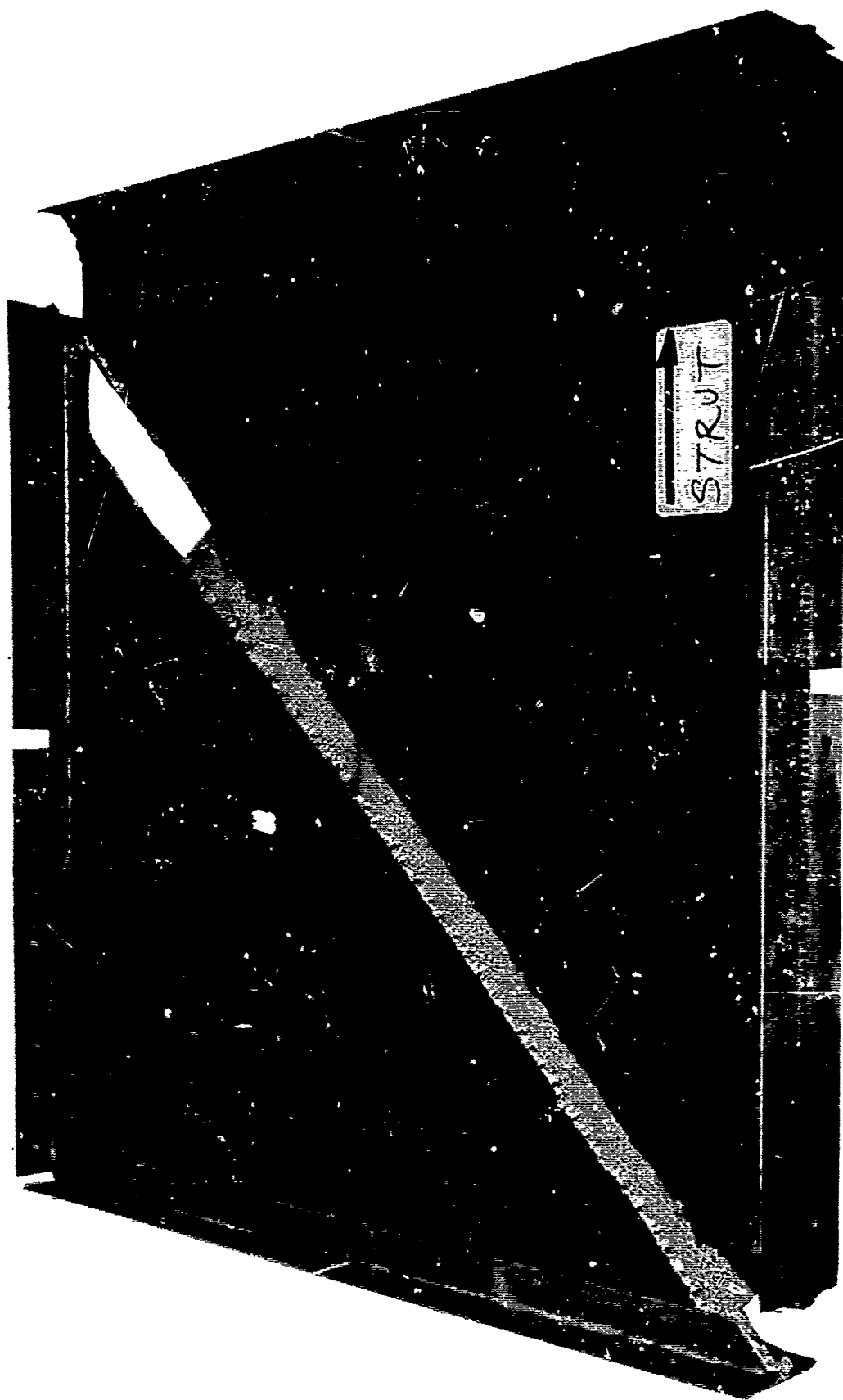
Figure 137. Test Specimen 3B1E1 After Failure, Back Side, Inplane Shear

Figure 138. Test Specimen 3B1E2 After Failure, Front Side, Inplane Shear
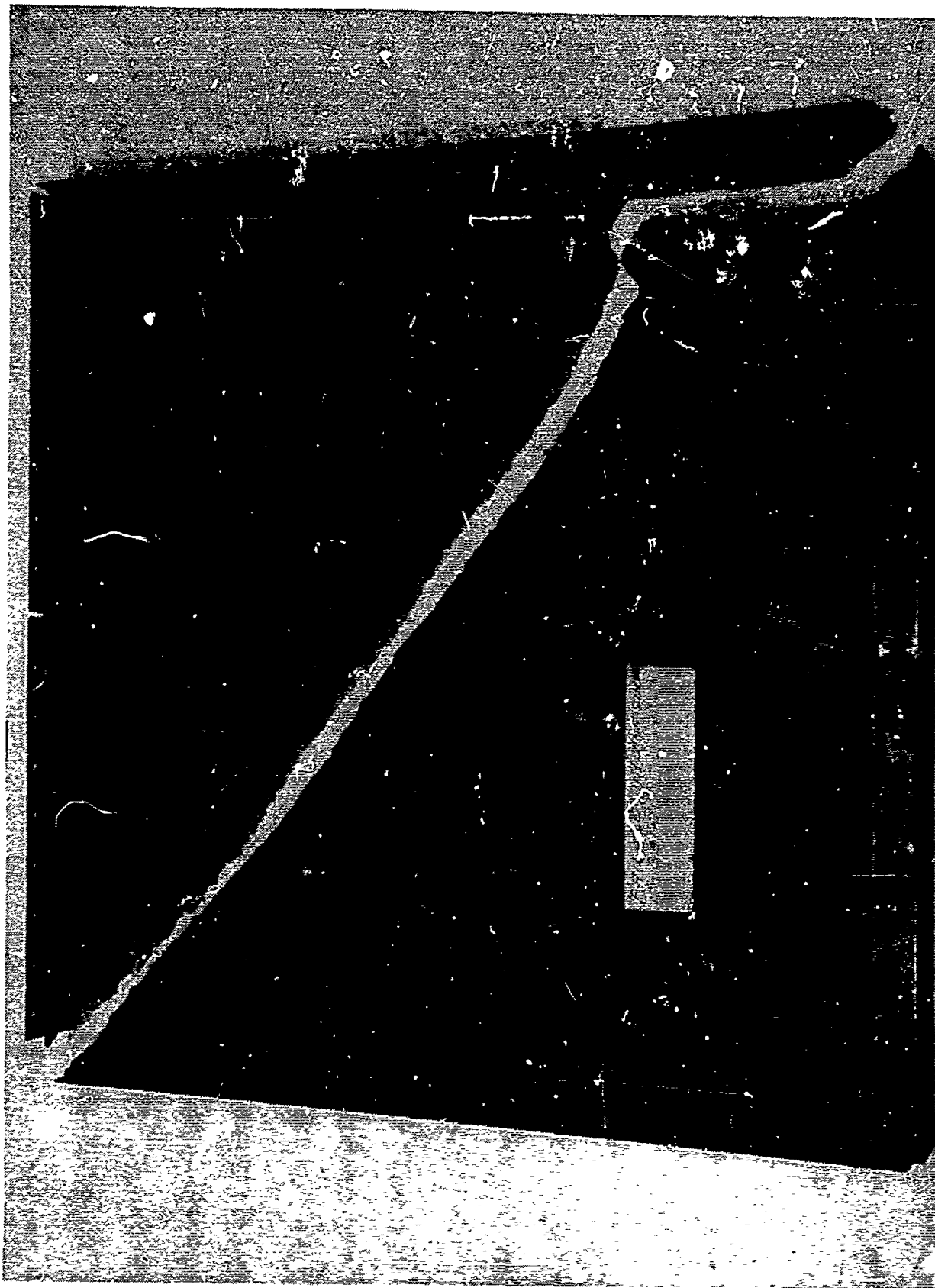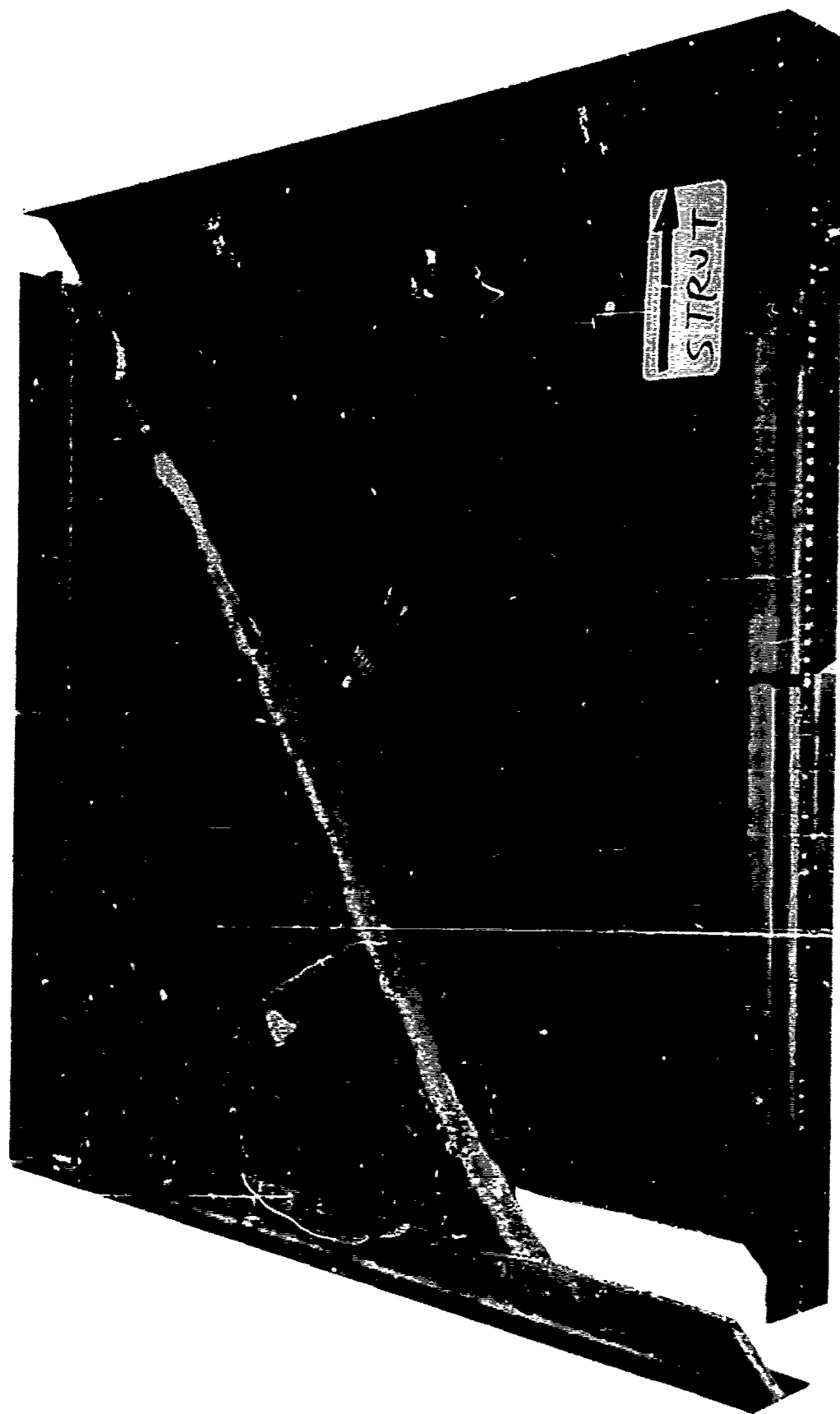
Figure 139. Test Specimen 3B1E2 After Failure, Back Side, Inplane Shear
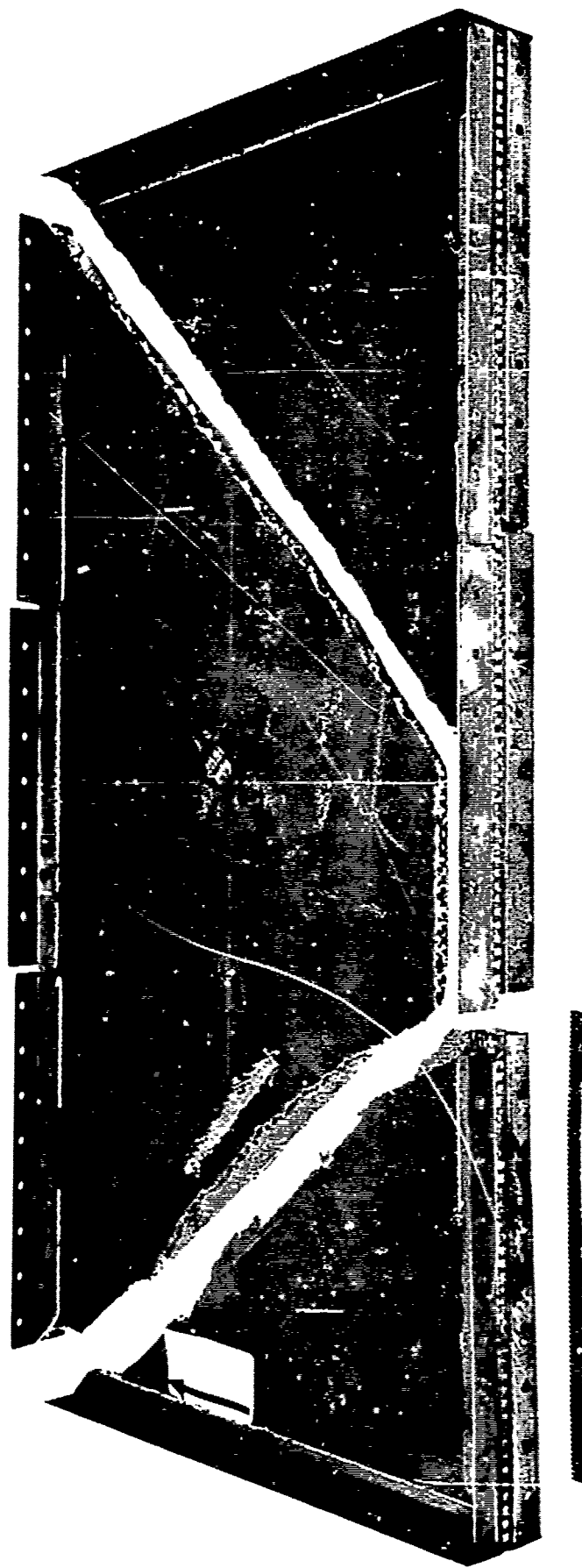
Figure 140.   Test Specimen 3B2R1 After Failure, Inplane Shear

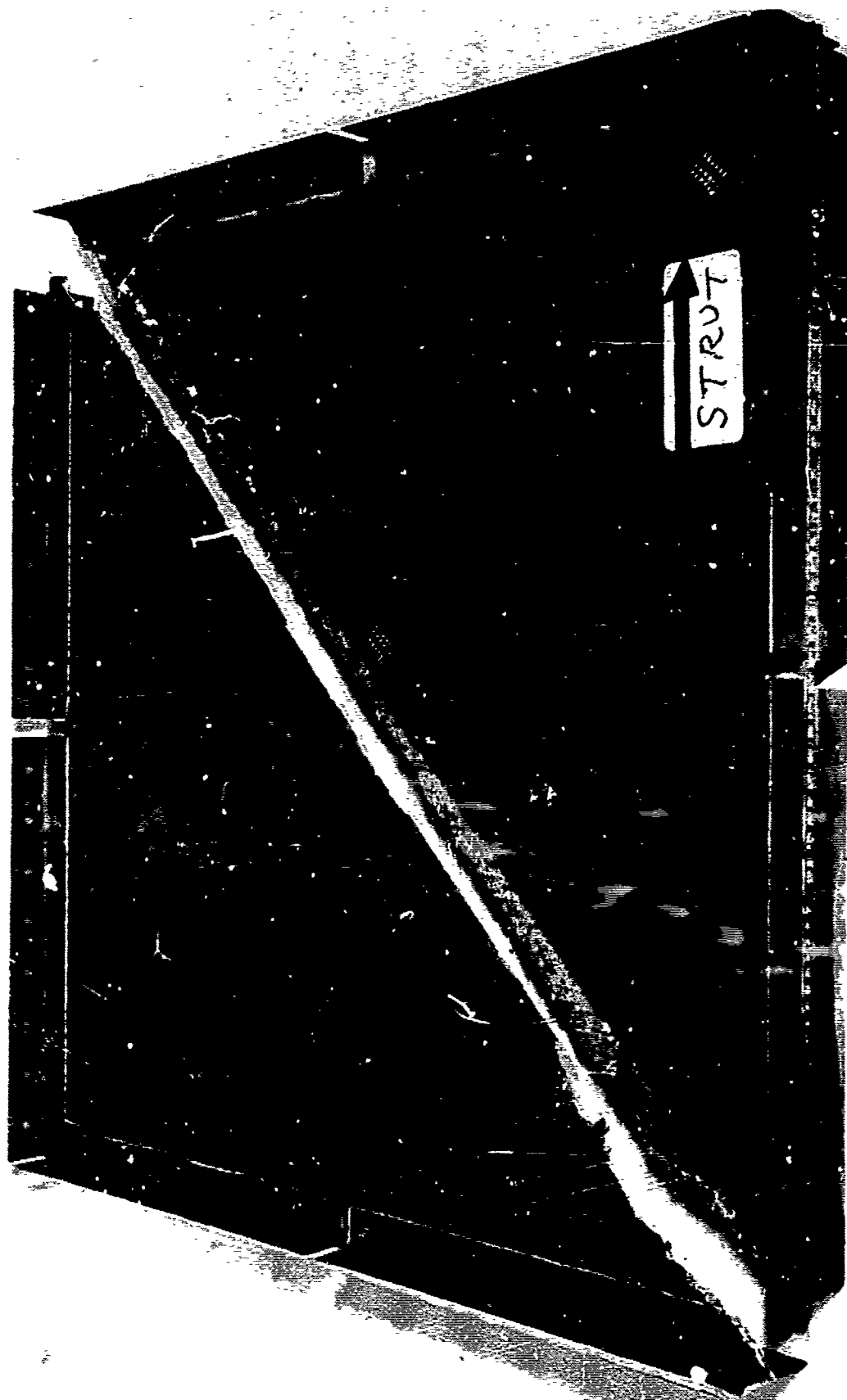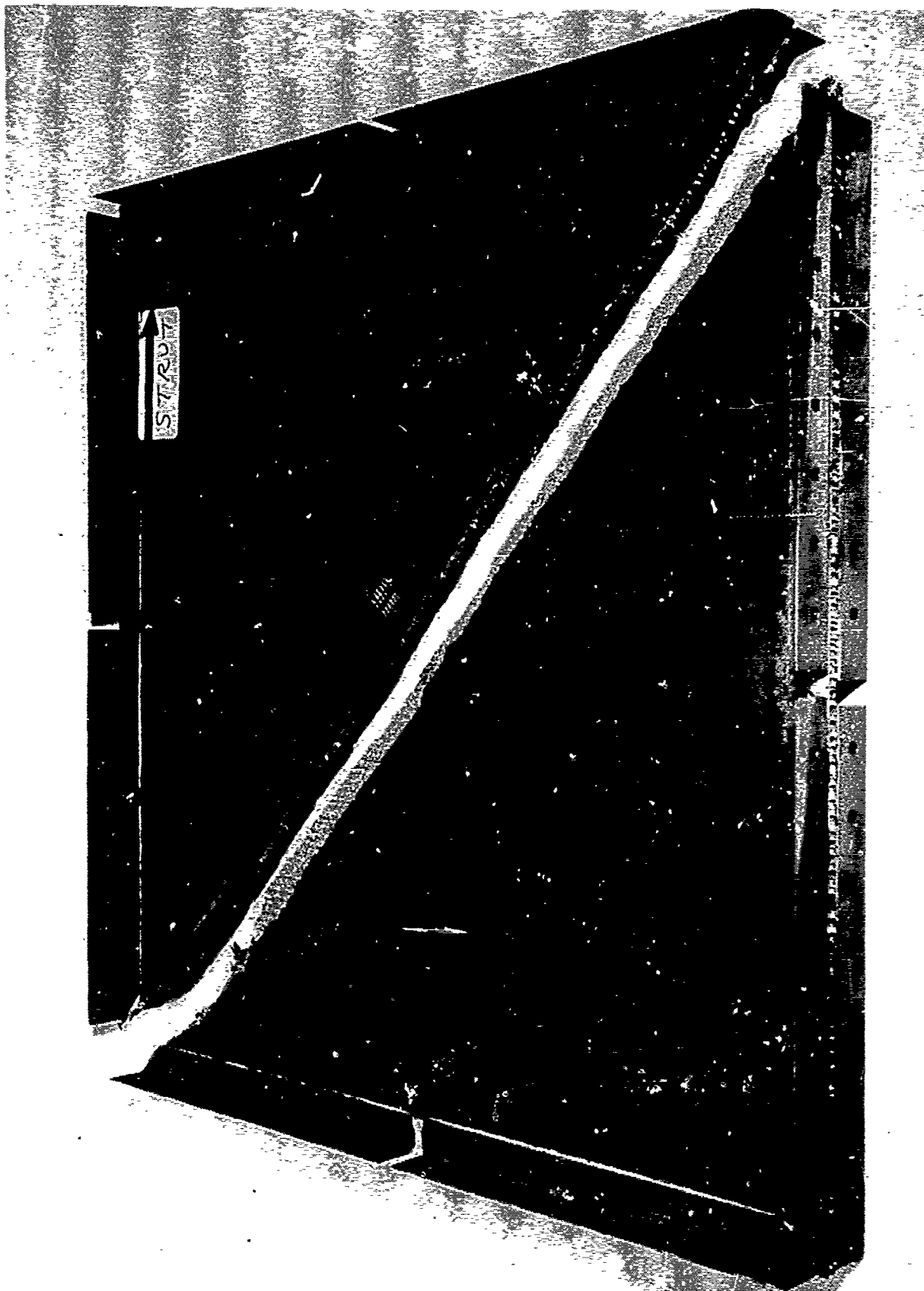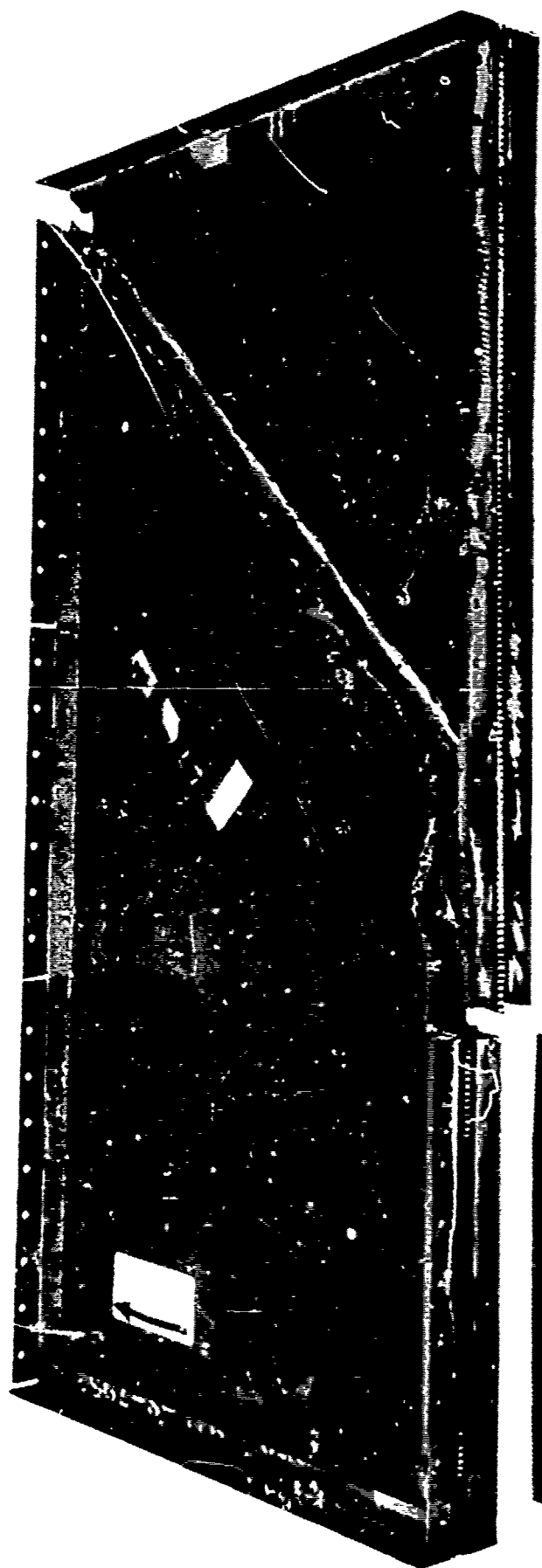Figure 141. Test Specimen 3B2E1 After Failure, Inplane Shear
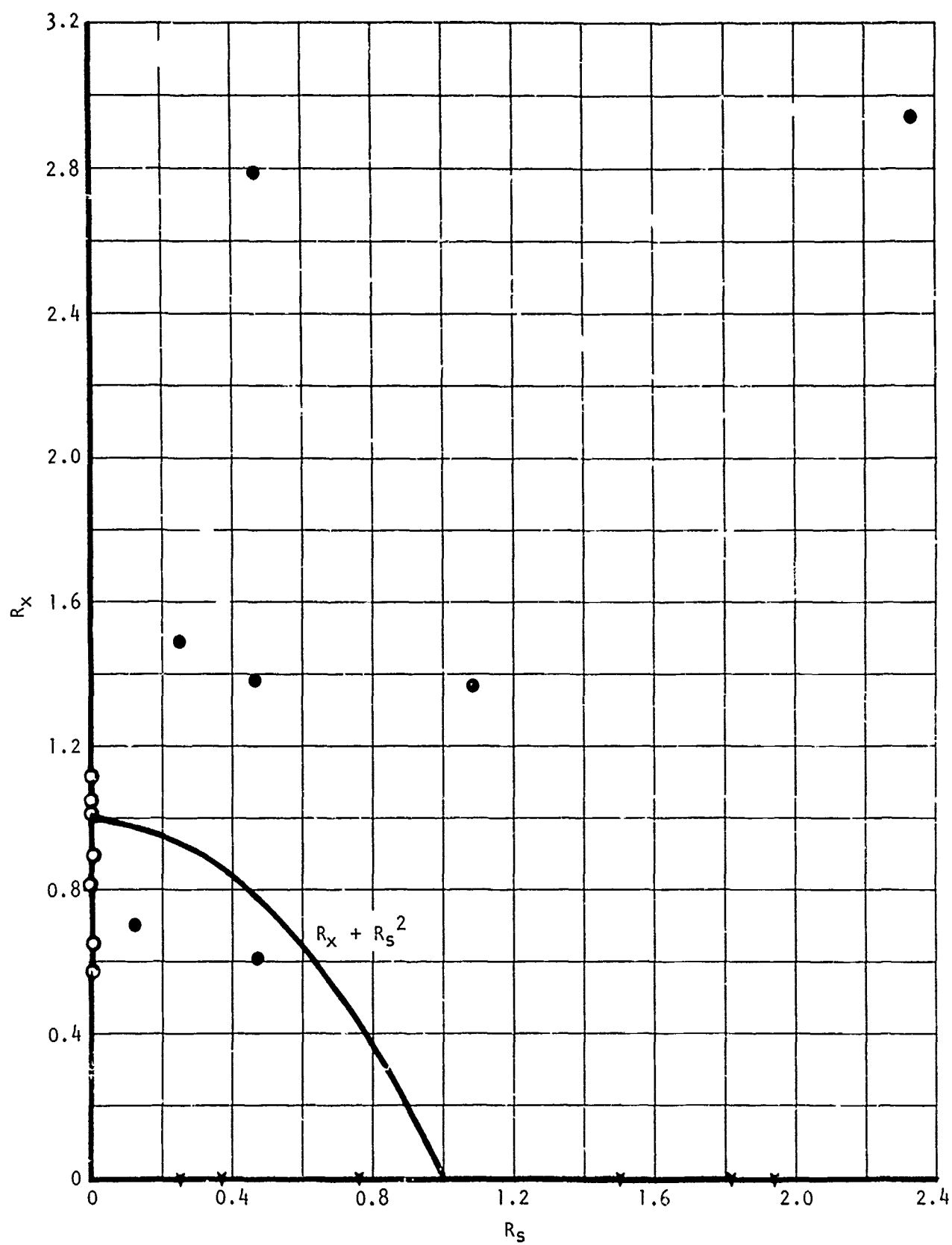
Figure 142. Interaction Curve, Uniaxial Compression and Shear Loading

The plot axes are labeled R_x (vertical) and R_s (horizontal). The curve is labeled $R_x + R_s^2$.

where (n_{xcr})test and (n_{xycr})test are the test buckling loads obtained by evaluations of back-to-back strain gages (refer to series 3B tests). The test results for the compression only and shear panels are also shown in figure 142 for comparison purposes. The results are shown in table XXVIII. Figures 143 through 149 are photographs of the test specimens after failure.

TABLE XXVIII.   TEST VERSUS THEORY FOR COMBINED UNIAXIAL COMPRESSION
AND SHEAR LOADED HONEYCOMB SANDWICH PANELS

Panel	Temp (°F)	a (in.)	b (in.)	α	ψ (Msi)	ν	Theory		Test				$\frac{n_{xycr}}{N_{xycr}}$ R_{xy}	$\frac{n_{xcr}}{N_{xcr}}$ P_x
							N_{xycr} (lb/in.)	N_{xcr} (lb/in.)	n_{xycr} (lb/in.)	n_{xcr} (lb/in.)	$n_{xy_{fail}}$ (lb/in.)	$n_{x_{fail}}$ (lb/in.)		
4B1R1	RT	26	26	1.0	9.15	0.0040	726	316	312	881	214	551	0.17	2.79
1R2	---	26	26	---	---	---	---	---	785	433	669	369	1.08	1.37
1E1	350	26	26	1.0	8.19	0.0058	671	297	166	442	97	259	0.25	1.49
1F2	---	---	---	---	---	---	---	---	5?1	409	169	222	0.46	1.38
2R1	RT	38	19	1.0	9.15	0.0075	865	581	*	*	167	656	*	*
2R2	---	38	19	---	---	---	---	---	2,021	1,708	520	270	2.54	2.91
2E1	350	38	19	1.0	8.19	0.0108	840	537	97	377	132	512	0.12	0.70
2E2	---	---	---	---	---	---	---	---	392	326	310	285	0.47	0.61

*Results were highly inconclusive.

184

Figure 143. Test Specimen 4B1R2 After Failure

Figure 144. Test Specimen 4B1E1 After Failure

Figure 145. Test Specimen 4B1E2 After Failure
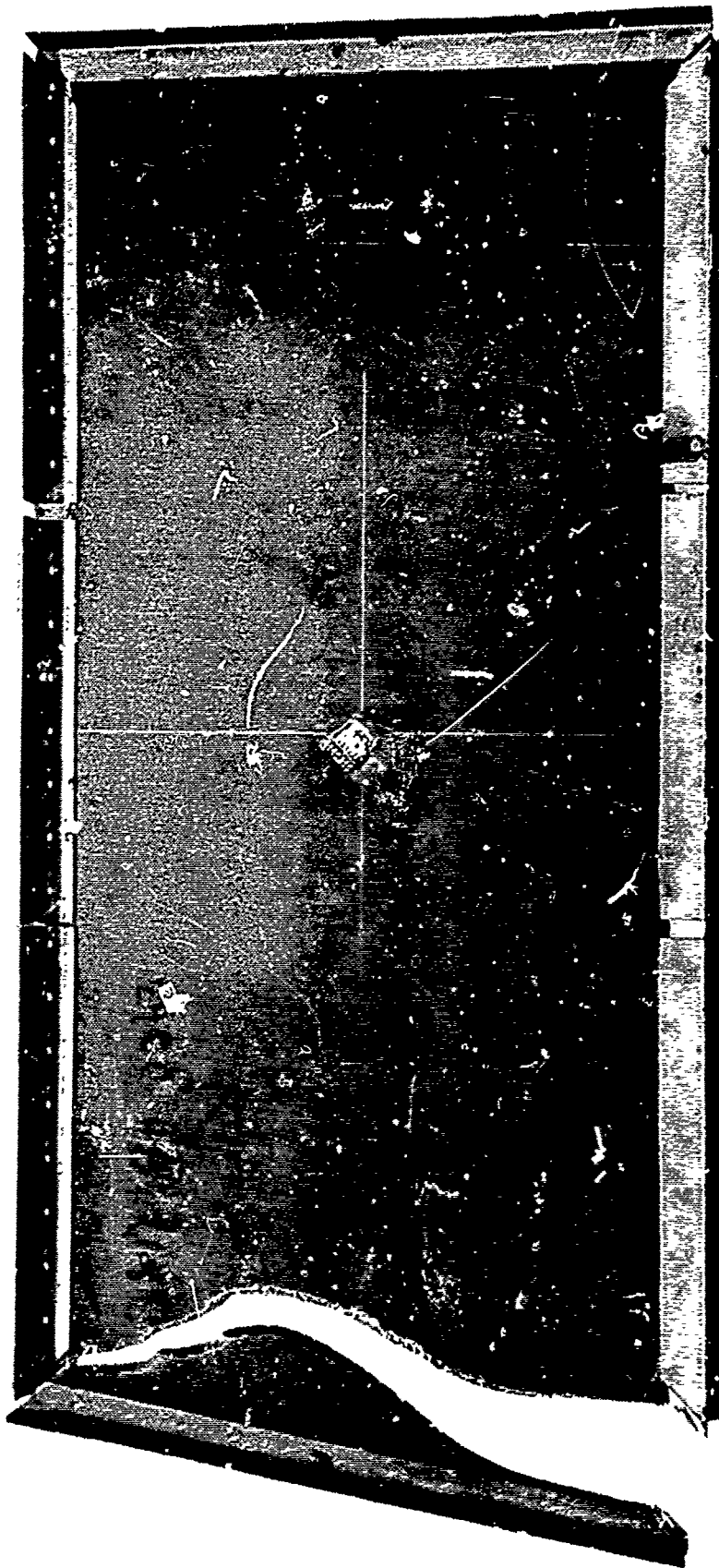
Figure 146. Test Specimen 4B2R1 After Failure

Figure 147. Test Specimen 4R2R2 After Failure

189
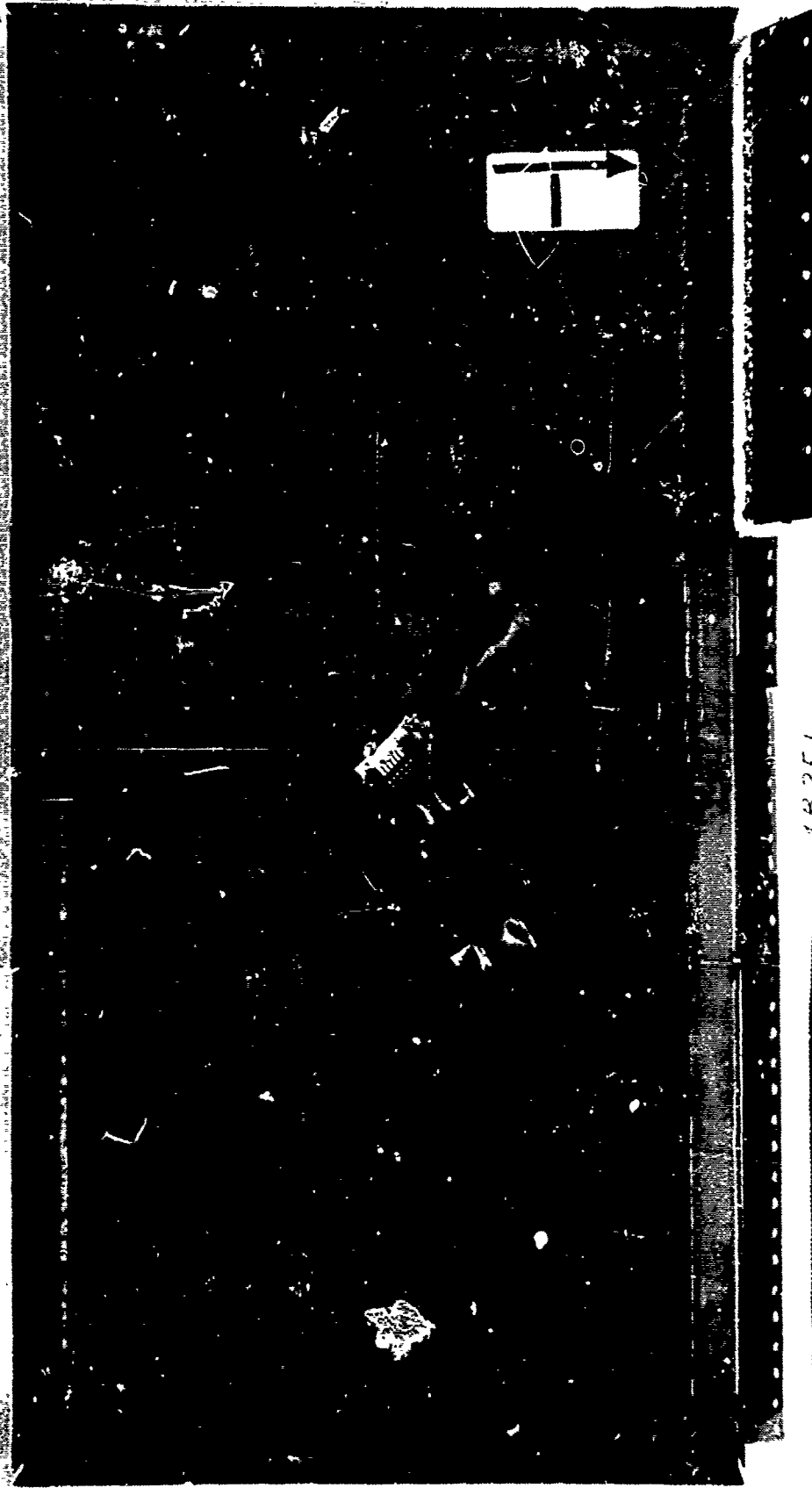
Figure 148. Test Specimen 4B2E1 After Failure
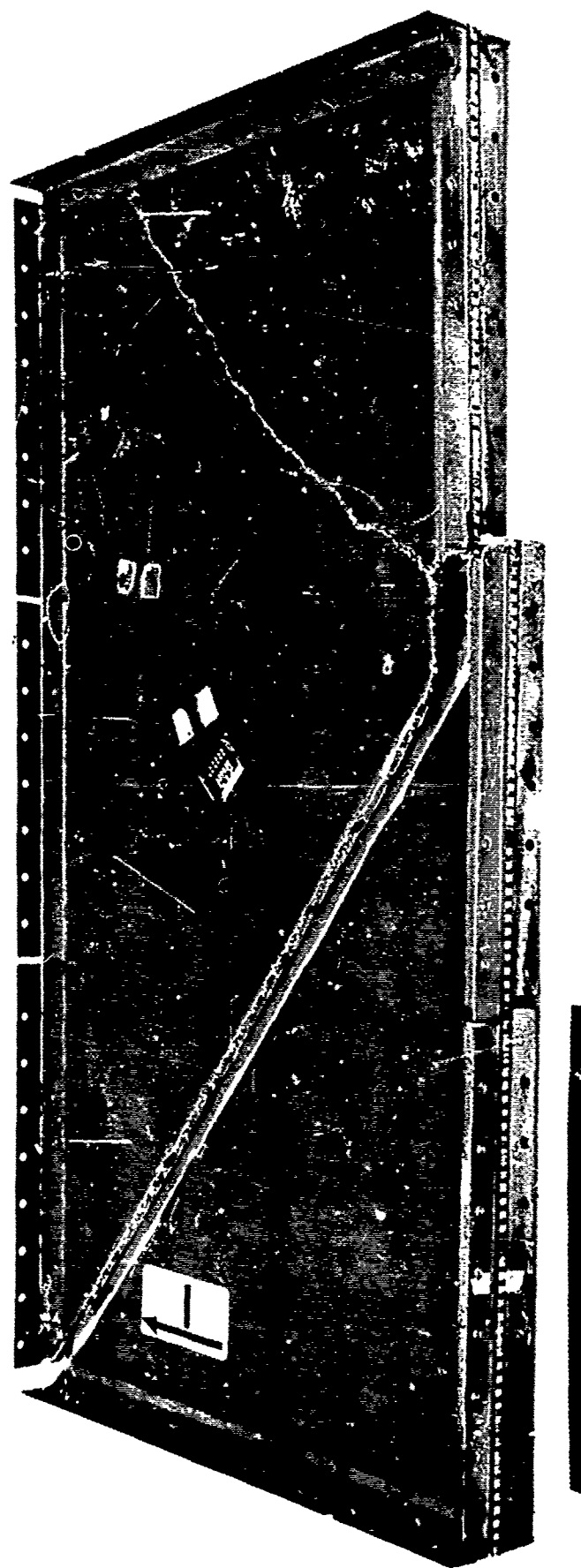
Figure 149. Test Specimen 4B2E2 After Failure

NORMAL PRESSURE (SERIES 5B)

Static Pressure

The analytical prediction methods for the response behavior of simply supported honeycomb sandwich panels with orthotropic faces and core have been developed and appear in Volume III of this report. For the simply supported panel shown in figure 150, subjected to a normal pressure q, the predicted maximum panel deflection and internal moments and shear forces are given in figure 151 and table XXIX. These data were obtained from computer program AC-7, described in Volume III.

The 5B series honeycomb pressure panels were all fabricated with $[0/\pm45/0]_S$ faces and 5056 aluminum, 8.1 lb/ft^3, 2-mil core with a 1/8-inch cell. The properties used in the analysis are tabulated below.

$$t_F \qquad = \quad 8 \text{ plies x } 0.0052 \text{ in./ply} = 0.0416 \text{ in.}$$

$$c \qquad = \quad 0.500 \text{ in.}$$

$$(G'_{cx})_{RT} \qquad = \quad 126{,}000 \text{ psi}$$

$$(G'_{cx})_{350°F} \quad = \quad 116{,}000 \text{ psi}$$
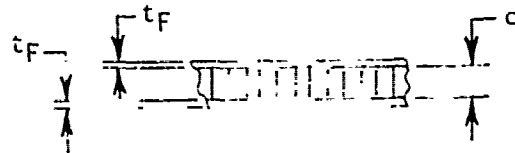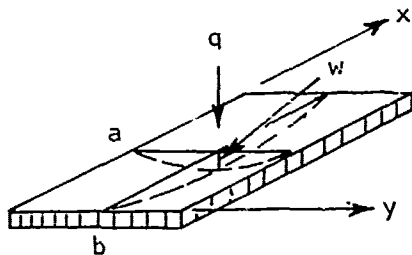
Figure 150. Simply Supported Honeycomb Sandwich Panel Subjected to Normal Pressure
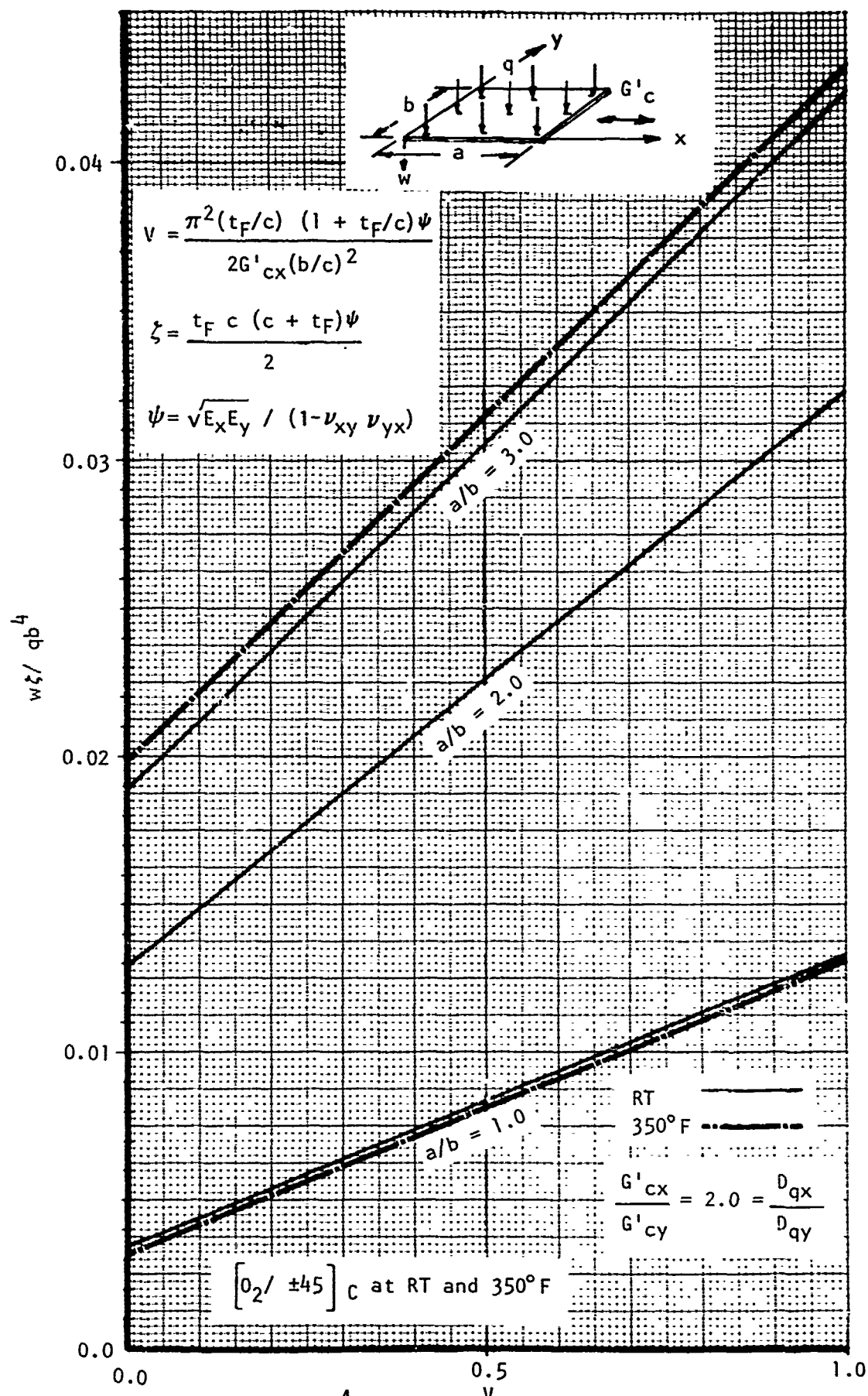
Figure 151. Parameter $w\zeta/qb^4$ Versus V for Simply-Supported Honeycomb Panel

TABLE XXIX. INTERNAL MOMENT AND SHEAR COEFFICIENTS FOR SIMPLY
SUPPORTED PANELS*

a/b	Temp (°F)	M_x/qb^2 x/a = 0.5 y/b = 0.5	M_y/qb^2 x/a = 0.5 y/b = 0.5	Q_x/qb x/a = 0.0 y/b = 0.5	Q_y/qb x/a = 0.5 y/b = 0.0
1.0	RT	0.073	0.027	0.396	0.262
	350	0.072	0.026	0.396	0.254
2.0	RT	0.094	0.077	0.485	0.408
	350	0.104	0.071	0.512	0.395
3.0	RT	0.092	0.104	0.496	0.461
	350	0.107	0.099	0.533	0.451

*Laminate Orientation - $[0/\pm45/0]_S$
Material - Narmco 5505
$$\frac{G'_{cx}}{G'_{cy}} = \frac{D_{qx}}{D_{qy}} = 2.0$$

Table XXX lists the material properties used in the analysis.

TABLE XXX. MATERIAL PROPERTY DATA FOR 5B SERIES PANELS

Temp (°F)	Face Sheet Properties						Sandwich Properties	
	E_x (Msi)	E_y (Msi)	G_{xy} (Msi)	ν_{xy}	ν_{yx}	ψ (Msi)	ξ (10^4 lb-in.)	Vb^2 (in.^{2})
RT	16.67	5.06	4.30	0.701	0.213	10.79	6.07	9.50
350	15.78	3.86	3.97	0.840	0.205	9.42	5.30	9.05

where

$$\psi = \sqrt{E_x E_y} \Big/ (1 - \nu_{xy}\nu_{yx})$$

and

$$\xi = \frac{t_F c\ (c + t_F)\psi}{2}$$

Thus, for 5B1 series

$$a/b = 1: \quad V_{RT} \quad = 9.50/15^2 = 0.042$$

$$V_{350°F} = 9.05/15^2 = 0.040$$

$$a/b = 3: \quad V_{RT} \quad = 9.50/13^2 = 0.056$$

$$V_{350°F} = 9.05/13^2 = 0.053$$

A comparison of the predicted maximum normal deflection and the test data are given in table XXXI.

TABLE XXXI. TEST VERSUS THEORY FOR MAXIMUM NORMAL DEFLECTION OF PANELS

Specimen	Temp (°F)	Failure Pressure q (psi)	a/b	b (in.)	$w\xi/qh^4$ (figure 151)	(w/q) Theory	(w/q) Test
5B1R1	RT	58.0	1.0	15.0	0.0038	0.0032	0.0040
1R2	RT	57.0	1.0	15.0	0.0038	0.0032	0.0035
1E1	350	55.0	1.0	15.0	0.0035	0.0033	0.0044
3R1	RT	27.0	3.0	13.0	0.020	0.0094	0.0100
3E1	RT	18.5	3.0	13.0	0.021	0.0112	0.0125

With the use of table XXXI and the material allowables in table XXXII, the critical stress for the test panels considered was found to be the transverse stress in the center of the tension face of the H/C panel; i.e., the stress parallel to the Y axis.

TABLE XXXII. MATERIAL ALLOWABLES FOR $[0/\pm45/0]_C$

Temp (°F)	F_y^{tu} (psi)	F_x^{tu} (psi)
RT	16,500	103,000
350	13,800	91,300

The theoretical failure pressure can then be calculated from the relation:

$$F_y^{tu} = \frac{(M_y)(c+t_F)/2}{t_F(c+t_F)^2/2} = \alpha q b^2 / [t_F(c+t_F)]$$

or

$$(q)_{failure} = F_y^{tu}(c+t_F)t_F / [\alpha b^2]$$

where α is obtained from the fourth column of table XXIX. Figures 152 and 153 compare the predicted panel deflections and failure pressure to the test data. As can be seen from these figures, the theory and test are in good agreement. Typical failed specimens are shown in figures 159 through 164. Figures 154 through 158 show plots of the midpoint deflection for the panels.

Alternating Pressure

Two panels with geometry identical to 5B3R1 were subjected to fatigue loading by cycling the positive normal pressure applied to the panels from zero to peak pressure q. The pressure spectrum for the alternating loading is given in table XXXIII.

196

Figure 152. Maximum Normal Deflection for Simply Supported Honeycomb Panels

FACE SHEETS

$[0/\pm45/0]_S$

$G'_{cx}/G'_{cy} = 2.0$

$\rho_c = 8.1$ LB/FT^3 (ALUM)

⊙ RT; a/b = 1; b = 15 IN.

⊕ 350° F ; a/b = 1; b = 15 IN.

◈ RT ; a/b = 3; b = 13 IN.

◈ 350° F; a/b = 3; b = 13 IN.

(W/q) PREDICTED

(W/q) ACTUAL
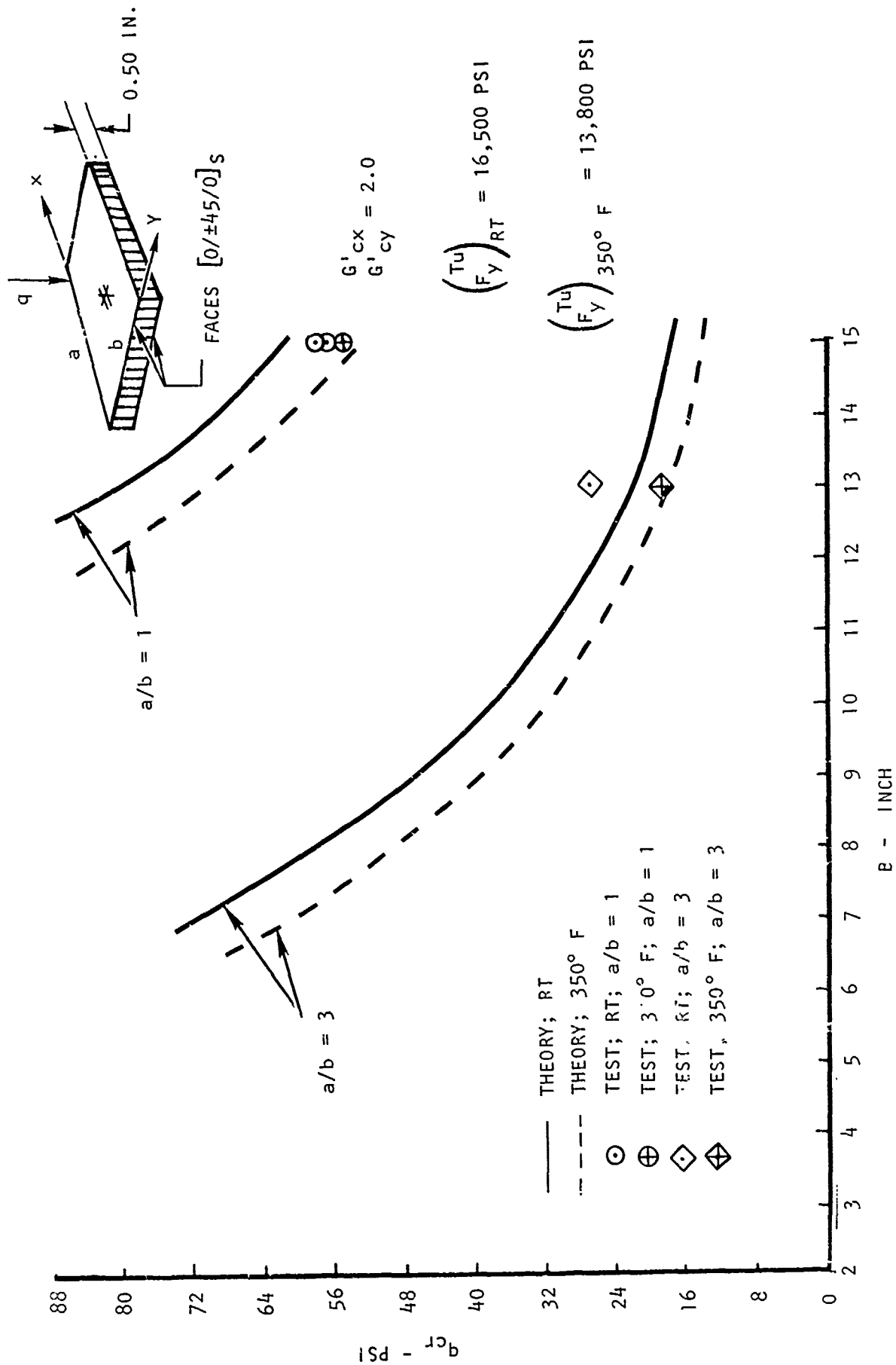
Figure 153. Normal Failure Pressure q_{cr} Versus Panel Width

0.50 IN.

FACES $[0/\pm45/0]_S$

$G'_{cx} = 2.0$
G'_{cy}

$\left(\dfrac{T_u}{F_y}\right)_{RT} = 16{,}500$ PSI

$\left(\dfrac{T_u}{F_y}\right)_{350° F} = 13{,}800$ PSI

$a/b = 1$

$a/b = 3$

——— THEORY; RT
– – – THEORY; 350° F
⊙ TEST; RT; a/b = 1
⊕ TEST; 350° F; a/b = 1
◇ TEST; RT; a/b = 3
⊕ TEST; 350° F; a/b = 3

B - INCH

q_{cr} - PSI
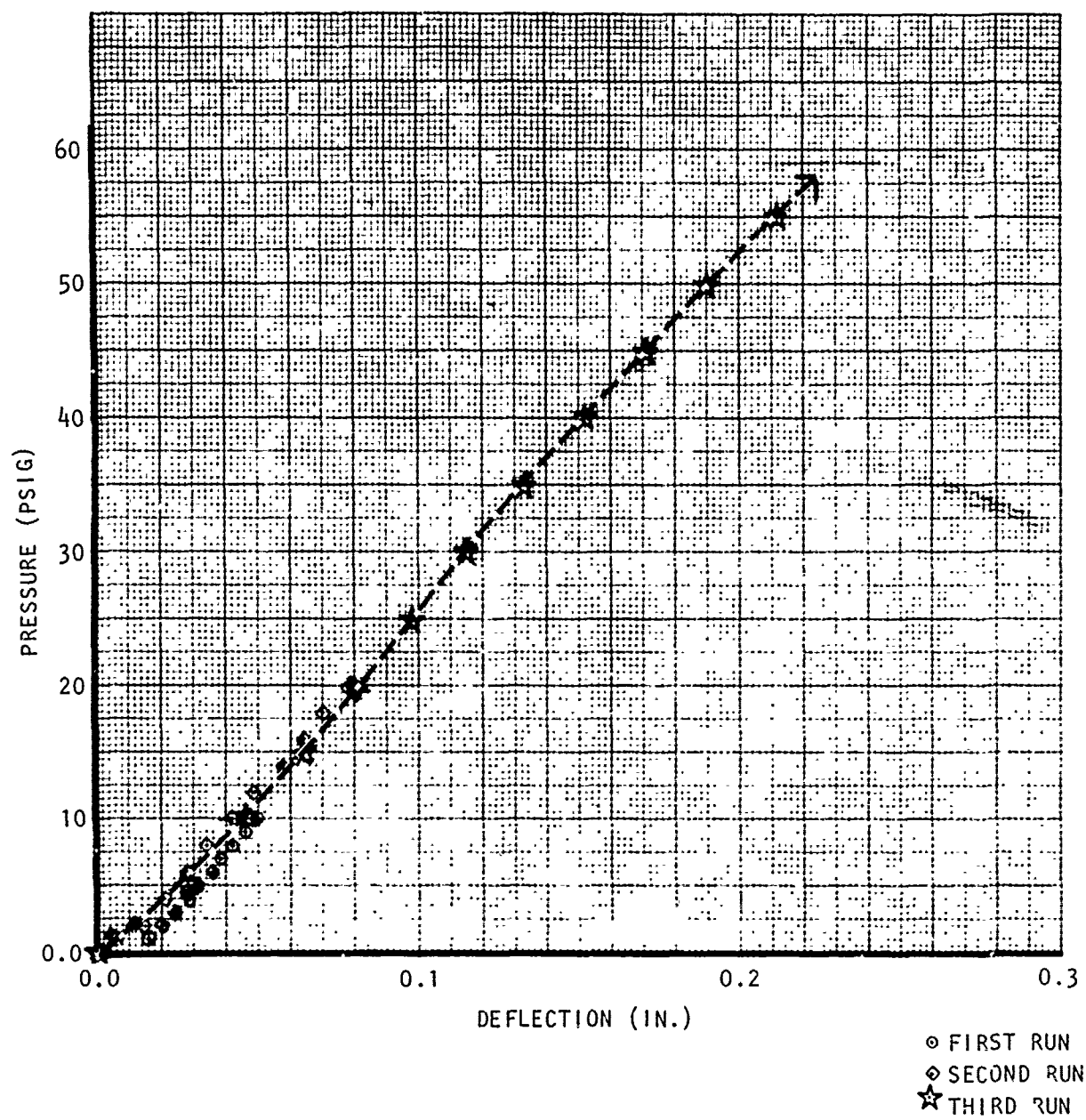
Figure 154. Midpoint Deflection vs Pressure for Panel 5B1R1
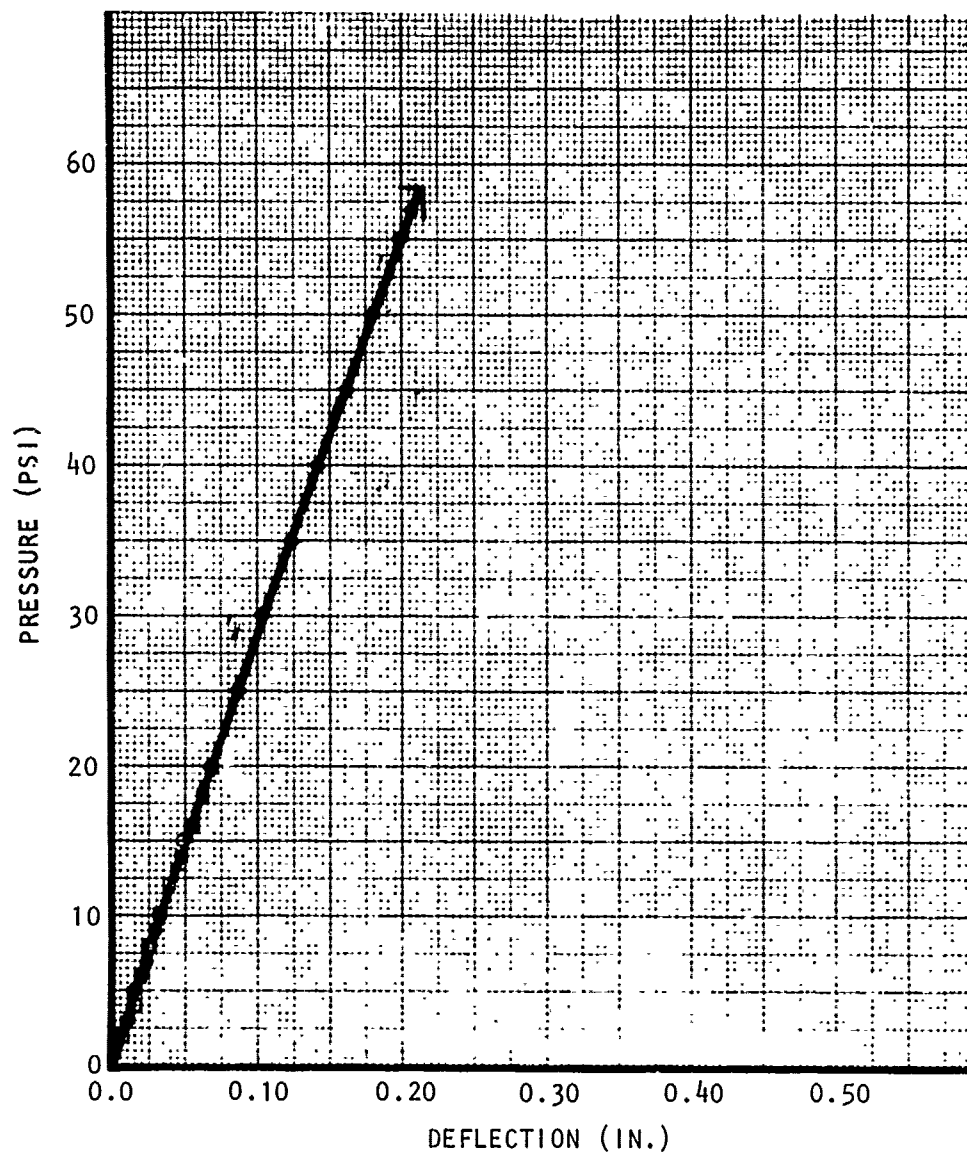
Figure 155. Midpoint Deflection vs Pressure for Panel 5B1R2
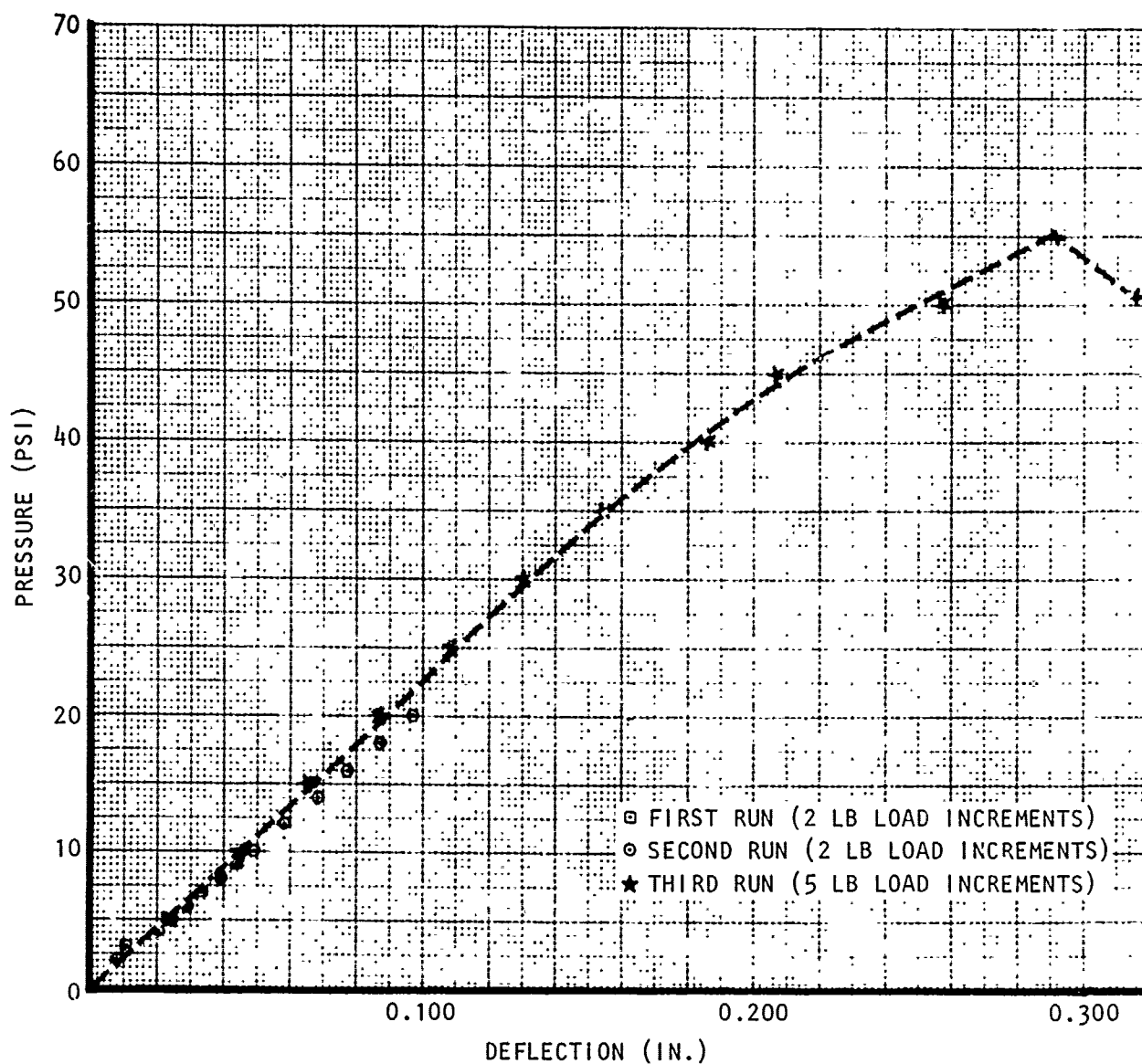
Figure 156. Midpoint Deflection vs Pressure for Panel 5B1E1
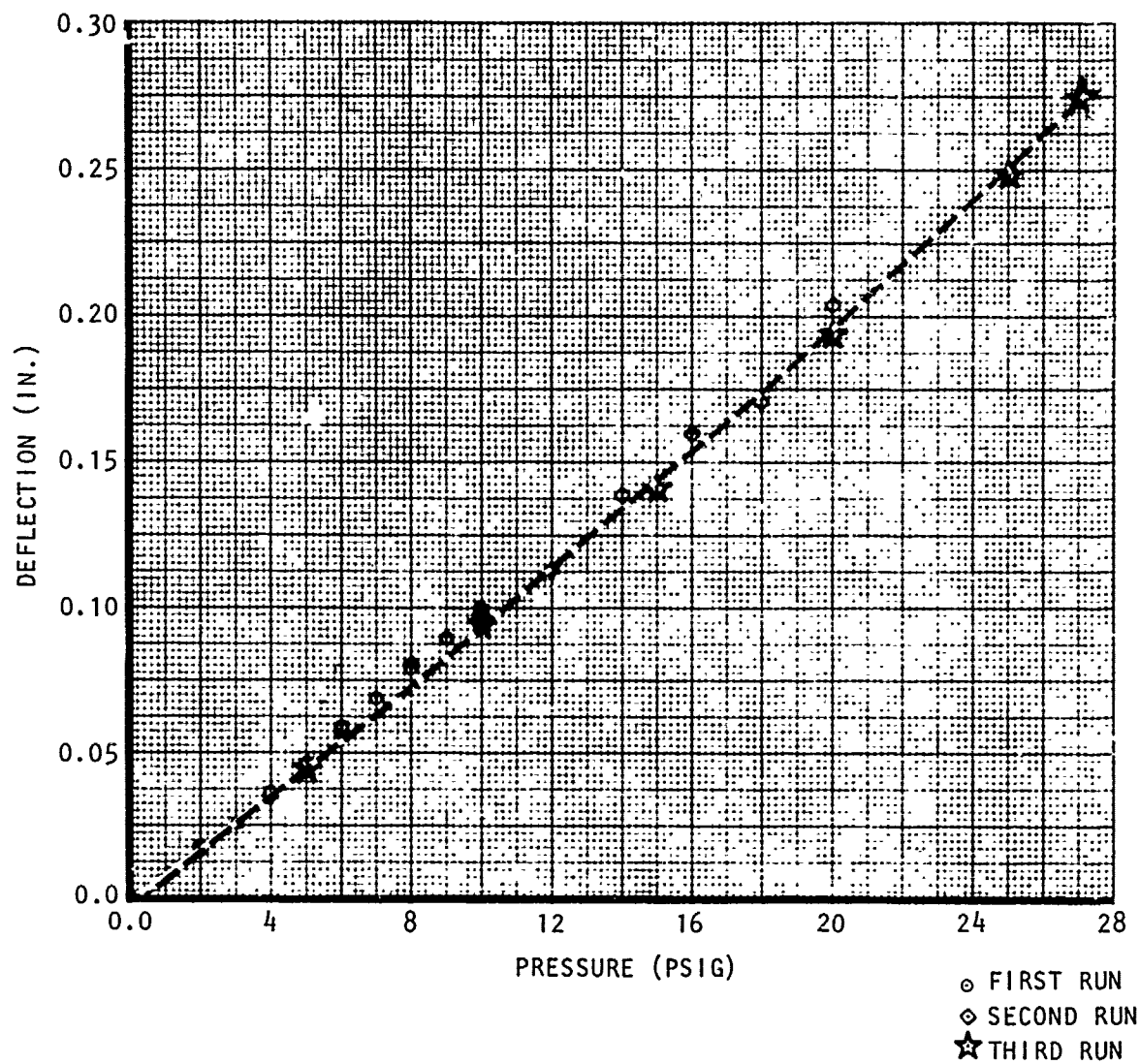
Figure 157. Midpoint Deflection vs Pressure for Panel 5B3R1
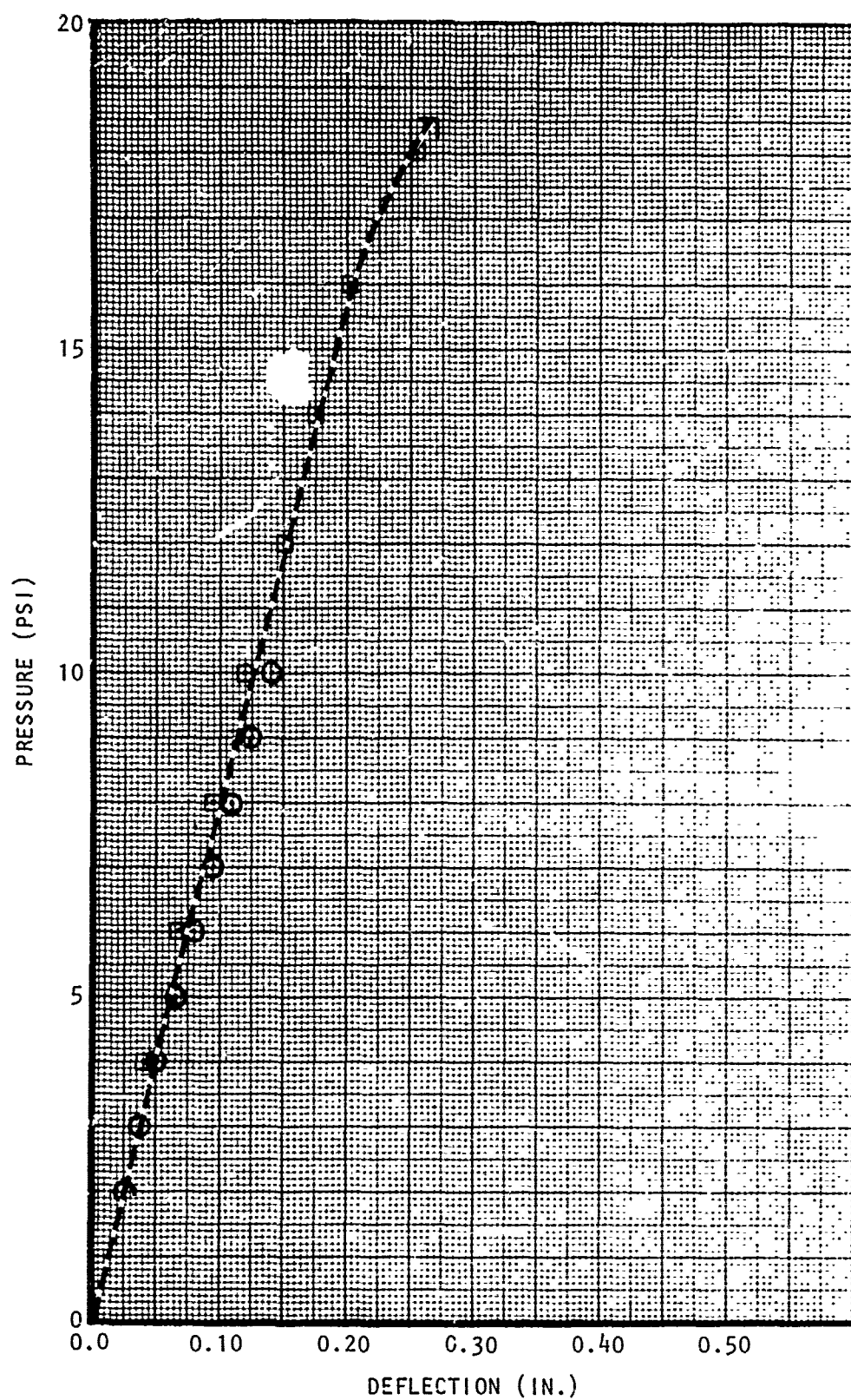
Figure 158. Midpoint Deflection vs Pressure for Panel 5B3E1
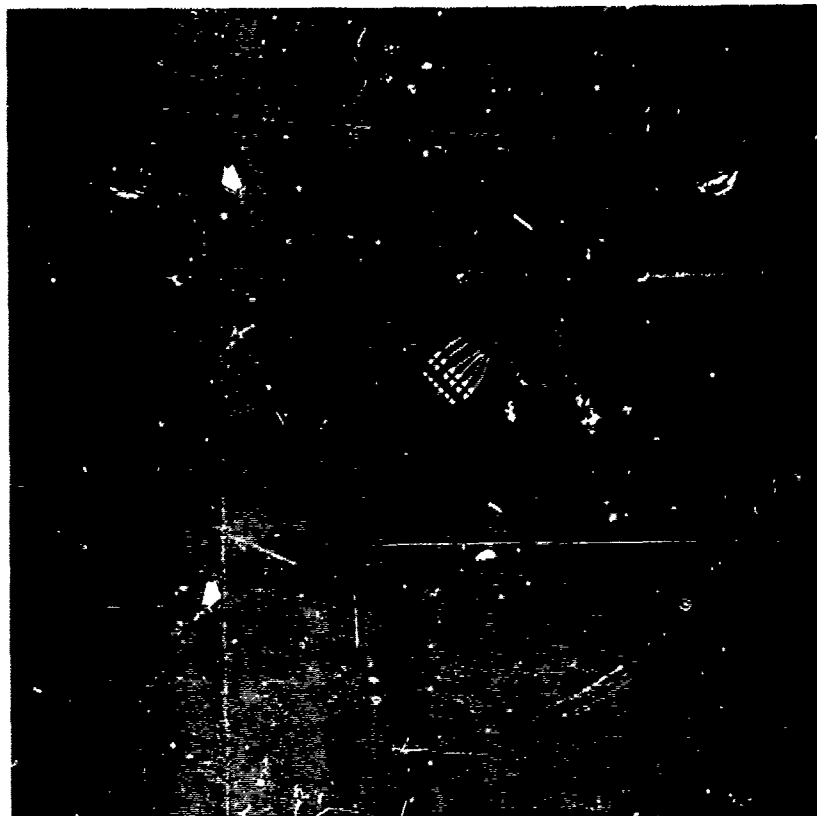
Figure 159. Panel 5B1R1 After Normal Pressure Failure

Figure 160. Panel 5B1R2 After Normal Pressure Failure
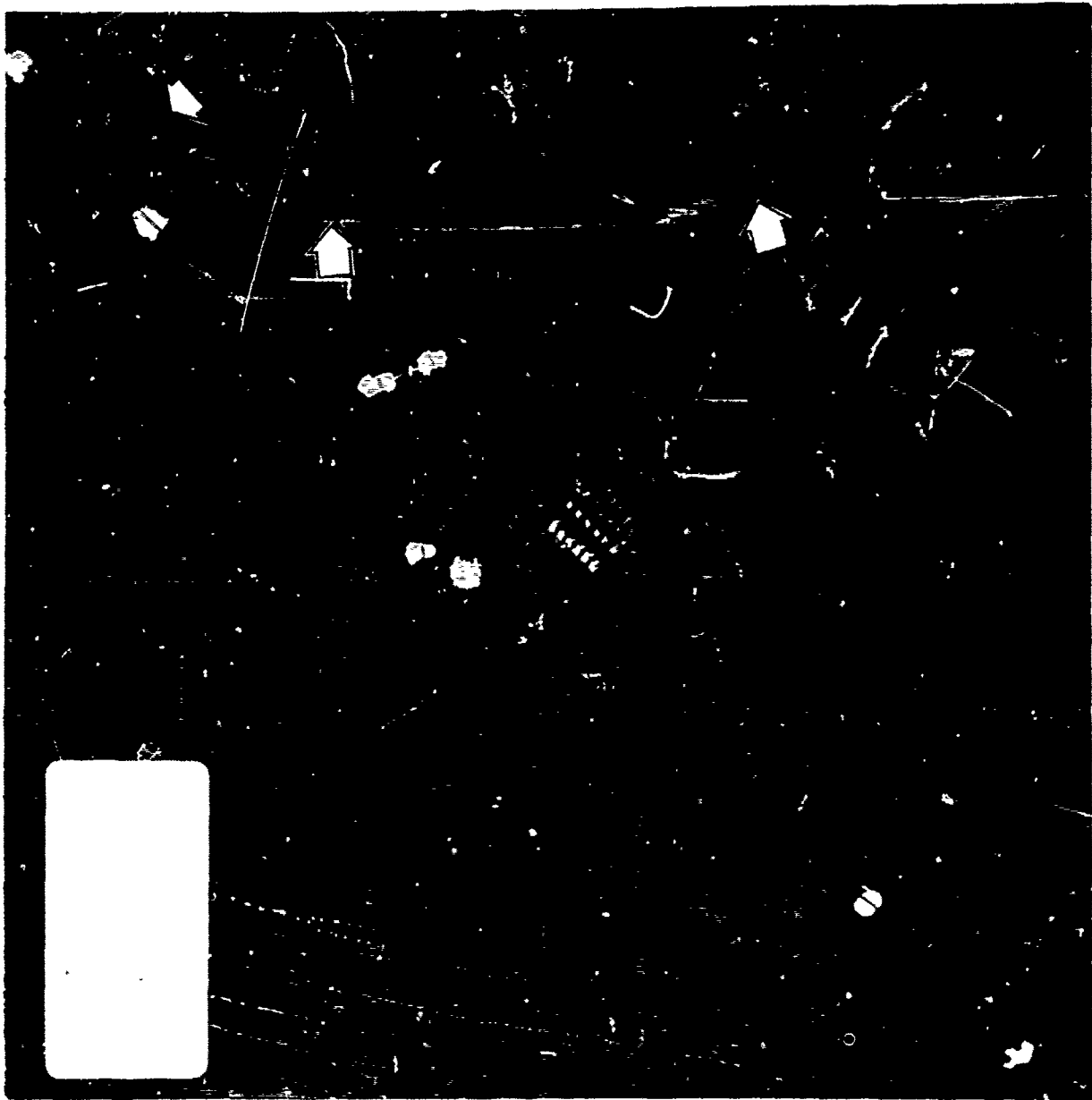
Figure 161.   Panel 5B1E1 After Normal Pressure Failure

Figure 162.   Panel 5B3R1 After Normal Pressure Failure
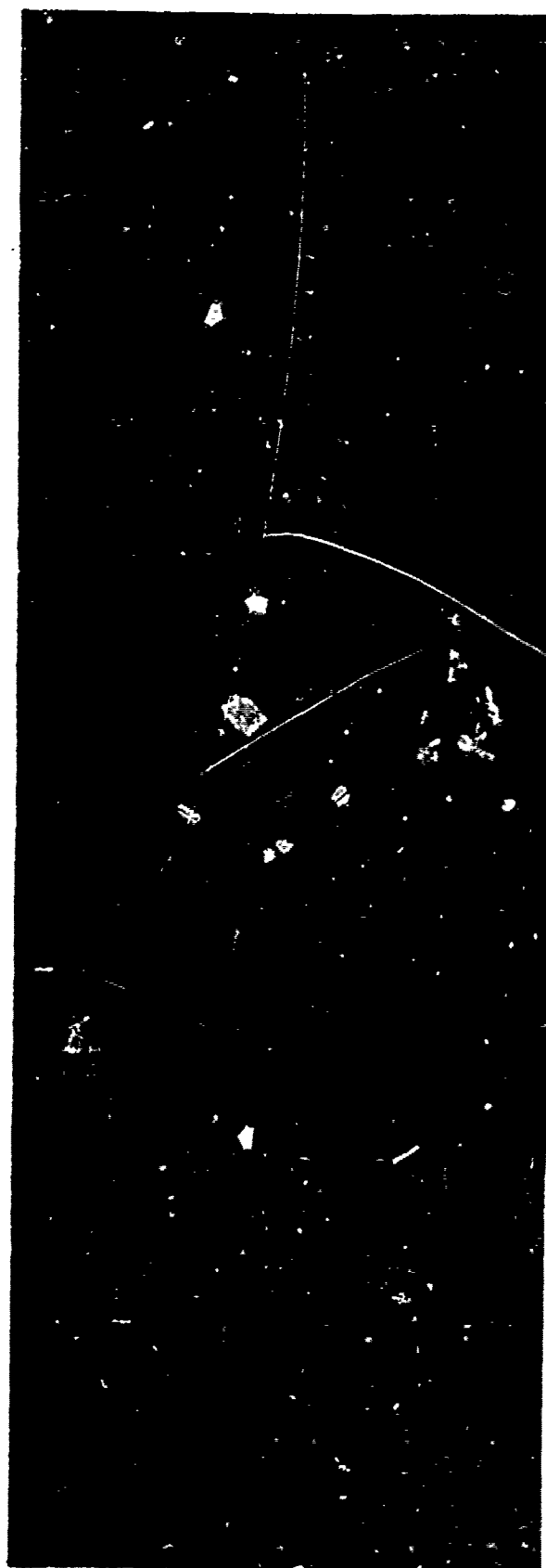
Figure 163. Panel 5B5E1 After Normal Pressure Failure
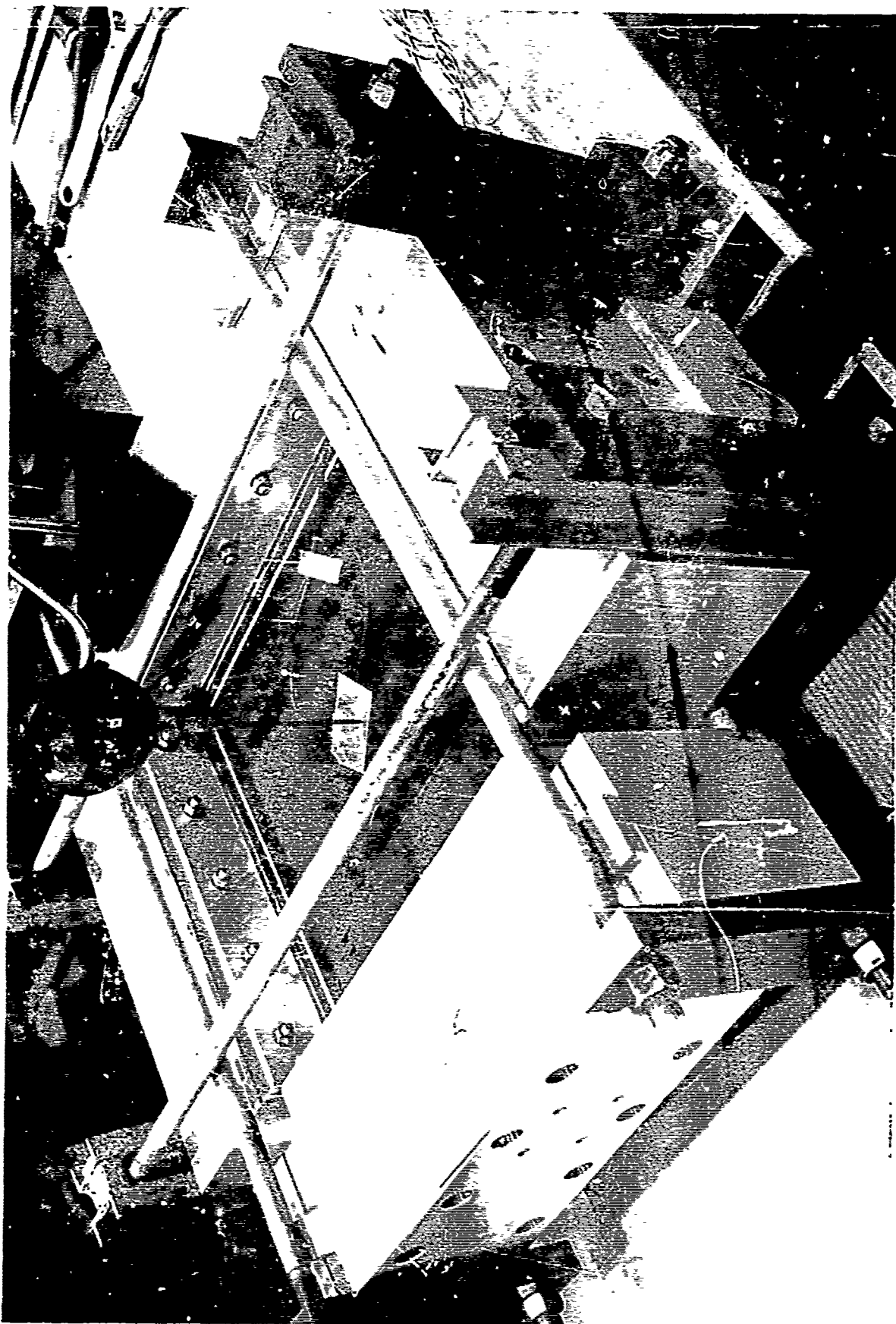
Figure 164. Typical Test Setup, Panel 5B1R1

TABLE XXXIII.   FATIGUE LOADING SPECTRUM (R = 0.10)

| Peak Normal Pressure q (psi)	No. of Applied Cycles		Remarks
	Panel 5B3R1F	Panel 5B3R2F	
20	16,928	--	
23	84	--	Panel failed in static mode.
21	--	1,400	Panel failed in static mode.

From table XXXI, we obtain the static pressure at which the panel failed in a transverse tension mode, q = 27.0 psi. This value, rather than the theoretical value of 22.0 psi, is used as the failing static pressure for the fatigue test panels. The higher static test value indicates some fixity of the test panels and is used in this evaluation in order to establish accurately the percent of F_y^{tu} at which the panel face sheets were being cycled.

Miner's linear accumulative damage theory is used to compare actual versus predicted damage. The results are shown in Table XXXIV and are based on the equation

$$D = \sum_{i=1}^{p} \frac{n_i}{N_i}$$

where

D = panel damage (with failure occurring at $D \geq 1$)

n_i = cycles at stress amplitude σ_i

N_i = cycle life for stress amplitude σ_i

p = number of values of σ_i

N_i is obtained from figure 165. Figures 166 and 167 are photographs of the test specimen after failure.
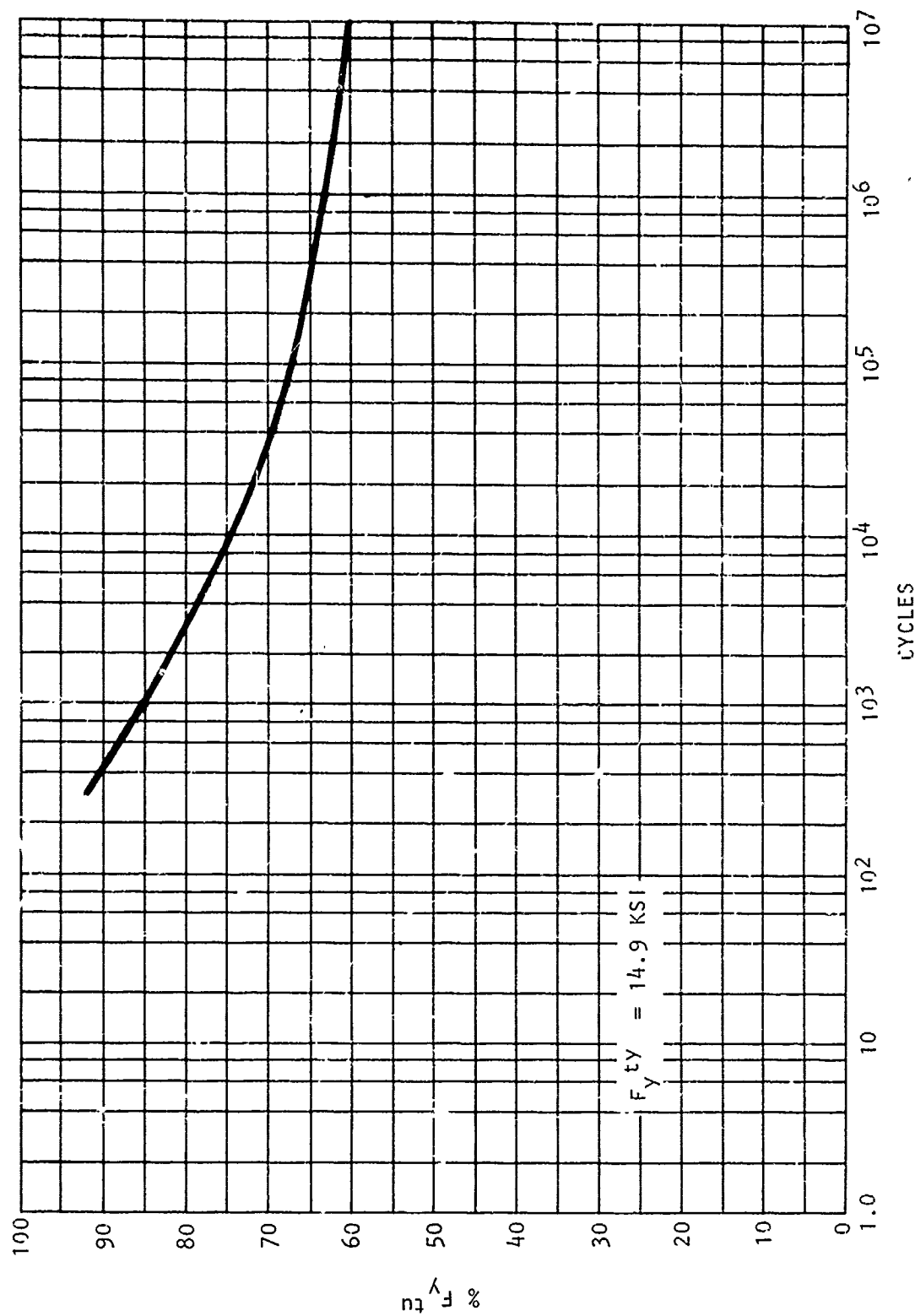
Figure 165. Constant Amplitude Fatigue Diagram $[90_2/\pm YS]_c$ at R.T., R = 0.10

211
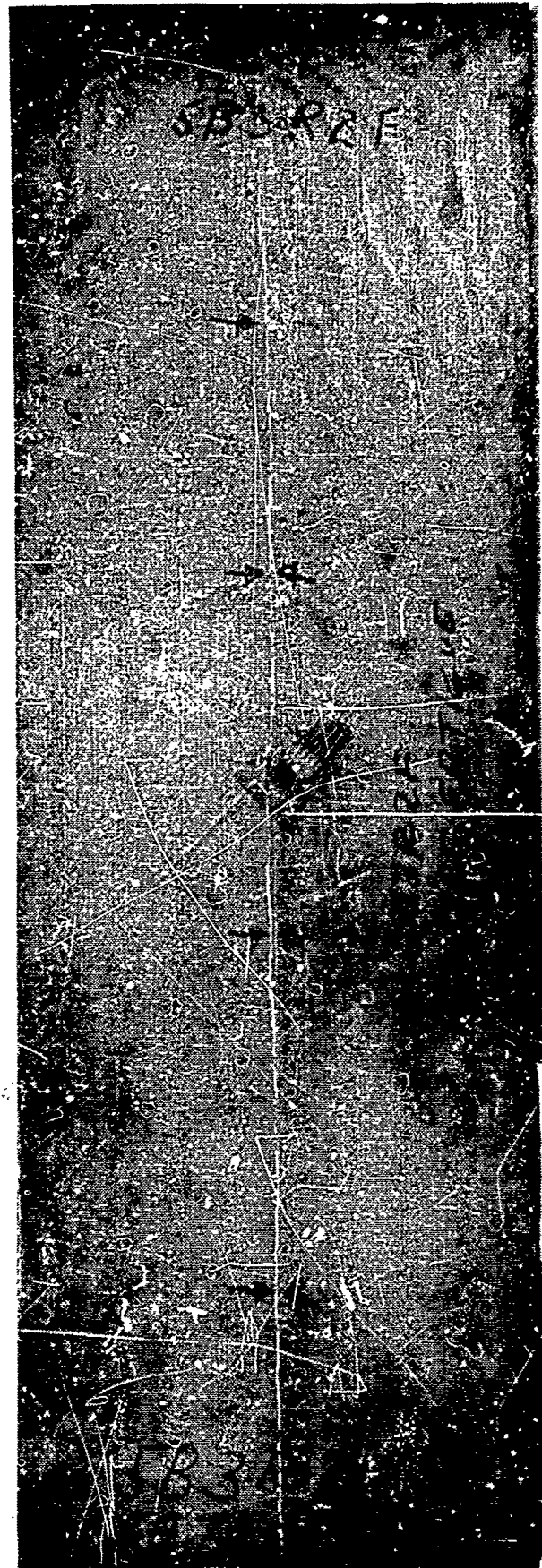
Figure 166. Panel 5B3R2F After Normal Pressure Failure (Fatigue)

Figure 167. Panel 5B3R1F After Normal Pressure Failure (Fatigue)

TABLE XXXIV. MINER'S DAMAGE PREDICTION VERSUS ACTUAL DAMAGE FOR R = 0.10

Specimen	Percent F_y^{tu}		C	N_1 Cycles	n_2 Cycles	N_2 Cycles	Miner's D
	$\overline{\sigma}_1$	$\overline{\sigma}_2$					
5B3R1F	74*	85**	6,928	12,000	84	1,000	1.50
3R2F	78***	--	1,400	4,700	--	--	0.30

* $\overline{\sigma}_1 = (20/27) \times 100 \times F_y^{tu}$

** $\overline{\sigma}_2 = (23/27) \times 100 \times F_y^{tu}$

*** $\overline{\sigma}_1 = (21/27) \times 100 \times F_y^{tu}$

THERMAL GRADIENT (SERIES 6B)

The series 6B honeycomb thermal gradient panels were fabricated with $[0/\pm45/0]_S$ face sheets and 8.1 lb/ft^3 Al-5056 (2-20) core. All four sides of the panel were supposed to be hinged; i.e., they were free to rotate (simple support) but not allowed to translate. Thus, thermal stresses due to the gradient, $\Delta T = T(t_f)-T(t_o)$, were allowed to develop. The purpose of the tests was to verify the thermal stresses and the buckling loads. The basic material properties are given in tables I through III. The geometries are as follows:

Panel	a (in.)	b (in.)	t_F (in.)	c (in.)	s (in.)	t_c (in.)
6B1E1	15	15	0.0416	0.50	1/8	0.002
3E1	39	13	0.0416	0.50	1/8	0.002

NOTE The parameters listed are defined in figure 172.

N^*_{xt} and N^*_{yt}, the theoretical stresses induced by the thermal gradient, were obtained by using the method given for series 6A panels. The boundaries were assumed to remain stationary. Given these thermal stresses, the buckling stresses were predicted by using the procedures delineated in the series 2B panels.

The thermal stresses based on the strain gage readings were not credible. This was probably due to strain gage drift (refer to section III). Methods for rectifying this effect are not presently available. Therefore, to avoid false conclusions, these data were not presented.

The data to predict thermal stresses and buckling predictions above 350°F were not available. Rather than to extrapolate the material properties, it has been decided herein to extrapolate the predicted and buckling loads. Figure 168 shows the predicted thermal loads and buckling loads for the two panels. Panel 6B1E1 delaminated at 425°F, which is somewhat below the predicted 580°F temperature. Panel 6B3E1 was not tested above 425°F and no failure occurred. Since the predicted failure temperature is 455°F, this test was satisfactory.

Figure 169 shows the strain gage data for panel 6B1E1; figures 170 and 171 show photographs of the failed test specimens.

PRESSURE AND THERMAL GRADIENT (SERIES 7B)

The series 7B honeycomb panels were fabricated with $[0/\pm45/0]_S$ face sheets and 8.1 lb/ft^3 (2-20) Al-5056 honeycomb core. The geometries are shown in table XXXV and figure 172. The basic properties are given in tables I through III. The panels were tested for a combined thermal gradient and pressure loading. The first step in the loading was to raise the temperature of the panel from RT to 200°F while constraining the edges from translation but not rotation (i.e., hinged). While maintaining the panel at this temperature, a uniform pressure loading was applied incrementally until failure.

As in the 6B series panels, the thermal stresses were obtained from the method presented for the 6A panels. Given these thermal stresses, the effects of pressure were obtained in the same manner as delineated for the series 8B panels.

Because of the strain gage drift mentioned in connection with the previous series, it was not possible to obtain reliable thermal gradient stresses. However, since temperature was subsequently maintained at 200°F, the incremental stresses due to the pressure loading were assumed to be reliable. The results are presented in figures 173 and 174. It should be noted that both
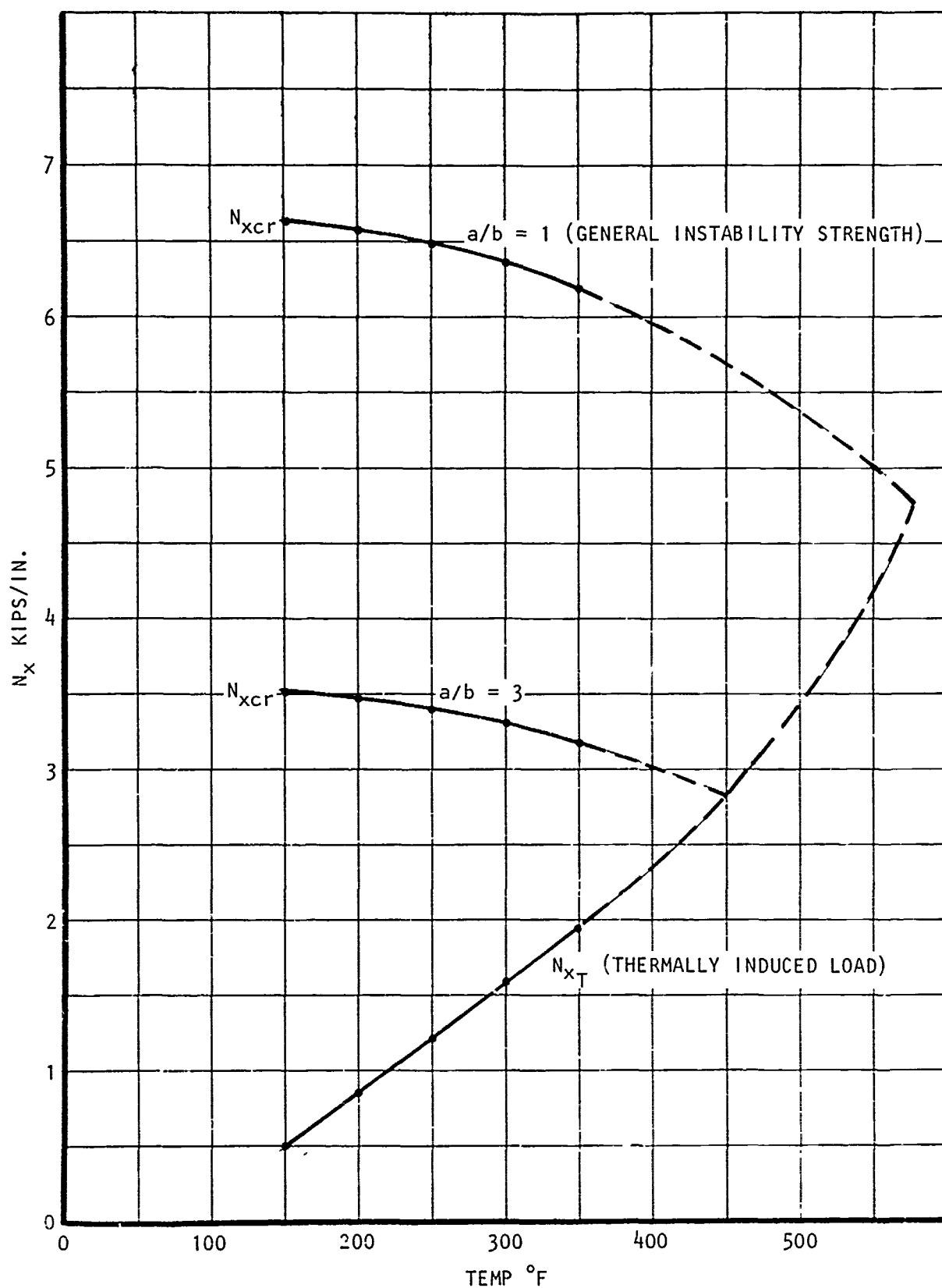
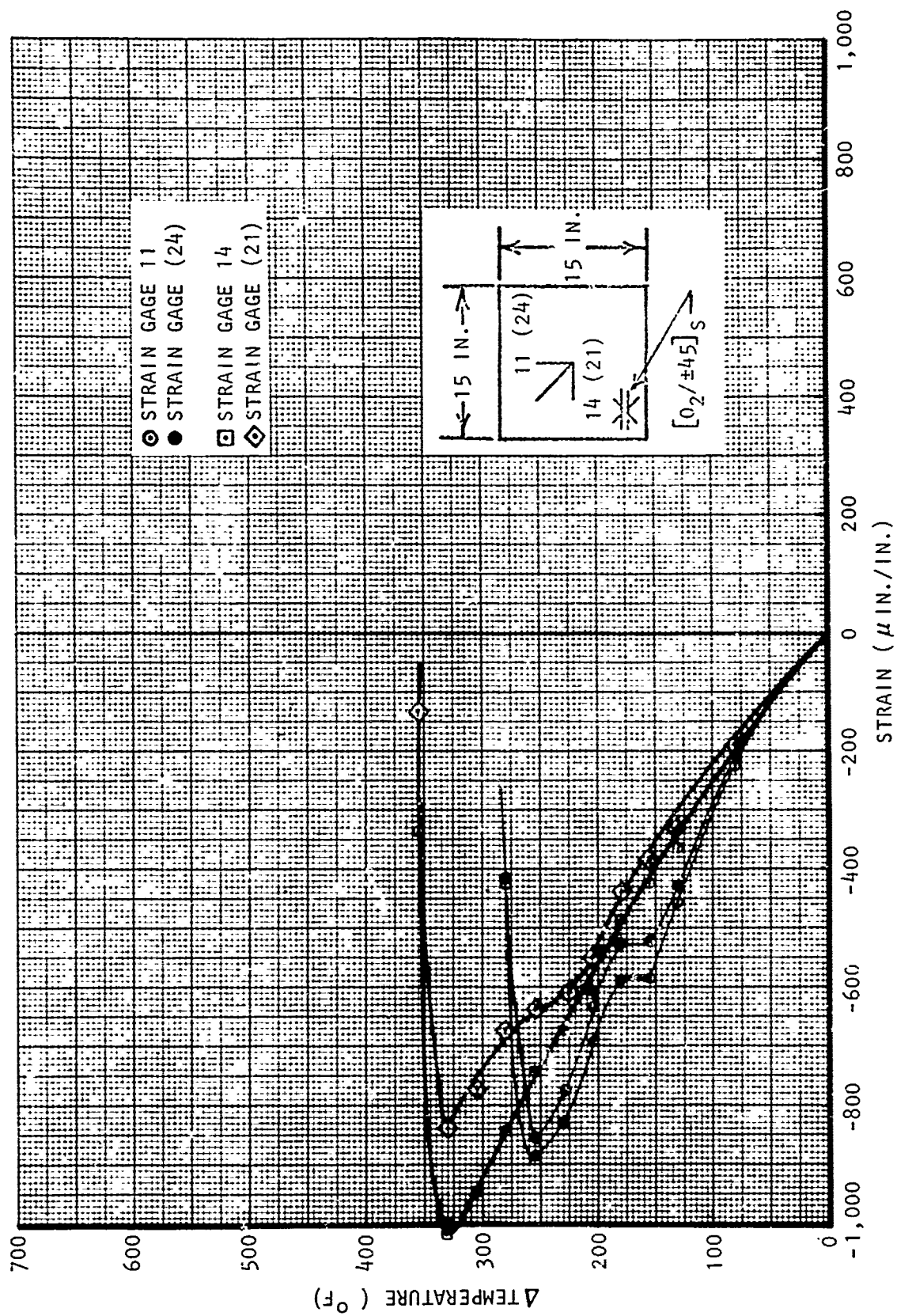Figure 168.   Thermally Induced Edge Loading in Honeycomb Panels

Figure 169. Temperature vs Strain to Determine "Top of the Knee" Buckling Load for Specimen 6B1E1
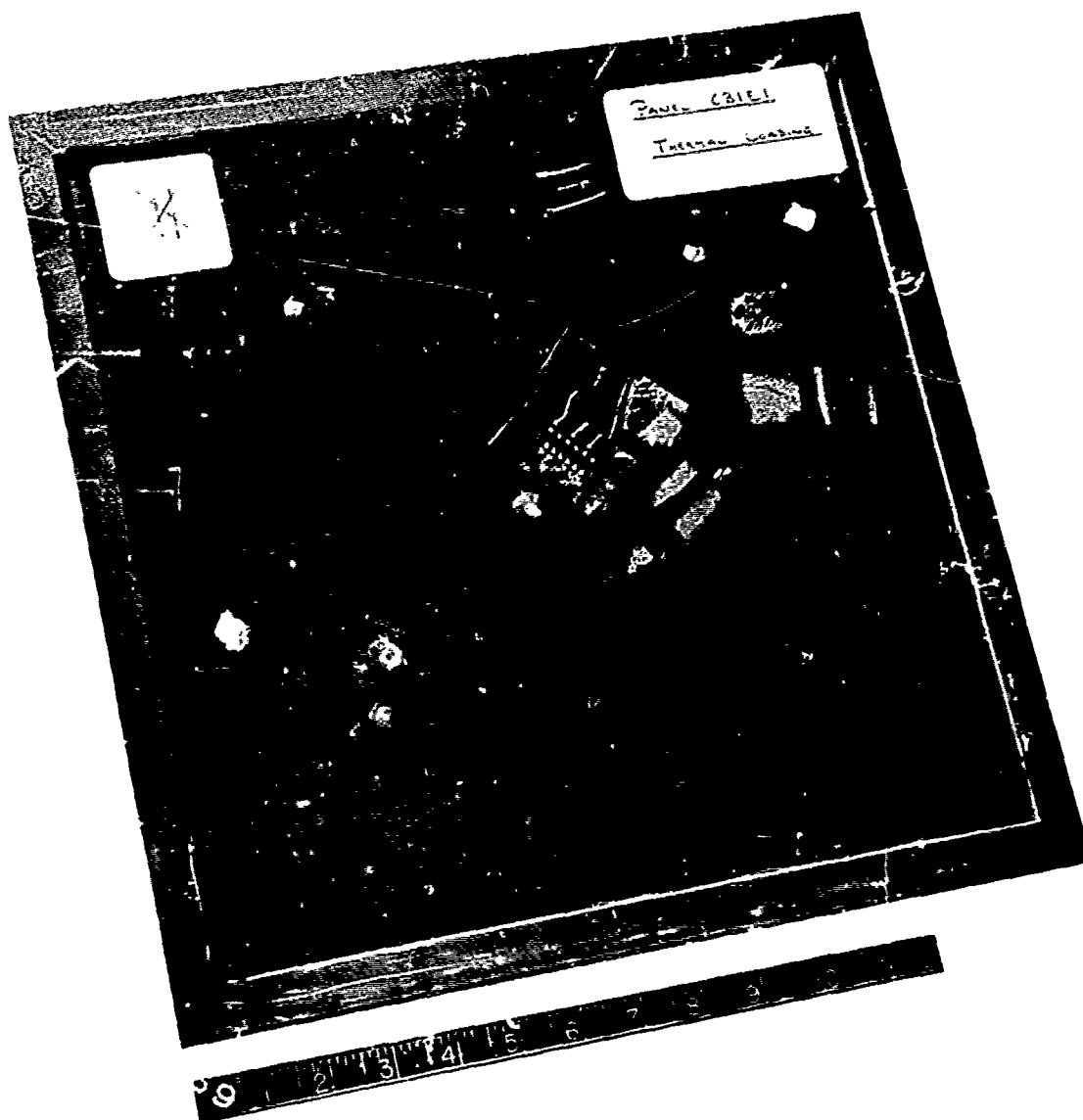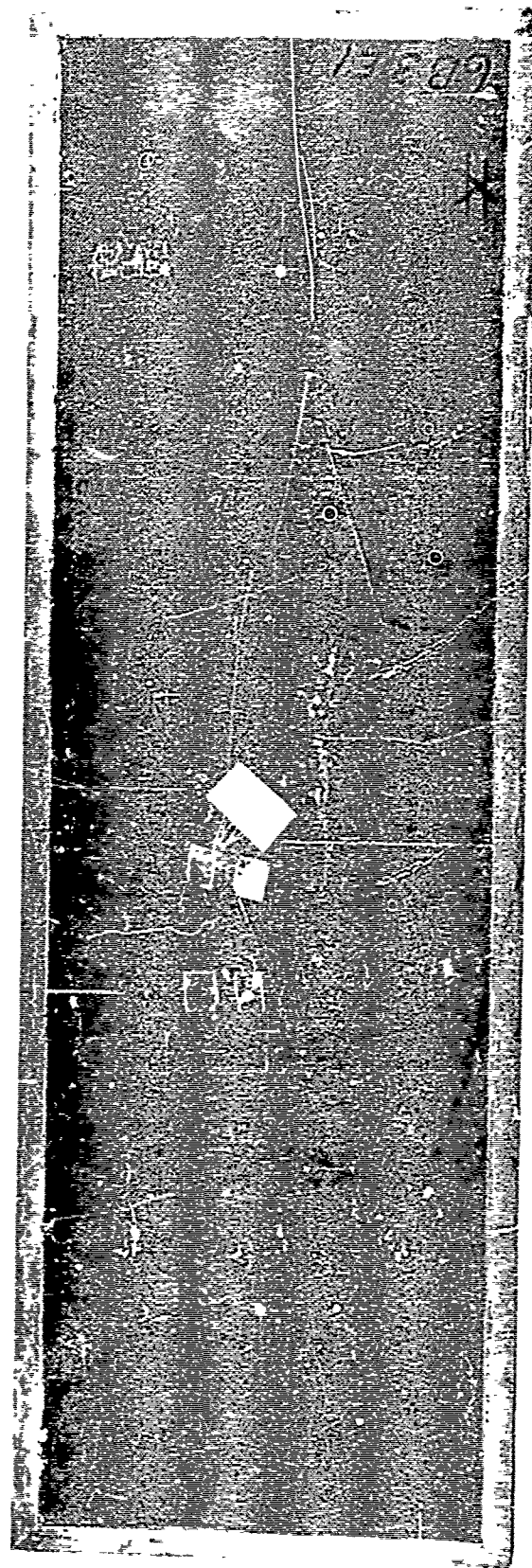
217

Figure 170. Specimen 6B1E1 After Failure

Figure 171. Specimen 6B3E1 After Failure

TABLE XXXV.   GEOMETRY FOR 7B SERIES PANELS

Panel	a (in.)	b (in.)	t_f (in.)	c (in.)	s (in.)	t_c (in.)
7B1E1	15	15	0.0416	0.50	2/16	0.0020
3E1	39	13	0.0416	0.50	2/16	0.0020

the predicted and strain gage stresses have been reduced to consider the effects of incremental pressure (given the axial loads due to the thermal gradient).

Deflection results were obtained only for panel 7B3E1, and were approximately 30 percent low. This is probably due to the partial damping action of the edge supports. The stresses for this panel were also in the same low range, thus supporting this conjecture. The 7B1E1 panel stresses, on the other hand, were 30 to 50 percent high on the tension side and 5 to 20 percent low on the compression side at 65 psi. The stresses at 30 psi, on the other hand, were within 10 percent of prediction. This is indicative that there was some initial deflection in the panel, although not too significant.

PRESSURE AND UNIAXIAL COMPRESSION (SERIES 8B)

The analytical prediction method for the response behavior of simply supported 8B series sandwich panels with orthotrophic faces and core subjected to normal pressure and inplane loading are reported in Volume III of this report. For both the aspect ratios 1 and 3 panels, the applied N_x compression
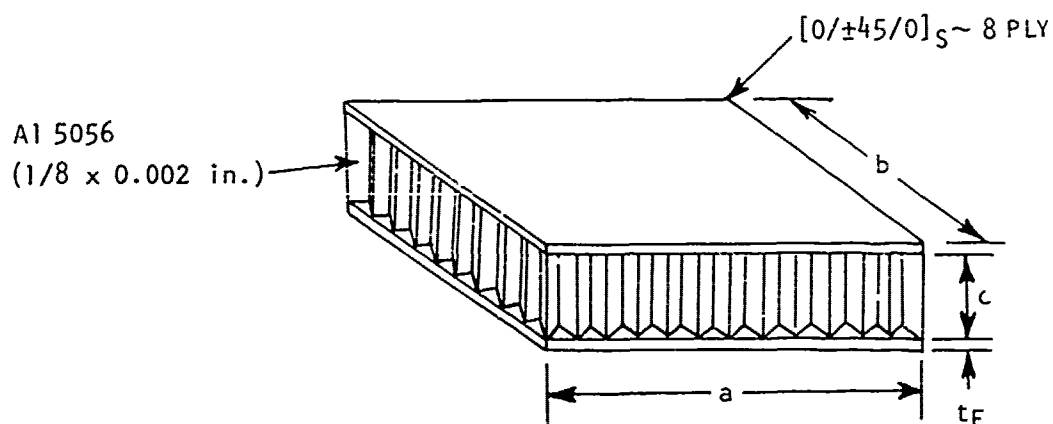
Figure 172.   Typical Honeycomb Sandwich Panel

Figure 173. Test vs Predicted Stresses for a Honeycomb Sandwich Panel Under Uniaxial Compression and Pressure Loading. (7B1E1)
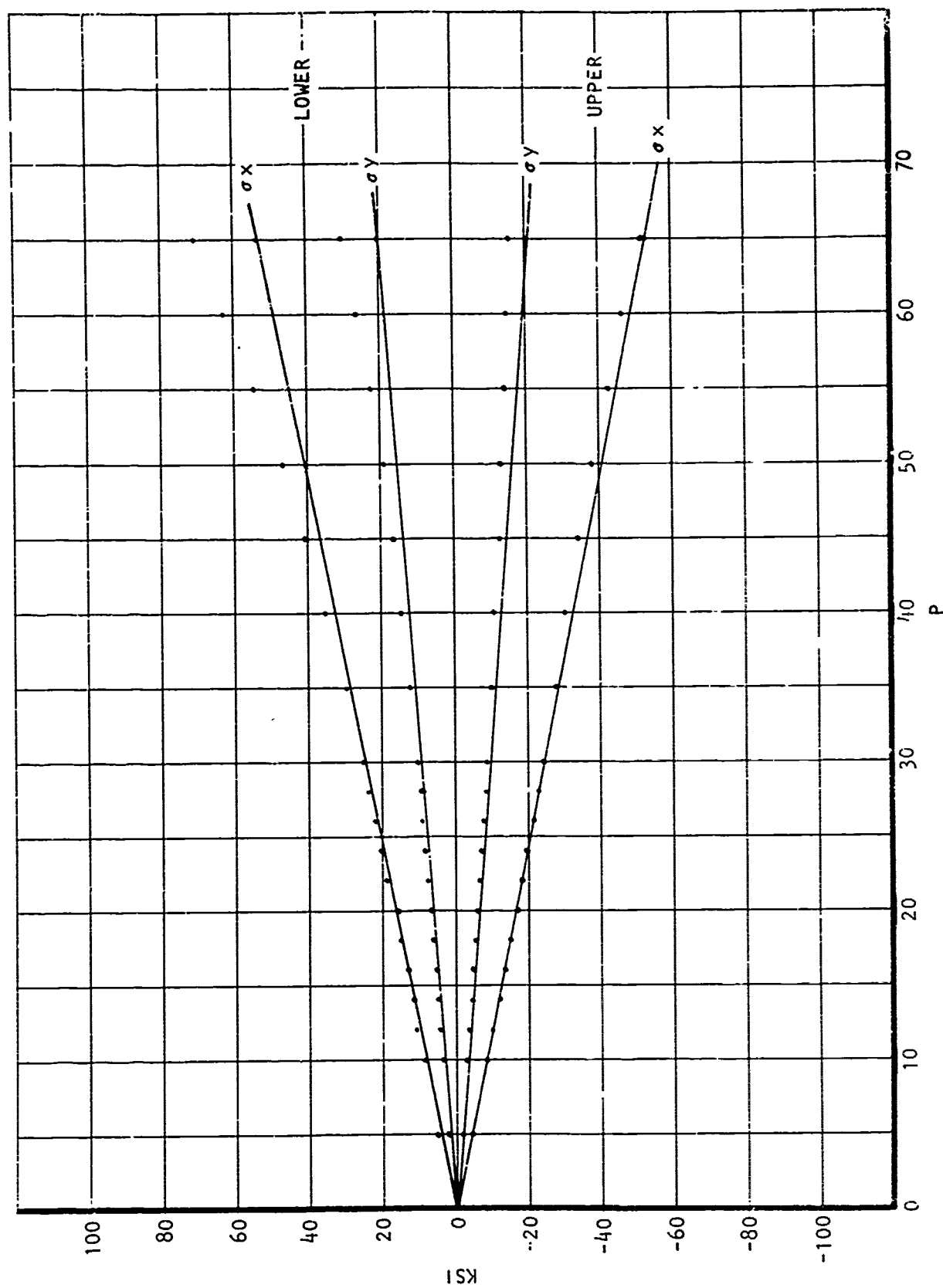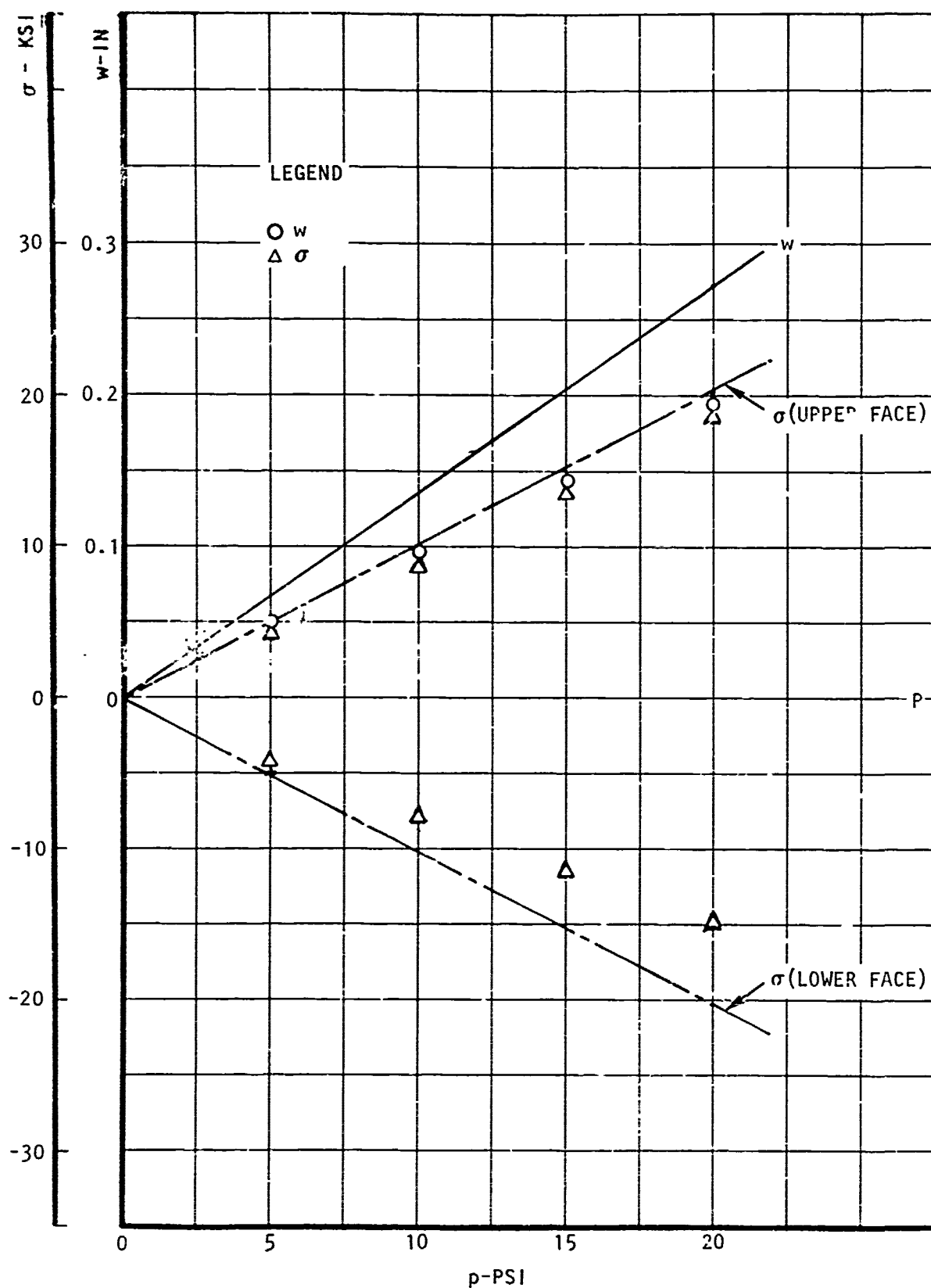
Figure 174. Test vs Predicted Data for a Honeycomb Sandwich Panel under Uniaxial Compression and Pressure Loading (7B3E1)
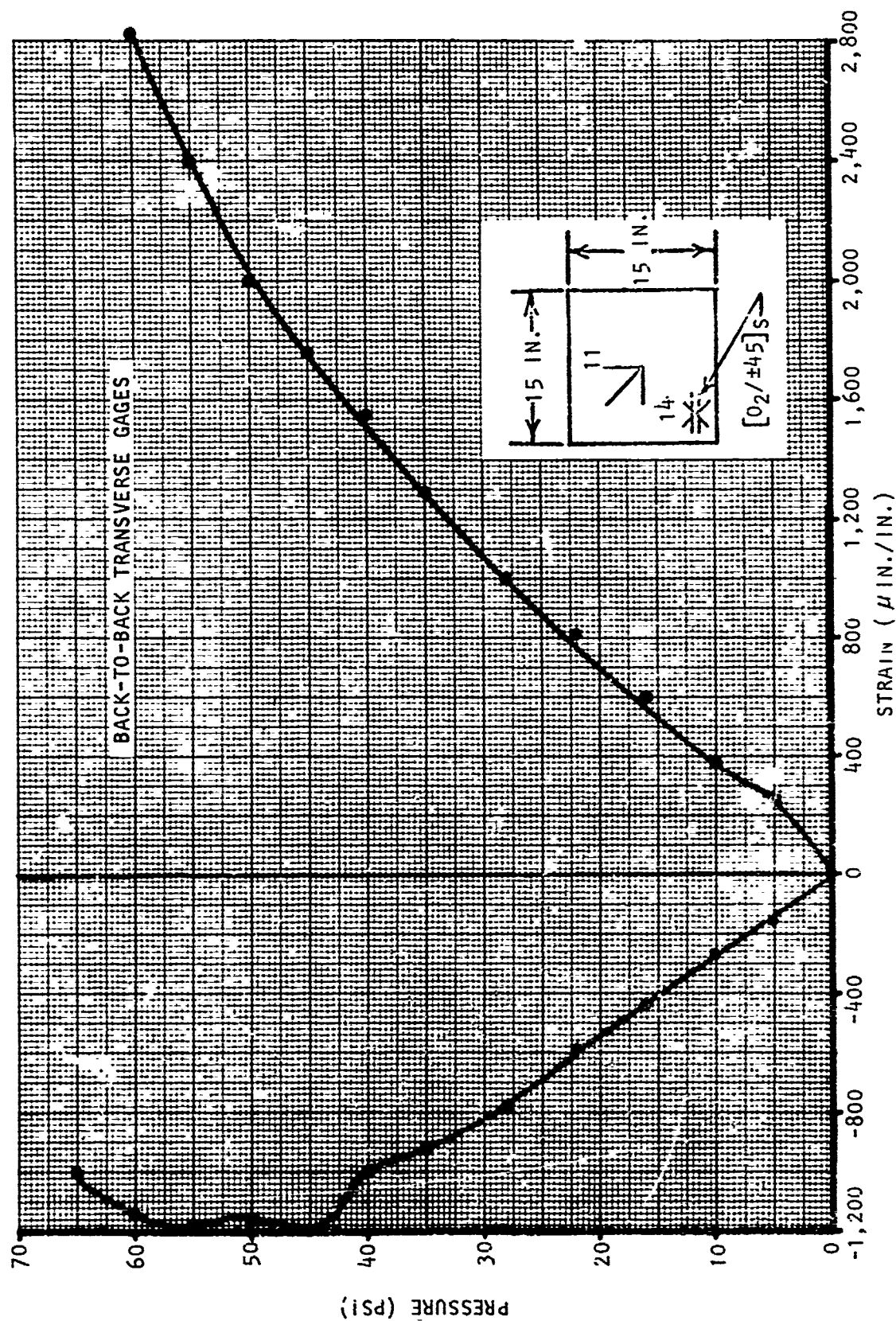
Figure 175. Normal Pressure Plus Thermal Loading (200°F) vs Strain Reading to Determine "Top of the Knee" Buckling Load for Panel 7B1E1
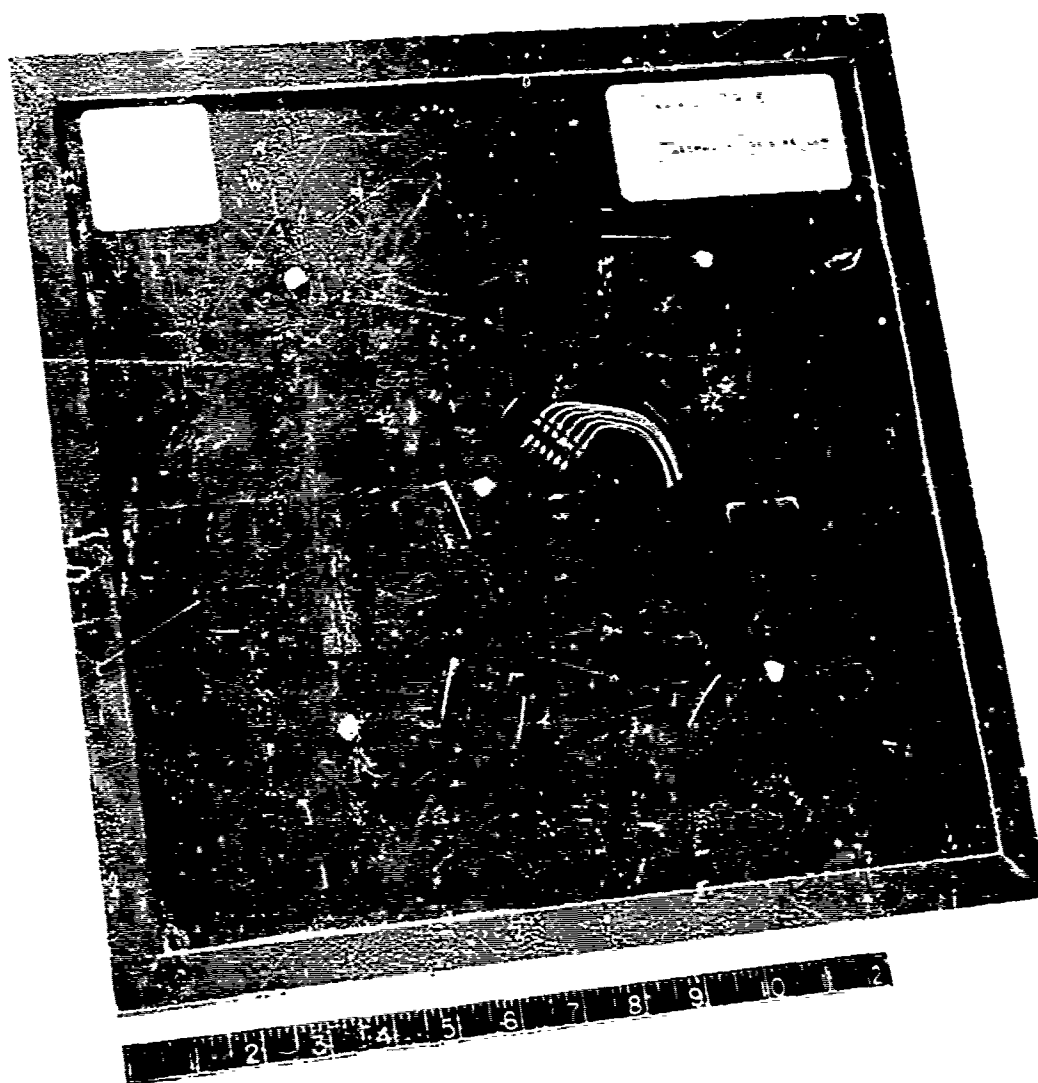
223

Figure 176. Specimen 7B1E1 After failure

Figure 177. Specimen 7B3E1 After Failure

load was approximately $1/2(N_{xcr})$; consequently, the predicted internal moments and plate deflections, shown in table XXXVI, were obtained from section IV of Volume III, which has data for (N_x/N_{xcr}) equal to 1/3.

TABLE XXXVI. PREDICTED CENTER DEFLECTION AND TRANSVERSE MOMENT FOR TEST PANELS

a/b	Temp (°F)	$W\xi/qb^4$* $x/a = 0.50$ $y/b = 0.50$	α M_y/qb^2* $x/a = 0.5$ $y/b = 0.5$
1.0	RT	0.00581	0.044
	350	0.00547	0.040
3.0	RT	0.0290	0.149
	350	0.0308	0.145

*Value for honeycomb sandwich with $[0/\pm45/0]_S$ face sheets and (G'_{cx}/G'_{cy}) = D_{qx}/D_{qy} = 2.0; with $\xi = \sqrt{D_{11}D_{22}}$ = t_F $c(c+t_F)\psi/2$

The geometry of the test panels was identical to the 5B series pressure panels and is summarized together with the loadings for the test panels, in table XXXVII, with typical loading illustrated in figure 178.

TABLE XXXVII. GEOMETRIC* AND LOAD DATA FOR 8B SERIES PANELS

Specimen No.	Test Temperature (°F)	a/b	b (in.)	ξ $(10^4 lb\text{-}in.)$	(N_x)applied (lb/in.)	$(N_x)cr$*** (lb/in.)
8B1R1	RT	1.0	15.0	6.07	3,333	10,300
1R2	RT	1.0	15.0	6.07	3,333	10,300
1E1	350	1.0	15.0	5.30	**	--
3R1	RT	3.0	13.0	6.07	4,615	12,900
3E1	350	3.0	13.0	5.30	3,846	12,590

*Same as 5B series.
**Panel failed prematurely
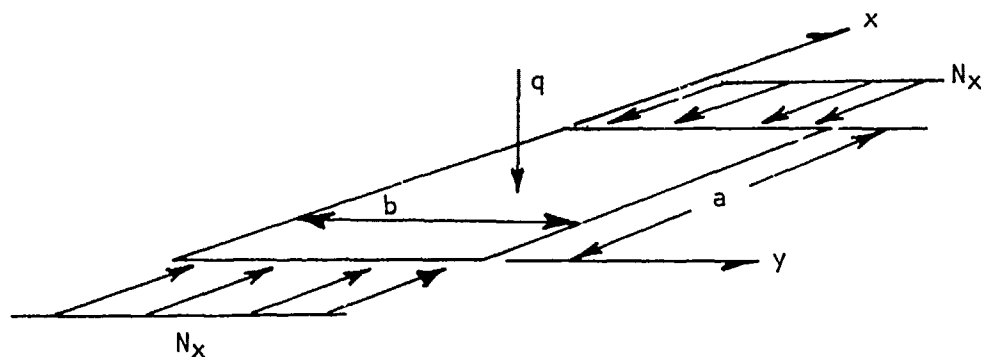***Obtained from 1B series data

Figure 178. Typical Pressure Plus Uniaxial-Compression-Loaded Sandwich Panel

A comparison of the predicted maximum deflections, based on table XXXVI, with test data is given in table XXXVIII.

TABLE XXXVIII. TEST VERSUS THEORY FOR MAXIMUM NORMAL DEFLECTION OF PANELS

Specimen	Test Temp (°F)	a/b	b (in.)	$W\xi/qb^4$ (Theory)	W/q (Theory)	W/q (Test)
8B1R1	RT	1.0	15.0	0.00581	0.00484	0.00415
1R2	RT	1.0	15.0	0.00581	0.00484	0.00426
3R1	RT	3.0	13.0	0.0290	0.0136	0.0141
3E1	350	3.0	13.0	0.0308	0.0204	0.0160

The theoretical failure pressure can be obtained from the relation

$$(q)_{failure} = F_y^{tu} (c+t_F) t_F / (\alpha b^2)$$

where α is obtained from the fourth column of table XXXVI. A comparison of predicted and actual failure pressure, with the axial compression load N_x held constant at the value shown in table XXXVII, is given in table XXXIX. Figures 179 through 184 show photographs of the failed test specimens.
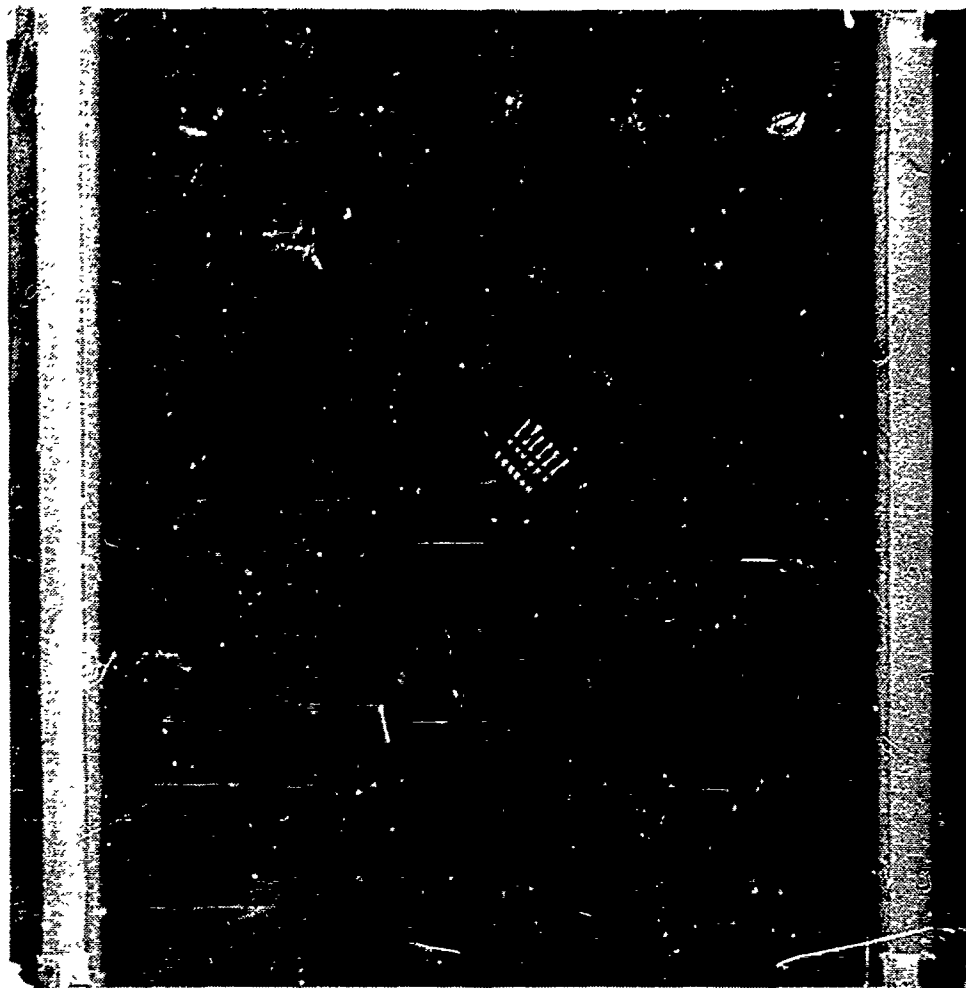
Figure 179. Specimen 8B1R1 After Failure

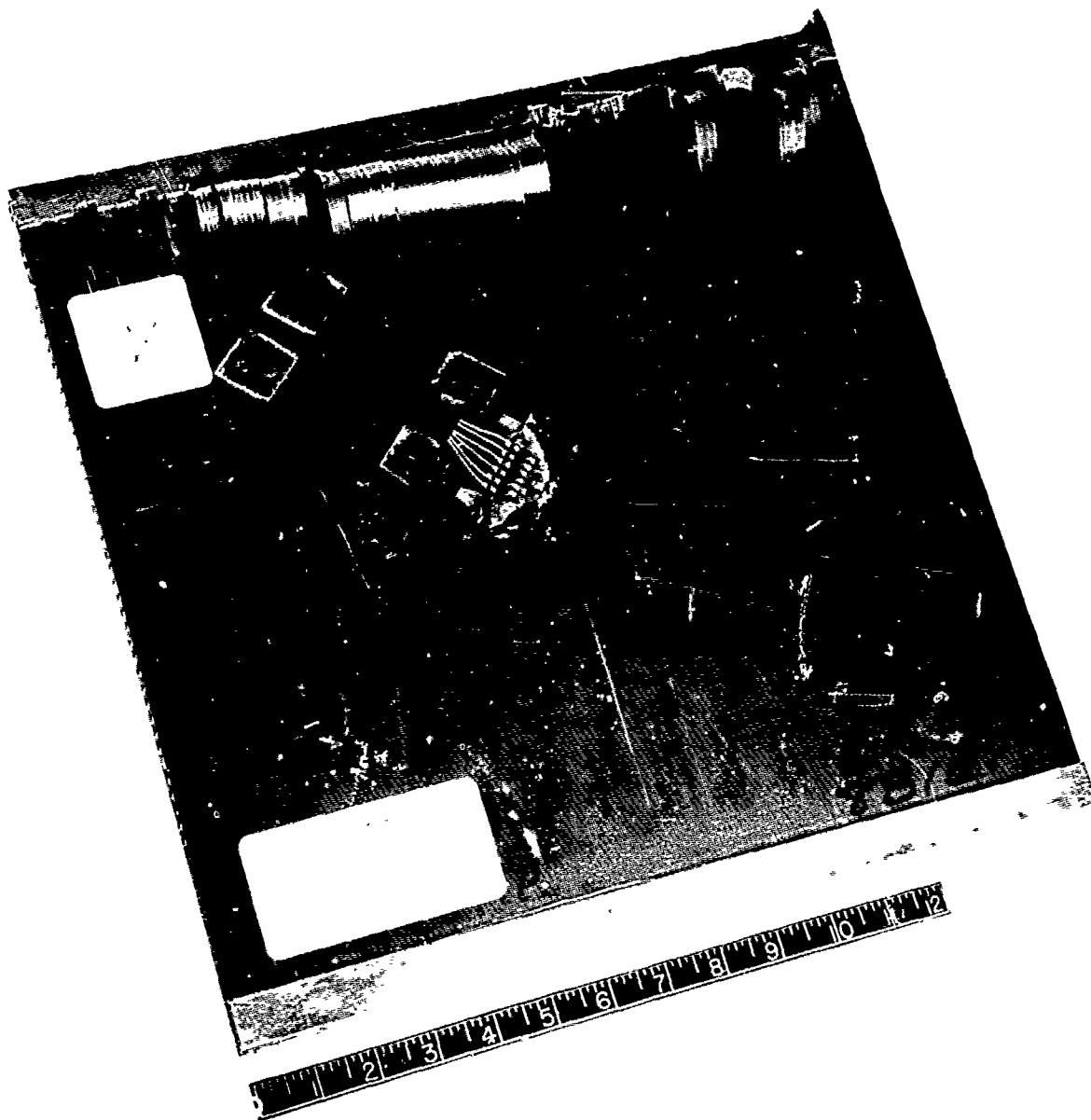Figure 180. Specimen 8B1R2 After Failure

Figure 181.   Specimen 8BiEl After Failure
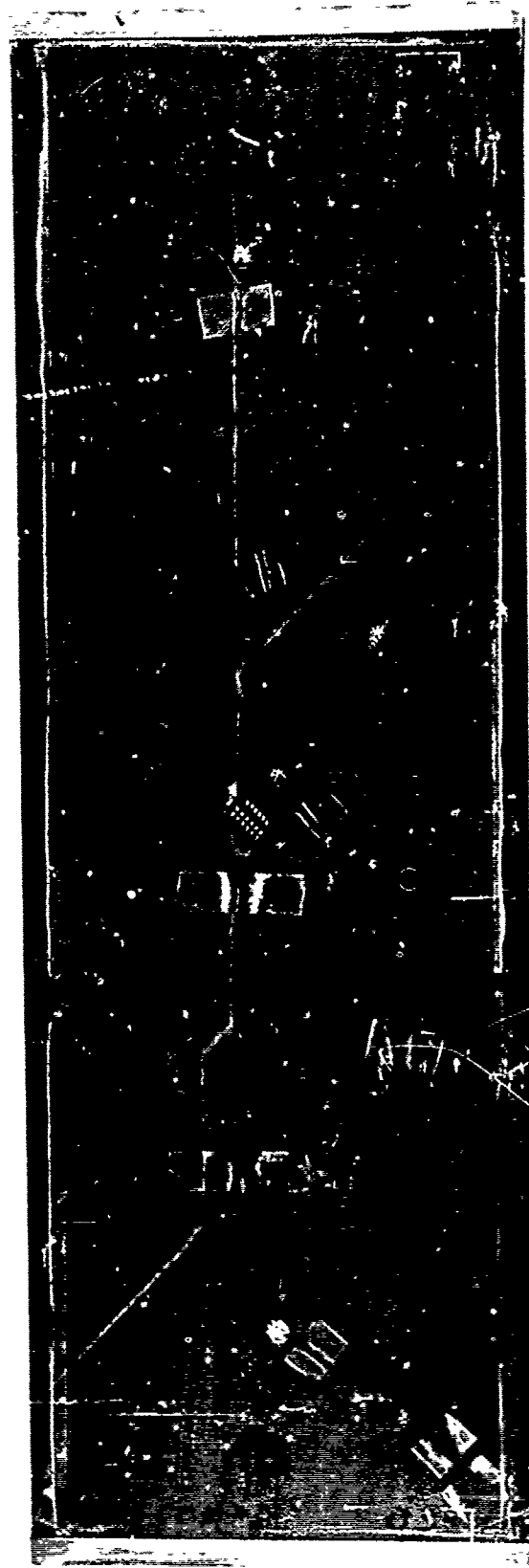
Figure 182. Specimen 8B3R1 After Failure

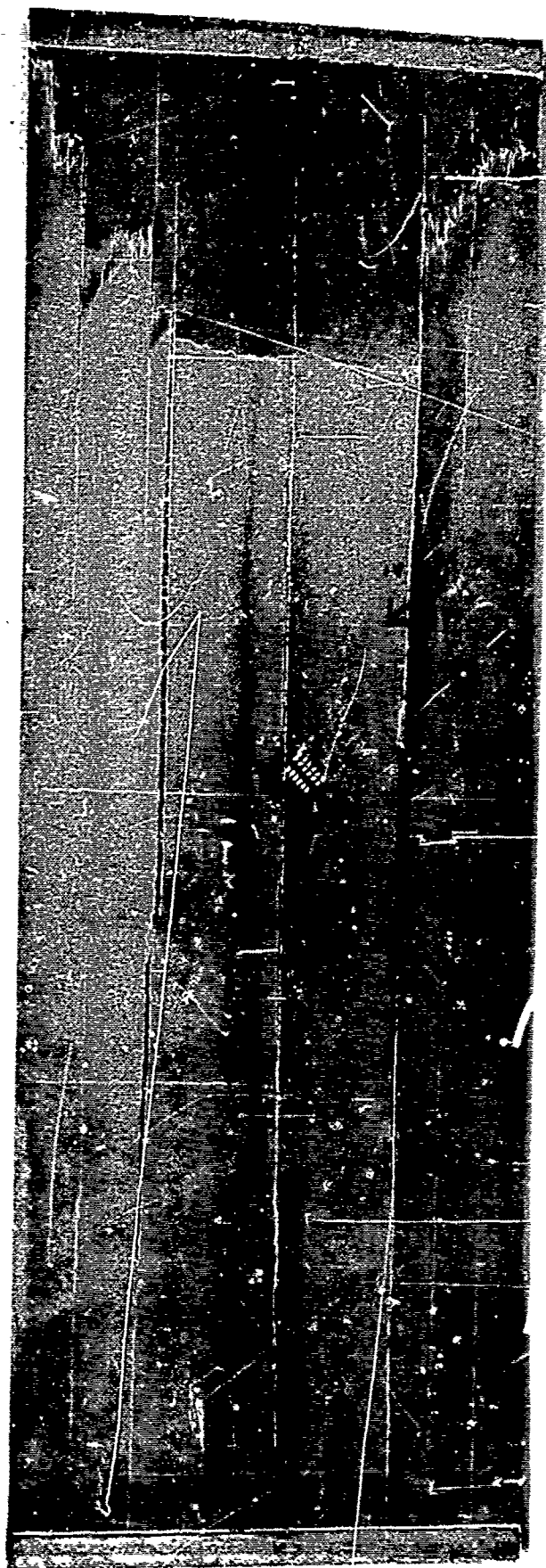Figure 183. Specimen SB3E1 After Failure

232

Figure 184. Specimen 8B3R2F After Failure (Fatigue)

TABLE XXIX. TEST VERSUS THEORETICAL FAILURE PRESSURE WITH N_x/N_{xcr} = 0.333

Specimen	$(q)_{failure}$ (Test)	$(q)_{failure}$ (Theory)
8B1R1	55.0	37.6
1R2	55.0	37.6
3R1	24.0	14.8
3E1	15.0	12.7

where, for $[0/\pm 45/0]_S$ face sheets:

$$(F_y^{tu})_{RT} = 16,500 \text{ psi}$$

$$(F_y^{tu})_{350°F} = 13,800 \text{ psi}$$

CREEP BUCKLING (SERIES 9B AND 10B)

Specimen series 9B and 10B were honeycomb panel creep tests, with the panels loaded in uniaxial compression. The 9B panels were columns (i.e., the unloaded edges were unsupported), while the 10B panels had simply supported unloaded edges. The purpose of the tests was to determine the load-displacement characteristics of the panel (as a function of time) and the time to failure.

Table XL presents the geometry for the panels. Figures 185 through 190 and 195 through 200 present the midpoint lateral deflections and midpoint longitudinal strains for the back-to-back gages. Figures 191 through 194 and 201 through 203 illustrate the failed specimens.

Figure 185.   Honeycomb Column Creep; Panel 9B1E1 Back-to-Back Strain
             Longitudinal Strain Gages

Figure 186. Honeycomb Column Creep; Panel 9B1E2 Back-to-Back Longitudinal Strain Gages

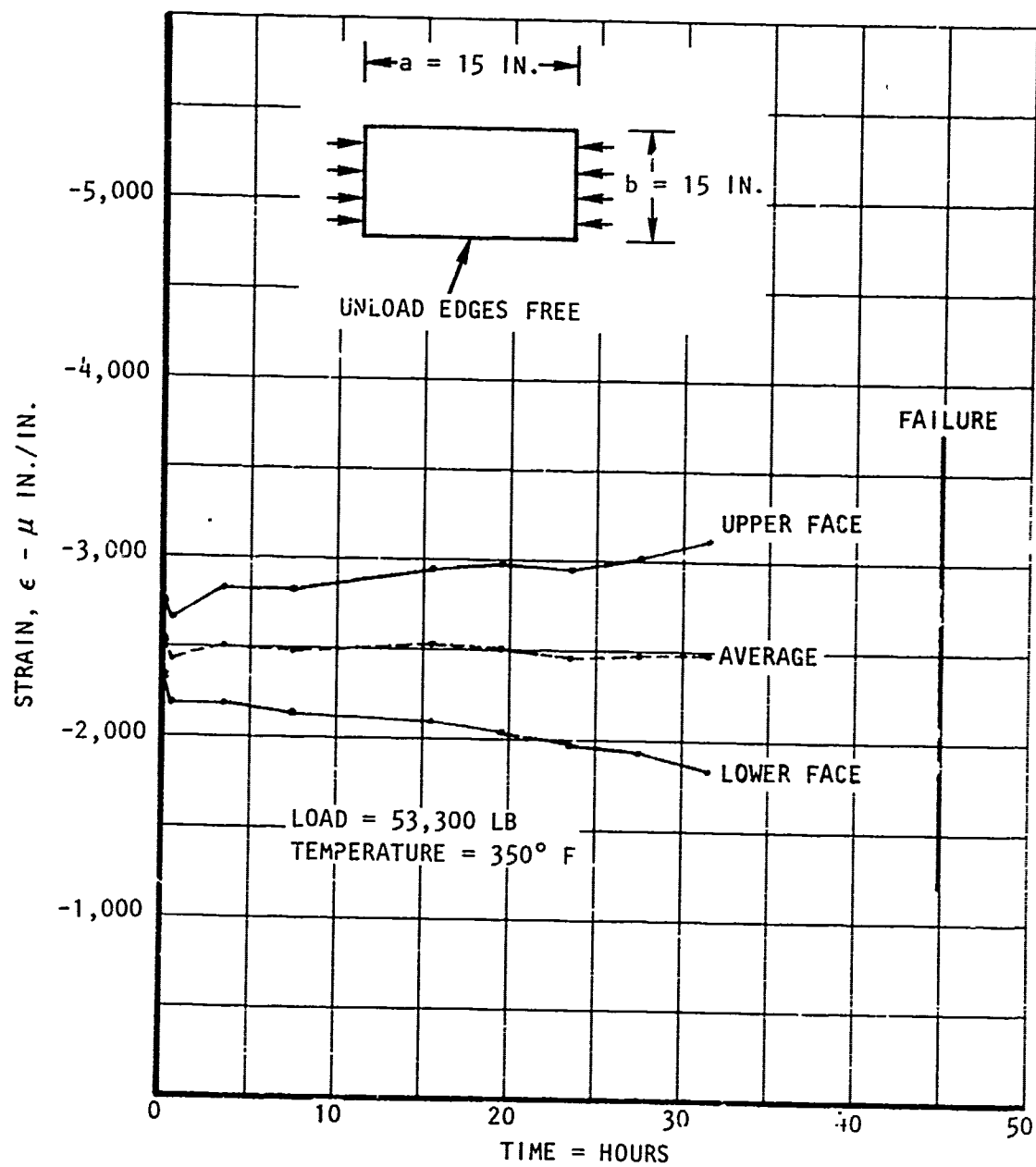Figure 187. Honeycomb Column Creep; Panel 9B1E3 Back-to-Back Longitudinal Strain Gages

Figure 188. Honeycomb Column Creep; Panel 9B2E1 Back-to-Back Longitudinal Strain Gages

Figure 189. Honeycomb Column Creep; Panel 9B2E2 Back-to-Back Longitudinal
Strain Gages

Figure 190. Honeycomb Column Creep; Panel 9B2E3 (Rerun) Back-to-Back Longitudinal Gages

Figure 191. Specimen 9B1F1 After Failure, Front Side

241

Figure 192. Specimen 9B1E1 After Failure, Back Side
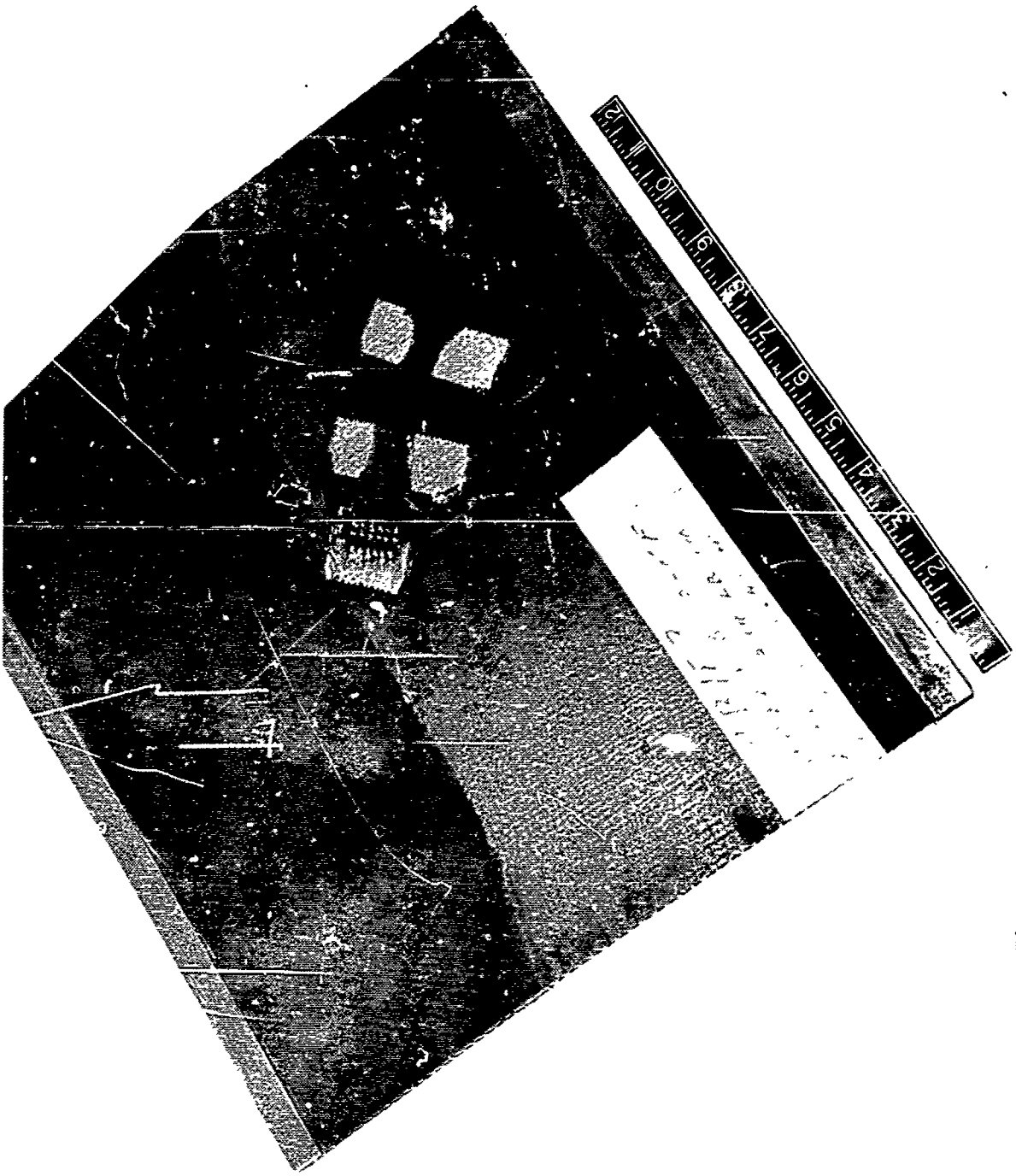
Figure 193. Specimen 9B1E3 After Failure, Front Side

Figure 194. Specimen 9B1E3 After Failure, Back Side
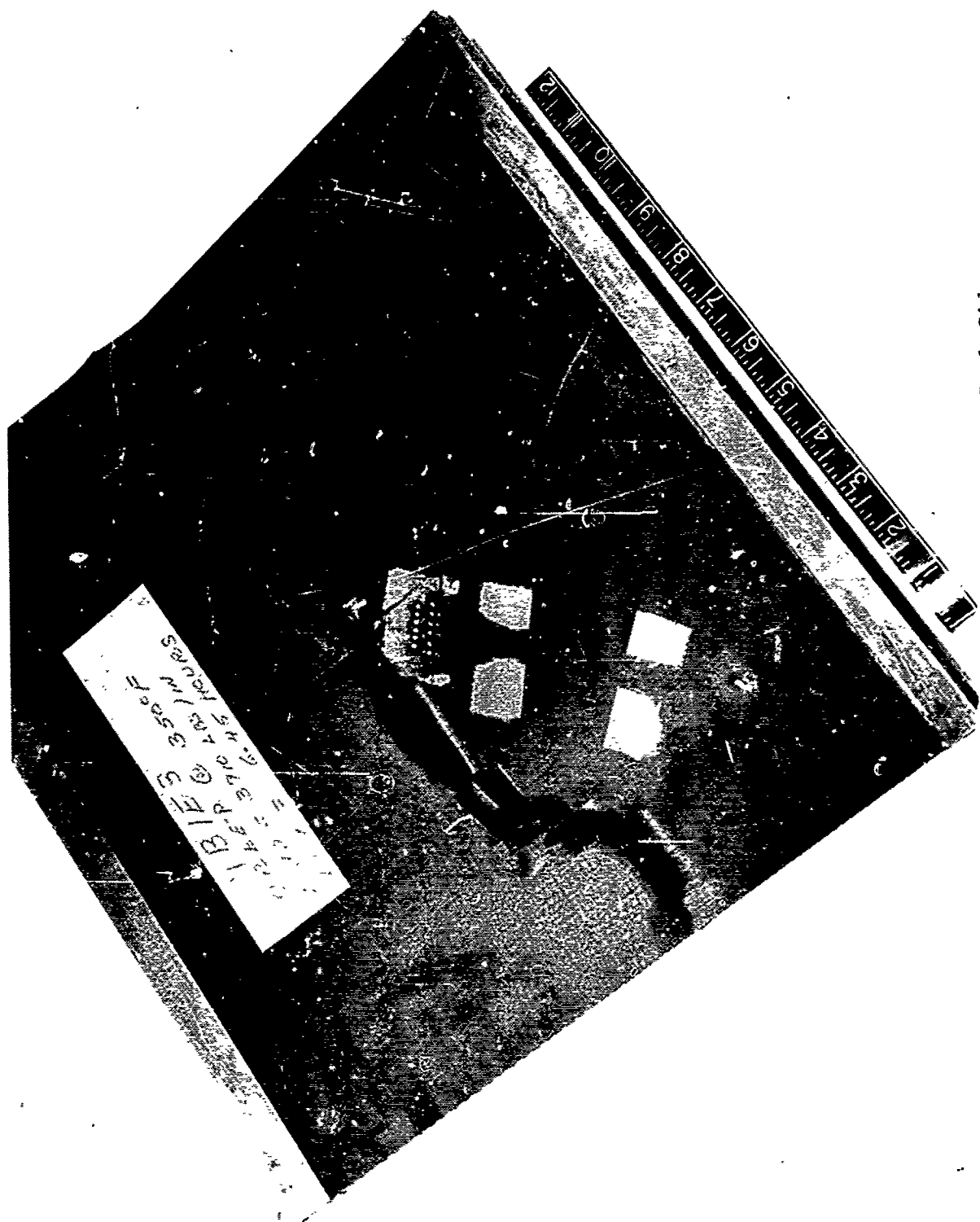
Figure 195. Honeycomb Panel Creep; Panel 10B1E1 Back-to-Back Longitudinal Strain Gages
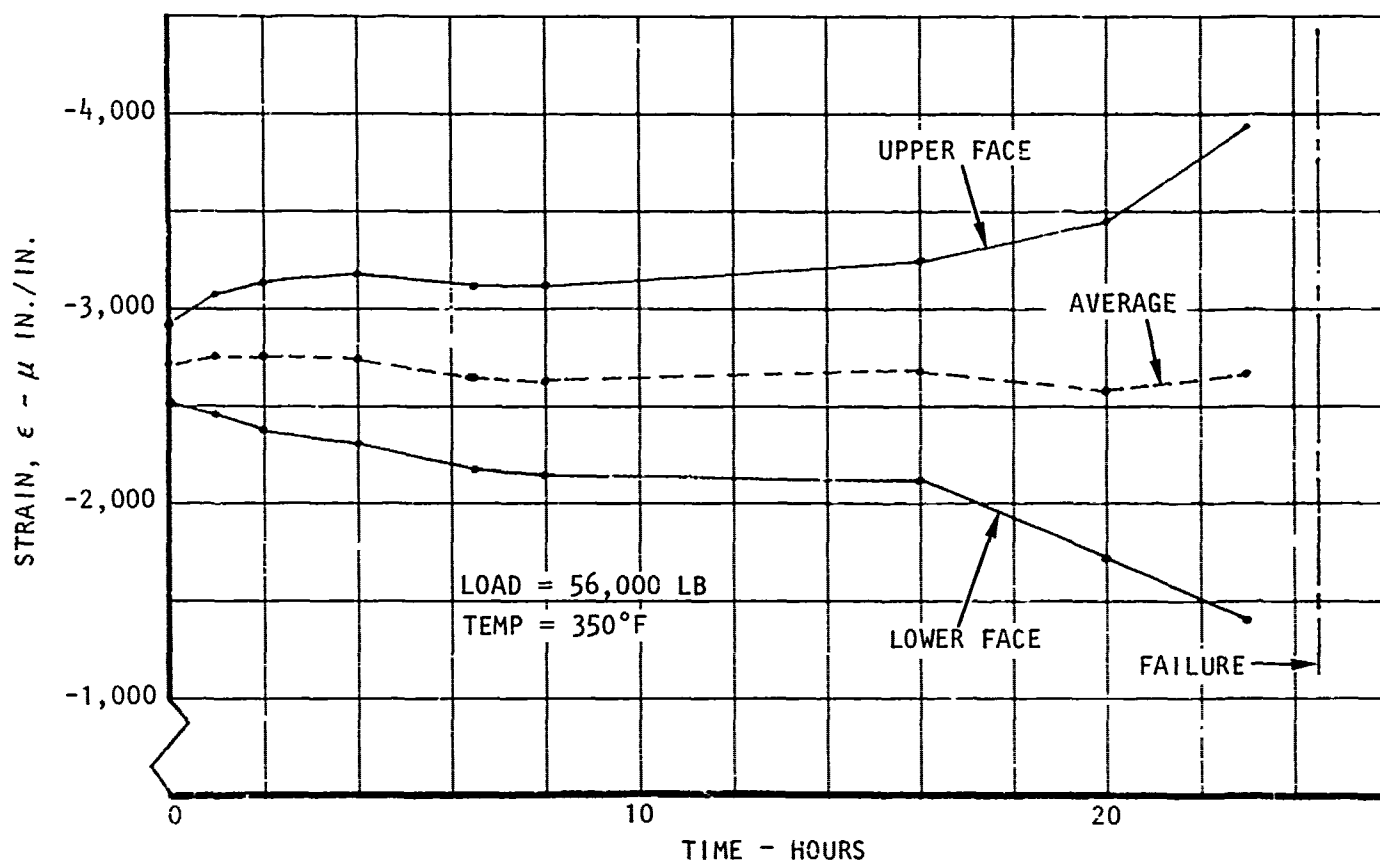
Figure 196. Honeycomb Panel Creep; Panel 10B1E2 Back-to-Back Longitudinal Strain Gages
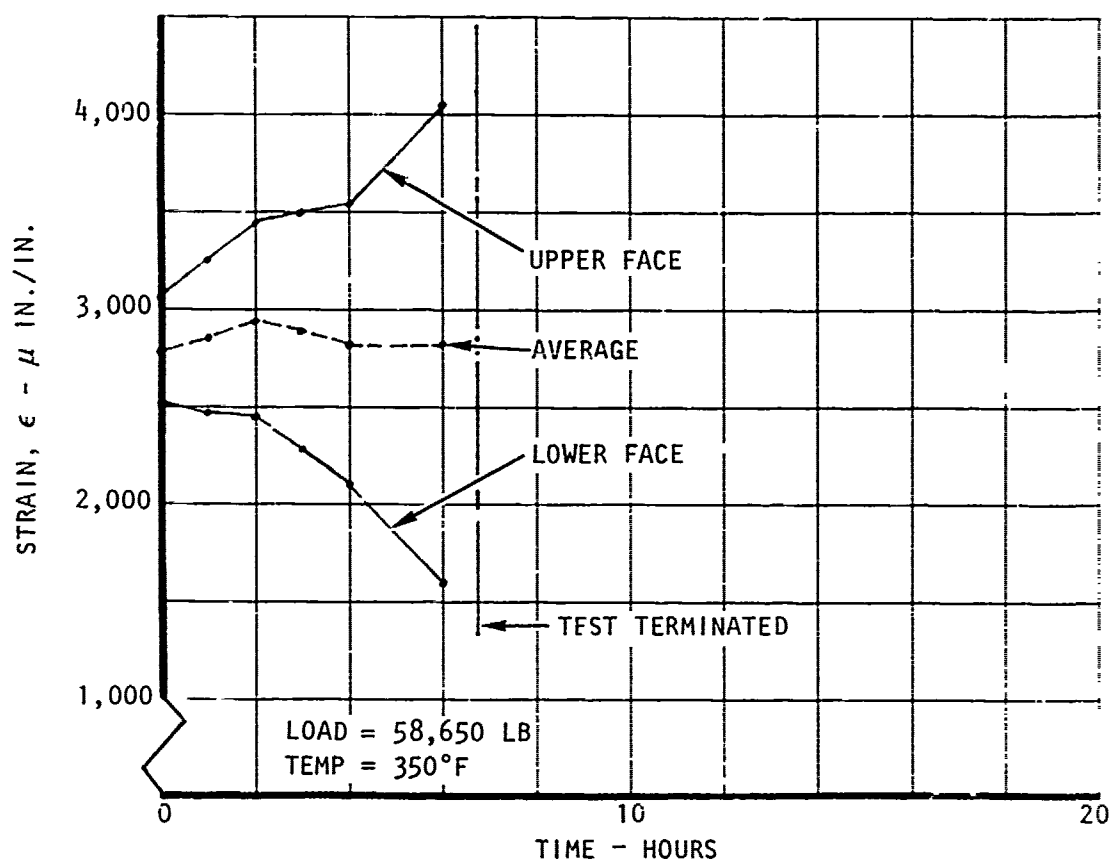
Figure 197. Honeycomb Panel Creep; Panel 10B1E3 Back-to-Back Longitudinal Strain Gages
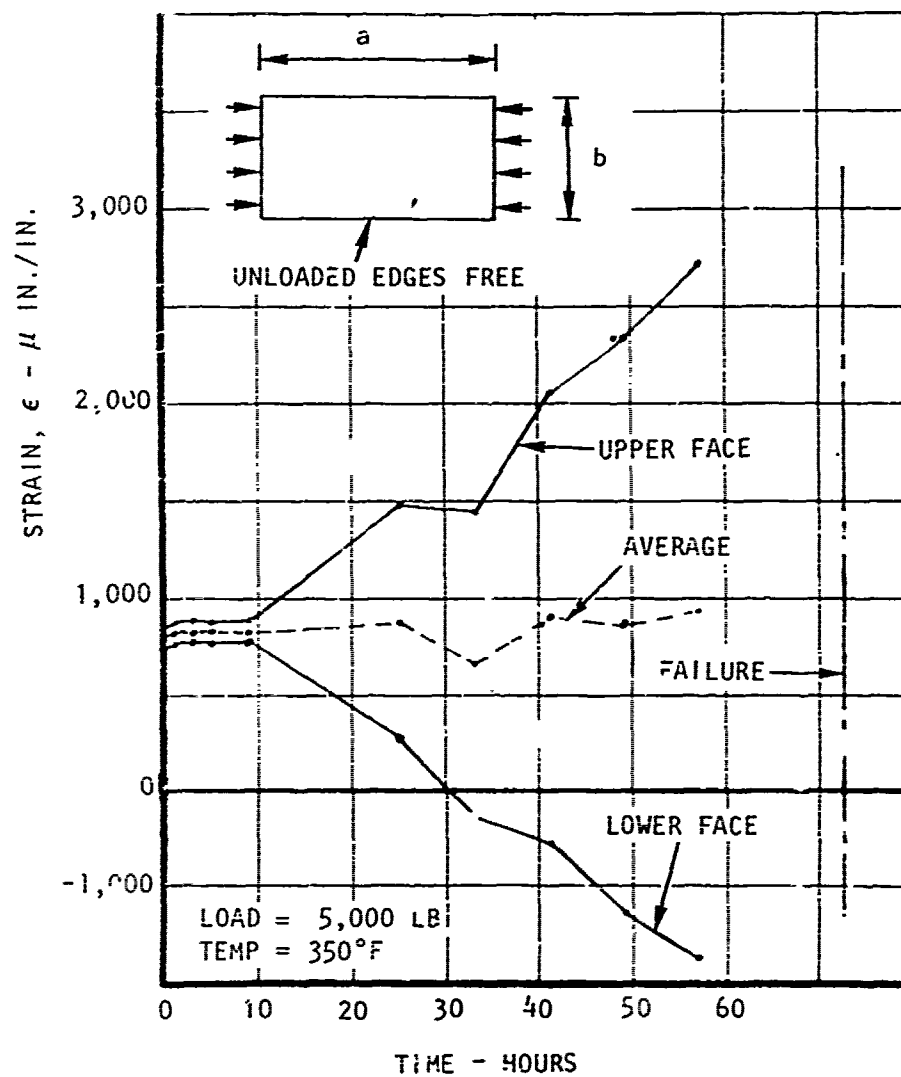
Figure 198. Honeycomb Panel Creep; Panel 10B2E1 Back-to-Back Longitudinal Strain Gages
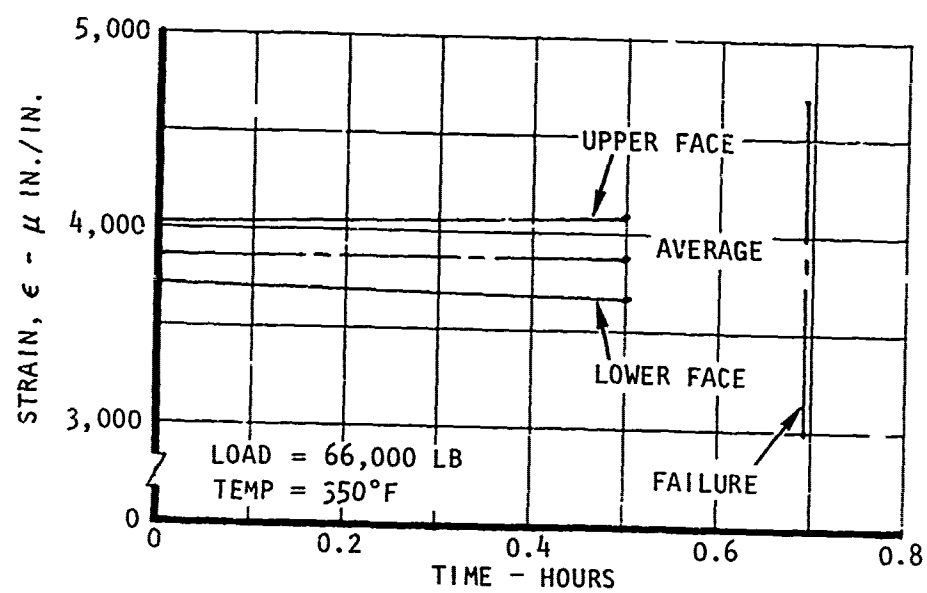
Figure 199. Honeycomb Panel Creep; Panel 10B2E2 Back-to-Back Longitudinal Strain Gages
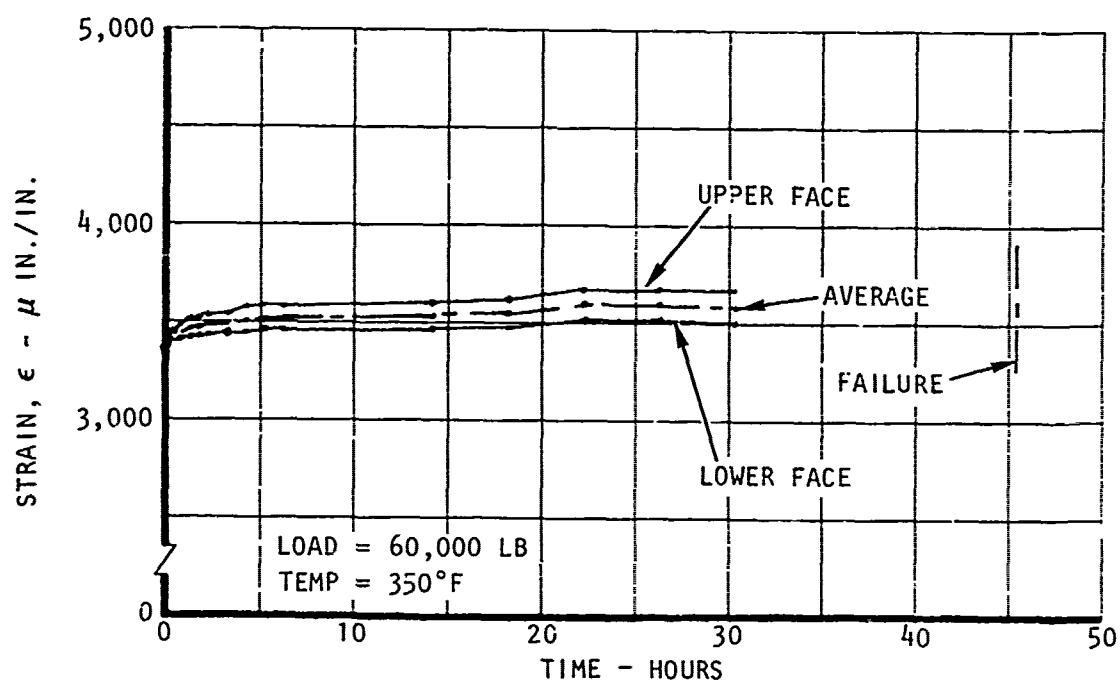
Figure 200. Honeycomb Panel Creep; Panel 10B2E3 Back-to-Back Longitudinal Strain Gages

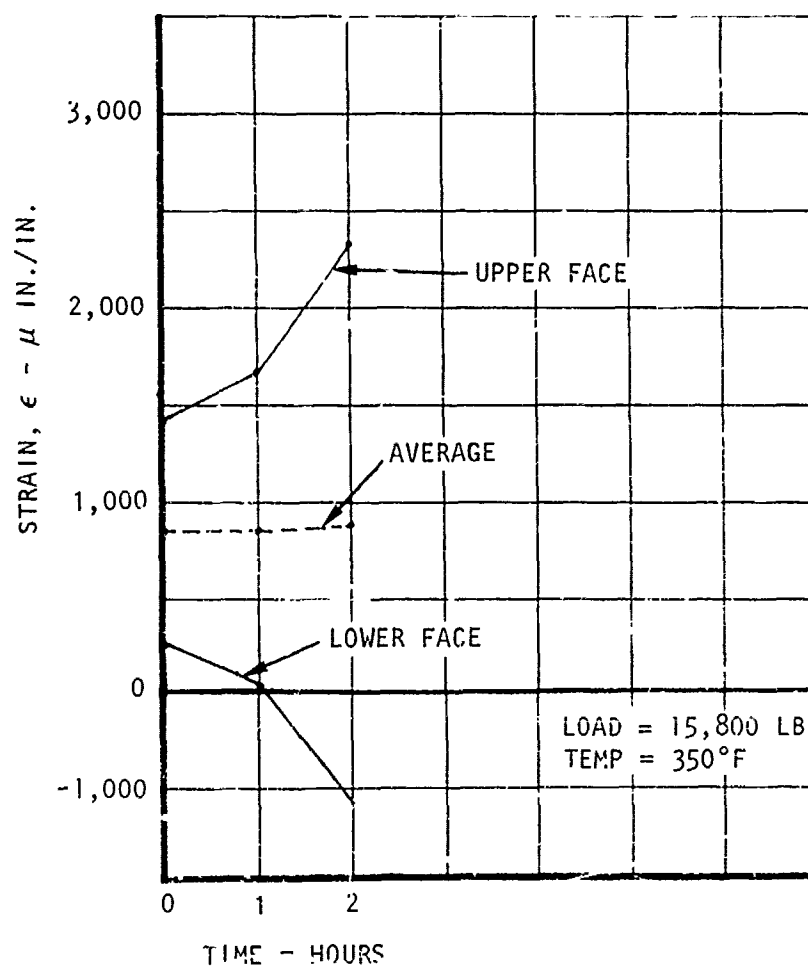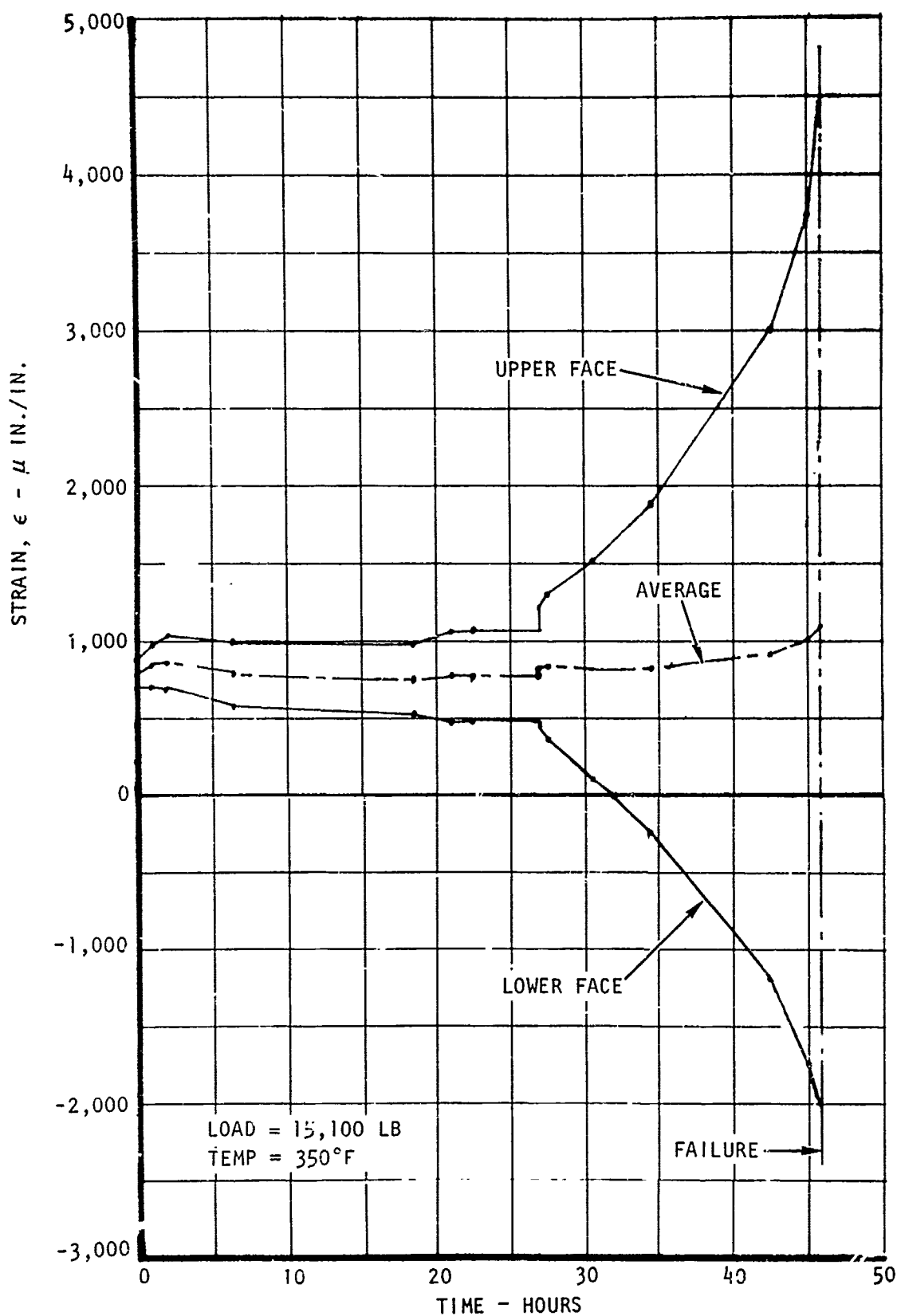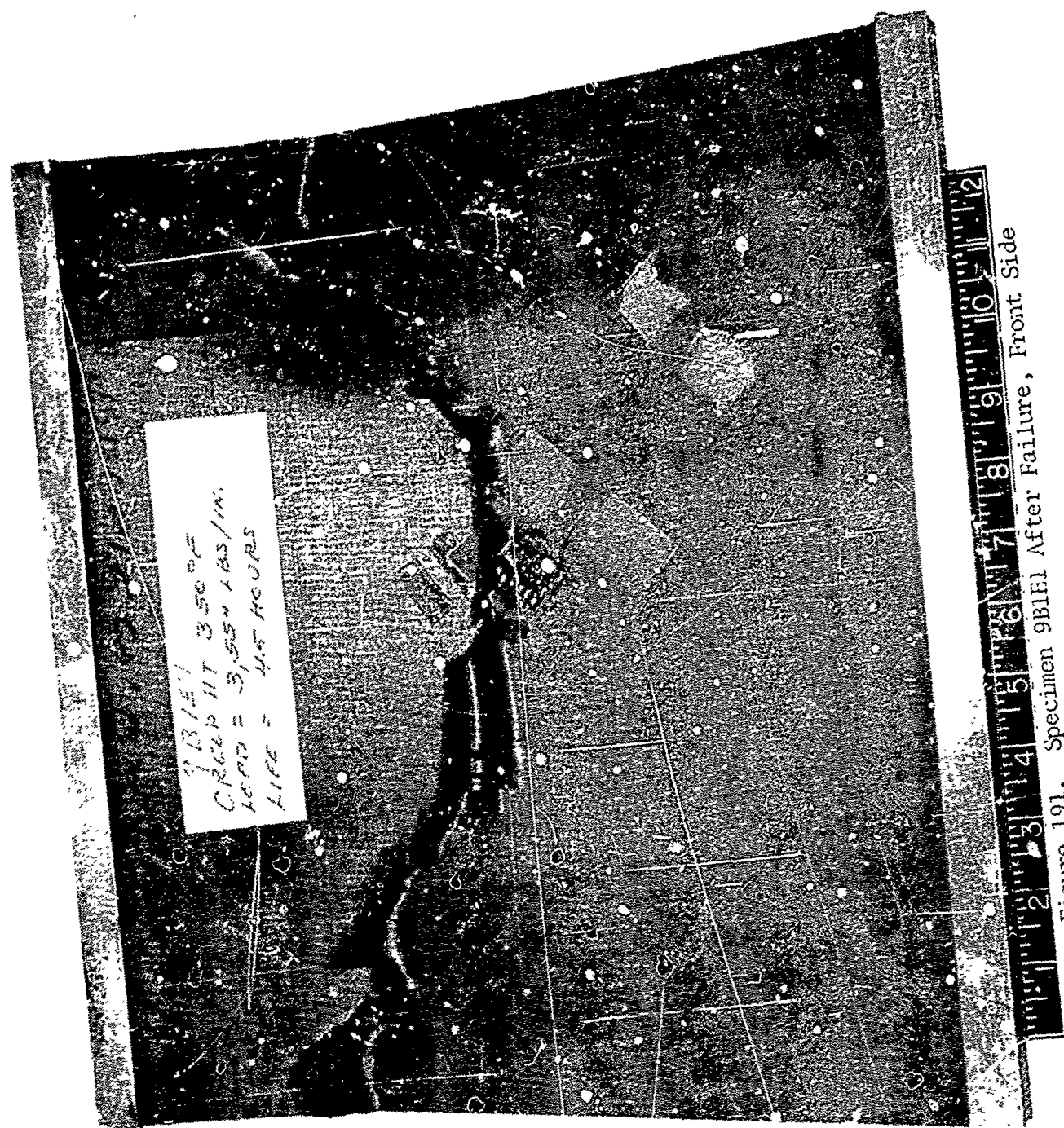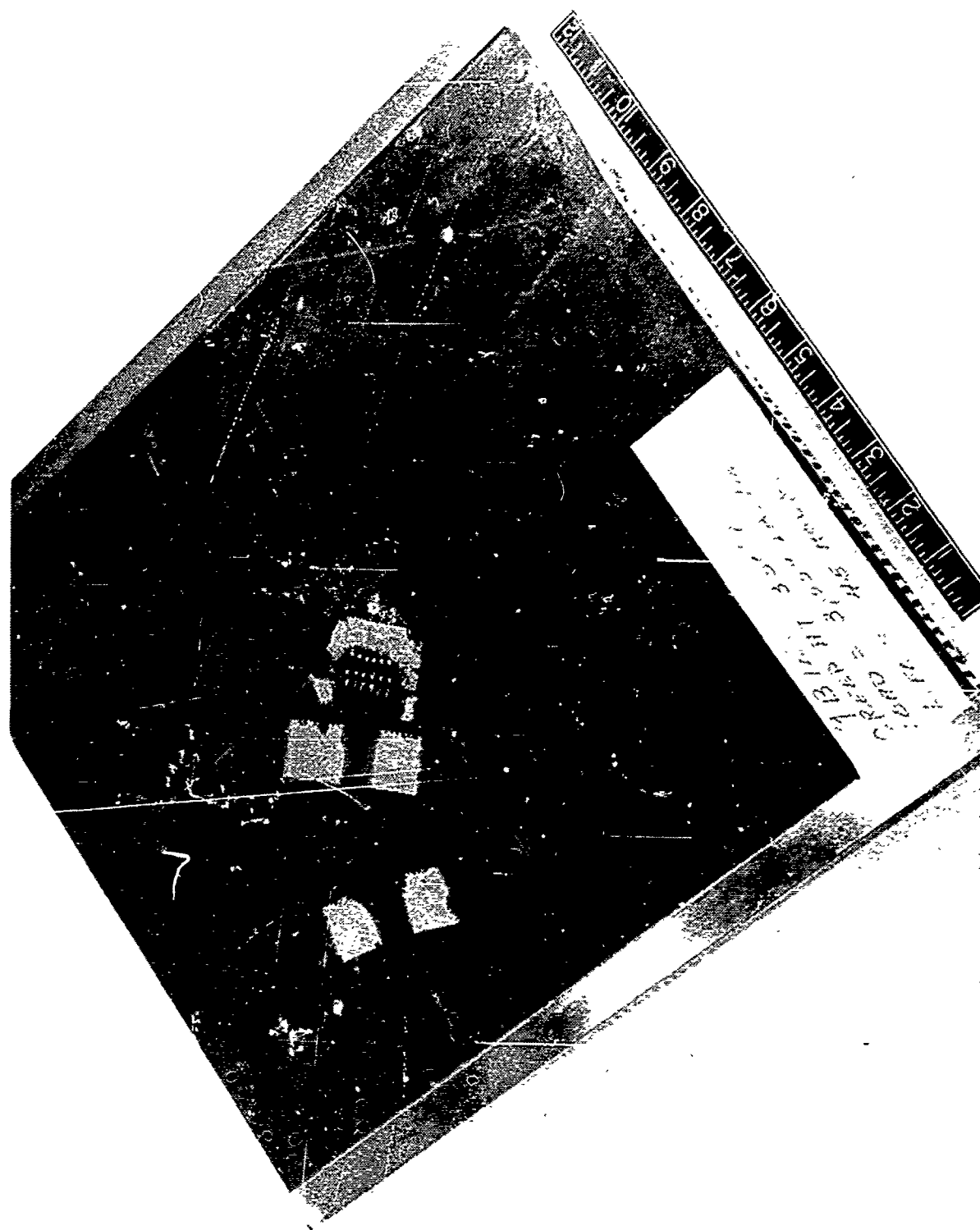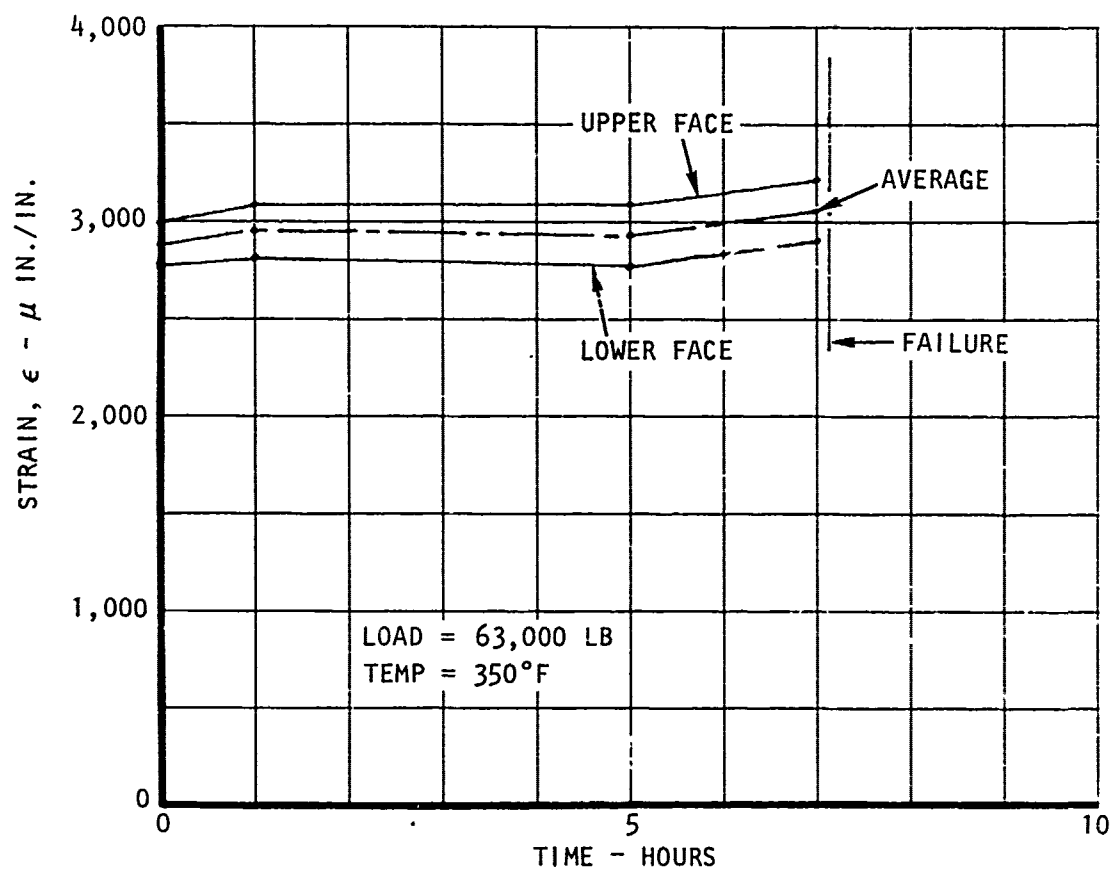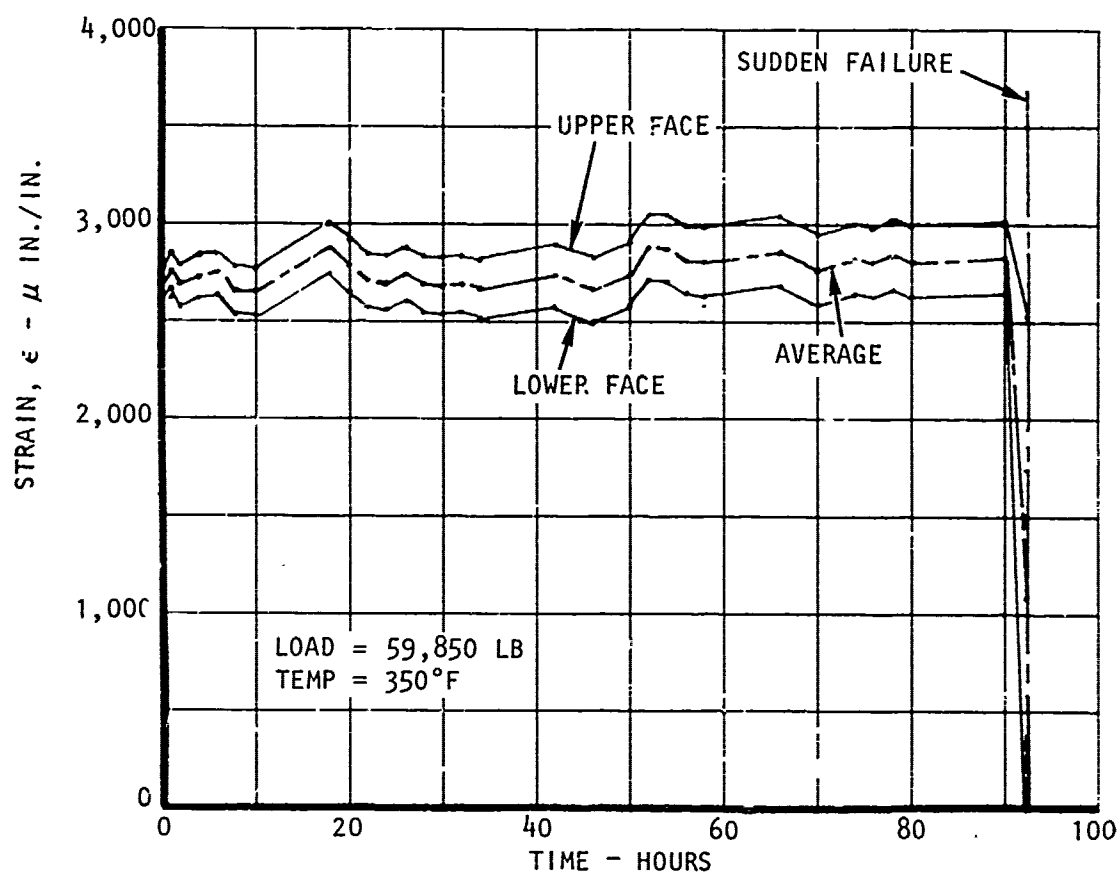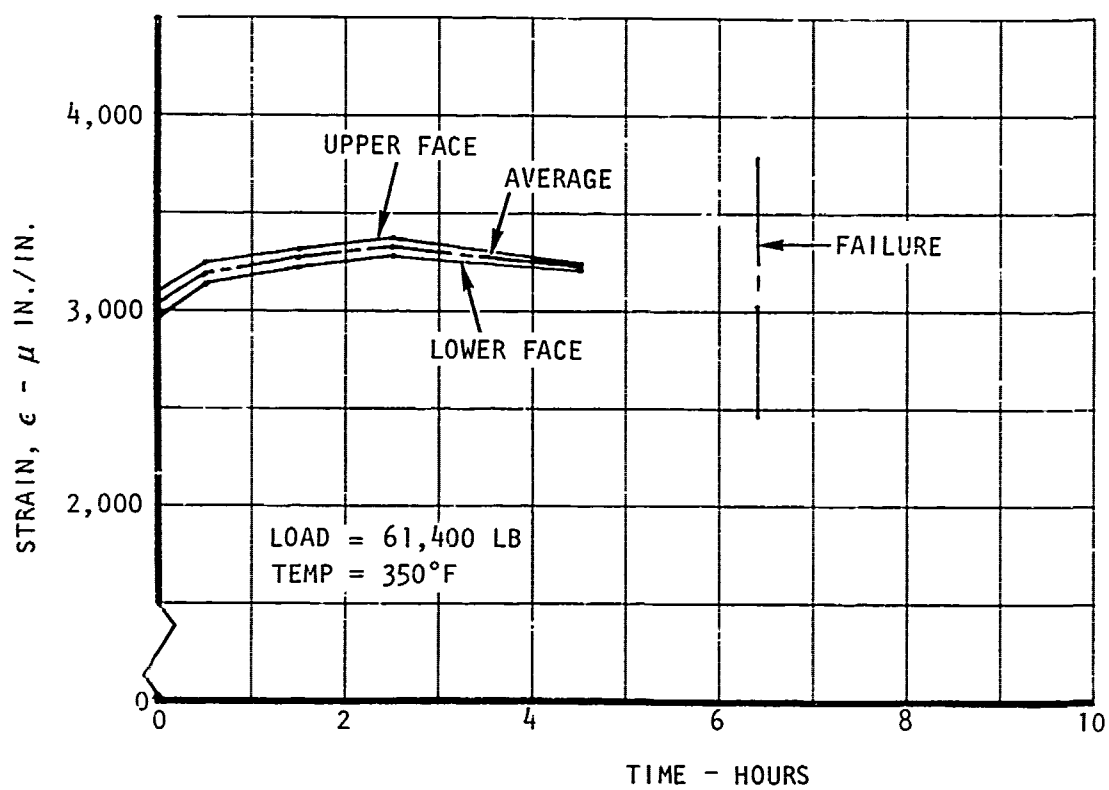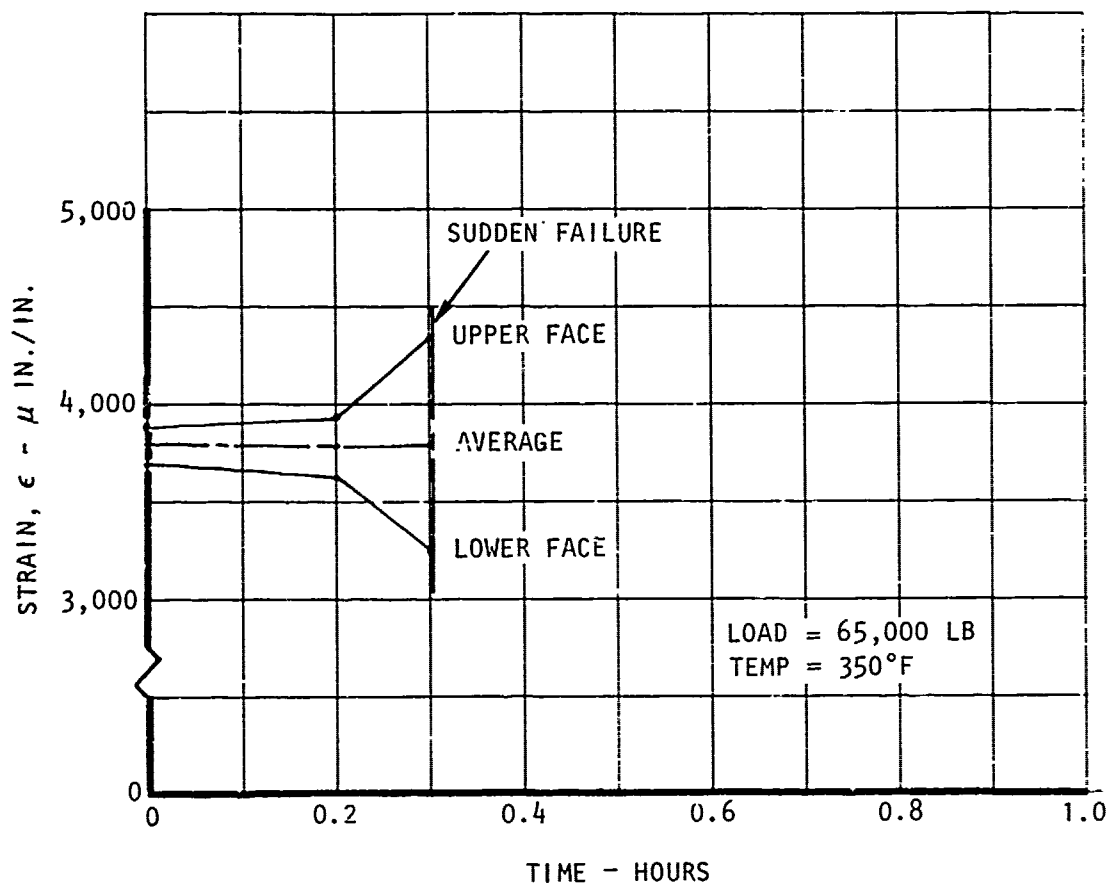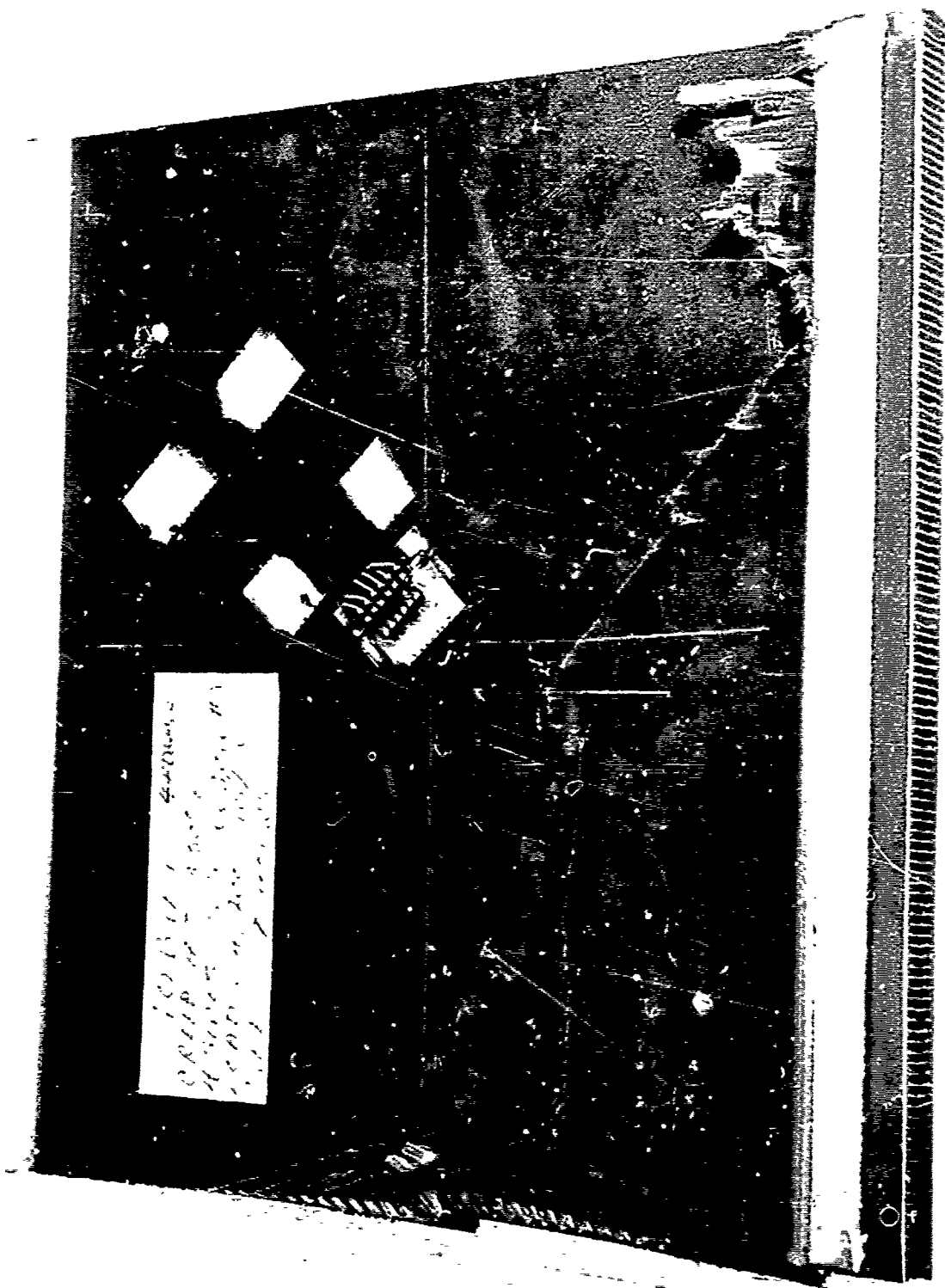Figure 201. Specimen 10B1E1 After Failure

251
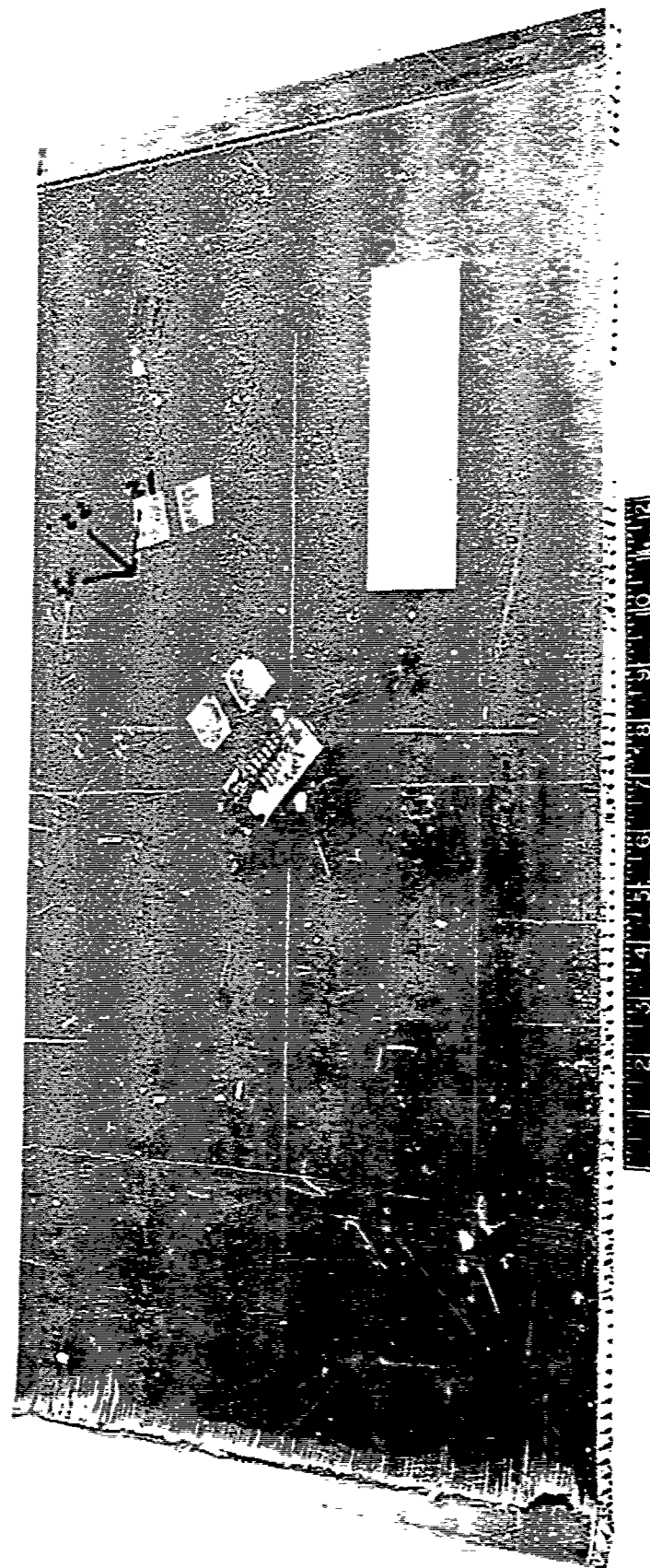
Figure 202. Specimen 10B2E1 After Failure
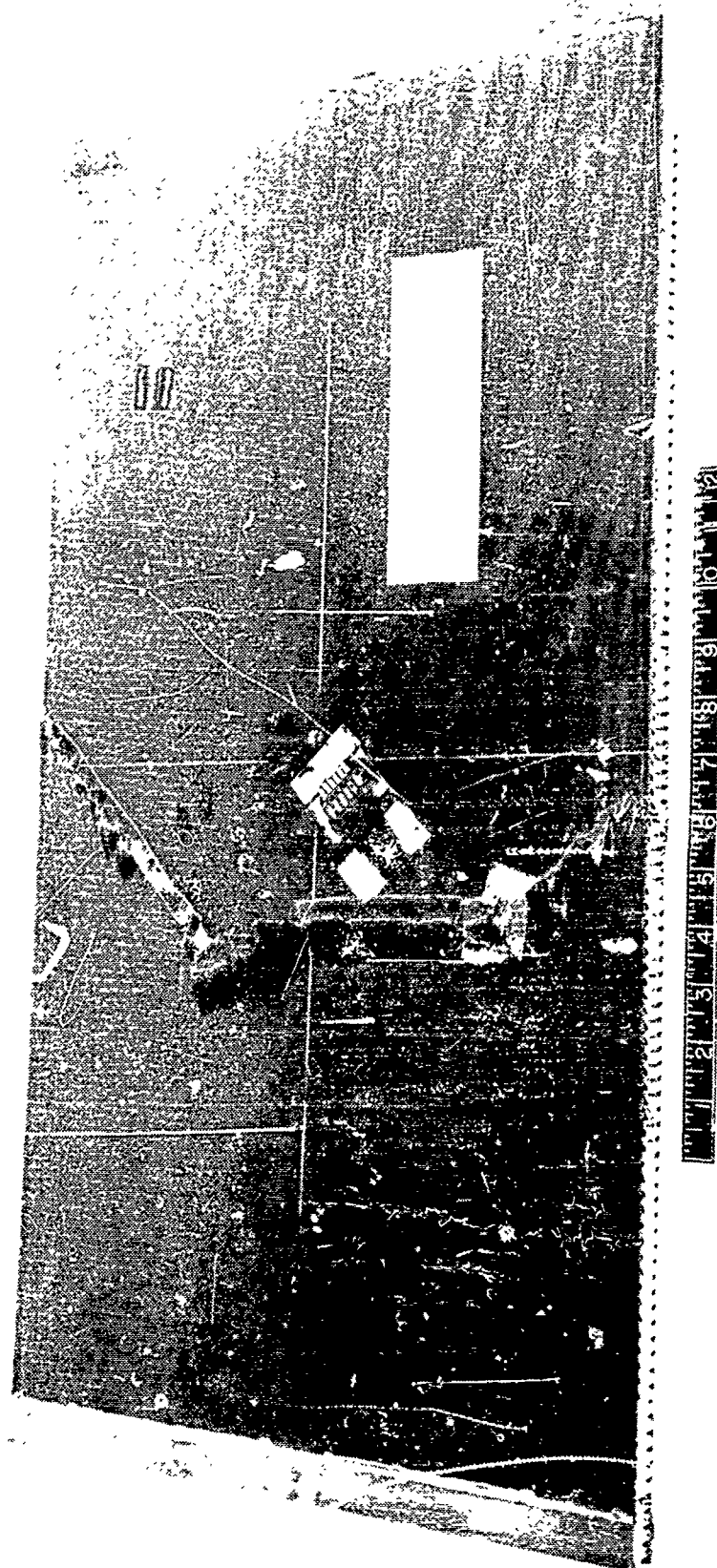
Figure 203. Specimen 10B2E3 After Failure

253

TABLE XL. GEOMETRIC DATA FOR CREEP TEST SPECIMENS

Panel	Config	a (in.)	b (in.)	t_F (in.)	c (in.)	s (inch/16)	t_C (mils)
9B1E1	$[0/\pm45/0]_S$	15.01	14.95	0.0416	0.5	2	2.0
1E2	$[0/\pm45/0]_S$	15	15	0.0416	0.5	?	2.0
1E3	$[0/\pm45/0]_S$	15	15	0.0416	0.5	2	2.0
2E1	$[0/\pm45/0]_S$	27.97	14.01	0.0416	0.5	2	2.0
2E2	$[0/\pm45/0]_S$	27.95	14	0.0416	0.5	2	2.0
2E3	$[0/\pm45/0]_S$	27.95	14.01	0.0416	0.5	2	2.0
10B1E1	$[0/\pm45/0]_S$	15	15	0.0416	0.5	2	2.0
1E2	$[0/\pm45/0]_S$	14.93	15	0.0416	0.5	2	2.0
1E3	$[0/\pm45/0]_S$	15	15	0.0416	0.5	2	2.0
2E1	$[0/\pm45/0]_S$	28	14	0.0416	0.5	2	2.0
2E2	$[0/\pm45/0]_S$	28	14	0.0416	0.5	2	2.0
2E3	$[0/\pm45/0]_S$	27.95	14.15	0.0416	0.5	2	2.0

STIFFENED SKIN

UNIAXIAL COMPRESSION (SERIES 1C AND 1D)

The series 1C and 1D stiffened-skin columns were fabricated with $[0/\pm45/0]_S$ skins and $[0]_{nT}$ stiffeners. The 1C series were Z-stiffened, while the 1D series were hat-stiffened. The geometries are shown by ures 204 and 20%. and table XLI. The loaded edges were simply supported, while the unloaded edges were unsupported. Tests were conducted at room temperature and 350°F. Two types of failures were considered: general and local instability. The columns were analyzed for general instability by using the equation
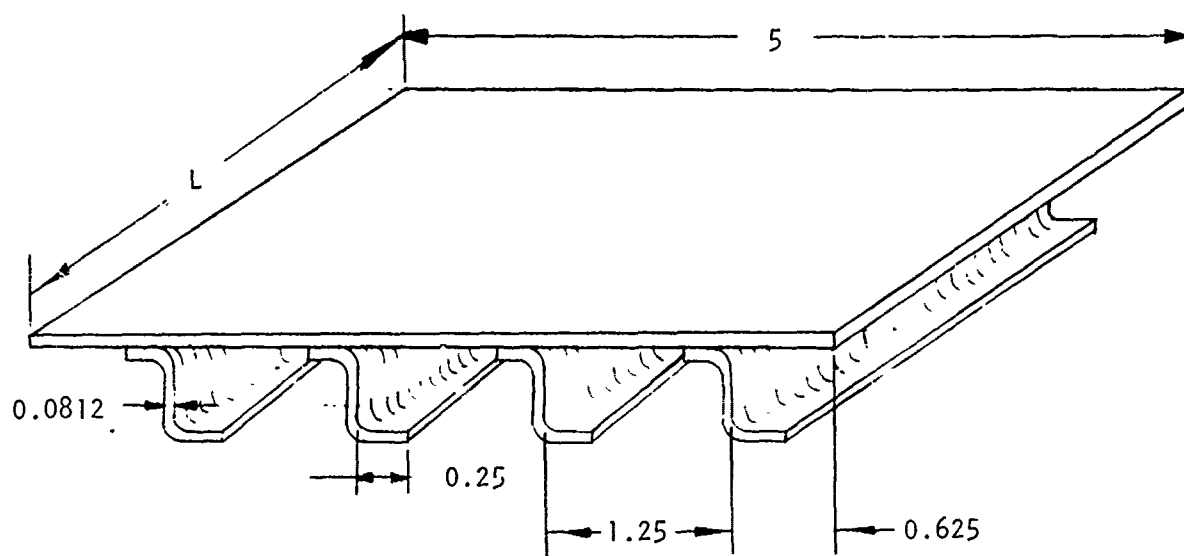
Figure 204.   Zee-Stiffened Skin Geometry
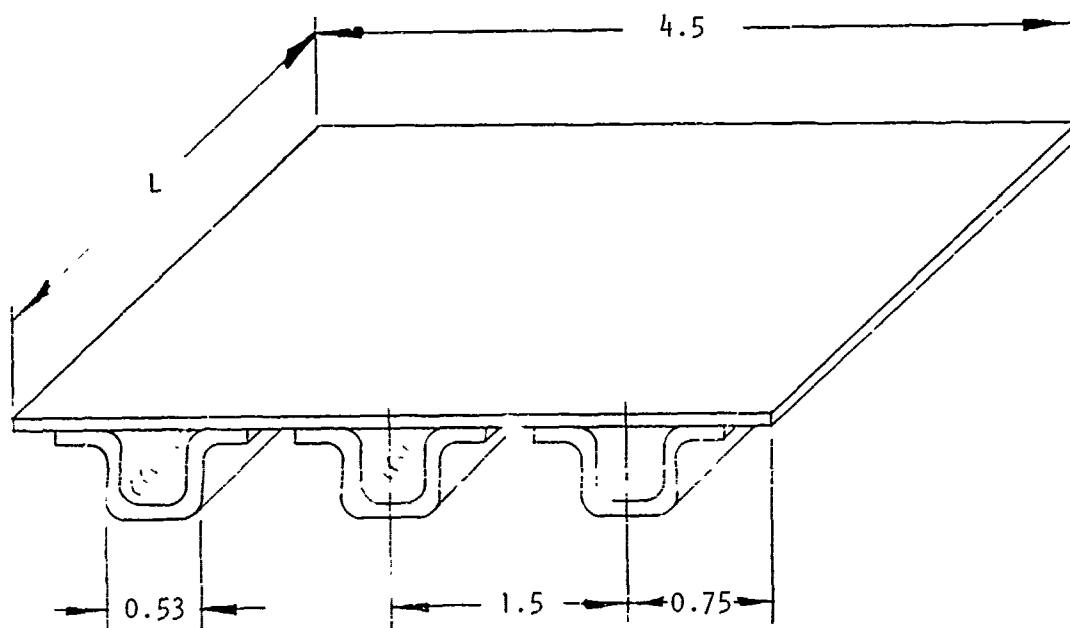
Figure 205.   Hat-Stiffened Skin Geometry

TABLE XLI. GEOMETRIC DATA FOR STIFFENED SKIN PANELS

Specimen	Skin	Stiffener		L (in.)	W (in.)	b_s (in.)	b_e (in.)	Temp (°F)	Failure Load (lb)
1C1R1	$[0/\pm45/0]_S$	Zee	$[0]_6$	2.650	5.00	1.25	0.625	RT	11,975
1R2			$[0]_6$	2.825				RT	14,850
1E1			$[0]_7$	2.975				350	10,130
1C2R1			$[0]_6$	4.700				RT	9,420
2R2			$[0]_6$	4.960				RT	11,900
2E1			$[0]_7$	4.925				350	8,290
1C3R1				12 395				RT	6,480
3R2				12.440				RT	7,500
3E1	$[0/\pm45/0]_S$	Zee	$[0]_7$	12.610	4.99	1.25	0.625	350	4,700
1D1R1	$[0/\pm45/0]_S$	Hat	$[0]_5$	2.840	5.00	1.50	0.75	RT	20,275
1R2			$[0]_5$	2.80				RT	24,900
1E1			$[0]_6$	2.945				350	11,225
LD2R1				4.840				RT	9,025
2R2				4.785				RT	17,600
2E1				4.935				350	12,650
1D3R1				17.815				RT	7,440
3R2				17.755				RT	12,000
3E1	$[0/\pm45/0]_S$	Hat	$[0]_6$	17.455	5.00	1.50	0.75	350	5,420

$$N_{co} = \frac{\pi^2 D_1}{L^2}.$$

where N_{co} is the load per inch of the column, D_1 is given in Volume III on page 81 and is the flexural rigidity in the X direction, and L is the effective length of the column. For a simply supported panel, the effective length is equal to its actual length. Since the local instability or crippling strength techniques shown for the series 20C and 21D series tests were inconclusive, the method shown in sections V and VI of Volume III was used,

256

where the stiffeners are analyzed as individual flat plates simply supported at intersections. The results are shown in table XLII. Figures 206 and 207 show plots of these data. It should be noted here that the column predictions were based on the elastic properties shown in tables I through III.

The test data for the zee-stiffened 1C panels were rather low (average $P_{fail}/P_{pred} = 0.63$), whereas the hat-stiffened 1D panels failed as predicted or slightly high ($P_{fail}/P_{pred} = 1.09$). The reason for this apparent discrepancy is in the analysis, which assumes that the skins are simply supported for the width of the stiffener spacing. Although this approximation is reasonably valid for the zee-stiffened skins, it is quite conservative for the hat section, which has an unsupported span of only about 1/2 inch for the nominal analytical spacing of 1-1/2 inches. Thus, it can be seen that the method produces reasonable correlation. For design purposes, a strength of 50 percent of the results of this prediction technique produces reasonable design values.

TRANSVERSE SHEAR (SERIES 3C AND 3D)

The series 3C and 3D stiffened skin transverse shear panels were fabricated with $[0/\pm 45/0]_S$ skins and $[0]_{nT}$ stiffeners, where the 3C specimens were zee-stiffened, and the 3D specimens were hat-stiffened. The geometries are shown by figures 204 and 205. Tests were conducted at room temperature and 550°F. Two types of failures were considered, general instability and local instability.

The general instability strength was calculated by using the anisotropic material theory which neglects the coupling effect between inplane and rotational displacements and stress resultants. The governing equilibrium equation is

$$D_1 W_{,xxxx} + 4D_{16} W_{,xxxy} + 2(D_{12}+2D_{66}) W_{,xxyy} + 4D_{26} W_{,xyyy} + D_{22} W_{,yyyy}$$

$$= 2\overline{N}_{xy}, W_{,xy}$$

The predictions are based on the General Dynamics RA-5 anisotropic program described in reference 1. Simply supported boundary conditions were assumed for these predictions.

The crippling strength was calculated by using the procedure set forth from reference 5. The basic crippling strength of the face sheet is

TABLE XLII.   TEST VERSUS THEORY FOR STIFFENED-SKIN PANELS[*]

| Specimen	P_f (Kips)	P_{fco} (Kips)	P_{fcc} (Kips)	L (in.)	A (in.^{2})	F_f (Ksi)	F_{co} (Ksi)	F_{cc} (Ksi)	P_f/P_{min}
1C1R1	11.98	258.3	16.62	2.65	0.314	38.2	822.6	52.9	0.720
1R2	14.85	227.3	16.62	2.83	0.314	47.3	723.9	52.9	0.894
1E1	10.23	226.6	15.58	2.98	0.332	30.8	682.5	46.9	0.657
2R1	9.42	82.1	16.62	4.70	0.314	30.0	261.5	52.9	0.567
2R2	11.90	73.7	16.62	4.96	0.314	37.9	234.7	52.9	0.716
2E1	8.29	82.7	15.58	4.93	0.332	24.96	249.1	46.9	0.532
3R1	6.48	11.81	16.62	12.40	0.314	20.6	37.6	52.9	0.549
3R2	7.50	11.72	16.62	12.44	0.314	23.88	37.3	52.9	0.640
3E1	4.70	12.61	15.58	12.61	0.332	14.2	38.0	36.9	0.373
1D1R1	20.28	>> 1	13.46	2.84	0.342	59.4	High	39.4	1.507
1R2	24.90	>> 1	13.46	2.80	0.342	72.9	High	39.4	1.850
1E1	11.23	>> 1	13.47	2.95	0.373	30.1	High	36.2	0.834
2R1	9.03	122.5	13.46	4.84	0.342	26.4	358.7	39.4	0.671
2R2	17.60	125.3	13.46	4.79	0.342	51.5	3 ,.7	39.4	1.308
2E1	12.65	131.5	13.47	4.94	0.373	33.95	352.9	36.2	0.939
3R1	7.44	9.04	13.46	17.82	0.342	21.8	26.5	39.4	0.823
3R2	12.00	9.10	13.46	17.76	0.342	35.1	26.6	39.4	1.319
3E1	5.42	10.51	13.47	17.46	0.373	14.5	28.2	36.2	0.516

[*]$[0_2/\pm45]$; F_L^{pl} = 154 Ksi
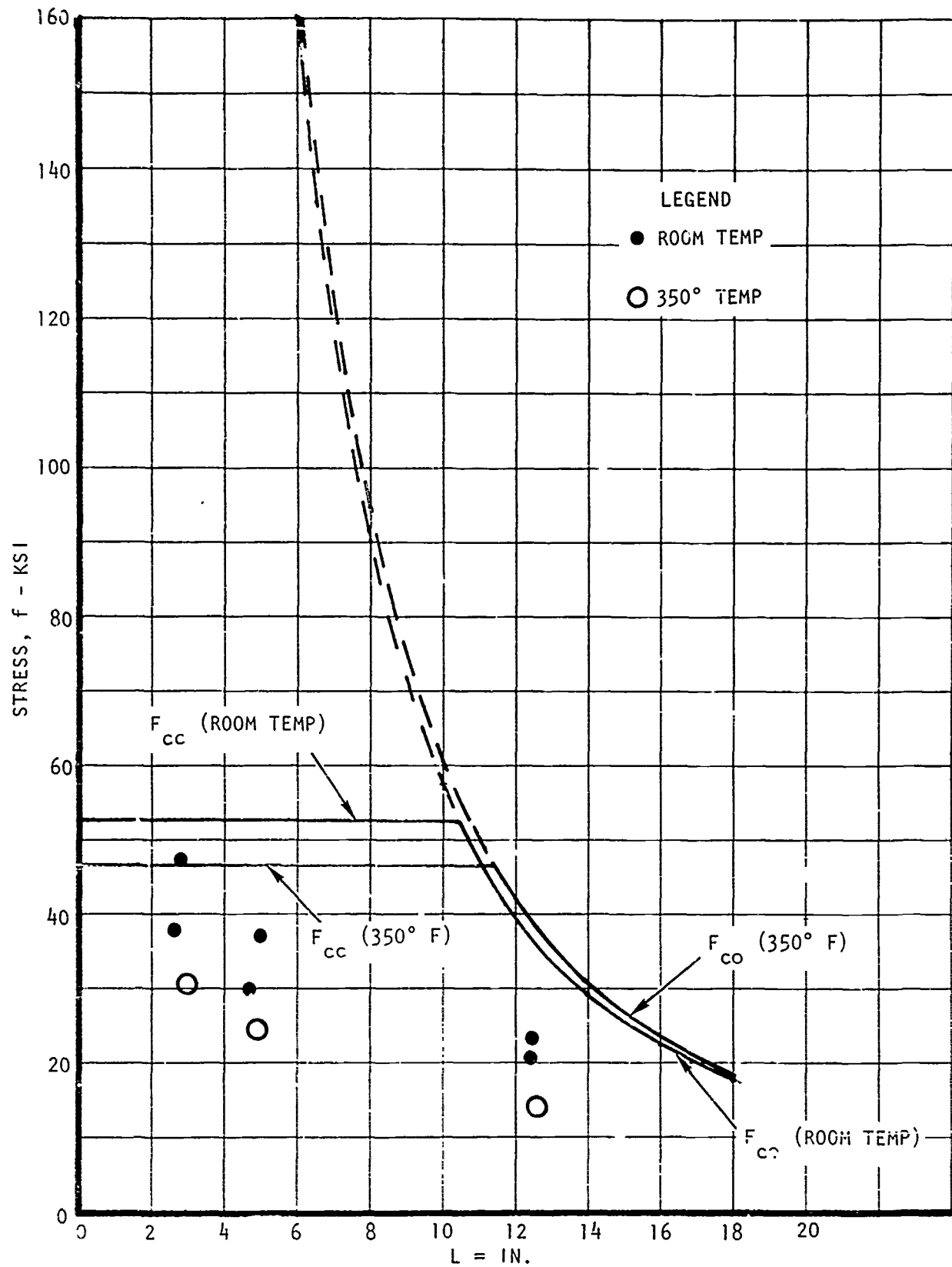
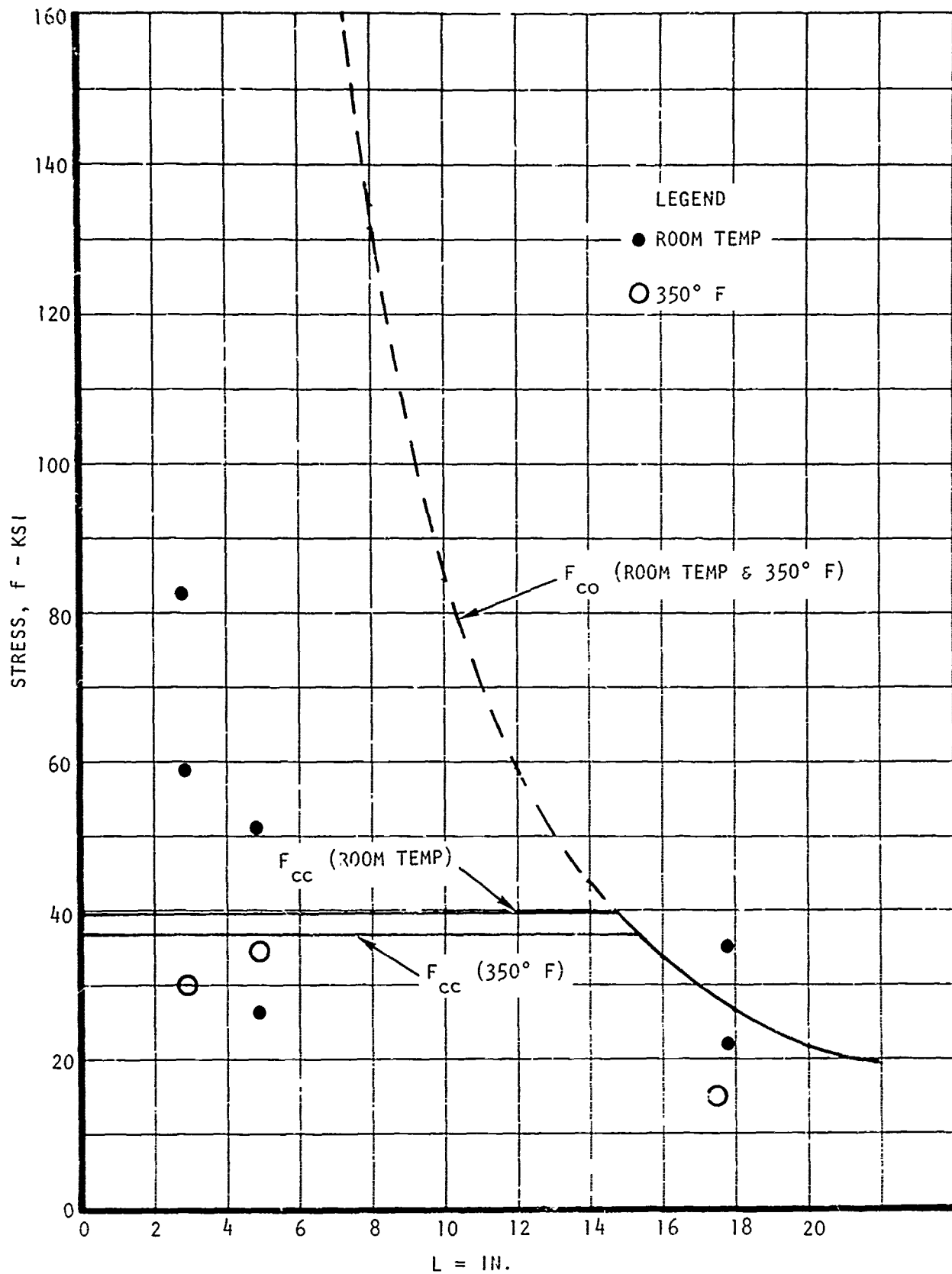Figure 206. Test Versus Predicted Stresses for Hat-Stiffened Columns

Figure 207. Test Versus Predicted Stresses for Zee-Stiffened Columns

assumed to be its general instability strength for simple supports at the center line of the stiffeners. This basic strength must then be modified by the multiplicative factor

$$R_1 = \left[\frac{1}{2} \left(\frac{b_s}{b} \right)^3 (1 - R_h) + R_h \right]$$

to account for the actual support provided for by the stiffeners. R_h can be obtained from figure 208 and was empirically derived for angle-type stiffeners as shown. This procedure would appear to be conservative on three accounts:

1. The unsupported panel width is much less than the stiffener spacing.

2. The stiffeners should lend more support than an angle section.

3. The axial rigidity (EA) of the stiffener is inherently greater than it would be were it made from the same material as the skin.

The results are shown in table XLIII, where R_1 is taken from table XLIV. Figures 209 and 210 show plots of these data. It should be noted here that the predictions are based on elastic properties. For the case of general instability strength prediction, some of the values should be reduced for plasticity effects. As in the compression specimens, 1C and 1D series, the zee-stiffened panels failed somewhat low. A prediction of 55 percent of the theoretical technique would be a good estimate at the present time. The hat-stiffened specimen, on the other hand, because of the inherent conservatism in the technique, failed somewhat high. For these specimens, a prediction of 110 percent of the theoretical technique is justified. Figures 211 through 218 show photographs of the test specimens after failure.
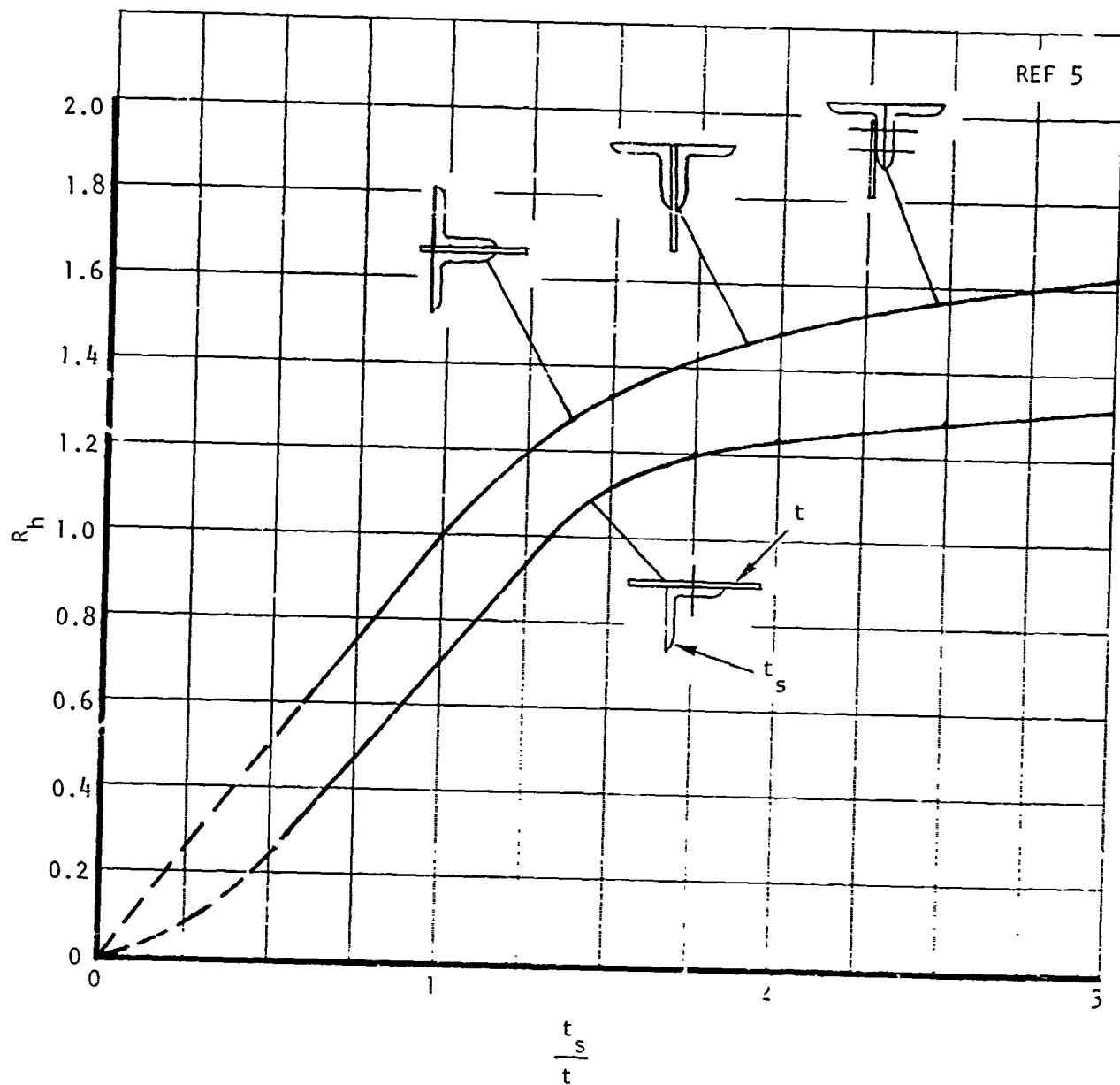
Figure 208. Empirical Restraint Coefficients for Stiffened Sheets
Under Shear Loading

TABLE XLIII. TEST VERSUS THEORY FOR SHEAR-LOADED STIFFENED-SKIN PANELS

Specimen	Temp (°F)	Stiffener Type	Stiffener Orientation	a (in.)	b (in.)	b_s (in.)	b_e (in.)	Predicted F^s_{cr} (Ksi)	Predicted R_1	Predicted F^s_{cc} (Ksi)	Test F^s (Ksi)
3C1R1	RT	Zee	$[0]_6$	8.00	8.00	1.25	1.50	81.13	0.457	13.99	9.98
1R2	RT		$[0]_6$	8.00	8.00		1.50	81.13	0.457	13.99	11.18
1E1	550		$[0]_7$	8.00	8.00		1.50	82.64	0.575	13.44	10.82
2R1	RT		$[0]_6$	16.00	8.00		1.50	21.06	0.450	13.77	10.07
2R2	RT		$[0]_6$	16.00	8.00		1.50	21.06	0.450	13.77	7.75
2E1	550		$[0]_7$	16.00	8.00		1.50	20.62	0.570	15.34	11.90
3R1	RT		$[0]_6$	18.00	6.00		1.125	17.67	0.450	13.77	9.71
3R2	RT		$[0]_6$	18.00	6.00		1.125	17.67	0.450	13.77	7.21
3E1	550	Zee	$[0]_7$	18.00	6.00	1.25	1.125	17.05	0.570	13.34	9.86
3D1R1	RT	Hat	$[0]_5$	8.00	8.00	1.50	1.50	127.21	0.327	7.04	7.67
1R2	RT		$[0]_5$	8.00	8.00		1.50	127.21	0.327	7.04	8.99
1E1	550		$[0]_6$	8.00	8.00		1.50	133.51	0.452	7.50	12.62
2R1	RT		$[0]_5$	16.00	8.00		1.50	31.32	0.325	7.00	7.98
2R2	RT		$[0]_5$	16.00	8.00		1.50	31.32	0.325	7.00	9.57
2E1	550		$[0]_6$	16.00	8.00		1.50	31.63	0.450	7.48	9.47
3R1	RT		$[0]_5$	18.00	6.00		1.125	25.84	0.325	7.00	7.86
3R2	RT		$[0]_5$	18.00	6.00		1.125	25.84	0.325	7.00	10.48
3E1	550	Hat	$[0]_6$	18.00	6.00	1.50	1.125	25.72	0.450	7.48	9.98

TABLE XLIV. REDUCTION FACTORS FOR STIFFENED-SKIN CONSTRUCTION

	Temp (°F)	a_s (in.)	b (in.)	t_s (in.)	t (in.)	t_s/t	R_h	K'_{ss}/K_{ss} (R$_1$)
Zee-stiffened	RT	1.25	8	0.0312	0.0416	0.750	0.450	0.457
	RT	1.25	16	0.0312	0.0416	0.750	0.450	0.450
	RT	1.25	18	0.0312	0.0416	0.750	0.450	0.450
	350	1.25	8	0.0364	0.0416	0.875	0.570	0.575
	350	1.25	16	0.0364	0.0416	0.875	0.570	0.570
	350	1.25	18	0.0364	0.0416	0.875	0.570	0.570
Hat-stiffened	RT	1.5	8	0.0260	0.0416	0.625	0.325	0.327
	RT	1.5	16	0.0260	0.0416	0.625	0.325	0.325
	RT	1.5	18	0.0260	0.0416	0.625	0.325	0.325
	350	1.5	8	0.0312	0.0416	0.750	0.450	0.452
	350	1.5	16	0.0312	0.0416	0.750	0.450	0.325
	350	1.5	18	0.0312	0.0416	0.750	0.450	0.325
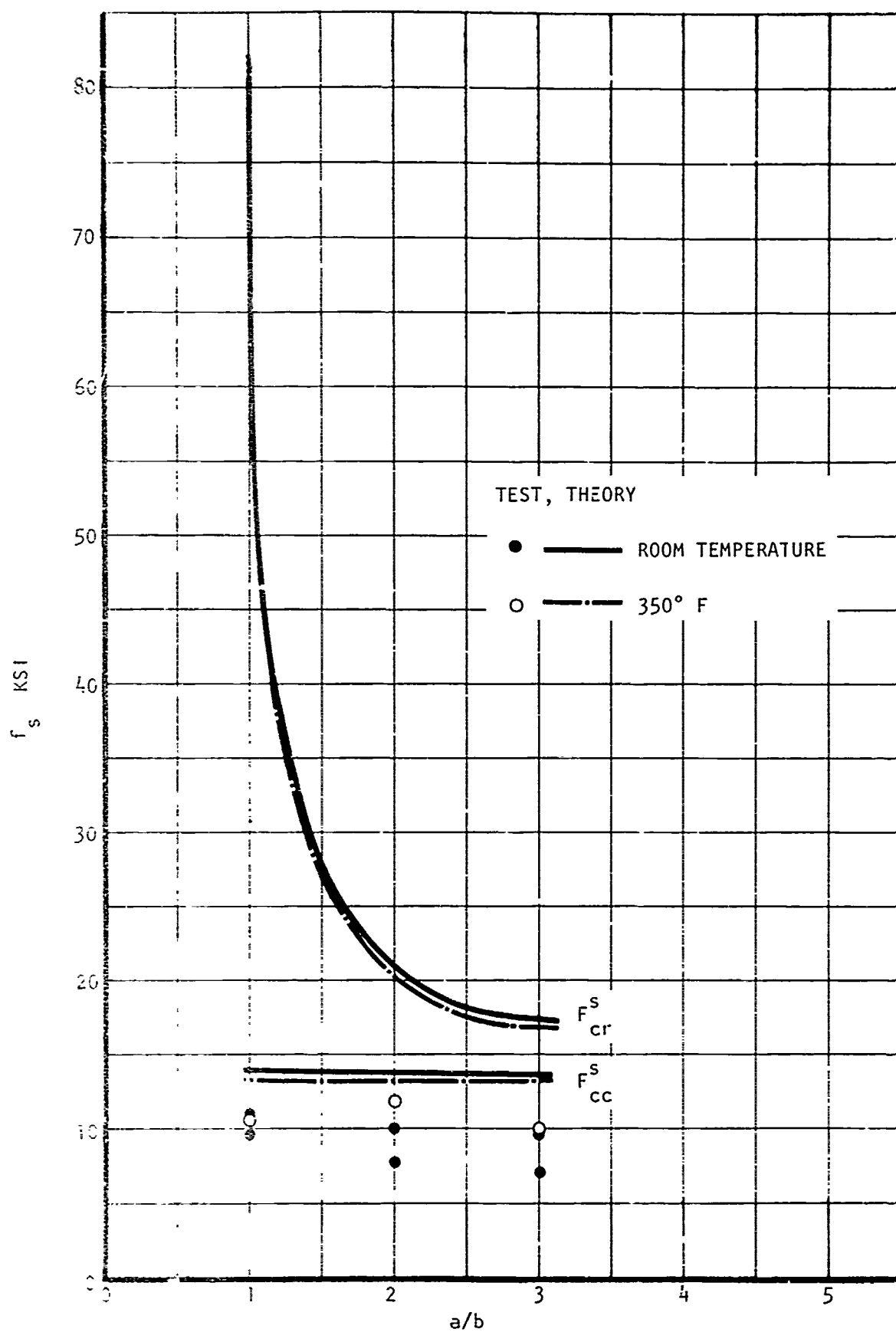
Figure 285. Test Versus Theory for Zee-Stiffened Panels in Shear
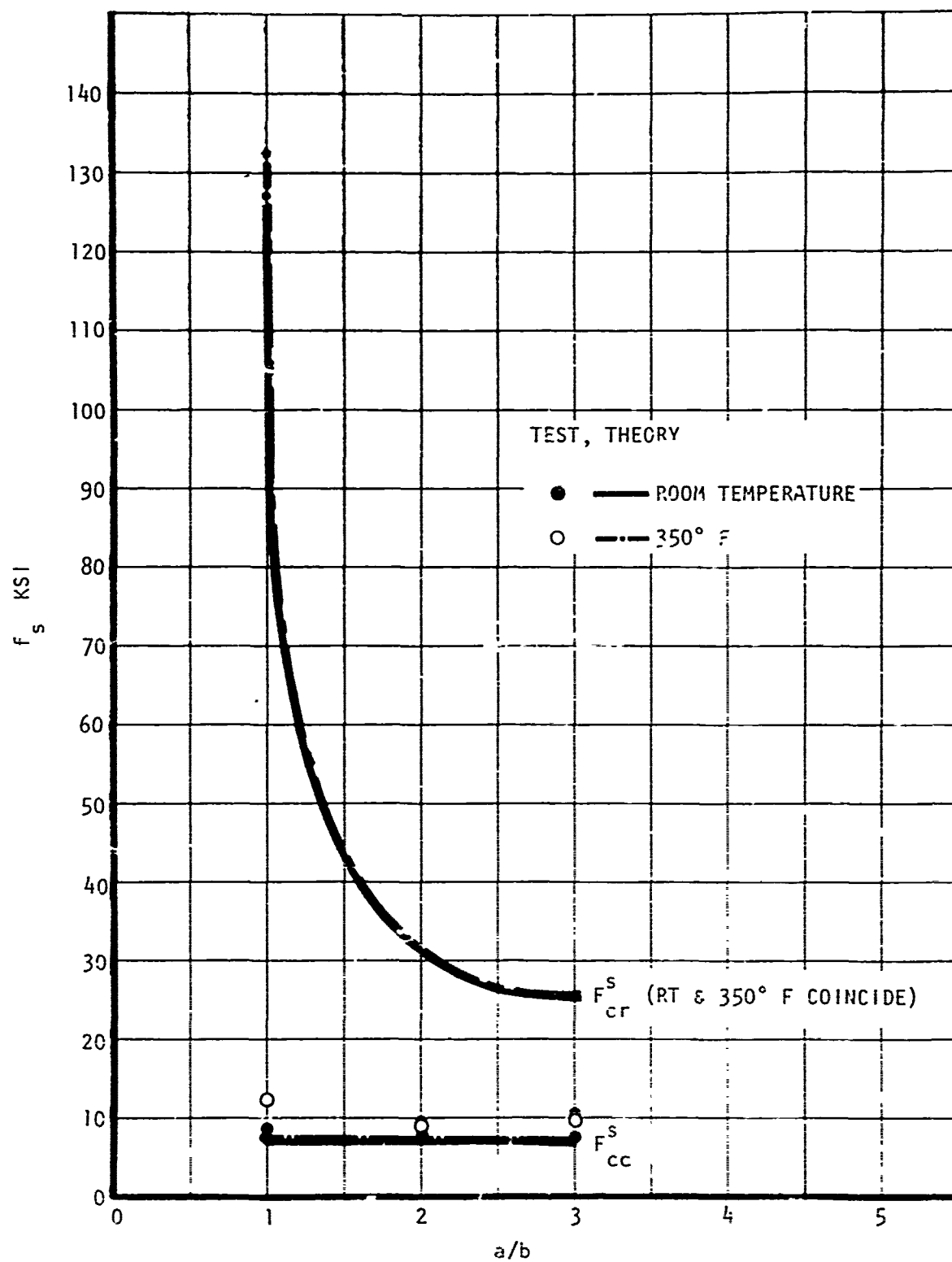
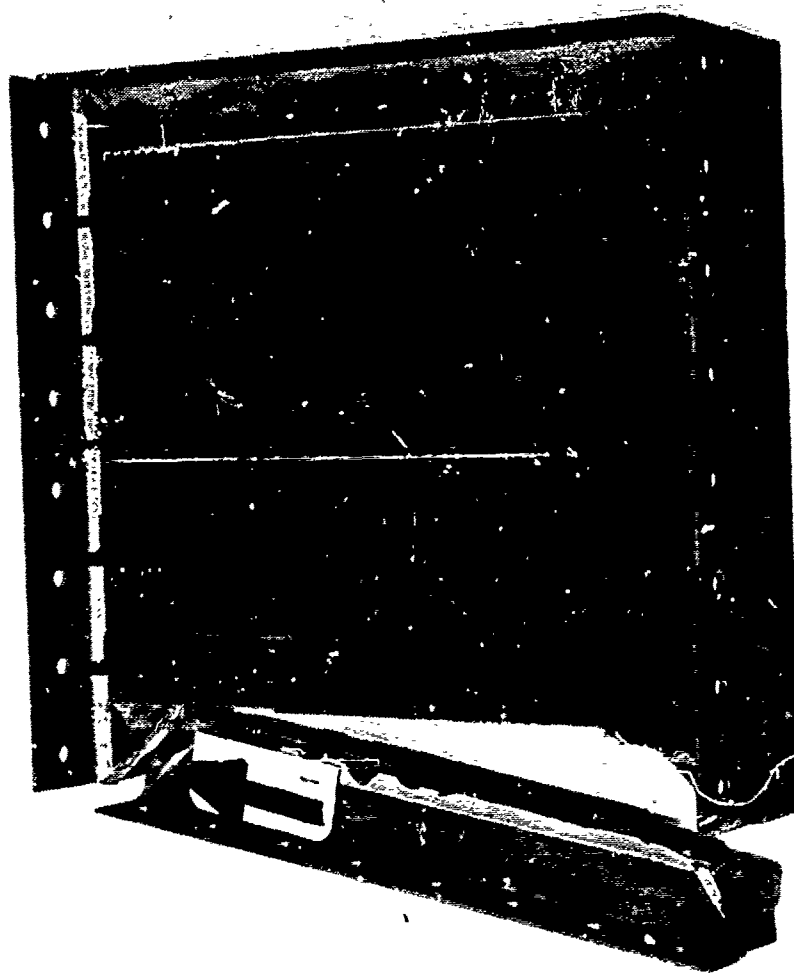Figure 210. Test Versus Theory for Hat-Section-Stiffened Panels in Shear
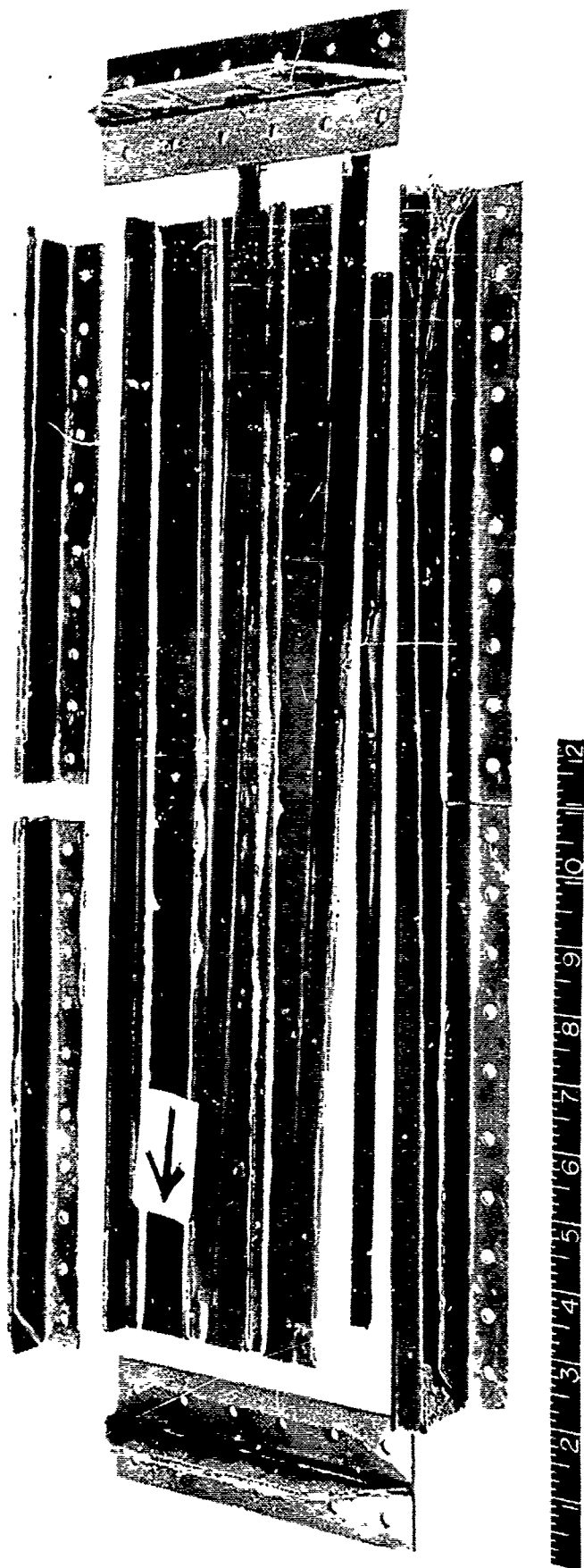
Figure 211. Specimen 3C1R1 After Failure
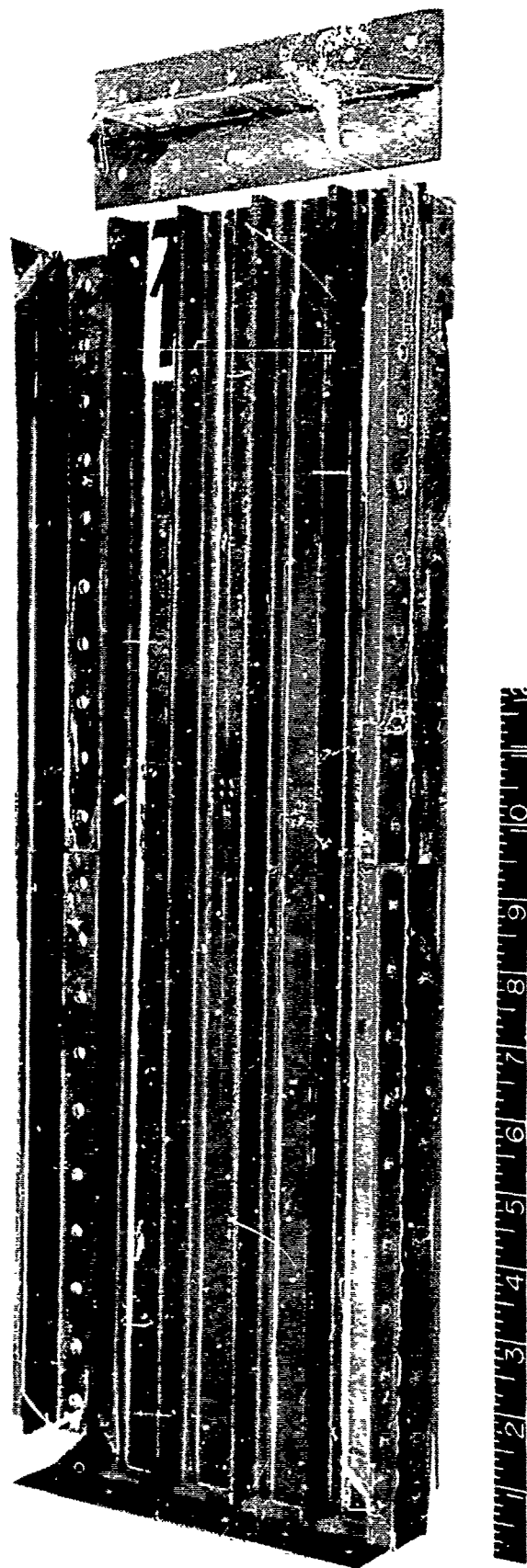
Figure 212. Specimen 3C3R1 After Failure

Figure 213. Specimen 3CR2 After Failure.
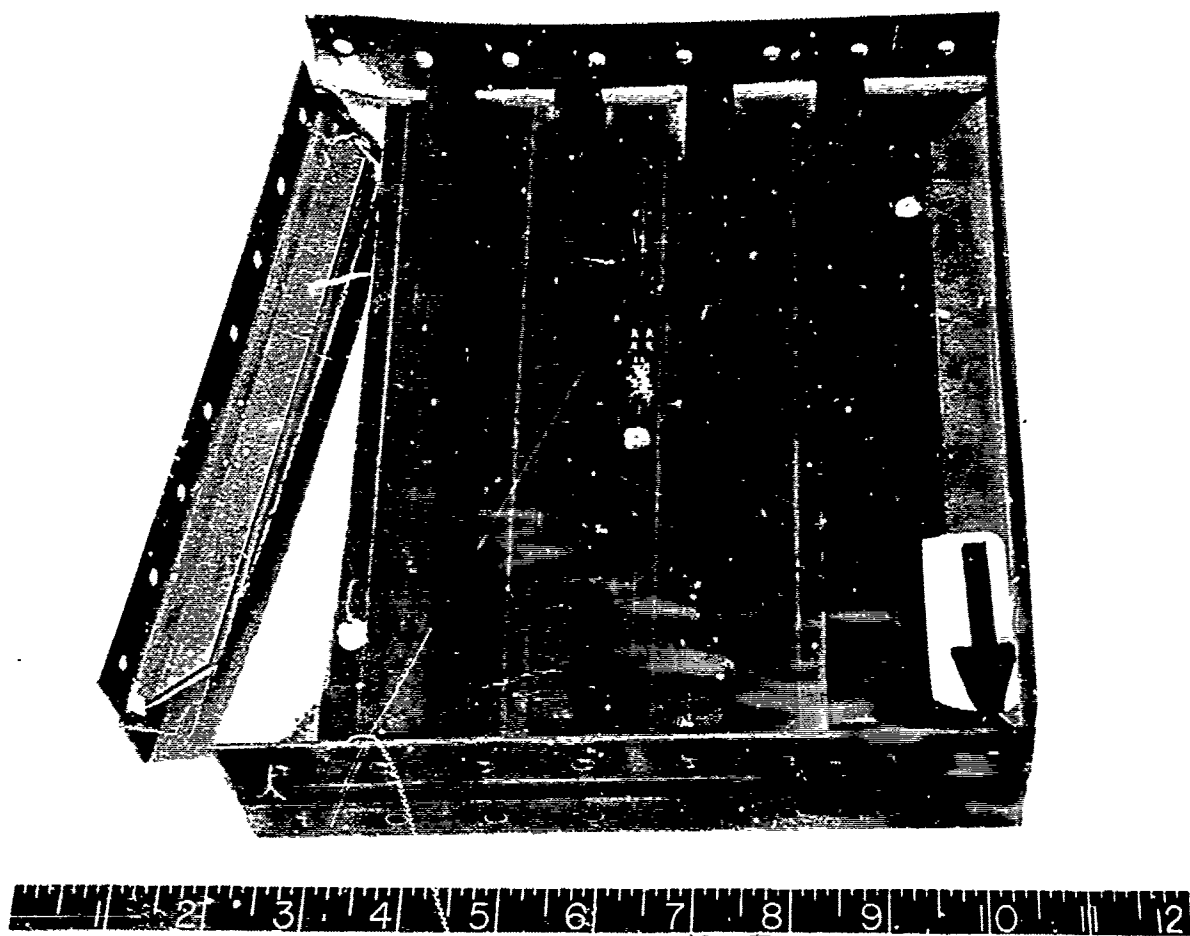
269

Figure 214. Specimen 3C3E1 After Failure

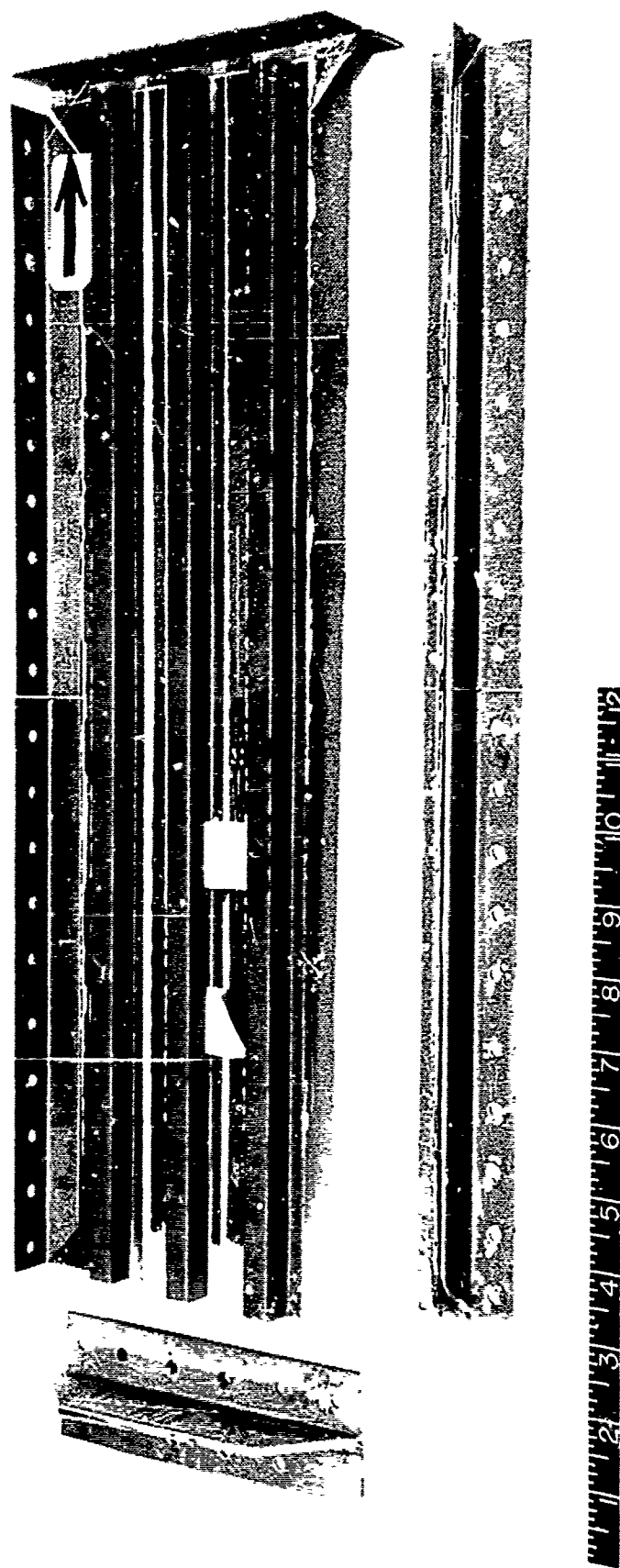Figure 215. Specimen 3D1E1 After Failure
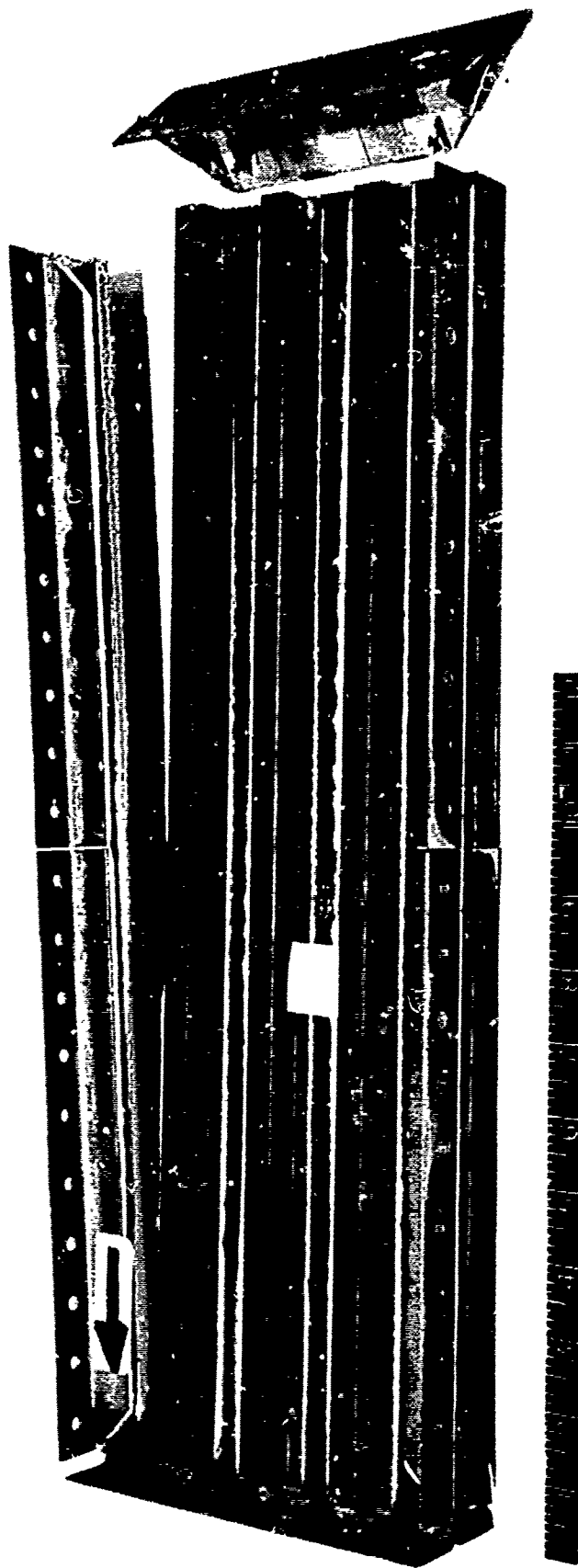
Figure 216. Specimen 3D3R1 After Failure

Figure 217. Specimen 3D3R2 After Failure

Figure 218. Specimen 3D3E1 After Failure

SECTION V

CONCLUSIONS AND RECOMMENDATIONS

This program was the first step in the generation and presentation of basic engineering data necessary to perform high-confidence-level structural design of primary aircraft structures utilizing advanced composite materials. Because of the scope of the program, many problems encountered throughout the program are not yet resolved. These have been delineated in the text. Although, for the most part, there were analytical techniques available to compare with the test data, there was often not enough test data available to modify the techniques when the comparison was wanting. In particular, further efforts should be devoted to the cutout test and the crippling test sections. Since these are problem areas for monolithic materials, the results were not surprising; although, in the crippling area, a recommendation was made to revise the basic element test specimen. In the area of creep, there were enough data generated to formulate an empirical creep equation. Further effort in the area should prove fruitful.

Most of the data, however, showed very good correlation with the analytic methods considered. In particular, the test results for membrane-loaded and combined-membrane-and-pressure-loaded unstiffened skin and honeycomb sandwich panels correlated well.

The analytic techniques, or empirical modifications thereto, shown in the text can be used for those orientations tested. Exptrapolations to other orientations can be made with assurance for those cases where the analytical methods were verified, although further "spot-testing" for other orientations is desirable. Similar test programs should be conducted for other material systems.

APPENDIX

SPECIMEN DRAWINGS

FOREWORD

This appendix comprises the individual drawings used in this program to define and fabricate the structural element test specimens. Each drawing delineates the panel to be fabricated, the layout of the specimens and coupons to be cut from it, and a summary of the test parameters.
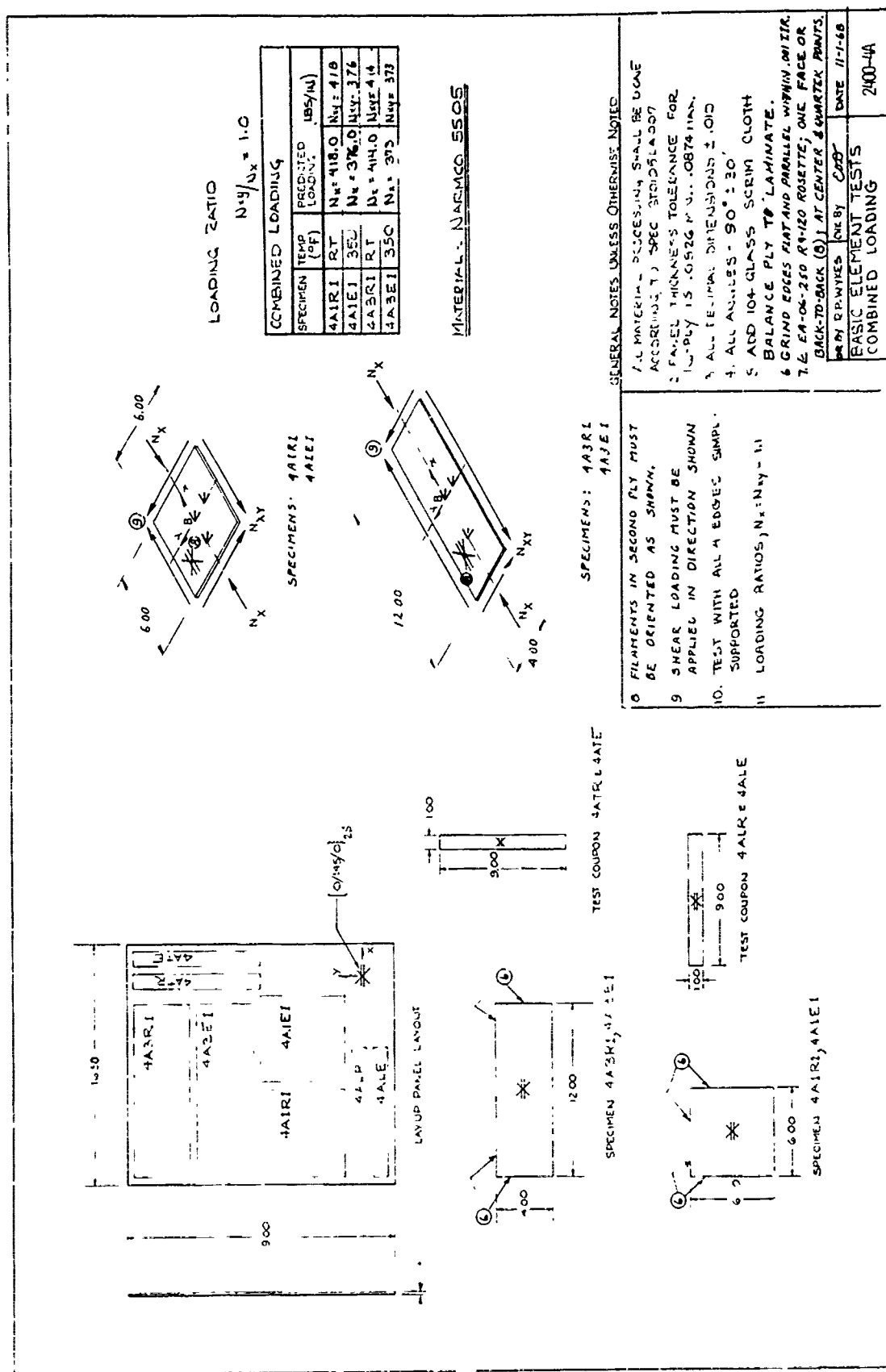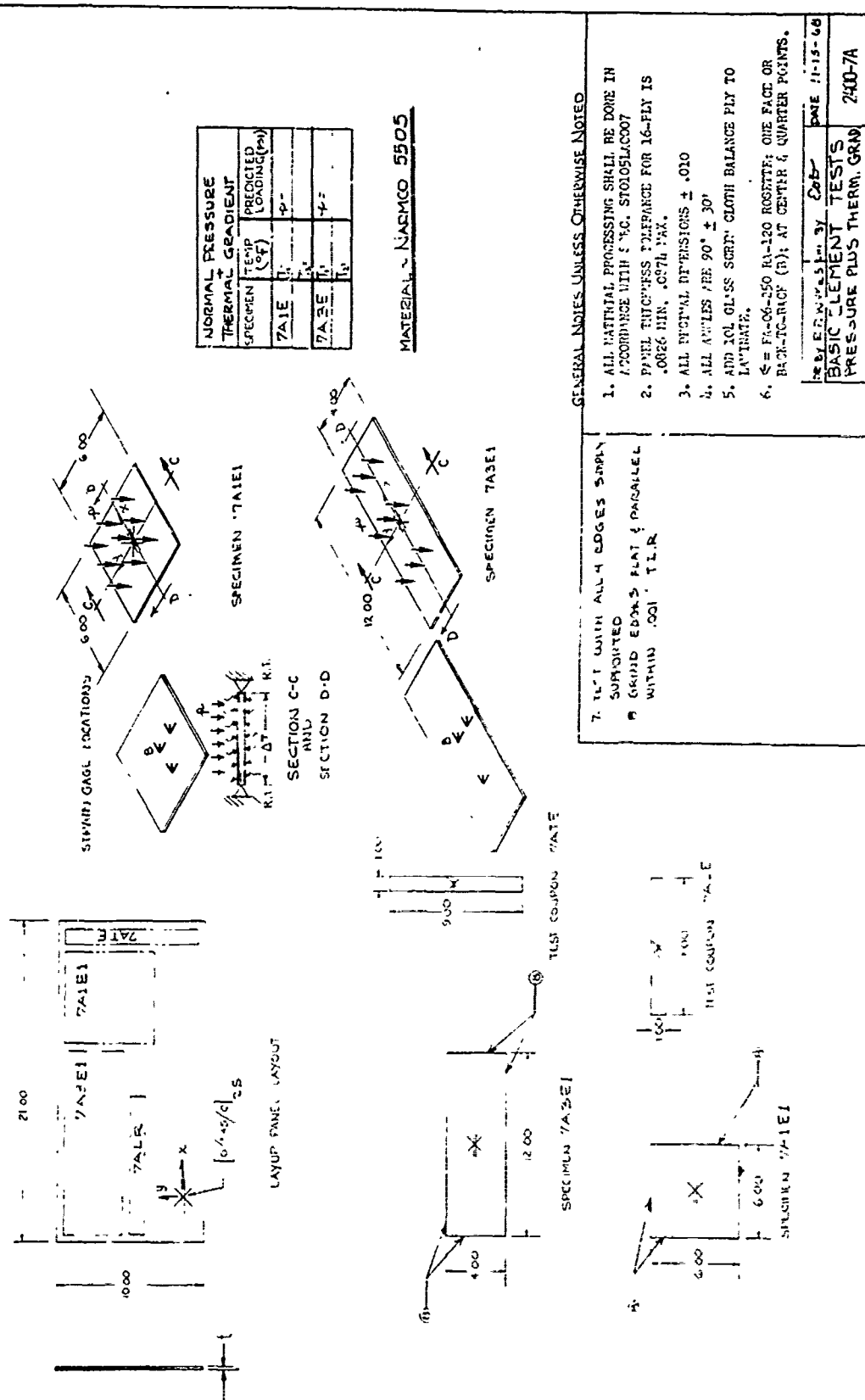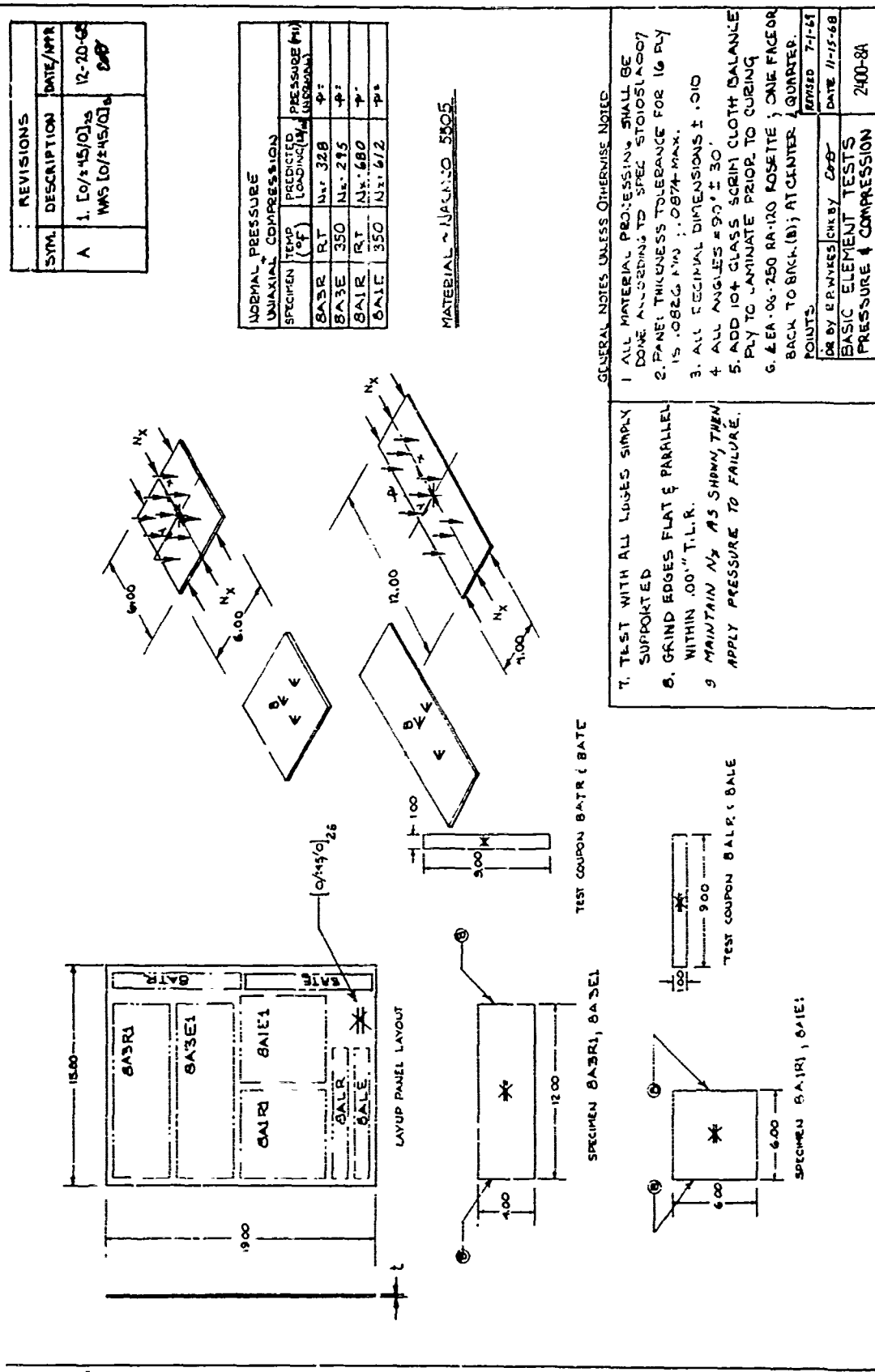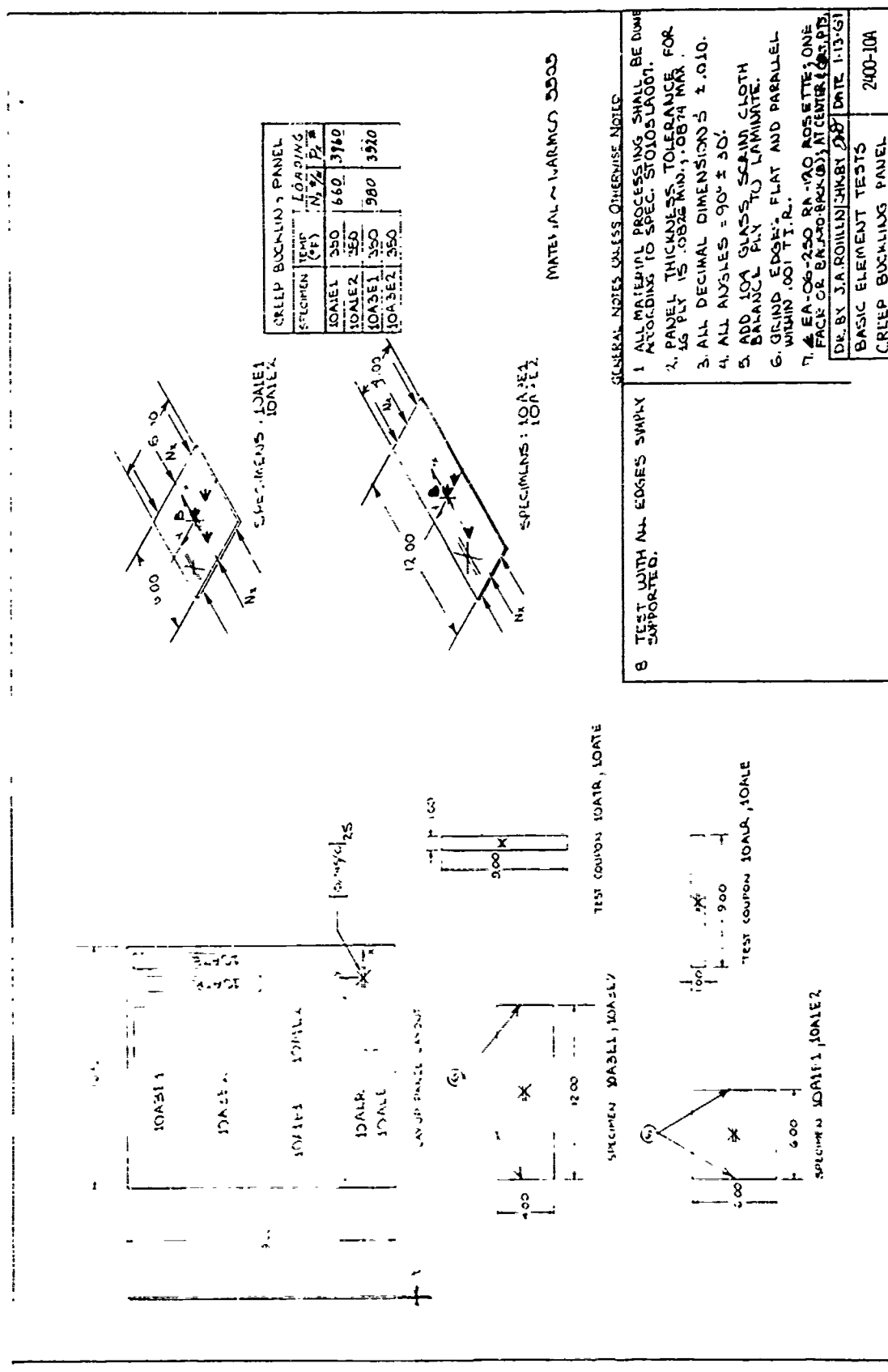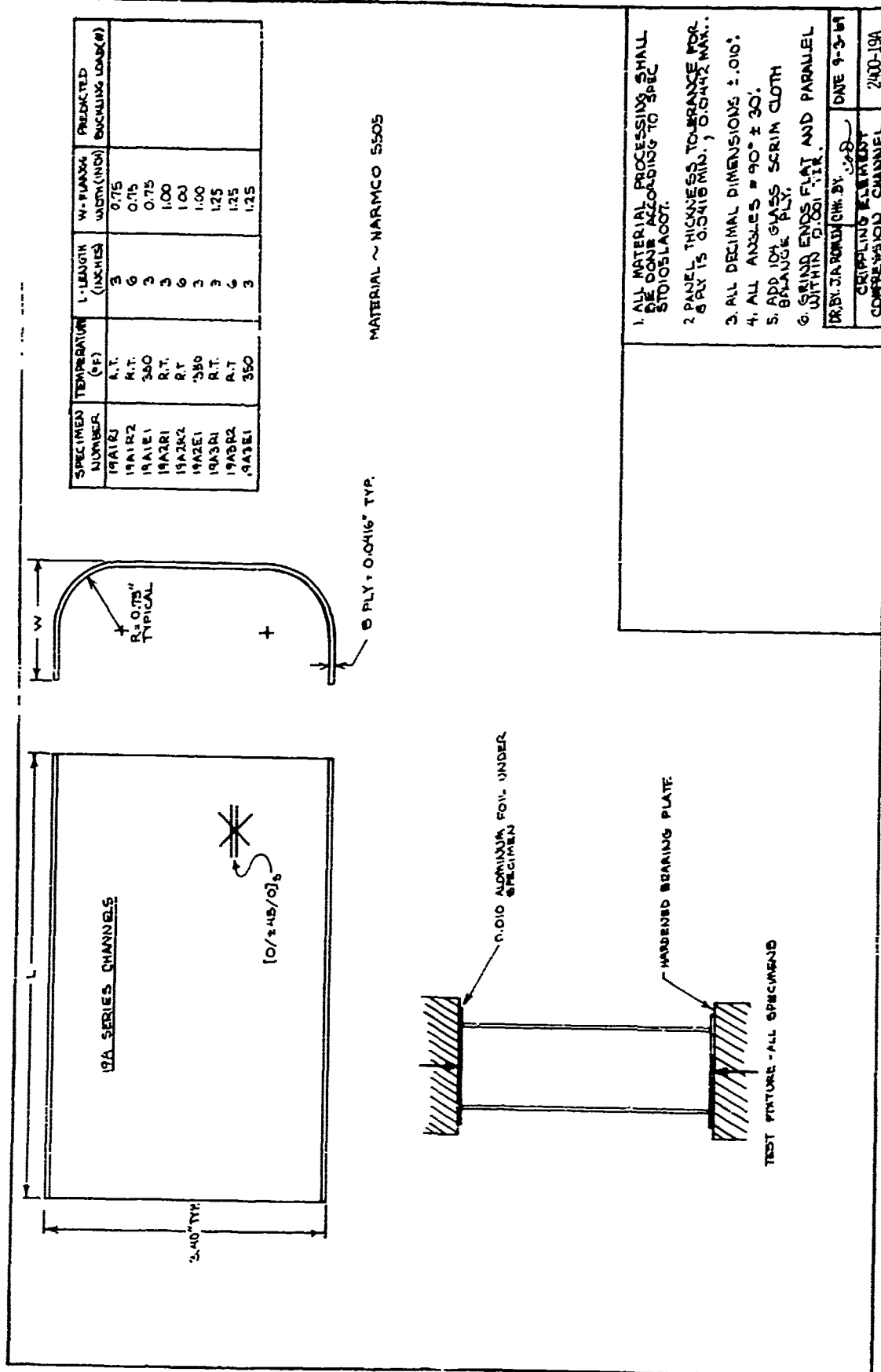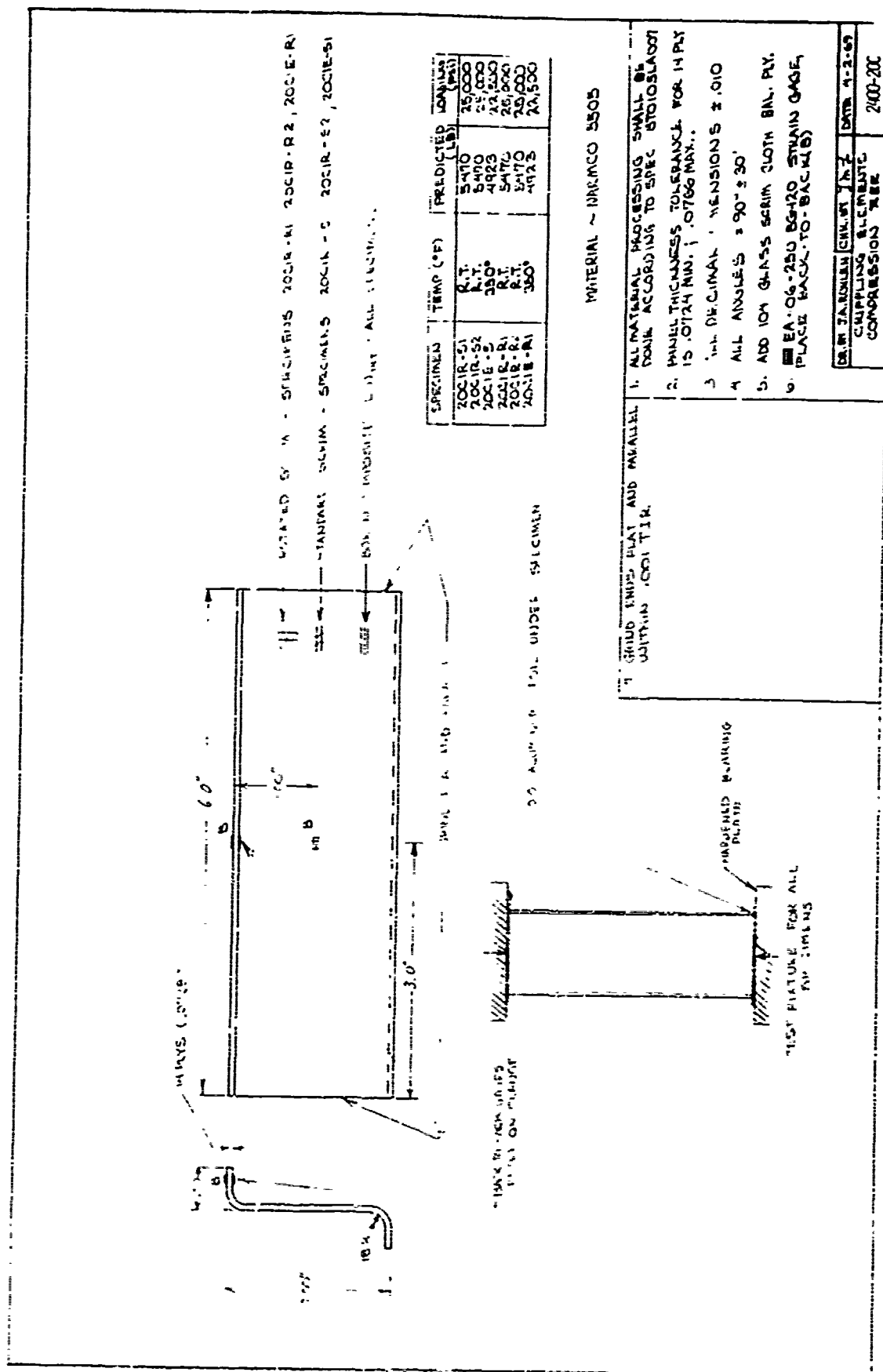
Figure 219.

279

Figure 220.

Figure 221.

Figure 222.

Figure 223.

283

Figure 224.

Figure 225.

Figure 226.

Figure 227.

Figure 228.

Figure 229.

289

Figure 230.

290

Figure 231.

REVISIONS

SYM	DESCRIPTION	DATE/APPR
4	CHANGED PER SYMBOL	5-12-11
	ADDED ELEV TEMP.	

SPECIMEN CODE	TYPE OF SPECIMEN	NO. REQUIRED	
		R+R.T	E+35°F
1	Warp Transverse Tension	3	3
2	Warp Longitudinal Tension	3	3
3	Warp Transverse Flexure	3	3
4	Warp Longitudinal Flexure	2	2
5	±45° 60° Interlaminar Shear	3	3

MATERIAL ~ NARMCO 5505

(c) Jor Boron Composite Rotated Scrim Cloth

rotated scrim cloth

6. ─ EA-06-250 B9-in STRAIN GAGE.

MATERIAL ~ NARMCO 5505

DATE 4-10-35
CRIPPLING ELEMENTS ROTATED SCRIM COUPON
2400-20/21-RSC

Figure 232.

Figure 233.
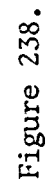
293

Figure 234.

Figure 235.

295

Figure 236.

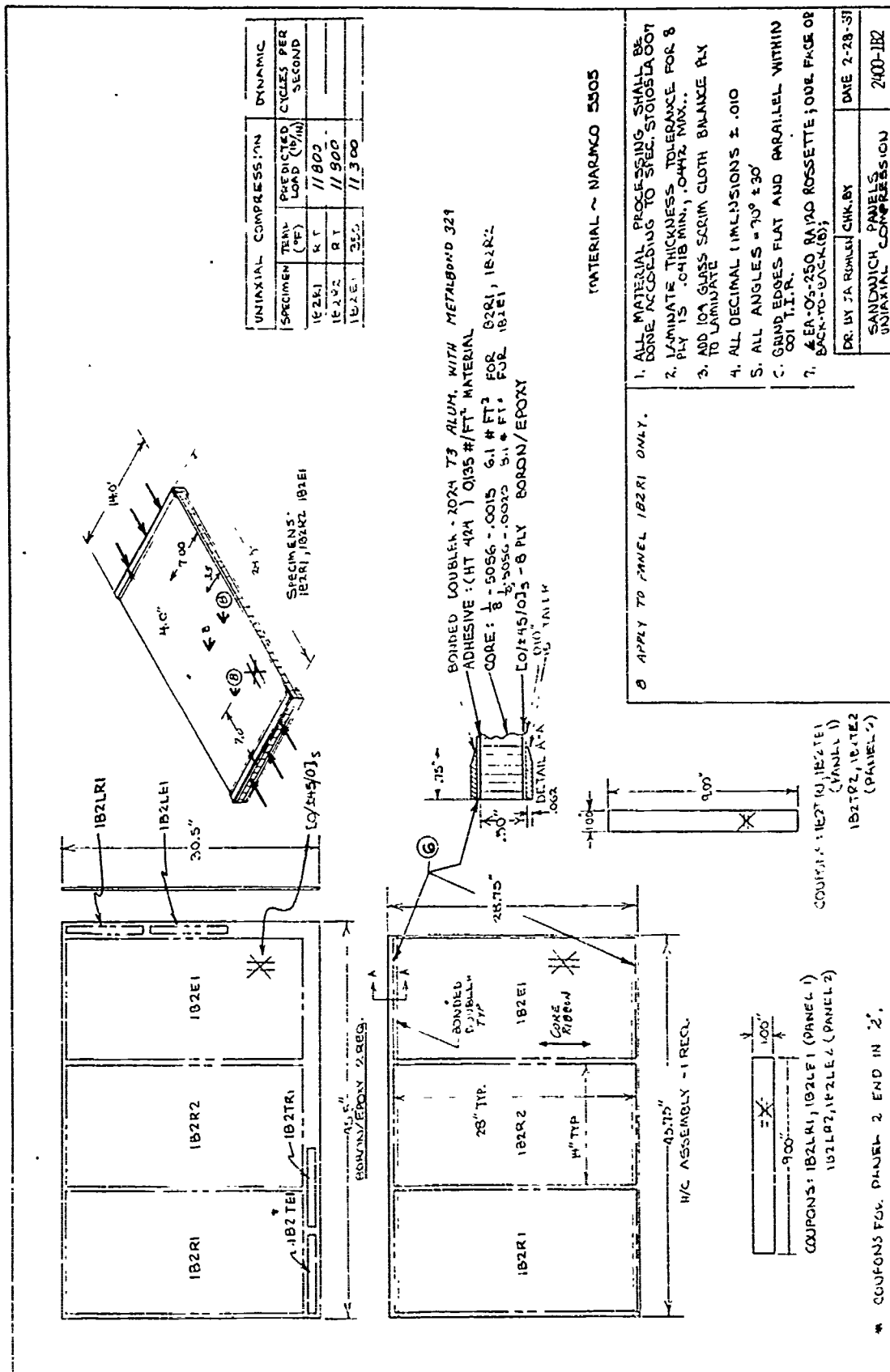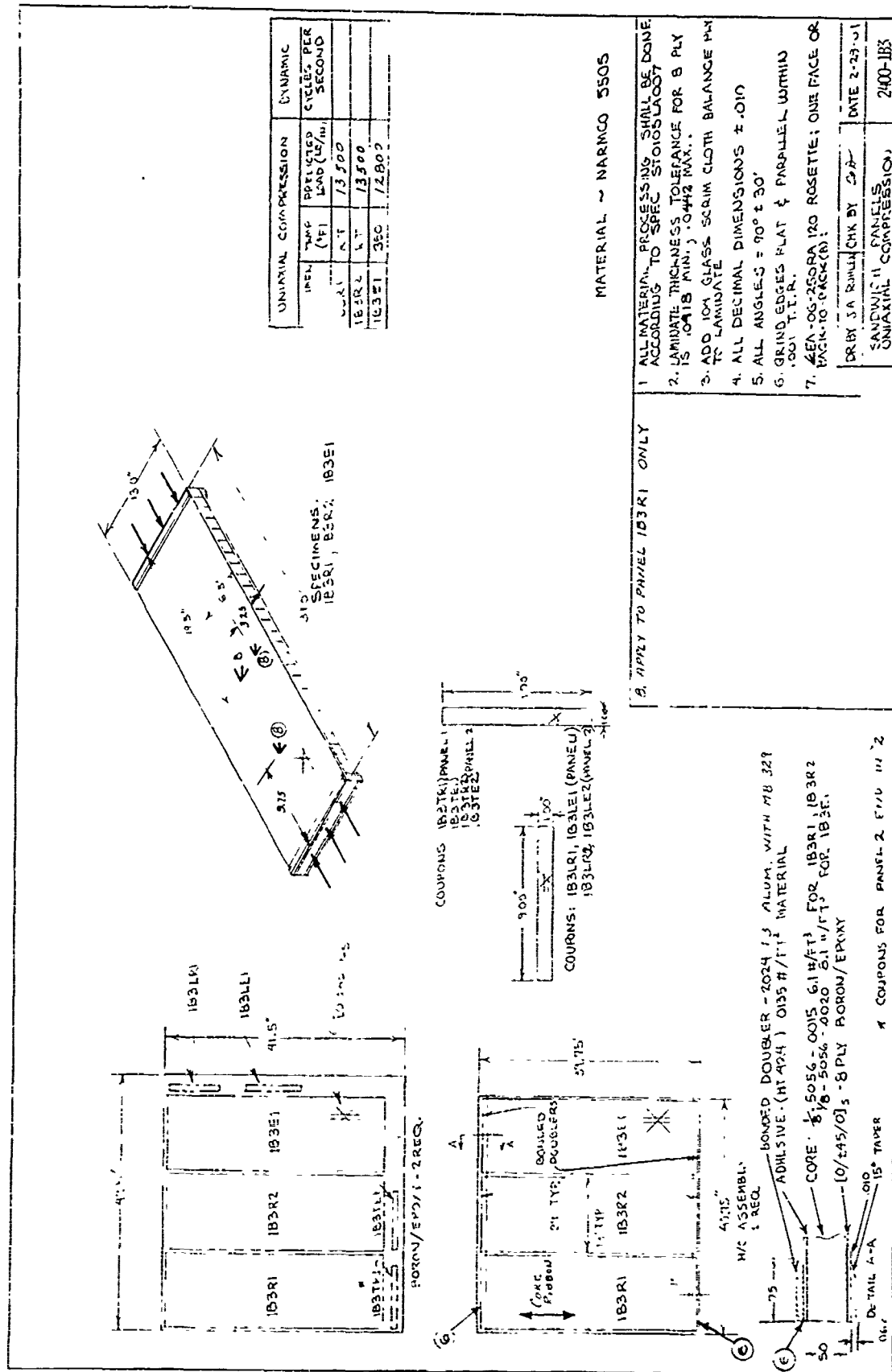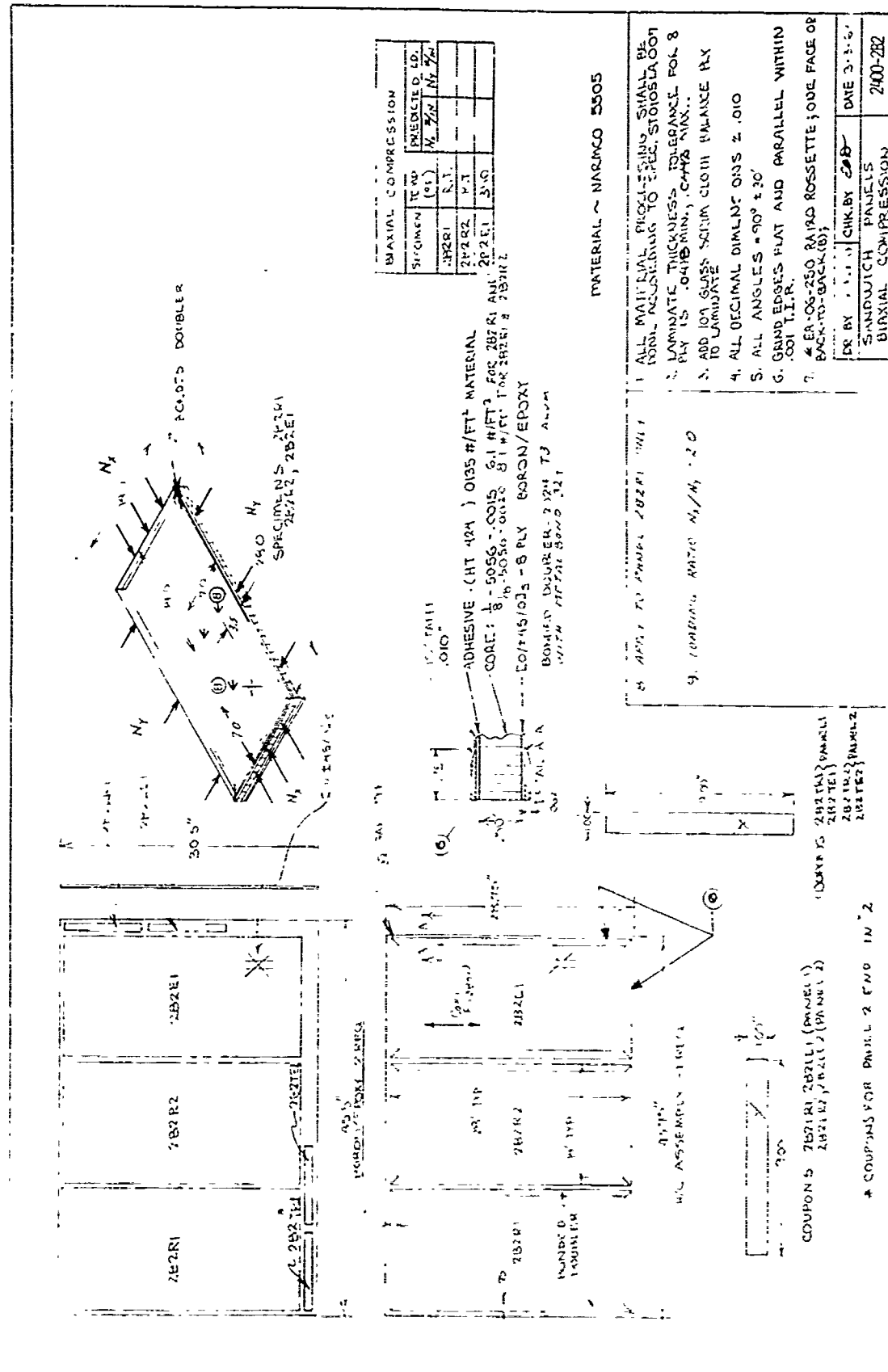Figure 237.

297

Figure 238.

29

Figure 239.

Figure 240.

Figure 241.

301

Figure 242.

Figure 243.

Figure 244.

Figure 245.

Figure 246.

Figure 247.

307

Figure 248.

Figure 249.

Figure 250.

310

Figure 251.

Figure 252.

Figure 253.

313
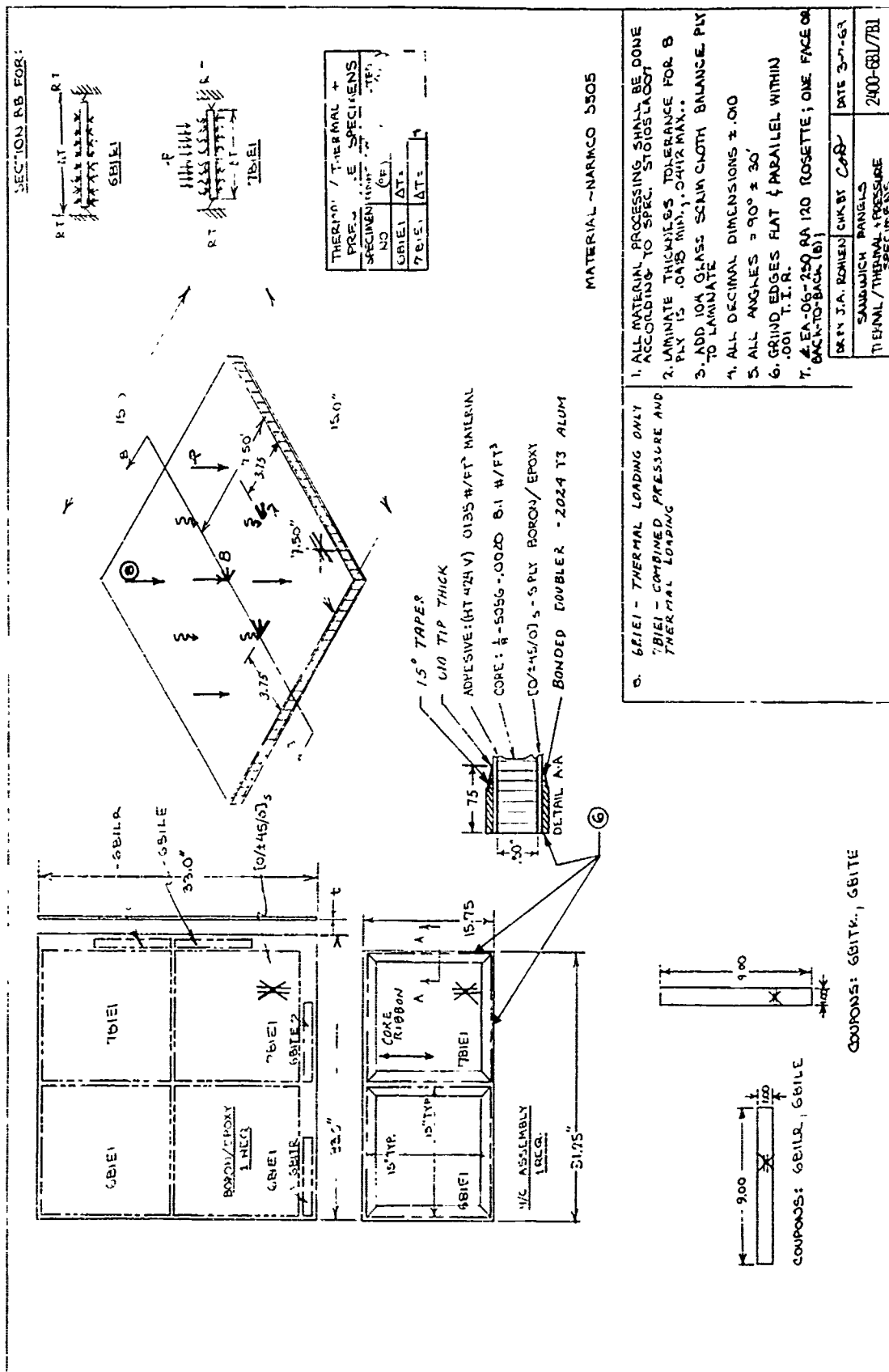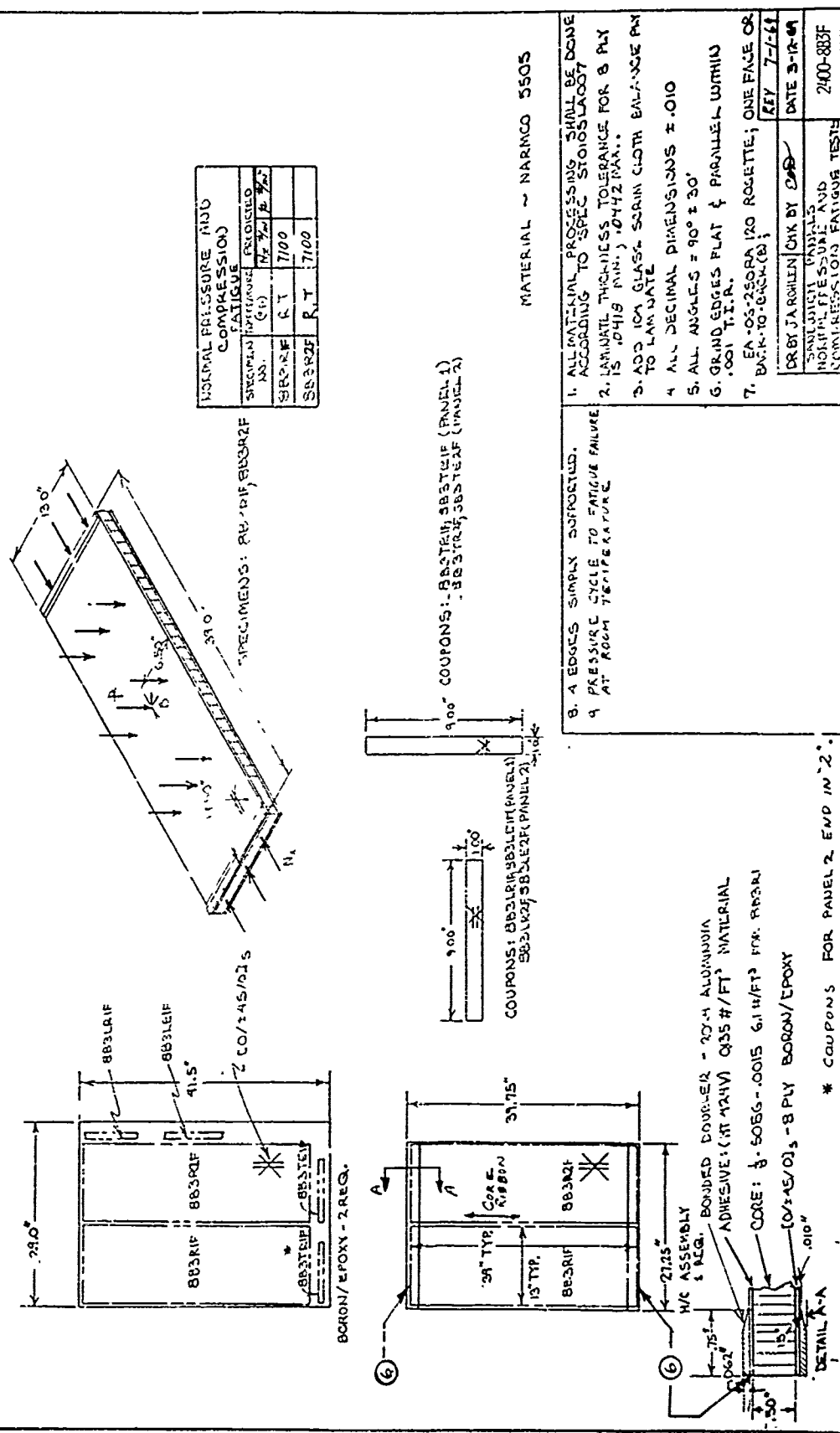
Figure 254.

Figure 255.

Figure 256.

Figure 257.

317

Figure 258.

318
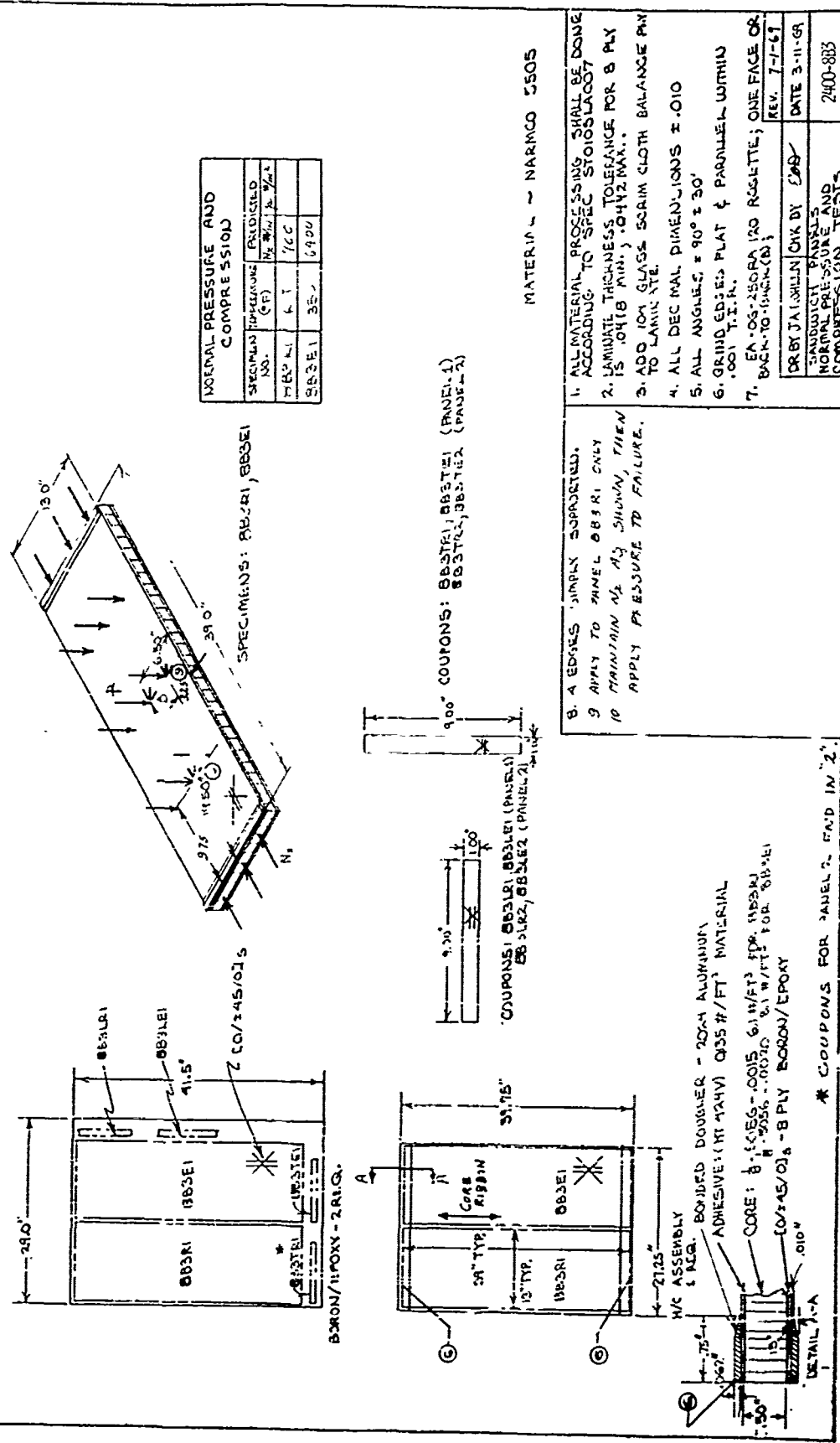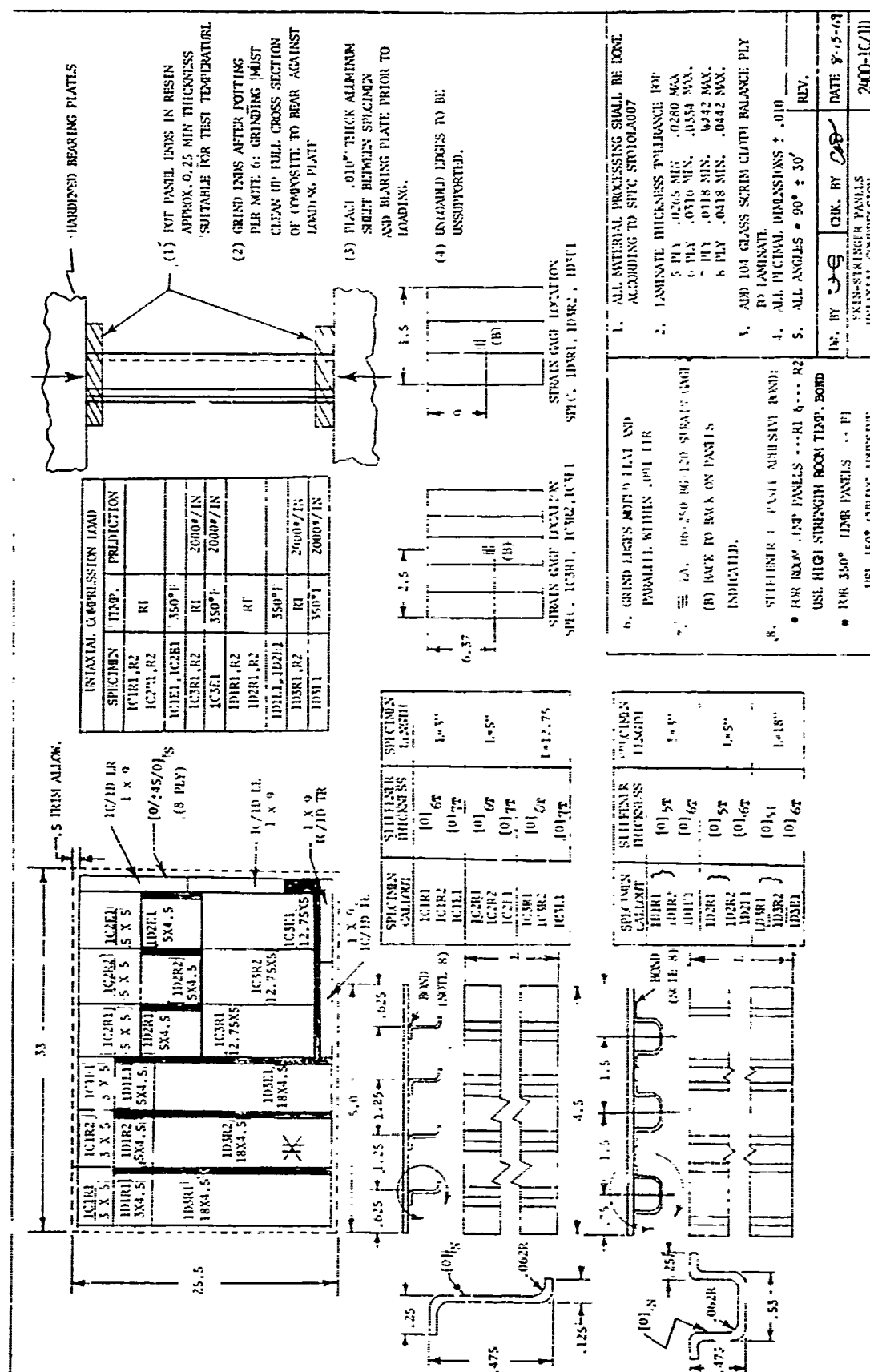
Figure 259.

Figure 260.
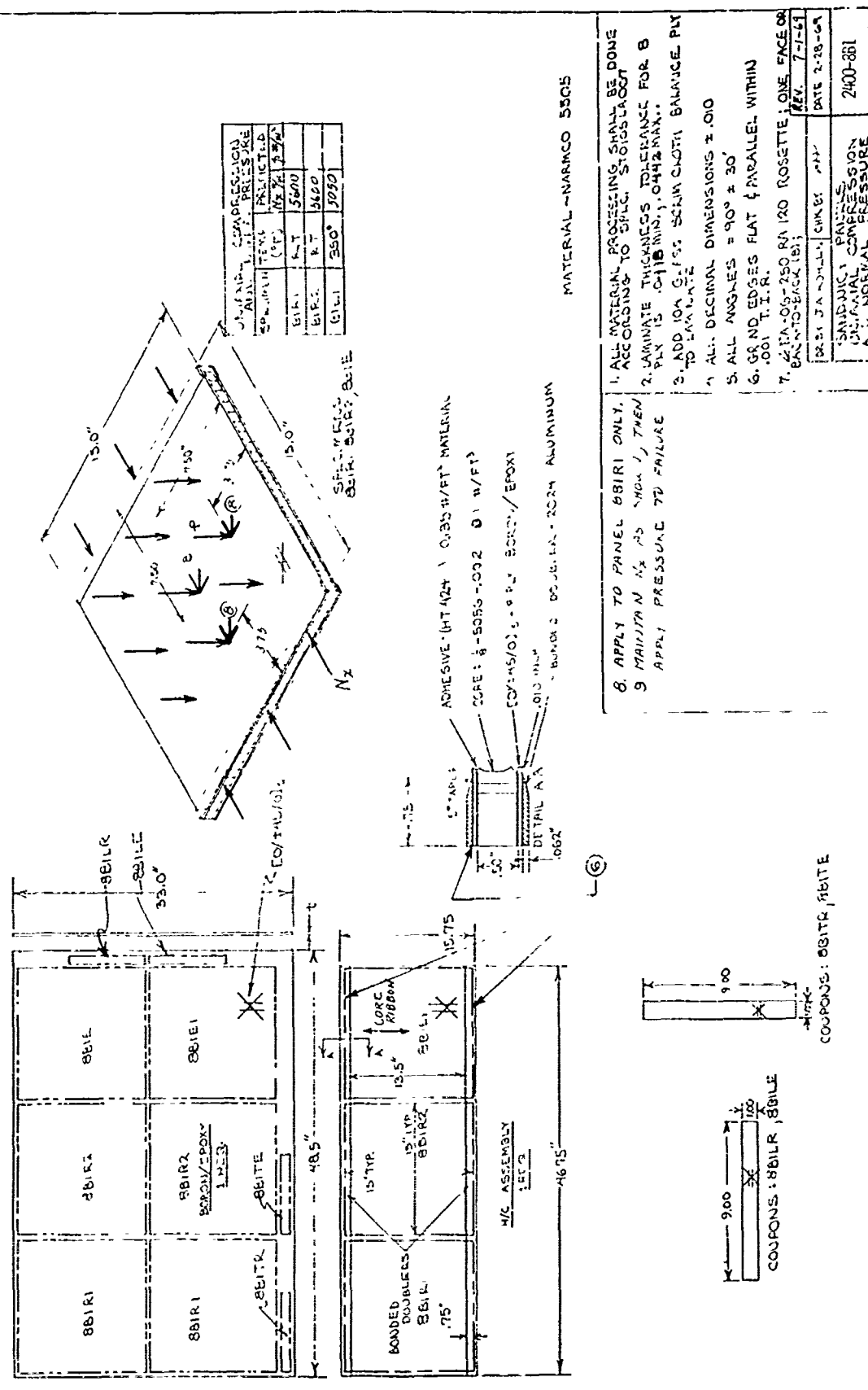
Figure 261.

321
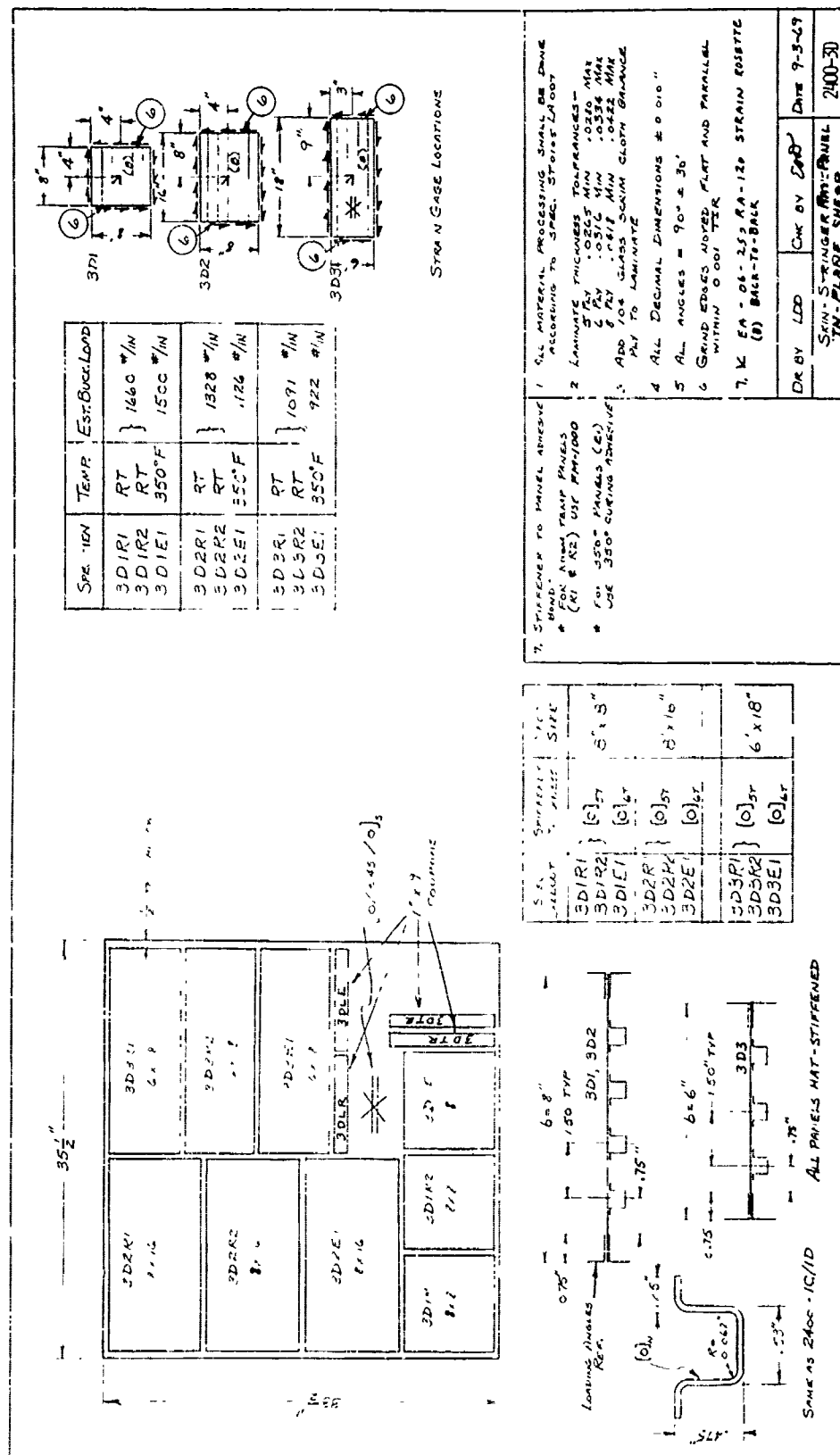
Figure 2b2.

REFERENCES

1. Ashton, J. E., "Anisotropic Plate Analysis," General Dynamics/ Fort Worth Division, Report No. FZM-4899, Contract AF33(615)-5257, October 1967

2. Structural Design Guide for Advanced Composite Applications, Second Edition, Contract F33615-69-C-1368, North American Rockwell/Los Angeles Division, January 1971

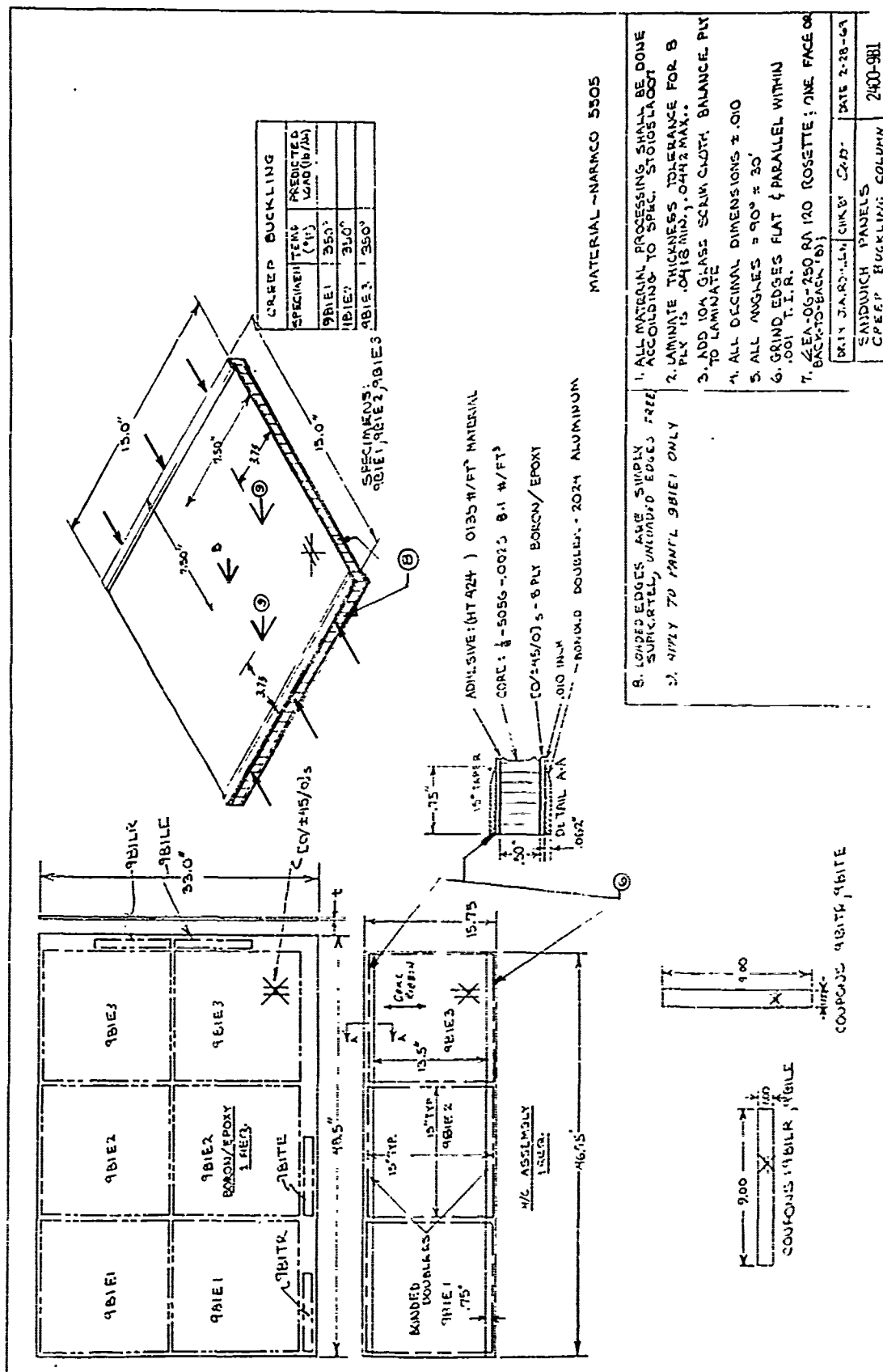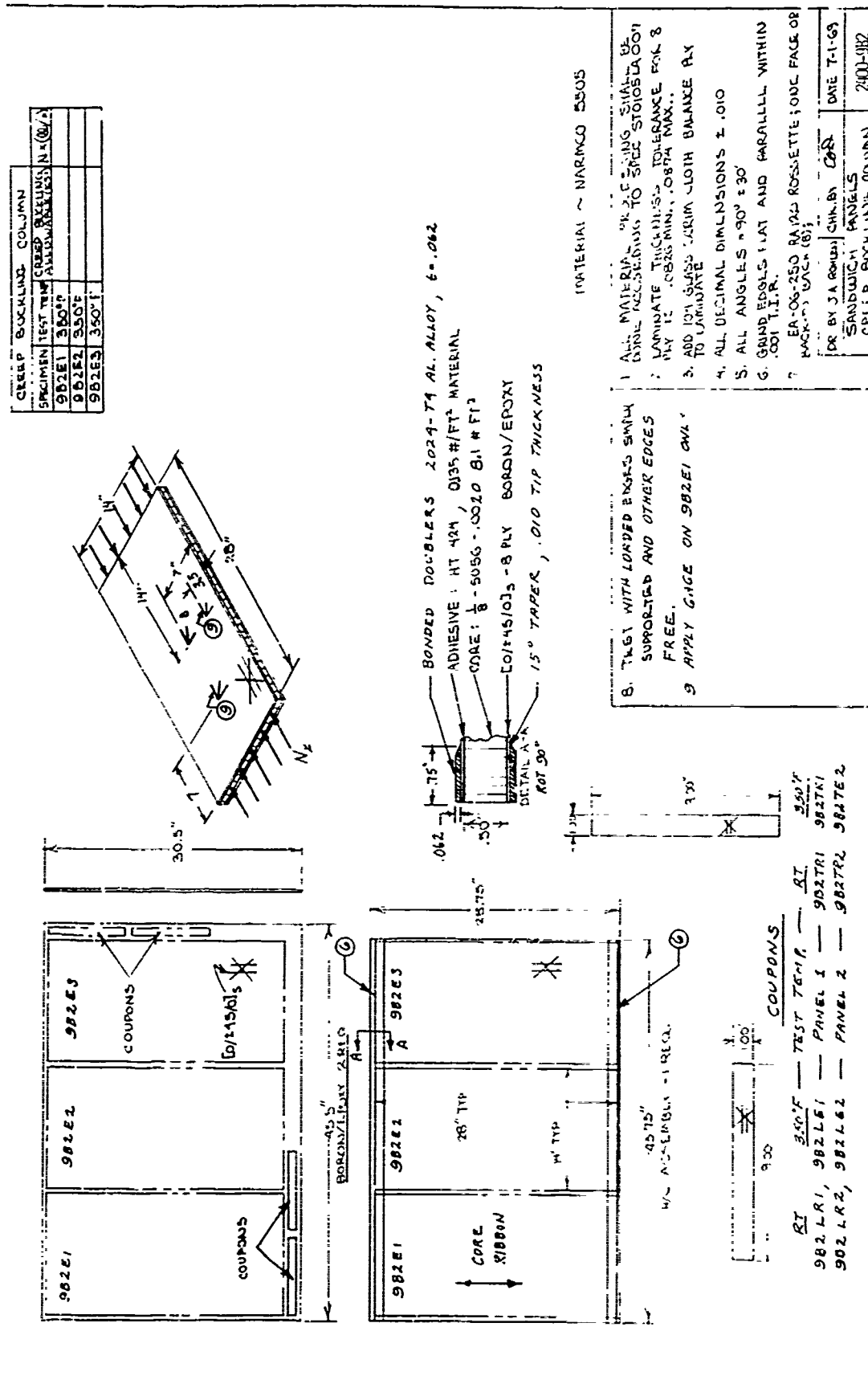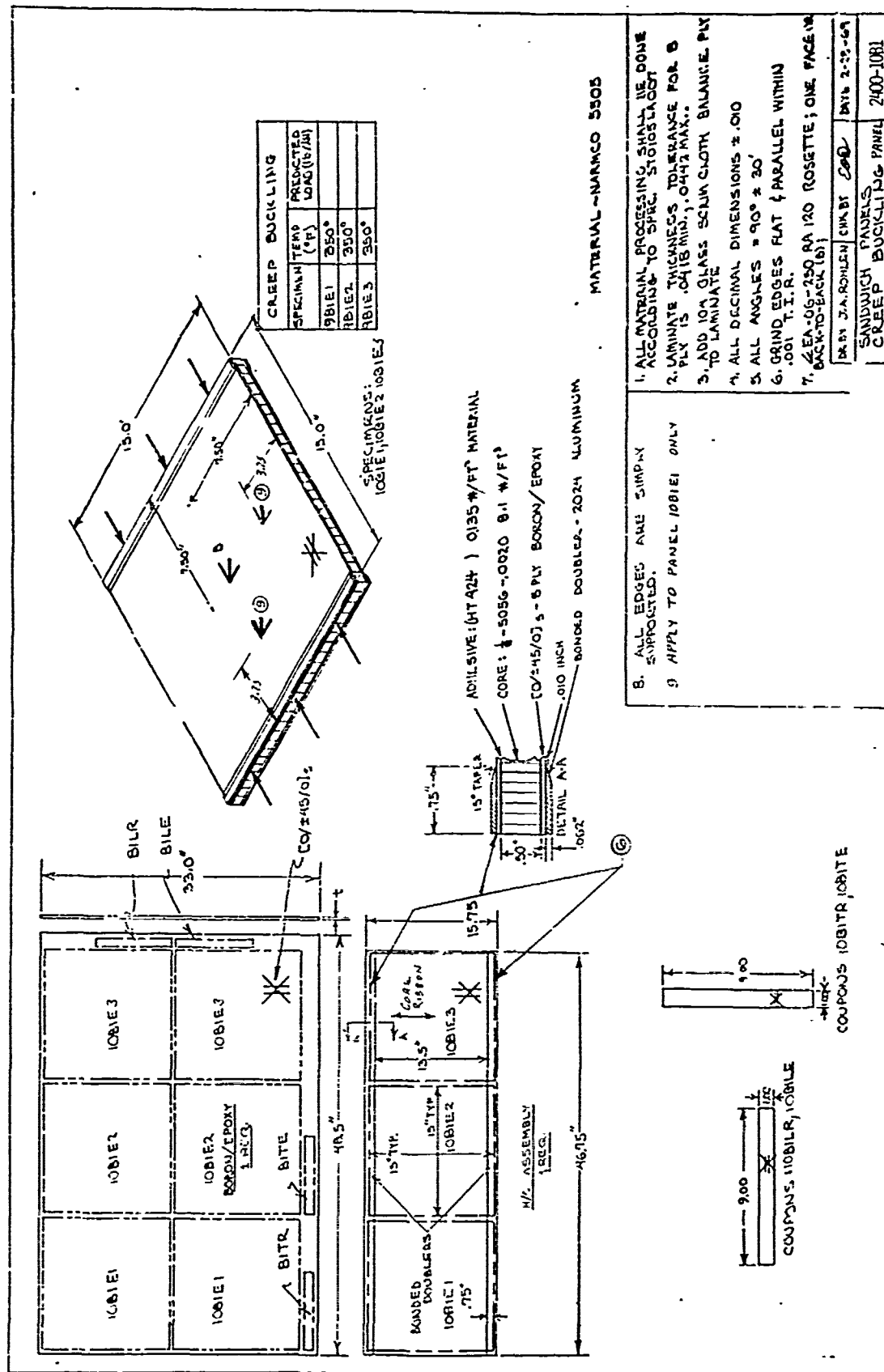3. Perry, David J., Aircraft Structures, McGraw-Hill Book Company, Inc, New York, 1950, pp 371-376

4. "Development of Engineering Data for Advanced Composite Materials," Air Force Materials Laboratory Report AFML-TR-69-108, General Dynamics/Fort Worth Division, 197^

5. Kuhn, P., Peterson, J., and Levin, L., "A Summary of Diagonal Tension; Part I - Methods of Analysis," National Advisory Committee for Aeronautics Technical Note 2661, Langley Aeronautical Laboratory, Langley Field, Va., May 1952

323

DOCUMENT CONTROL, DATA - R & D

(Security classification of title, body of abstract and indexing annotation must be entered when the overall report is classified)

1 ORIGINATING ACTIVITY (Corporate author)	2a. REPORT SECURITY CLASSIFICATION
North American Rockwell Corporation Los Angeles Division Los Angeles, California 40009	Unclassified
	2b. GROUP N/A

3 REPORT TITLE

Advanced Composites Data for Aircraft Structural Design
Volume II: Structural Element Behavior - Test and Analytical Determination.

4 DESCRIPTIVE NOTES (Type of report and inclusive dates)

Final Technical Report, 15 March 1968 - 15 March 70.

5 AUTHOR(S) (First name, middle initial, last name)

Leslie M. Lackman. Donald Y. Konishi

6 REPORT DATE	7a. TOTAL NO. OF PAGES	7b NO OF REFS
March 72	344 p.	5
8a CONTRACT OR GRANT NO F33615-68-C-1489	9a. ORIGINATOR'S REPORT NUMBER(S) AFML TR-70-58 Vol - 2	
b. PROJECT NO AF- 6169CW		
c.	9b. OTHER REPORT NO(S) (Any other numbers that may be assigned this report)	
d.		

10 DISTRIBUTION STATEMENT

Distribution limited to U.S. Government Agencies and designated recipients only since this report concerns the test and evaluation of technology directly applicable to military hardware. Requests for additional copies or further distribution of this document must be referred to AFML/LC, Wright-Patterson AFB, OH 45433.

11 SUPPLEMENTARY NOTES	12 SPONSORING MILITARY ACTIVITY
	Advanced Composites Division (AFML/LC) Air Force Materials Laboratory Wright-Patterson Air Force Base, Ohio

13 ABSTRACT

This volume summarizes that portion of the program concerned with the fabrication, testing, and analysis of basic element specimens composed partially or entirely of the boron/epoxy advanced composite material referred to herein as Narmco 5505.

The main body of this volume comprises independent sections on the fabrication of basic structural elements, testing of basic structural elements, and the analysis of unstiffened skin, honeycomb sandwich, and stiffened skin-element tests.

403 239

DD FORM 1473 (1 NOV 65)

KEY WORDS	LINK A		LINK B		LINK C	
	ROLE	WT	ROLE	WT	ROLE	WT
Aircraft Structural Design						
Advanced Composite Materials						
Advanced Composite Structure						
Filamentary Composite Materials						
Filamentary Composite Structure						
Fiber-Reinforced Materials						
Composite Material						
Composite Structure						
Anisotropic Analysis						
Micromechanics						
Strength Properties of Composites						
Elastic Constants of Composites						
Thermoelastic Analysis						
Orthotropic Sandwich						